

CRANFIELD UNIVERSITY

NURUL MUSFIRAH MAZLAN

ASSESSING/OPTIMISING BIO-FUEL COMBUSTION  
TECHNOLOGIES FOR REDUCING CIVIL AIRCRAFT EMISSIONS

SCHOOL OF ENGINEERING  
Department of Power and Propulsion

PhD  
Academic Year: 2009 - 2012

Supervisor: Prof Mark Savill  
Dec 2012



CRANFIELD UNIVERSITY

SCHOOL OF ENGINEERING  
Department of Power and Propulsion

PhD

Academic Year 2009 - 2012

NURUL MUSFIRAH MAZLAN

Assessing/Optimising Bio-fuel Combustion Technologies for  
Reducing Civil Aircraft Emissions

Supervisor: Prof Mark Savill

Dec 2012

This thesis is submitted in partial fulfilment of the requirements for  
the degree of PhD

***(NB. This section can be removed if the award of the degree is  
based solely on examination of the thesis)***

© Cranfield University 2012. All rights reserved. No part of this  
publication may be reproduced without the written permission of the  
copyright owner.



## **ABSTRACT**

Gas turbines are extensively used in aviation because of their advantageous volume as weight characteristics. The objective of this project proposed was to look at advanced propulsion systems and the close coupling of the airframe with advanced prime mover cycles. The investigation encompassed a comparative assessment of traditional and novel prime mover options including the design, off-design, degraded performance of the engine and the environmental and economic analysis of the system. The originality of the work lies in the technical and economic optimisation of gas turbine based on current and novel cycles for a novel airframes application in a wide range of climatic conditions.

The study has been designed mainly to develop a methodology for evaluating and optimising biofuel combustion technology in addressing the concerns related to over-dependence on crude oil (Jet-A) and the increase in pollution emissions. The main contributions of this work to existing knowledge are as follows: (i) development of a so-called greener-based methodology for assessing the potential of biofuels in reducing the dependency on conventional fuel and the amount of pollution emission generated, (ii) prediction of fuel spray characteristics as one of the major controlling factors regarding emissions, (iii) evaluation of engine performance and emission through the adaptation of a fuel's properties into the in-house computer tools, (iv) development of optimisation work to obtain a trade-off between engine performance and emissions, and (v) development of CFD work to explore the practical issues related to the engine emission combustion modelling.

Several tasks have been proposed. The first task concerns the comparative study of droplet lifetime and spray penetration of biofuels with Jet-A. In this task, the properties of the selected biofuels are implemented into the equations related to the evaporation process. Jatropha Bio-synthetic Paraffinic Kerosine (JSPK), Camelina Bio-synthetic Paraffinic Kerosine (CSPK), Rapeseed Methyl Ester (RME) and Ethanol are used and are evaluated as pure fuel. Additionally, the mixture of 50% JSPK with 50% Jet-A are used to examine the effects of

blend fuel. Results revealed the effects of fuel volatility, density and viscosity on droplet lifetime and spray penetration. It is concluded that low volatile fuel has longer droplet lifetime while highly dense and viscous fuel penetrates longer. Regarding to the blending fuel, an increase in the percentage of JSPK in the blend reduces the droplet lifetime and length of the spray penetration.

An assessment of the effect of JSPK and CSPK on engine performance and emissions also has been proposed. The evaluation is conducted for the civil aircraft engine flying at cruise and at constant mass flow condition. At both conditions results revealed relative increases in thrust as the percentage of biofuel in the mixture was increased, whilst a reduction in fuel flow during cruise was noted. The increase in engine thrust at both conditions was observed due to high LHV and heat capacity, while the reduction in fuel flow was found to correspond to the low density of the fuel. Regarding the engine emissions, reduction in  $\text{NO}_x$  and CO was noted as the composition of biofuels in the mixture increased. This reduction is due to factors such as flame temperature, boiling temperature, density and volatility of the fuel. While at constant mass flow condition, increases in CO were noted due to the influence of low flame temperature which leads to the incompleteness of oxidation of carbon atoms.

Additionally, trade-off between engine thrust,  $\text{NO}_x$ , and CO through the application of multi-objective genetic algorithm for the test case related to the fuel design has been proposed. The aim involves designing an optimal percentage of the biofuel/Jet-A mixture for maximum engine thrust and minimum engine emissions. The Pareto front obtained and the characteristics of the optimal fuel designs are examined. Definitive trades between the thrust and CO emissions and between thrust and  $\text{NO}_x$  emissions are shown while little trade-off between  $\text{NO}_x$  and CO emissions is noted. Furthermore, the practical issues related to the engine emissions combustion modelling have been evaluated. The effect of assumptions considered in HEPHAESTUS on the predicted temperature profile and  $\text{NO}_x$  generation were explored.

Finally, the future works regarding this research field are identified and discussed.

## **ACKNOWLEDGEMENTS**

First of all my deepest thanks go to ALLAH for His blessings.

I would like to state my gratitude to my supervisor, Professor Mark Savill and my advisor, Dr Timos Kipouros, for consistently offering encouragement, supervision and help throughout this research. Huge thanks also to all the professors, lecturers, researchers and staff of Cranfield University, particularly in the Department of Power and Propulsion, who gave me the opportunity to pursue and helping me in completing my PhD study.

Special thanks also are dedicated to the Universiti Sains Malaysia, Malaysia, for the financial and funding support throughout this course.

I would like to express my thanks to my parents, Mazlan Rozali and Mastura Jamari, and all my siblings for their duas, support and encouragement and valuable advice.

I am indebted to my husband, Amil Saleh Amilasan for his patience and help, especially in looking after my son during my studies, not forgetting the special thanks due to my lovely son, Amil Azfar Amil Saleh, for understanding my situation. I also dedicate thanks to my husband's family for their constant support and encouragement.

Last but not least, my appreciation to all my colleagues, John, Christos, Apostolos, Janthanee, Gilberto and Salwan who give me their valuable time for discussion.



# TABLE OF CONTENTS

ABSTRACT .....	iii
ACKNOWLEDGEMENTS.....	v
LIST OF FIGURES.....	xi
LIST OF TABLES .....	xiv
NOTATIONS .....	xvi
ABBREVIATIONS AND FORMULAE .....	xx
1 INTRODUCTION TO THE RESEARCH TOPIC.....	23
1.1 General Introduction.....	23
1.1.1 Introduction.....	23
1.1.2 Research Motivation and Problem of Statement.....	23
1.1.3 Research Gap.....	26
1.1.4 Aim and Objectives.....	26
1.1.5 Contribution to Knowledge.....	27
1.1.6 Thesis Layout .....	27
1.2 General Literature Survey .....	29
1.2.1 Introduction.....	29
1.2.2 Alternative Fuel's Issues .....	34
1.2.3 'Drop-in' Jet Fuel.....	37
1.2.4 Flight Tests Using 'Drop-in' Jet Fuel.....	38
1.2.5 Performance and Emissions of 'Drop-in' Jet Fuel .....	39
1.3 Methodology.....	41
1.3.1 Introduction .....	41
1.3.2 Flowchart .....	42
1.3.3 Evaporation Analysis .....	44
1.3.4 PYTHIA Software.....	44
1.3.5 HEPHAESTUS Software .....	46
1.3.6 Optimisation using GATAC Optimisation Tool .....	49
2 EVALUATION OF BIO-FUEL'S SPRAY BEHAVIOUR.....	52
2.1 General Introduction.....	52
2.2 Factors Affecting Combustion Performance of Liquid Fuels.....	52
2.3 Requirement of Biofuels Spray Evaluation .....	56
2.3.1 Physical Modelling of the Liquid Phase .....	57
2.3.2 Finding and Derivation of the Necessary Fuel Properties.....	60
2.4 Results .....	73
2.4.1 The Comparison of Fuel's Properties .....	73
2.4.2 The Evaluation of Droplet Lifetime.....	77
2.4.3 The Comparison of Spray Penetration.....	78
2.5 Discussions .....	80
2.5.1 The Effect of Boiling Temperature on Droplet Lifetime .....	80
2.5.2 The Effect of Density on Penetration Length .....	81
2.5.3 The Effect of Fuel's Viscosity on Spray Penetration .....	82
2.5.4 The Influence of Mixing Biofuel with Kerosine .....	83
2.6 Conclusions.....	87
3 EVALUATION OF BIOFUELS ENGINE PERFORMANCE .....	90
3.1 General Introduction.....	90

3.2	Gas Turbines and the Factors that Affect the Performance .....	90
3.3	Requirement for the Engine Performance Evaluation .....	93
3.3.1	Computer Tools Used.....	94
3.3.2	Fuels' Caloric Properties Data Generation .....	95
3.3.3	Validation of Data Generation.....	96
3.3.4	Evaluation of Bio-fuel in Two-Spool High Bypass Turbofan Aircraft Engine 97	
3.4	Results .....	100
3.4.1	Data Validation .....	100
3.4.2	Engine Performance Validation .....	101
3.4.3	The Influence of Biofuel Mixture during Cruise Condition .....	102
3.4.4	The Influence of Biofuel Mixture at Constant Mass Flow Condition 105	
3.5	Discussion.....	107
3.5.1	The Influence of LHV on the Engine Thrust.....	107
3.5.2	The Effect of Heat Capacity on Engine Thrust.....	107
3.5.3	The Effect of Fuel Density on Fuel Consumption.....	109
3.6	Conclusions.....	110
4	EVALUATION OF BIOFUELS ENGINE EMISSIONS .....	113
4.1	General Introduction.....	113
4.2	Formation of Pollutant Emissions and Its Impact on the Environment and Human Health .....	113
4.3	Effect of Fuel Properties on Emissions.....	116
4.4	Engine Emissions Evaluation Requirements.....	119
4.4.1	Introduction to the HEPHAESTUS.....	119
4.4.2	Engine emissions evaluation .....	122
4.5	Results .....	122
4.5.1	The Comparison of NO <sub>x</sub> and CO with the Literature .....	122
4.5.2	Formation of NO <sub>x</sub> during Cruise Condition.....	124
4.5.3	Formation of CO during Cruise Condition.....	127
4.5.4	Formation of NO <sub>x</sub> during Constant Mass Flow Condition.....	128
4.5.5	Formation of CO during Constant Mass Flow Condition.....	131
4.6	Discussion.....	131
4.6.1	The Effect of LHV, Heat Capacity and FAR on Combustor Outlet Temperature and NO <sub>x</sub> Formation .....	132
4.6.2	The Effect of Boiling Temperature on NO <sub>x</sub> Formation.....	135
4.6.3	The effect of fuel density on NO <sub>x</sub> formation .....	136
4.6.4	The Effect of Flame Temperature on CO Formation at constant mass flow condition .....	137
4.6.5	The Effect of Fuel Volatility on Evaporation Rate and CO Formation at Cruise Condition.....	139
4.7	Conclusions.....	139
5	OPTIMISATION ASSESSMENT .....	141
5.1	Introduction .....	141
5.2	Optimisation in general.....	142
5.3	Requirement for the Optimisation Assessment .....	143
5.3.1	About GATAC – The Optimisation Framework .....	143

5.3.2	Non-dominated Searching Genetic Algorithm (NSGA) - based Optimiser.....	144
5.3.3	Test cases Implementation.....	145
5.3.4	Comparative Study with MOTS2.....	148
5.4	Results and Discussions .....	149
5.4.1	Trade studies – Test case 1 .....	149
5.4.2	Extreme Designs – Test case 1 .....	151
5.4.3	Compromise Design – Test case 1.....	152
5.4.4	Trade Studies – Test case 2.....	153
5.4.5	Extreme Designs - Test case 2.....	154
5.4.6	Compromise Design – Test case 2.....	156
5.4.7	Comparison between NSGAMO with MOTS2 .....	157
5.5	Conclusions.....	162
6	CFD MODELLING APPROACH.....	165
6.1	General Introduction.....	165
6.2	The Comparison of RANS model with DNS and LES models .....	165
6.3	Problem description.....	167
6.4	Results and Discussion .....	170
6.4.1	Comparison of Combustor Temperature Profile .....	170
6.4.2	The Comparison of NO <sub>x</sub> Generation .....	173
6.4.3	The Comparison Result between HEPHAESTUS with URANS and LES for the case of Generic Combustor.....	180
6.5	Conclusions.....	182
7	GENERAL RESULTS AND DISCUSSIONS .....	183
7.1	Biofuel's Spray Behaviour Evaluation.....	183
7.2	Biofuel's Engine Performance Evaluation .....	185
7.3	Biofuel's Engine Emissions Evaluation.....	186
7.4	Optimisation Assessment.....	188
7.5	CFD Modelling Approach .....	191
8	CONCLUSIONS AND FUTURE WORKS .....	193
8.1	Conclusions.....	193
8.2	Future Works.....	199
9	REFERENCES.....	202
10	APPENDICES .....	214
10.1	Appendix A - List of Publications.....	214
10.2	Appendix B - Evaporation Calculation for Kerosine .....	215
10.3	Appendix C - Calculation of Molecular Formula and Enthalpy of Formation.....	217
10.4	Appendix D - Equations of Mixing Properties of Two Fuels .....	220
10.5	Appendix E - Hephaestus Input File.....	221



## LIST OF FIGURES

Figure 1-1: Percentage of Pollutants Produced from Aircraft Engine (GAO report, 2009).....	30
Figure 1-2: The Winglets Invention Reducing Induced Drag at the Tips of the Wings by Weakening the Vortex at the Wingtip. (Source: <a href="http://www.grc.nasa.gov/WWW/k-12/airplane/winglets.html">http://www.grc.nasa.gov/WWW/k-12/airplane/winglets.html</a> ) .....	32
Figure 1-3: The Challenges of Implementing Aircraft with Ethanol (Dagget <i>et al.</i> (2006)).....	35
Figure 1-4: The Tendency of Biodiesel to Freeze at Cold Temperature (Melanie, 2006).....	36
Figure 1-5: Additional Process Introduced to Overcome Freezing-fuel Issue (Dagget <i>et al.</i> (2006)) .....	36
Figure 1-6: The Flowchart Representing the Proposed Tasks Conducted in Present Research Work .....	42
Figure 2-1: Density of Jet-A as a Function of Temperature.....	61
Figure 2-2: Vapour Pressure of Kerosine as a Function of Temperature .....	62
Figure 2-3: Specific Heat Capacity of Kerosine as a Function of Temperature	63
Figure 2-4: Density of Rix Biodiesel as a Function of Temperature.....	64
Figure 2-5: Vapour Pressure of Rix Biodiesel as a Function of Temperature...	66
Figure 2-6: Specific Heat Capacity of RME as a Function of Temperature .....	66
Figure 2-7: Ethanol's Density Varying with Temperature.....	67
Figure 2-8: Ethanol's Vapour Pressure as a Function of Temperature.....	68
Figure 2-9: Density of CSPK Reduces as Temperature Increases.....	69
Figure 2-10: Vapour Pressure of CSPK Varies with Temperature.....	69
Figure 2-11: Heat Capacity of CSPK Increases Linearly with Temperature .....	70
Figure 2-12: Density of JSPK at Various Temperatures .....	71
Figure 2-13: The Variation of Vapour Pressure as a Function of Temperature	72
Figure 2-14: The Variation of Heat Capacity as a Function of Temperature ...	73
Figure 2-15: Comparison of Fuels' Density as Function of Temperature .....	74
Figure 2-16: The Comparison of Heat Capacity as a Function of Temperature	75
Figure 2-17: The Comparison of Vapour Pressure as a Function of Temperature .....	76
Figure 2-18: The Comparison of Jet-A, JSPK and CSPK as a Function of Temperature.....	76
Figure 2-19: The Comparison of Penetration Length .....	79
Figure 2-20: Linear Increases of Spray Penetration Observed After 0.08 ms ..	80
Figure 2-21: The Comparison of Density between B50, Jet-A and Pure JSPK	84
Figure 2-22: The Comparison of Heat Capacity between B50, Jet-A and Pure JSPK .....	85
Figure 2-23: The Comparison of the Penetration Length Predicted between B50, Jet-A, and Pure JSPK.....	86
Figure 3-1: Schematic Diagram of Turbojet Engine (Mattingly, 1996).....	91
Figure 3-2: Effect of Fuel Heating Value on Turbine Output (Brooks, 2000) ....	92
Figure 3-3: Effect of FAR, Pressure Ratio and Maximum Temperature on Thrust at Sea Level (Palmer, 1945).....	93
Figure 3-4: Components in Two Spool High Bypass Turbofan Engine.....	97

Figure 3-5: Schematic Diagram of Two Spools High Bypass Turbofan Engine used in this Work.....	98
Figure 3-6: The comparison of Fuel flow and Heating Value with Literature ..	101
Figure 3-7: Comparison of Thrust, Fuel Flow, and SFC of Pure CSPK and CSPK/Jet-A blend with Jet-A.....	103
Figure 3-8: Comparison of Thrust, Fuel Flow, and SFC of JSPK/Jet-A blend with Jet-A.....	104
Figure 3-9: Comparison of Thrust, TET, and SFC of CSPK/Jet-A blend Compared to Jet-A .....	105
Figure 3-10: Difference of Thrust, TET, and SFC of JSPK/Jet-A blend Compared to Jet-A .....	106
Figure 3-11: The Effect of Heat Capacity on Engine Thrust .....	108
Figure 3-12: The Effect of Fuel Density on Fuel Consumption .....	109
Figure 4-1: The Formation of Emissions from the Aero-engine (Norman <i>et al.</i> , 2003).....	114
Figure 4-2: The Arrangement of PSR and PaSR in Representing the Combustor (Celis, 2010).....	120
Figure 4-3: The Comparison of Engine Emissions Predicted in this Work with Literature .....	123
Figure 4-4: Percentage Difference of NO <sub>x</sub> and Adiabatic Flame Temperature as a Function of CSPK Level .....	124
Figure 4-5: Percentage Difference of NO <sub>x</sub> Pollution and Adiabatic Flame Temperature as a Function of JSPK level .....	125
Figure 4-6: Percentage Difference of NO <sub>x</sub> as a Function of Biofuel Percentage .....	126
Figure 4-7: The Reduction of CO during Cruise Condition as a Function of Biofuel Composition .....	127
Figure 4-8: Percentage Difference of NO <sub>x</sub> and Adiabatic Flame Temperature as a Function of CSPK Percentage Quantified at Constant Mass Flow Condition.....	128
Figure 4-9: Percentage Difference of NO <sub>x</sub> and Adiabatic Flame Temperature as a Function of JSPK Level at Constant Mass Flow Condition.....	129
Figure 4-10: Percentage Difference of NO <sub>x</sub> Generated as a Function of Biofuel Mixture during Constant Mass Flow Condition .....	130
Figure 4-11: Percentage difference of CO between JSPK and CSPK relative to Jet-A during the constant mass flow condition .....	131
Figure 4-12: The Effect of LHV on Flame Temperature as a Function of Biofuel Composition .....	133
Figure 4-13: The Effect of FAR on Flame Temperature as a Function of Biofuel Composition .....	134
Figure 4-14: The Effect of C <sub>p</sub> on Flame Temperature as a Function of Biofuel Composition .....	135
Figure 4-15: The Effect of Boiling Temperature on NO <sub>x</sub> .....	136
Figure 4-16: The Influence of Density on NO <sub>x</sub> Formation.....	137
Figure 4-17: The Effect of Flame Temperature on CO Formation .....	138
Figure 4-18: The Effect of AFR on Flame Temperature .....	138
Figure 5-1: The Test Case Configuration Set up in GATAC Framework .....	147

Figure 5-2: 3D and 2D Plots of NSGAMO Optimisation Result (Blue (x) – Pareto front, Magenta (circle) – datum point, Green (square) – Min NO <sub>x</sub> design (Design A), Red (square) – Min CO design (Design B), Cyan (square) – Max Thrust design (Design C)) for test case 1 .....	150
Figure 5-3: 3D and 2D Plots of NSGAMO Optimisation Result (Blue (x) – Pareto front, Magenta (circle) – datum point, Green (square) – Min NO <sub>x</sub> design, Cyan (square) – Max Thrust design, Red (square) – Min CO design) for test case 2 – Arrow Shows the Target Direction .....	154
Figure 5-4: The Comparison of Pareto Front for Test Case 1 - (Red circle - MOTS2 Pareto Front, Black circle – NSGAMO Pareto Front, Black square – Datum point, Cyan square – Max thrust design (MOTS2), Cyan diamond – Max thrust design (NSGAMO), Green square – Min NO <sub>x</sub> design (MOTS2), Green diamond – Min NO <sub>x</sub> design (NSGAMO), Blue square – Min CO design (MOTS2), Blue square – Min CO design (NSGAMO))....	157
Figure 5-5: The Comparison of Pareto Front for Test Case 2 (Red circle - MOTS2 Pareto Front, Black circle – NSGAMO Pareto Front, Black square – Datum point, Cyan square – Max thrust design (MOTS2), Cyan diamond – Max thrust design (NSGAMO), Green square – Min NO <sub>x</sub> design (MOTS2), Green diamond – Min NO <sub>x</sub> design (NSGAMO), Blue square – Min CO design (MOTS2), Blue square – Min CO design (NSGAMO))....	158
Figure 6-1: Configuration of Combustor Considered in HEPHAESTUS .....	167
Figure 6-2: (a) The combustor configuration showing the location of the fuel injector, holes for the core cooling and annular ring for the wall cooling along the chamber (b) The combustor with the total cells of 154 235 non-structural mesh.....	169
Figure 6-3: The Temperature Profile of HEPHAESTUS (H) in Comparison to CFD (1 = FF, 2 = PZ, 3 = IZ, 4 = DZ) .....	171
Figure 6-4: Velocity Vector of the Static Temperature .....	173
Figure 6-5: The Temperature Contour Shows the Maximum Temperature which Recorded at the IZ .....	176
Figure 6-6: The Contour of NO <sub>x</sub> Mass Fraction Shows the Highest NO <sub>x</sub> Mass Fraction Downstream of the Chamber .....	176

## LIST OF TABLES

Table 1-1: Summary of Conducted Flight Tests (Kinder and Rahmes, 2009) ..	25
Table 1-2: List of Design Parameters, Constraints and Design Objectives for Both Cases.....	49
Table 2-1: Different Types of Biofuels Selected for the Evaluation.....	56
Table 2-2: Rix Biodiesel Fatty Acid Methyl Ester (Rochaya, 2007) .....	64
Table 2-3: Antoine Constant of FAME (Yuan <i>et al.</i> , 2005) .....	65
Table 2-4: Constants for Ethanol's Vapour Pressure .....	67
Table 2-5: Droplet Lifetime Comparison.....	77
Table 2-6: The Relation between Boiling Temperature and Viscosity with Droplet Lifetime .....	81
Table 2-7: The Influence of Density on Spray Penetration .....	82
Table 2-8: The Comparison of Droplet Lifetime for the Blend Fuel.....	86
Table 2-9: The Comparison of Penetration Length Measured at 0.12 ms .....	87
Table 3-1: Estimation of Molecular Formula and Enthalpy of Formation for JSPK and CSPK .....	96
Table 3-2: Parameters for the Chosen Engine .....	99
Table 3-3: Average Error of Data Generated Relative to Data from Literature	100
Table 4-1: Difference in Emission Level during Different Operating Condition (Penner <i>et al.</i> , 2013) .....	115
Table 4-2: The Impact of Aircraft Pollution onto Human Health and Environment .....	116
Table 5-1: List of Design Parameters (Test case 1) .....	146
Table 5-2: List of Design Parameters (Test case 2) .....	146
Table 5-3: List of Design Objectives and Design Constraints.....	146
Table 5-4: The Optimiser Set up .....	147
Table 5-5: Comparison between the Optimiser Solutions with Baseline Point	151
Table 5-6: Improvement of Objective Functions for Each Solution Relative to Baseline Point .....	151
Table 5-7: The Comparison of Optimal Design and the Improvement Relative to Datum Point .....	153
Table 5-8: Comparison between the Optimiser Solutions with Baseline Point	155
Table 5-9: Improvement of Objective Functions for Each Solution Relative to Baseline Point .....	156
Table 5-10: The Optimal Solution and the Improvement Relation to Datum Point .....	156
Table 5-11: The Comparison of Extreme Designs Solution given between NSGAMO and MOTS2 – Test case 1 .....	159
Table 5-12: The Comparison of Extreme Designs Solution given between NSGAMO and MOTS2 – Test case 2 .....	160
Table 5-13: The Comparison of Optimal Design between NSGAMO and MOTS2 - Test Case 1.....	161
Table 5-14: The Comparison of Optimal Design between NSGAMO and MOTS2 - Test case 2 .....	162
Table 6-1: Combustor Geometry .....	167
Table 6-2: Fraction of Air at the Core and Wall of the Combustor Section .....	168

Table 6-3: Amount of Air Entering Each Section of the Combustor .....	168
Table 6-4: Combustion Chamber Boundary Condition .....	170
Table 6-5: The Comparison of Temperature and NO <sub>x</sub> between HEPHAESTUS and CFD.....	174
Table 6-6: The Comparison of Reaction Parameters Considered in HEPHAESTUS and CFD for Each Elementary Reaction .....	178
Table 6-7: The Reaction Considered in Modified HEPHAESTUS .....	179
Table 6-8: The Comparison of NO <sub>x</sub> between the Initial HEPHAESTUS, Modified HEPHAESTUS and CFD.....	179
Table 6-9: The Boundary Condition for the Generic Combustor.....	180
Table 6-10: Average Control Volume of the Generic Combustor .....	181
Table 6-11: The Temperature Predicted by HEPHAESTUS for Each Zone of the Generic Combustor .....	181
Table 6-12: The Comparison of Outlet Temperature, Flame Temperature and NO <sub>x</sub> Generation between HEPHAESTUS and CFD Simulation .....	181
Table 10-1: HEPHAESTUS Input File for Jet-A at Cruise Condition .....	221
Table 10-2: Engine Parameters of CSPK and the Blend as an Input file for HEPHAESTUS.....	223
Table 10-3: Engine Parameters of JSPK and the Blends as an Input File for HEPHAESTUS.....	223
Table 10-4: Hephaestus Input File for Constant Mass Flow Evaluation .....	224

## NOTATIONS

Symbol	Definition	Unit
		$\text{m}^3/\text{kgmols}^{**}$
$\dot{V}$	Volumetric Flow rate	$\text{m}^3/\text{s}$
$\dot{m}$	Mass Flow Rate	$\text{kg}/\text{s}$
$\dot{m}_0$	Total Mass Flow Rate	$\text{kg}/\text{s}$
$\tau_\lambda$	Ratio of the Burner Exit Enthalpy to the Ambient Enthalpy	
$\tau_c$	Compressor Temperature Ratio	
$\tau_t$	Turbine Temperature Ratio	
$\tau_r$	Ratio of Total to Static Temperature of the Free Stream	
A	Pre-exponential Factor	$\text{m}^3/\text{gmols}^{**}$
A	Area	$\text{m}^2^{**}$
A, B and C	Antoine Constant	-
$A_p$	Particle area	$\text{m}^2$
$C_D$	Drag coefficient	-
$C_i$ ,	Vapour concentration of vapour gas	$\text{kgmolm}^{-3}$
$C_{i,s}$	Vapour concentration at droplet surface	$\text{kgmolm}^{-3}$
$C_p$	Heat capacity of particle	$\text{Jkg}^{-1}\text{K}^{-1}$
$D_0$	Nozzle Diameter	mm
$D_{i,m}$	Diffusion coefficient of vapour pressure in the bulk	$\text{m}^2\text{s}^{-1}$
$E_a$	Arrhenius equation	$\text{J}/\text{kgmol}$
$E_{\text{INO}_x}$	$\text{NO}_x$ Emission Index	$\text{g}/\text{kg fuel}$
ER	Equivalence Ratio	-
F	Engine Thrust	N
FAR	Fuel to Air Ratio	-
GP	Caloric Property	- <sup>**</sup>
H/C	Hydrogen to Carbon ratio	-

$M_0$	Mach Number	
$MW_p$	Particle molecular weight	kg
$N_i$	Molar flux of droplet's vapour	-
$P_v$	Vapour Pressure	Pa
$P_{vi}$	Vapour Pressure of Fatty Acid	Pa
$P_{vmix}$	Vapour Pressure of Fatty Acid Mixture	Pa
$R$	Universal gas constant	$Jkg^{-1}K^{-1}$ **
$R$	Universal Gas Constant	$J/kgmolK$ **
$Re_p$	Particle Reynolds number	-
$Sc$	Schmidt number	-
SFC	Specific Fuel Consumption	mg/N sec
SMD	Sauter Mean Diameter	mm
$T$	Gas temperature	K
$T_3$	Temperature at the Compressor Inlet	K
$T_4$	Temperature at Compressor Outlet	K
$T_5$	Temperature at the Nozzle Outlet	K
TET	Turbine Entry Temperature	K
$T_p$	Particle temperature	K
TSFC	Thrust Specific Fuel Consumption	lbm/h lbf
$V$	Air Velocity	$ms^{-1}$
$V_0$	Velocity of the Intake	$ms^{-1}$
$V_{19}$	Velocity of the Fan Nozzle	$ms^{-1}$
$V_9$	Velocity of the Core Nozzle	$ms^{-1}$
$V_{in}$	Initial Velocity	$ms^{-1}$
$V_p$	Particle velocity	$ms^{-1}$
$W$	Air Mass flow rate	kg/sec **
$W$	Work Produced from Gas Turbine	Joule **
$X_i$	Local bulk fraction of species i	-
$x_i$	Mole Fraction of Fatty Acid	-
$a_0$	Speed of Sound	m/s
$d_0$	Initial Droplet	$\mu m$
$d_p$	Particle Diameter	$\mu m$

$g_c$	Newton's constant = 1	
$h$	Convective heat transfer coefficient	$Wm^{-2}K^{-1}$
$h_{fg}$	Latent heat of vaporisation	$Jkg^{-1}$
$k_c$	Mass transfer coefficient	$ms^{-1}$
$p$	Gas pressure	Pa
$p_{sat}$	Particle saturated vapour pressure	Pa
$s$	Penetration Distance	mm
$x_i$	Mole Fraction of Fatty Acid	-
$\alpha$	Bypass Ratio	
$\alpha_d$	Volume Fractions of Droplet	-
$\beta$	Temperature Exponential	-
$\Delta H$	Enthalpy differentiation	-
$\Delta S$	Entropy differentiation	-
$\theta$	Half Angle of the Spray Cone	degree
$\mu$	Molecular Viscosity	$kgm^{-1}s^{-1}$
$\rho$	Air density	$kgm^{-3}$
$\rho_i$	Density of component i	$kg/m^3$
$\rho_p$	Particle Density	$kgm^{-3}$
$\phi_i$	Percentage of component i	-

\*\* Depending on context

## Subscripts

<b>Symbol</b>	<b>Definition</b>
F	Fan
SMD	Sauter Mean Diameter
TET	Turbine Entry Temperature
a	Air
amb	Ambient
c	Compressor
f	Fuel
p	Particle
ref	From Literature
table	From the Present Work

## ABBREVIATIONS AND FORMULAE

AFna	Africa Natural gas
ANZ	Air New Zealand
B100	Pure
B50	Blend of 50% Biofuel with 50% Kerosine
Bio-SPK	Bio-Synthetic Paraffinic kerosine
BPR	Bypass Ratio
CAL	Continental Airlines
CFD	Computational Fluid Dynamic
CME	Canola Methyl Ester
CO	Carbon Monoxide
CO <sub>2</sub>	Carbon Dioxide
CSPK	Camelina Bio-synthetic Paraffinic Kerosine
DZ	Dilution Zone
FAME	Fatty Acid Methyl Esters
FAR	Fuel to Air Ratio
FF	Flame Front
FPR	Fan Pressure Ratio
GATAC	Greener Aircraft Trajectories under Atmospheric Constraints (GATAC)
GIACC	International Aviation and Climate Change
H	Hydrogen Atom
H <sub>2</sub>	Hydrogen
H <sub>2</sub> O	Water Vapour
H <sub>2</sub> SO <sub>4</sub>	Sulphuric Acid
HF	Hog-fat
HPCPR	High Pressure Compressor Pressure Ratio
HPT	High Pressure Turbine
HVO	Hydro-treated Vegetable Oil
IARC	International Agency for Research on Cancer
ICAO	International Civil Aviation Organization

IPCPR	Intermediate Pressure Compressor Pressure Ratio
IZ	Intermediate Zone
JAL	Japan Airlines
JSPK	Jatropha Bio-synthetic Paraffinic Kerosine
kg	kilogram
LBO	Lean Blow-Out
LHV	Low Heating Value
M	Mach Number
MJ	Mega Joule
MOTS2	Multi-Objective Tabu Search
N	Nitrogen Atom
N <sub>2</sub>	Nitrogen Molecule
N <sub>2</sub> O	Nitrous oxide
NASA CEA	NASA Chemical Equilibrium Application
NO	Nitric Oxide
NO <sub>x</sub>	Nitrogen Oxide
NSGA	Non-sorted Genetic Algorithm
NSGAMO	Non-Sorted Genetic Algorithm Multi-Objective
O	Oxygen Atom
O <sub>2</sub>	Oxygen Molecule
OPR	Overall Pressure Ratio
PaSR	Partially-Stirred Reactor
PSR	Perfectly Stirred Reactor
PSRS	Perfectly Stirred Reactor Series
PZ	Primary Zone
RANS	Reynolds Average Navier-Stokes
RME	Rapeseed Methyl Ester
RRME	Recycled Rapeseed Methyl Ester
SME	Soy Methyl Ester
SO <sub>3</sub>	Sulphur Trioxide
SO <sub>x</sub>	Sulphur Oxide
UHC	Unburned Hydrocarbon

UKna	UK Natural gas
UNFCC	United Nations Framework Convention on Climate Change
URANS	Unsteady RANS
VEGA	Vector Evaluated Genetic Algorithm
mm	Milimeter
ms	Milisecond
$\mu\text{m}$	Micrometer

# **1 INTRODUCTION TO THE RESEARCH TOPIC**

## **1.1 General Introduction**

### **1.1.1 Introduction**

This chapter provides a brief introduction to the topic of this research, which includes the motivation of the study, aim and objectives, the contribution of this research to the knowledge, methodology, and computer tools used in this work. The organisation of this thesis is also presented.

### **1.1.2 Research Motivation and Problem of Statement**

In this modernised world, where most people use airplanes to travel from one place to another, there has been the encouragement of airline industries to grow extensively. Nevertheless, such extensive growth in terms of airline industries comprises problems, both in terms of oil demand, which, in turn, increases fuel price. This has become more challenging when such growth also contributes to the increase in pollutant generation emitted into the atmosphere.

Notably, total emissions produced by an aircraft are associated with the fuel it consumes. Presently, aviation consumes approximately 2–3% of all total fossil fuel used worldwide, with more than 80% of the fuel used by civil aviation operations (Lee *et al.*, 2004; ICAO report, 2002).

Aware of the problem of fuel price and the environmental issues associated with crude oil, aviation industries are now looking forward to using biofuels in aircraft engines. More recently, a technology referred to as ‘drop-in’—or, in other words, blend fuel—has become an interesting topic as it promises future ‘greener’ aircraft and reduced dependency on crude oil. It is indeed an approach that has been introduced with the aim of avoiding any additional modifications or adaptation in aircraft engines—particularly in modern low NO<sub>x</sub> combustors. In other words, this approach can be used in aircrafts that are currently in service. Previous studies on blend fuels have made improvements in both engine performance and pollutant generation, particularly in regard to NO<sub>x</sub>.

Studies on biofuel blends have actually been carried out as early as 1998 by Baylor Institute for Air Science, which conducted an experimental work investigating emissions and engine performance for up to 30% biofuel blends with Jet-A. The biofuels used were derived from waste cooking oil, plants, and animal matter. Other experimental works later followed. Notably, all studies revealed improvements in engine performance and emissions—especially in NO<sub>x</sub>.

As the attention towards biofuel has grown, studies on the influence of biofuels on engine performance and emissions were not only conducted experimentally within the laboratory setting, but recently were also extended into the series of flight tests. For instance, the first commercial flight on the biofuel blend took place by Virgin Atlantic Airways 747-400 on February 24, 2008, running with 20% biofuel derived from Brazilian Babassu nuts and coconuts, blended with 80% kerosine in one of its four engines.

Following the successful flight, another test programme was implemented with the use of a commercial aircraft by an air transport industry team consisting of Boeing, Air New Zealand (ANZ), Continental Airlines (CAL), Japan Airlines (JAL), General Electric Aviation, CFM International, Pratt & Whitney, Rolls-Royce and Honeywell's UOP. The test programme used a 50% mixture of biofuels deriving from *Jatropha*, *Camelina* and *Algae* (Rahmes *et al.*, 2009). This successful flight has proved the capability of bio-fuels as an alternative option in terms of reducing dependency on crude oil whilst simultaneously providing greener future aircraft. The implementation of bio-fuels in gas turbine engines is now not limited to the civil aircraft engine, but has also been implemented in the helicopter. For example, there is the AH-64D Apache—built by Boeing—which is the first military helicopter to have successfully flown on a 50% blend of aviation bio-fuel (made from algae and used cooking oil) and 50% conventional jet fuel, without there being any modification made to the engine (Klopper, 2010). Many more test flights that have been conducted intentionally to evaluate capability of biofuels are summarised in Table 1-1 below.

**Table 1-1: Summary of Conducted Flight Tests (Kinder and Rahmes, 2009)**

<b>Airline</b>	<b>Air New Zealand</b>	<b>Continental Airlines</b>	<b>Japan Airlines</b>
<b>Aircraft</b>	Boeing 747-400	Boeing 737-800	Boeing 747-300
<b>Engine</b>	Rolls-Royce RB211-534G	CFM International CFM56-7B	Pratt & Whitney JT9D-7R4G2
<b>Plant feedstock</b>	50% Jatropha	47.5% Jatropha, 2.5% Algae	42% Camelina 8% Jatropha/Algae
<b>Flight date</b>	Dec 30, 2008	Jan 7, 2009	Jan 30, 2009
<b>Engine tests/ground run results</b>	Comparison of fuel flow with expected heat of combustion	Engine Operability & Emissions Tests for various blend percentages	Engine Operability & Emissions on Neste Oil-provided paraffins for ground test only

In evaluating new fuels, Sharp (1951) listed the requirement that has to be followed to ensure that fuel can be used appropriately in gas turbine engine. The requirements highlighted in Sharp (1951) are listed as follows:

- i. Adequate combustion efficiency
- ii. Adequate stability performance
- iii. Smooth operation
- iv. Quick and easy ignition even under adverse condition
- v. Adequate combustion intensity
- vi. Low pressure loss
- vii. Satisfactory outlet temperature distribution
- viii. Combustion products which harm no engine components
- ix. Freedom from harmful deposits.

In this study, Sharp (1951) also has stressed some of the important fuel properties that affecting the above requirements. The effect of fuel volatility is of importance in regard to combustion efficiency, ignition, exhaust temperature distribution, and safety, while increase in carbon/hydrogen ratio was found to affect the tendency of carbon to deposit in the combustion chamber. Additionally, vapour pressure, viscosity, and density were all found to have an impact on evaporation and atomisation, whilst fuel calorific value is known to

affect the amount of fuel consumed by the gas turbine. The calorific value of the fuel was influenced by the molecular weight of the fuels. The heaviest fuel will normally have the highest calorific value hence reduce the fuel consumption. All the requirements stated in this study can be used as indicators in selecting a suitable fuel to be utilised in a gas turbine engine.

### **1.1.3 Research Gap**

As far as the interest on biofuel and the fuel requirements is concerned, there is a clear motivation for this research to be developed. In corresponds to the fuel requirements mentioned above, it is essential in this work to explore the influence of fuel properties in regard to the spray characteristics which are influenced by the evaporation and atomisation process.

It is also noted from literature that most of the studies conducted have used up to 50% biofuel in the biofuel/kerosine mixture. There has been no research work until this moment—neither through experiment nor numerical—that investigates the optimal level of fuel blend able to provide maximum engine performance and minimum level of engine emissions. This, indeed, motivates this present research work to develop a method in predicting the optimal level of biofuel that can be used in the mixture within certain objective and constraints.

Additionally, it is also worth indicating here that, since Cranfield University has developed in-house engine performance and emissions computer tools, therefore it is essential in this study to extend the capability of these tools in quantitatively evaluating biofuels.

### **1.1.4 Aim and Objectives**

This research was carried out with the main objective to reduce environmental impacts and to improve the performance of gas turbines generally and civil aviation specifically. Thus, specific objectives were highlighted in order to achieve the above contribution:

1. To investigate the chemical and physical properties of the selected biofuels to initiate the assessments.

2. To conduct an engine performance and emissions assessment using different type of computer tools available at Cranfield University. In order to do so, modification to these tools was introduced to provide the tools with biofuels properties before performing the tasks.
3. To perform an optimisation process by taking into account multidisciplinary aspects, such as performance and emissions from the engine.
4. To perform a CFD work in an attempt to authenticate the practical issues the predicted engine emission from the in-house computer tool.

### **1.1.5 Contribution to Knowledge**

The main contributions of this work to knowledge broadly comprise the following:

1. The development of a so-called greener-based methodology for assessing the potential of biofuels in reducing the dependency on conventional fuel and the amount of pollution emission generated,
2. The prediction of fuel spray characteristics as one of the major controlling factors regarding emissions,
3. The evaluation of engine performance and emission through the adaptation of a fuel's properties into the in-house computer tools,
4. The development of optimisation work to obtain a trade-off between engine performance and emissions, and
5. The development of CFD work to explore the practical issues related to the engine emission combustion modelling.

### **1.1.6 Thesis Layout**

This thesis comprises nine chapters:

The first chapter presents general introduction to the research topic, which consists of several sections. The first section (General Introduction) discusses briefly the problem statement that motivates this research to be carried out, followed by the aim and objectives of the research. The contribution of this

research to knowledge and the layout of this thesis are also presented in this section. The second section (General Literature Survey) presents previous state-of-art of the issues relating to the increases in crude oil price and pollution emission in general. This section also discusses in brief the options that might help to alleviate the problems. Amongst such options, the focus was given only to the alternative fuel, and therefore issues relating to biofuel will be presented further. Section three (Methodology) is centred on the approaches proposed and computer tools used throughout this research work.

Chapter Two deals with works carried out in regard to conducting an assessment centred on bio-fuel spray behaviour. This chapter begins with the general introduction of the assessment, which comprises the problem statement, aim, and objectives of the assessment. The chapter continues with the previous state-of-art of spray characteristics, as well as the importance of spray behaviour on the combustion performance. Detailed discussions surrounding the properties of bio-fuels, methods, and equations used in assessing the bio-fuel's spray behaviour follow subsequently. The analysis of the results obtained, and the discussions of the effect of bio-fuel on spray characteristics, such as droplet lifetime, evaporation rate, and spray penetration in comparison to Jet-A are presented at the end.

Chapter Three presents the work completed in order to evaluate the performance of the civil aircraft engine running with bio-fuels. A general introduction relating to the topic was discussed briefly. The previous literature on the works carried out in evaluating the performance of bio-fuel on the engine performance was discussed. Furthermore, the method that comprises generating caloric properties data and the software used to perform the evaluation were presented. Finally, the results from the assessment of the engine performance were analysed and discussed in-depth.

Chapter Four presents the assessment of bio-fuel engine emissions. Previous works on engine emissions evaluation—both experimentally and computationally—were discussed. Furthermore, detailed explanation about the procedures taken in this research work specifically in modifying the engine

emissions software and evaluating engine emissions is presented. This chapter continues with the analysis of results and discussions on the improvement of pollutant emissions generated by bio-fuel in comparison to Jet-A.

Chapter Five offers explanation relating to the optimisation work conducted. This consists of the literature survey on the optimisation method and the procedures carried out when carrying out the work. A detailed explanation of the selected test case will be presented. Moreover, the analysis and discussions of the results are also presented.

Chapter Six grants the CFD work that has been done in order to explore the practical issues relating to HEPHAESTUS engine emissions combustion modelling. The influences of assumptions considered in modelling HEPHAESTUS are discussed in detail in this chapter. Lastly, the analysis of the results garnered is presented at the end of the chapter.

All of the results obtained in the previous chapters will be discussed briefly in Chapter Seven.

Chapter Eight concluded the present research work while providing discussions towards the potential works that could be done in the future in order to provide the necessary understanding of bio-fuel potential in regard to the other aspects that might be of interest.

## **1.2 General Literature Survey**

### **1.2.1 Introduction**

The ability of aviation to move people and products safely and quickly cannot be denied. For this reason, aviation becomes important, and therefore rapid growth, over several decades, as well as increased demand on travel services, passenger travel, and freight transportation subsequently arise.

From an economic point of view, this growth is beneficial, although the influence of such development in regard to the potential environmental pollution is

undeniable. Like other vehicles, aircraft jet engines also produce carbon dioxide (CO<sub>2</sub>), nitrogen oxide (NO<sub>x</sub>), carbon monoxide (CO), water vapour (H<sub>2</sub>O), sulphur oxide (SO<sub>x</sub>), unburned hydrocarbon (UHC), and other trace compounds. However, aircraft emissions depend on whether or not they occur near the ground or at certain altitude. Pollutants occurring at the ground are considered local air quality pollutants, whilst pollutants occurring at the altitude are considered greenhouse pollution.

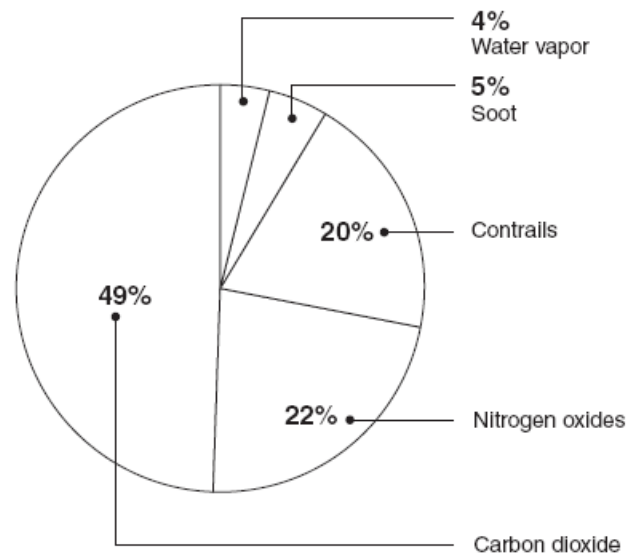


**Figure 1-1: Percentage of Pollutants Produced from Aircraft Engine (GAO report, 2009)**

Apparently, an aircraft produces the largest amount of CO<sub>2</sub> followed by NO<sub>x</sub> (22%), contrails (20%), soot (5%), and water vapour (4%). A number of different technologies and operational improvements related to the aircraft engine, aircraft design, aircraft operations, air traffic management and fuel sources are available in terms of helping to reduce the emissions and consumption of fuel, and therefore will improve aircraft energy efficiency.

### Improvement in Aircraft Engines

An improvement in aircraft engines is necessary to improve engine efficiency and to reduce engine emissions. Such an improvement may be a result of the increasing pressure and temperature of the engine, and also through improving

engine bypass ratio. As reported by Lee *et al.* (2001), approximately 40% improvement in engine efficiency was experienced during the period 1959–2000, with the improvement owing to the introduction of high bypass turbofan engines in the year 1970.

### Aircraft Improvements

The introduction of bypass engines, on the other hand, generates problems concerning engine diameter, weight, and aerodynamic drag with the increase of bypass ratios (Greene, 1992). For information, during this same period, improvements in terms of aerodynamic efficiency was approximate in terms of increasing an estimated 15% prior to better wing design and improved propulsion and airframe integration (Antoine & Kroo, 2005). Due to this problem, improvements in the aircraft itself were required. Such improvements may include the use of improved materials, namely lightweight composite, to decrease the aircraft weight, and the use of better wing design to improve the aerodynamics and reduce drag. However, during a longer period of time, a new design of aircraft might be helpful.

The replacement of traditional materials, such as aluminium with the lightweight composite material in building the aircraft—especially in the airframe construction—attributes to the reduction of the aircraft weight, and thus reduces fuel consumption. The use of composite materials in aircraft has been implemented over time. The Boeing 787, for example, has been built with 50% of the weight attributed by the composite materials compared with 12% composites in Boeing 777, whilst the A380 from Airbus also has benefitted from the composite materials, with approximately 25% of the airframe weight made from the composite.

As mentioned above, the improvement in aircraft aerodynamic is also helpful in increasing the aircraft's operating efficiency, hence reducing emissions and fuel burnt. For instance, a better wing design through the so-called winglets invention has been utilised in regard to all modern types of aircraft, and has

been found to reduce induced drag at the tips of the wings by weakening the vortex at the wingtip.

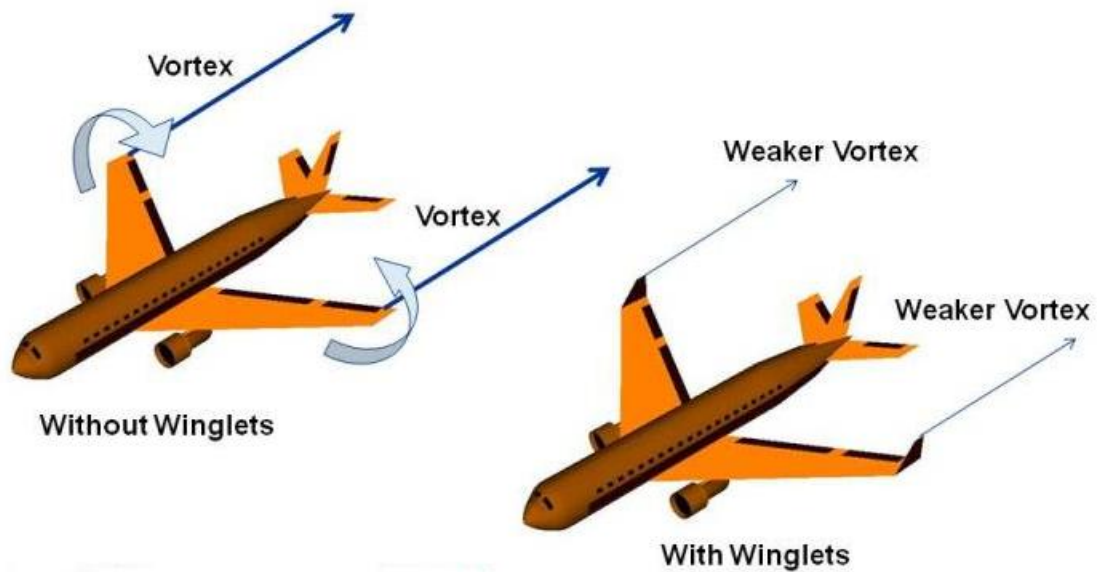


**Figure 1-2: The Winglets Invention Reducing Induced Drag at the Tips of the Wings by Weakening the Vortex at the Wingtip. (Source: <http://www.grc.nasa.gov/WWW/k-12/airplane/winglets.html>)**

### Improvement in Aircraft Operation

Other options that might be taken into account, as far as emissions are concerned, include improving the aircraft operation. Myhre & Stordal (2001) propose shifting the peak traffic periods towards sunrise and sunset, which could reduce contrail impact. Alternatively, there also appear to be another method concerning the reduction of the contrail in the atmosphere, which is through restricting cruise altitudes, as suggested by Sausen *et al.* (1998). In their study, it was found that elimination in contrail, contributed by changing cruise altitude of the aircraft, might limit the aircraft to operate at its maximum speed and efficiency, which subsequently might imply the total fuel burn and increment in CO<sub>2</sub>.

## Alternative Fuel

As opposed to improving aircraft design and changing the aircraft flight operation, utilising alternative fuels in aircraft engine is considered to be one of the options available to improving energy efficiency. The potential of alternative fuels in reducing gas emissions is also promising, even though there are certain concerns and challenges apparent. Although the contribution of alternative fuel has been assessed and was successfully observed in terms of reducing aircraft emissions when compared with fossil fuels, such as Jet-A, the sources of the alternative fuel itself were claimed to be unsuitable for use as biofuels owing to their negative impact towards the environment, and subsequently the economy. Not only that, the utilisation of alternative fuels in aviation can be considered not easy owing to their poor properties, which are not fully attuned to the combustion conditions of gas turbine jet engines.

In order to understand the influence of different fuels on the engine performance and environmental impact, the chemical compositions of the fuels become the important parameter that need to be focused on. The chemical compositions of the fuels will influence the fuel properties. For example, in comparison to kerosine ( $C_{12}H_{23}$ ), oxygenated fuel such as ethanol which has the chemical compositions of  $C_2H_5OH$  has advantage in the combustion process where the oxygen atom in the molecule can be treated as a partially oxidised hydrocarbon which helps in providing more oxygen for the combustion to burn lean, and consequently will reduce the CO (Pikunas et al, 2003). This also is consistent with study conducted by Palmer (1986) where he found that blending 10% ethanol in gasoline can reduce the CO formation by 30%. In regard to performance of the engine, thrust or power of the engine is primarily corresponds to the low heating value (LHV) of the fuel. The performance of the engine increases as the LHV of the fuel increases, whilst the LHV corresponds to the fuel composition. It is noted in Sahoo et al (2006) that fuel containing oxygen atom has low LHV, therefore depleting the engine performance.

All of the technologies mentioned above are important and worth exploration; however, this study concentrates only on the issues regarding the alternative fuel, as this option has been found to be achievable in the meantime.

### **1.2.2 Alternative Fuel's Issues**

Atmospheric pollution is caused mainly by fossil-fuel combustion: the more fossil-fuel is burned, the more pollution will be generated. Accordingly, there is the intention to reduce the dependency on the conventional fuel, as well as minimising its consumption. Indeed, this intention has led to rapid progression in alternative fuels studies, covering the need of developing alternative fuels, the selection of different types of alternative fuel, the concerns relating to their qualities, the issues surrounding sustainability, and the impact of such fuels in relation to aircrafts and engines.

Dagget *et al.* (2006) in their study highlight different types of alternative fuel that might be candidates towards the replacement of conventional fuel, namely hydrogen fuel (H<sub>2</sub>), other liquefied fuels (such as propane and butane), alcohols (such as ethanol and methanol), biofuels (combustible liquid manufactured from renewable sources such as animal fats and plants oils), and synthetic fuels (fuel produced from synthesis process, such as Fischer-Tropsch process). In addition, Demirbas (2007) also discuss the different types of alternative fuel, i.e. Fischer-Tropsch synthesis fuel, bio-ethanol, fatty acid (m) ethyl ester, bio-methanol and bio-hydrogen.

The sustainability of biofuels is important if there is a plan to use biofuels as a replacement to the traditional or conventional jet fuel. According to National Renewable Energy Lab (2004), the biofuel is considered sustainable if the quantity of crops used to produce the biofuel is sufficient enough to be grown in order to support fuel demand. Furthermore, O'Keeffe (2010) emphasises that the production of feedstock must not interfere with food or freshwater supply before it can be considered sustainable. This concern has referred to the second- and third-generation of biofuels, which has the high potential to replace the traditional fuel. *Jatropha*, *camelina*, algae, waste forest residues, organic

waste streams and the non-edible component of corn (corn stover) are examples of second- and third-generation feedstock. In addition, the biofuels were not considered sustainable if they contribute to the higher food prices due to the competition with food crops (Sims *et al.*, 2008). This concern has been considered in regard to the first-generation of biofuels, which are mainly produced from food crops such as soy and corn. Additionally, Dagget *et al.* (2007) emphasise that the biofuels must not cause any anthropogenic issues through deforestation, which could be harmed during the creation of sufficient farm land capacities.

Moreover, problems relating to biofuels—not only in terms of the sustainability of the fuel but also in relation to the properties of the biofuels itself: for instance, alcohol-based fuel, such as ethanol and methanol, are not able to be used in a commercial aircraft simply because of their poor mass and volumetric heat of combustions. With this noted, Dagget *et al.* (2006) report that powering an airplane by ethanol—which has low energy content (Figure 2.1) —requires 64% more storage volume for the same amount of energy contained in kerosine. Thus, 25% larger wings are required to carry the fuel. Consequently, such a scenario would increase the airplane’s empty weight by 20%. Moreover, since the ethanol itself has more weight, this would also increase the take-off weight of the airplane by 35%.

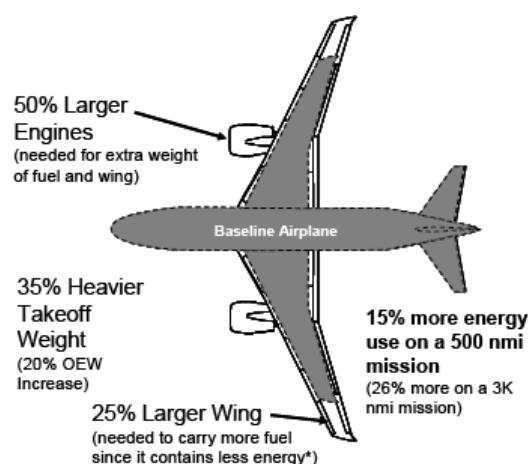


**Figure 1-3: The Challenges of Implementing Aircraft with Ethanol (Dagget *et al.* (2006))**

Another challenge of using biofuels in aircrafts which needs to be addressed is concerned with thermal stability issues and the tendency of the fuels to freeze at normal cruise temperature (i.e.,  $-20^{\circ}\text{C}$ ) (Figure 1-5).



**Figure 1-4: The Tendency of Biodiesel to Freeze at Cold Temperature (Melanie, 2006)**

Dagget *et al.* (2006) suggest an additional processing step to be included during the esterification process (which is the process of converting fatty acids from plants into biofuels) in order to overcome the freezing problem (Figure 1-6).

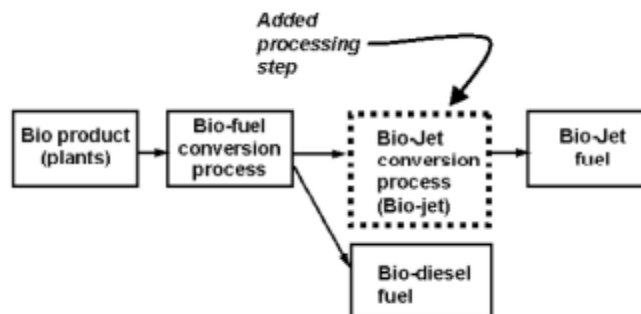


**Figure 1-5: Additional Process Introduced to Overcome Freezing-fuel Issue (Dagget *et al.* (2006))**

Dagget *et al.* (2007) also state that, in order to improve thermal stability and pass the jet fuel thermal stability requirements, biofuels have to be blended at a minimum of 20% of biofuel with 80% kerosine.

New technology in relation to fuel processing was also introduced in order to convert bio-derived oil rich with triglycerides and free fatty acids into biojet fuel, which has the composition of molecules already present in jet fuel. The process comprises the removal of oxygen atoms, the conversion of olefins to paraffin, and lastly the isomerisation and cracking of diesel range paraffin to branched-range paraffin. All processes have formed a biojet fuel, which has the higher heat of combustion, tremendously high thermal stability, and improvement at freezing point. This type of fuel is referred to as Bio-Synthetic Paraffinic kerosine (Bio-SPK).

### 1.2.3 'Drop-in' Jet Fuel

The definition of 'drop-in' was adopted by ICAO Group on International Aviation and Climate Change (GIACC) and the United Nations Framework Convention on Climate Change (UNFCCC), which was proposed by the Conference on Aviation and Alternative Fuels (2009), which stated:

*'Drop-in jet fuel is defined as a substitute for conventional jet fuel, that is completely interchangeable and compatible with conventional jet fuel when blended with conventional jet fuel. A drop-in fuel blend does not require adaptation of the aircraft/engine fuel system or the fuel distribution network and can be used 'as is' on currently flying turbine-powered aircraft'.*

A study carried out by Dagget *et al.* (2007), and Clercq & Aigner (2009) underlines a 'drop-in' or 'fit-for-purpose' technique (Clercq & Aigner, 2009) to be used in existing and short-term aircrafts. This approach was introduced with the aim of avoiding any additional modifications or adaptations in terms of the aircraft engine—particularly in modern low NO<sub>x</sub> combustors. In other words, this technique can be used in aircrafts currently in service.

The concept of 'drop-in' jet fuel—or, in other words, blends fuel—became an interesting topic amongst researchers, as it promises future 'greener' aircrafts and reductions of the dependency on crude oil. Rahmes *et al.* (2009) have investigated the properties of the blend of Bio-SPK fuel with conventional jet

fuel. Notably, the blend of Bio-SPK with conventional fuel is necessary to ensure that important fuel properties, such as density, meet the current specifications of aviation turbine fuel.

Furthermore, as discussed previously, Bio-SPK fuel has a high potential to be used in aircrafts since it improves various key issues that have been addressed (i.e. energy content, thermal stability and propensity to freeze). However, the evaluation in terms of fuel property—which has been conducted by Boeing, UOP and other organisations—indicates that the density of Bio-SPK fuel is lower than compared with conventional jet fuel; therefore, Bio-SPK has to be blended with conventional jet fuel in order to ensure that the density of the fuel meets the specification requirements of the turbine fuels.

#### **1.2.4 Flight Tests Using ‘Drop-in’ Jet Fuel**

In 2008–2009, there were three tests carried out in order to test the capability of drop-in fuel in existing aircraft engine.

In 2008, Air New Zealand successfully flew a Boeing 747-400 aircraft with only one of its four Rolls-Royce RB211-524 engines running with 50% blend of Jatropha with Jet-A-1 (Rahmes et al., 2009). However, no significant changes in performance have been revealed thus far (Warwick, 2009).

In 2009, another successful test flight was carried out by Japan Airline, which flew a Boeing 737-300 using a mixture of 42% Camelina, 8% of Jatropha and Algae with jet kerosine in one of the Pratt & Whitney JT9D-7R4G2 engines (Rahmes et al., 2009). No difference in performance was detected. Furthermore, Continental Airline flew a Boeing 737-800 aircraft in which only one engine (CFM56-7B) was allocated to run with the mixture of 47.5% Jatropha and 2.5% Algae with conventional jet fuel (Rahmes et al., 2009).

In the future, other flight tests have been planned. For instance, in 2012, Azul Brazilian Airline plans to conduct a flight demonstration with an Embraer twinjet. Only one of the GE CF34-10E engines will be running with a 20% blend of sugar-derived biofuel with conventional jet fuel. They might also consider

combinations of biofuel up to 50% (Kuhn, 2009). Moreover, another flight demonstration is planned by Interjet Mexico Airline, which is planning to fly an Airbus A320 aircraft running with salicornia type of algae; however, this flight has been rescheduled as Arizona Seawater has been unable to supply sufficient quantities of fuel (Sobie, 2010).

### **1.2.5 Performance and Emissions of 'Drop-in' Jet Fuel**

Interest in regard to the performance and emissions of the drop-in jet fuel blend-based engine motivates researchers to study different types of fuel and their blends with conventional jet fuel at different blending ratios. For instance, in the year 1998, an experimental study on the performance and emission of biofuels blend was carried out by the Baylor Institute for Air Science. This study took biofuels from waste cooking oil, and plant and animal matter, which were then blended with Jet-A up to 30% by volume in a modified gas turbine. Only nitric oxide (NO) was measured in this study. Nitric oxide (NO) concentration in the exhaust gases was found to be reduced with biofuel content, whilst Jet-A showed the highest; however, no significant changes were found in the engine performance or fuel consumption for Jet-A, and the blending of Jet-A with up to 20% biofuel.

Later, Krishna (2007) conducted an experimental study in order to measure CO and NO emissions of 30kW microturbine running with soy-based biofuel blended with No. 2 heating fuel oil. Adding biofuel resulting less both in NO and CO emissions.

On the other hand, Ellis et al. (2008) conducted an experimental work using semi-closed gas turbine operated with soy and palm oil biofuels, and a 20% blend of these fuels (by volume) with ultra-low sulphur No. 2 fuel oil. An increase in NO concentration but a decrease in CO concentrations was found.

Another experimental study was recently conducted by Habib et al. (2009) in an attempt to understand the effects of adding biofuels in Jet-A in terms of engine performance and emissions. Biofuels—namely soy methyl ester (SME), canola

methyl ester (CME), recycled rapeseed methyl ester (RRME) and hog-fat (HF) fuel—have been tested as pure (100% or B100) and blends (50% by volume, B50) with Jet-A in small scale (30kW) gas turbine. They noticed almost a linear increment of static thrust with engine speed for all fuels, and the measurements of all fuels fell within experimental uncertainties except for RRME, which did not follow the trend; however, no reason has been given to explain such. Moreover, adding biofuels in Jet-A provided no significant differences in TSFC as well as in thermal efficiency. Furthermore, pure biofuels showed slightly lower in TSFC and higher thermal efficiencies than Jet-A. Higher thermal efficiencies of B100 biofuels are believed to be owing to the presence of oxygen molecules in the biofuel. Furthermore, measurements of turbine inlet temperature for pure biofuels were found to be slightly lower than Jet-A at low speeds, but were nevertheless close to Jet-A at high speeds. Nevertheless, exhaust gas temperatures for all fuels were found to be almost similar to each other. Investigations into biofuel emissions resulted in decreases on CO and NO pollutant emission concentrations with biofuel. Interestingly, there was a greater reduction in CO and NO found with B50 blends.

During the same year, Rahmes *et al.* (2009) conducted off-wing engine ground tests in order to evaluate the impacts of Jatropha and Algae-derived Bio-SPK on engine performance and emissions. The test was carried out on a CFM56-7B engine, which was first run with Jet-A, followed by a 25% and then 50% blend of Bio-SPK fuel. Increases in heat of combustion and decreases in density and viscosity were noted as the blending percentage of the Bio-SPK increased. It was also noted that increases in the blending percentage of Bio-SPK improved the specific fuel consumption and fuel flow. Both 25% and 50% Bio-SPK blends showed reductions in fuel flow by 0.7% and 1.2% respectively, and were found to be consistent with differences in the heat of combustion (0.6% for 25% blend, and 1.1% for 50% blend respectively). They also summarise that the effects of additional Bio-SPK to the conventional jet fuel towards emissions is not markedly significant. Testing on engine emissions revealed a slight reduction in NO<sub>x</sub> (~1-5%) and smoke (~13-30%), whilst some increments in CO (~5-9%) and HC (~20-45%) were observed.

In addition, Rahmes *et al.* (2009) also report another test on engine emission that had been conducted with the use of a Pratt & Whitney Canada engine. In this test, 50% and 100% of diesel range hydro-treated vegetable oil (HVO) blends were used. Tests on engine emissions between Jet-A and a blend of HVO in Jet-A established no significant change in HC, CO, and NO<sub>x</sub>. Meanwhile, large reductions in smoke were noted following the increase of the percentage of biofuel in jet fuel.

In order to summarise the results from the engine emission test, a reduction in smoke number is known to correspond with the increment in the blending percentage of biofuel in jet fuel. Furthermore, absences of aromatics and a high H/C ratio of biofuel, compared with jet fuel, could be the reason for reductions in smoke number (Rahmes *et al.*, 2009).

## **1.3 Methodology**

### **1.3.1 Introduction**

This chapter discusses the methods of how the research will be conducted. Briefly, an introduction will be presented in regard to the fuels of interest, computer tools, and analysis that will be carried out in this research work.

### 1.3.2 Flowchart

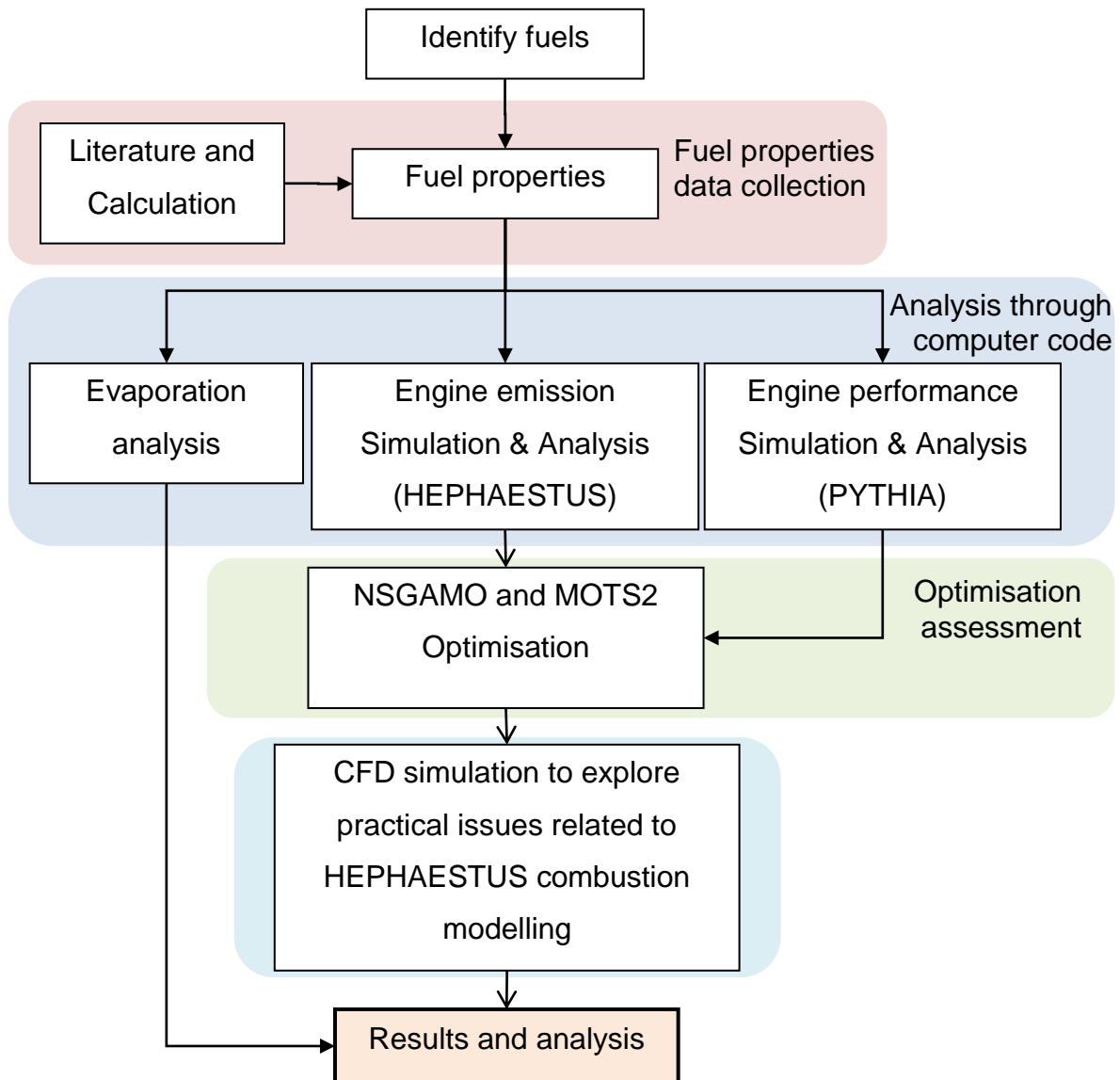


**Figure 1-6: The Flowchart Representing the Proposed Tasks Conducted in Present Research Work**

Figure 1-6 presents the flowchart of the way in which this research study will be conducted, which comprises several phases.

The first phase deals with the selection of biofuels that will be used in this work. This study focuses on the Bio-SPK type of fuel, which comes from Jatropha & Camelina as a feedstock. For the purposes of comparison, other biofuels, such as ethanol, rapeseed oil, Rix biodiesel—also referred to as rapeseed methyl

ester (RME)—were chosen. However, such fuels were used only to compare the characteristic of spray behaviour in the next stage. Only the bio-SPK type of fuels was used to carry out other following assessments. Important fuel properties which are necessary in this study will be collected from open literature. In the case of biofuels, such properties are not always easy to obtain; for this reason, calculation based on fatty acid composition in biofuels needs to be performed.

During the second phase, the impacts of adding fractions of biofuels in kerosine to the behaviour of spray characteristics, engine performance, and engine emissions have been investigated. The analysis on spray behaviour characteristic involves the evaporation rate, droplet lifetime, and spray penetration, which can be predicted from the evaporation process. Computational tools—namely PYTHIA—will be utilised to evaluate the engine performance, whilst HEPHAESTUS will be used to assess pollution in the context of the fuels selected. Both of these tools are available in Cranfield University, although appropriate modifications are required in order to develop the ability of these tools for the evaluation of biofuels.

In the third phase, the emission evaluation from HEPHAESTUS was validated through the simulation of the combustor considered in HEPHAESTUS in Computational Fluid Dynamic (CFD) computer tool. This validation assessment was implemented with the aim of exploring any practical issues related to the fluid behaviour within the combustor, which is not considered in HEPHAESTUS. This assessment is also deemed important for the optimisation work to be completed later.

An optimisation assessment was conducted at the next phase of the research. This analysis was carried out to evaluate the optimum percentage of biofuel in the biofuel/kerosine mixture, which minimises engine emissions and maximises engine performance at the same time. For this purpose, a multi-objective optimisation technique was used and was deployed throughout the process.

Last but not least, the results were analysed and discussed at the end of the stages.

### **1.3.3 Evaporation Analysis**

The evaluation of the fuel evaporation was predicted through a spreadsheet analysis developed previously by Mazlan (2008), which presents ethanol as a baseline demonstration fuel. This model focuses on the evaporation of a single droplet formed in a spray from a pressure swirl atomiser. This spreadsheet analysis was built based on the process of heat transfer, including droplet motion, energy equation, and boiling mass transfer. Equations regarding those processes were adopted from the FLUENT 6.3 User Guide.

In order to evaluate fuels in this model, fuel properties—such as density, vapour pressure, specific heat capacity, diffusivity and latent heat of vaporisation—are required. With the exception of density, the model developed by Mazlan (2008) did not take into account the variation of vapour pressure, specific heat capacity, diffusivity, and latent heat of vaporisation with temperature. With this noted, the present study extended and improved the model through the inclusion of the variation of fuel vapour pressure and diffusivity with temperature; this facilitated the gathering of more reliable evaluations.

### **1.3.4 PYTHIA Software**

PYTHIA is owned by Cranfield, which was developed over 30 years ago. This software is able to execute the performance calculation for both design-point and off-design for any type of open-cycle engine. Furthermore, this software is considered very user-friendly, with users only required to prepare the input file, describing the engine configuration and parameters for each component (Pachidis, 2006)

Major principles, limitations and the importance of this software to this study are listed and explained below:

## Major principles

- i. PYTHIA calculates engine performance by using the thermodynamic equations in which the fuel caloric properties which are density, heat capacity, entropy, enthalpy and gamma are used.
- ii. In simulating the gas turbine engine, PYTHIA requires the user to provide the components of the engine and the parameters of those components such as efficiencies and pressure ratio.
- iii. The outcomes of PYTHIA comprise the prediction of temperature and pressure at each component, engine thrust, fuel consumption, specific fuel consumption etc.

## Limitations

- i. PYTHIA was developed to calculate the engine performance of the gas turbine with the fuel option available at that time is only kerosine.
- ii. Therefore in order to evaluate the engine performance of the other fuels, set of calorific fuel properties of the new fuels have to be included into the software. These properties have to be generated and cover over wide range of temperature, pressure, fuel air ratio and water air ratio. The calorific properties required are heat capacity, entropy, enthalpy, and gamma. These properties can be generated using NASA CEA. However, in case of the fuel which is not included in NASA CEA's library, the molecular formula and enthalpy of formation of the fuel is necessary and need to be included in NASA CEA.

As previous mentioned PYTHIA has the capacity to generate engine performance characteristics, such as specific thrust, fuel consumption, and specific fuel consumption. Therefore, as this study aims to compare the performance of the engine that operated with different type of fuels, the usage of this software in performing the engine performance calculation is mandatory. Nevertheless, the intention of using this package in performing the calculation

also is important to provide the capability of PYTHIA in evaluating different type of fuels.

### **1.3.5 HEPHAESTUS Software**

HEPHAESTUS is a software developed by a previous PhD student at Cranfield University (Celis, 2010). This model was developed with the objective to predict pollutants emitted from gas turbine combustor, in which the stirred reactor method was applied. In regard to the inhomogeneities of the gas composition, this model utilised a stochastic method to represent turbulent mixing in the primary zone of the combustor. Outcomes obtained from HEPHAESTUS are in the form of NO<sub>x</sub>, CO, UHC, CO<sub>2</sub> and soot/smoke. HEPHAESTUS requires engine performance and combustor geometry as the input. Through the course of this research, input for engine performance was obtained from PYTHIA, whilst combustor geometry was taken as the same as in that of Celis (2010). Since HEPHAESTUS is not ready for simulating fuels other than Jet-A, several modifications were applied to the source code.

The prediction of NO<sub>x</sub> and CO is observed to follow the trend provided by ICAO but the prediction of UHC and soot are poor and therefore is not recommended to be used. Basic assumptions, major principles, limitations, and the importance of this software in this study is listed and explained below.

#### **Basic Assumptions**

HEPHAESTUS was developed based on the concept of stirred reactor (or physic-based approach) where NO<sub>x</sub>, CO, UHC and soot are estimated by utilising a number of stirred reactors.

- i. The combustor is assumed to be divided into Flame Front (FF) zone, Intermediate Zone (IZ), Primary Zone (PZ), and Dilution Zone (DZ). The FF was modelled by implementing a perfectly stirred reactor for the wall,

and partially stirred reactor for the core. The series of perfectly stirred reactor were used to represent the DZ and both wall and core of IZ and PZ.

- ii. The real combustor phenomenon such as evaporation, combustion unsteadiness and flow recirculation are not included to provide simplification to the pollution estimation.
- iii. In calculating CO, HEPHAESTUS assumed that during the combustion, all fuel react instantaneously to CO and water.
- iv. The prediction of NO<sub>x</sub> is based on works conducted by (ref) where the following assumptions as explained in Celis (2009) are utilised: (i) The concentrations of O<sub>2</sub>, N<sub>2</sub>, O, OH, and H are given by their equilibrium values at the local temperature, pressure and mixture fraction. In this assumption, the reactions of NO formation are slower than energy-releasing reactions, and (ii) The concentrations of N and N<sub>2</sub>O are in steady state where the formation rates of N and N<sub>2</sub>O are faster than NO formation rate.

### **Major principles**

- i. HEPHAESTUS predicts NO<sub>x</sub> by utilising the Zeldovich equations
- ii. To predict the emissions, HEPHAESTUS requires input file comprises of the information of flight altitude, ambient condition (temperature, pressure, humidity), air flow rate, fuel flow rate, combustor inlet condition (temperature and pressure), and also the combustor configuration.
- iii. Since HEPHAESTUS predict the combustion parameters using NASA CEA, therefore to evaluate different types of fuel (which doesn't provided in NASA CEA's library), the molecular formula of the fuel and the enthalpy formation of the fuel are required.

## Limitations

- i. HEPHAESTUS was developed to estimate the formation of pollution such as NO<sub>x</sub>, CO, UHC and soot. The estimation of NO<sub>x</sub> and CO is found to follow the trend provided by ICAO, but the prediction of UHC and soot is poor.
- ii. HEPHAESTUS was developed to provide the simplicity in estimating the gas turbine pollution. Therefore, major phenomenon regarding to the real combustion process such as evaporation and recirculation are neglected. By neglecting these processes, the output from HEPHAESTUS was underestimated.
- iii. HEPHAESTUS represents the core of the FF as a partially stirred reactor to describe statistically the gas composition, temperature and residence time which influence directly the rates of pollution particularly NO<sub>x</sub>. In partially stirred reactor, the unmixedness is difficult to estimate due to the issues such as fuel physical state, instantaneous mixing of gasses and air, and incomplete kinetic modelling, therefore, the correlation between the mixing parameter and the reactor equivalence ratio is utilised. However, this correlation has to be verified each time that a particular engine/combustor configuration is being modelled.
- iv. HEPHAESTUS only considered the formation of thermal-NO<sub>x</sub>, and prompt-NO<sub>x</sub>. While the formation of fuel-NO<sub>x</sub> is not included due to the fuel aviation fuel considered in HEPHAESTUS (Jet-A) does not contain significant levels of fuel-bounded nitrogen, therefore the contribution of fuel NO towards NO<sub>x</sub> formation is insignificant.

The importance of HEPHAESTUS in this study lies on it's capability to predict the NO<sub>x</sub> and CO emissions of the engine which are considered in this work. Although the ability of HEPHAESTUS to predict these pollutions is poor as it is only providing the similar trend as ICAO, but it is considered to be useful as far as biofuel is concerned, as it will become a baseline to further studies. Additionally, the prediction of pollution emissions through HEPHAESTUS is

nonetheless to test the capability of HEPHAESTUS to predict emissions generated from biofuels although further investigations are needed to clarify the output. It is also useful in this work to use HEPHAESTUS as a medium to predict the emissions as it will vary the fuels selection and make HEPHAESTUS more versatile. Although there are some other tools available to predict emissions, the use of HEPHAESTUS in this work is important due to the fact that the author has a control to the tool and able to include biofuels easily.

### 1.3.6 Optimisation using GATAC Optimisation Tool

In this study, the fuel design was carried out through the use of the multi-objective optimisation approach. This method was selected as there are several conflicting objective functions identified for obtaining the maximum biofuel that can be mixed with Jet-A, and could provide better engine performance whilst reducing pollution emissions. In order to achieve this, two cases were considered: 1) the optimisation assessment utilising CSPK and fuel flow as the variables; and 2) the optimisation assessment utilising JSPK and fuel flow as the variables. Both case studies have the same objective functions, which are NO<sub>x</sub> and CO minimisation and thrust maximisation. Besides achieving the design objectives decided, this assessment also takes into account the fuel's density and TET as constraints.

Design parameters, design constraints, and design objectives for both cases are summarised in Table 1-2 below.

**Table 1-2: List of Design Parameters, Constraints and Design Objectives for Both Cases**

<b>Design Parameters</b>	<b>Design Constraints</b>	<b>Design Objectives</b>
<ul style="list-style-type: none"> <li>• Fuel percentage</li> <li>• Mass flow rate</li> </ul>	<ul style="list-style-type: none"> <li>• Fuel's density</li> <li>• Turbine entry temperature (TET)</li> </ul>	<ul style="list-style-type: none"> <li>• Minimise NO<sub>x</sub></li> <li>• Minimise CO</li> <li>• Maximise Thrust</li> </ul>

The optimisation was carried out in GATAC, which is a tool developed for CLEAN SKY project. GATAC implements NSGAMO type of optimisation method (Dimech et al, 2011). The explanation about the major principles and limitations of GATAC is summarised as below. Additionally the importance of GATAC in this research work also is included.

### **Major principles**

- i. In principle, the optimisation method used in GATAC is a Non-Sorted Genetic Algorithm for Multi-Objective (NSGAMO). With this method, GATAC is known to handle more than one objective functions.
- ii. In GATAC, user has to include modules or the executable files, and properly defined the set up within the GATAC library to allow GATAC performs properly

### **Limitations**

- i. GATAC used in this work is the first version in which only one optimiser method (NSGAMO) is used. However, the second generation of GATAC is improved where Multi-objective Tabu Search (MOTS) is provided as an option.
- ii. Models available in GATAC are Aircraft Performance Model, Engine Performance Model, Emissions Model and Noise Model. However, the existence Engine Performance Model and Emissions Model are only available for kerosine which unfortunately is not enough to evaluate the optimum mixture of biofuel/kerosine as proposed in this work. Therefore, it is mandatory in this work to include the new model into the framework. To include the new model in GATAC, it is important to make sure that the model is able to run in the batch mode in order for GATAC to work properly.

## **The significance of GATAC in this work**

As mentioned in the Research Gap section (section 1.1.3), it has been noticed that most of the studies on the biofuels have used up to 50% biofuel in the biofuel/kerosine mixture, and there are no research work until this moment investigates the optimal percentage of biofuel in the blend, that can be used in providing the maximum engine performance and minimum engine emissions. Therefore it is mandatory in this work to optimise the percentage of biofuels chosen in this work that suitable to be blended with kerosine in order to get maximum engine performance and minimum engine emissions. In order to optimise the perfect mixture of the biofuel/kerosine with regard to the above problem, GATAC is used. GATAC was chosen to be used in this study by considering that the capability of GATAC to handle more than one objective functions. GATAC also was tested and was validated through the comparison work against the theoretical pareto of ZDT1 test case. Despite those above advantages, GATAC also is capable to handle any test cases as long as the system components such as Model Dictionary, Set up Model Dictionary, and Input and Output Handler are set up properly. Based on the capability and advantageous of GATAC, this optimisation framework is used for the test cases defined in this work.

## **2 EVALUATION OF BIO-FUEL'S SPRAY BEHAVIOUR**

### **2.1 General Introduction**

In the previous chapter we discussed how alternative fuel has proved capable of reducing and controlling the formation of pollution. Variables such as equivalence ratio and primary zone temperature, the homogeneity of the combustion process in the primary zone, residence time in the primary zone and the characteristics of linear wall quenching constitute the major factors in controlling such pollution. In the case however, of a combustor operated with liquid fuel, fuel spray characteristics also forms an important factor in controlling the pollution.

Spray characteristics, i.e. the spray mean drop size, distribution of drop size, the pattern of the spray, the spray cone angle and the spray penetration are important as they specify the pattern of the flame burning and temperature distribution within the primary zone, which consequently determines the combustor efficiency and formation of emissions. These characteristics are nonetheless affected by several factors such as ambient condition and fuel properties.

As the challenge exists of finding new fuel to replace conventional fuel, the influence of fuel properties becomes essential in evaluating the spray characteristics. Accordingly, the influence of fuel properties on spray characteristics, focusing on droplet lifetime and spray penetration is investigated.

### **2.2 Factors Affecting Combustion Performance of Liquid Fuels**

As mentioned, several factors influence combustion performance. For instance, a study conducted by Anderson *et al.* (1976) investigates the effect of liquid fuel drop size on liquid fuel combustion and generation of pollutant emissions by investigating the flame stability and thus measuring pollution for different sizes of fuel droplets at a different range of equivalence ratios. The main results

indicate significant reductions in the unburned hydrocarbon (UHC), NO and CO<sub>2</sub> levels but slight increases in CO levels as the drop size decreases. Reductions in CO<sub>2</sub> and increases in CO levels have also been noted by Tuttle *et al.* (1975). Anderson *et al.* (1976) believed that such behaviour is due to the fact that smaller drops require shorter times for igniting and evaporating. For this reason, large amounts of CO are produced and encountered during the oxidation process from CO to CO<sub>2</sub>, which is known to be a relatively slower process. Furthermore, Anderson *et al.* (1976) noted that the flame becomes very luminous as the size of drops increases. Moreover, the flame luminosity increases with the equivalence ratio. Conversely, the smaller drop size decreases the flame luminosity, and completely disappears when the smallest drop size is present.

Additionally, Datta and Som (1999) developed a numerical model of spray combustion in a gas turbine in order to identify the influence of Sauter Mean Diameter (SMD) and spray cone angle towards combustion efficiency and pattern factor for wall and exit temperature distribution. They observed that increases in mean drop diameter increase the combustion efficiency, and reaches maximum at an optimum value of mean drop diameter. Furthermore, the increment in droplet diameter subsequently reduces overall efficiency. The factor of the spray cone angle was also found to affect the combustion efficiency. In addition, increases in combustion efficiency were correspondingly found with increases in spray cone angle. Meanwhile, improvements in terms of pattern factors for exit temperature distribution were observed as the mean drop diameter or spray cone angle was increased. Furthermore, an increase in spray cone angle also increases the temperature distribution of the combustor wall.

The influence of mean drop size on soot formation was investigated by Rink and Lefebvre (1989) who used a tubular combustor in their experimental study. This combustor was fed with kerosine fuel and operated at a pressure of 1.52MPa. The investigation was performed for a set of equivalence ratio ranging from 0.9 to 1.2 and the mean drop size of 110  $\mu\text{m}$ , 70  $\mu\text{m}$  and 30  $\mu\text{m}$ . The results indicated an approximately half reduction of soot when the mean

drop size was reduced from 110 to 30  $\mu\text{m}$ . Rink and Lefebvre (1989) suggest that this is due to the evaporation of droplets that takes place as the fuel spray approaches the flame front. For the smallest droplet, it will have enough time to evaporate completely (become fuel vapour) before mixing with the combustion air and burning as premixed flame. Meanwhile, the largest droplets do not have time to evaporate completely and mix properly. As a result, the largest droplets are burnt as fuel-rich and therefore produce soot due the proportion of fuel burnt.

Sharma *et al.* (2001) conducted a numerical study in order to establish the effect of inlet air swirl (flow recirculation), inlet air pressure, inlet air temperature and spray cone angle on penetration and vaporisation histories for different sizes of droplet using the can type gas turbine combustor. It has been observed that the penetration of droplet increased with an increase in droplet diameter. This is mainly owing to the lower drag per unit mass of coarser diameter, subsequently requiring a longer time to completely vaporise. They also found that for each size of droplet the penetration decreased with an increase in inlet swirl number, primarily because of the strong flow of recirculation formed in the upstream of the combustor. Notably, both penetration and the rate of vaporisation of droplets were found to be reduced with increases in inlet air pressure. The results also revealed a significant reduction in droplet penetration if the spray cone angle was increased. Conversely, the penetration of droplet increased with rising air temperature; due to lower density at high air temperature, thereby reducing drag on the moving droplets.

Studies on the impact of fuel volatility towards combustion efficiency, exit temperature and the formation of  $\text{NO}_x$  have been conducted by Sharma and Som (2002), who developed a numerical model for a two-phase gas droplet flow, taking into account the variation in combustor pressure and inlet swirls. The fuels used in this study are *n*-hexane ( $\text{C}_6\text{H}_{14}$ ), kerosine ( $\text{C}_{10}\text{H}_{20}$ ) and *n*-dodecane ( $\text{C}_{12}\text{H}_{26}$ ). The study observed that increases in fuel volatility increase the efficiency of the combustor; however, this will affect only high pressure. In contrast at low pressure, the effect of fuel volatility is found to be unremarkable.

At low pressure, high-volatility fuel decreases the value of pattern factor but, for low-volatility fuel, the opposite trend was found. An increase in NO<sub>x</sub> emissions was observed with decreases in fuel volatility. For a given fuel, there was a reduction in the inlet combustor pressure and increases in inlet swirl number, which resulted in the reduction of NO<sub>x</sub> emissions.

Park *et al.* (2009) conducted an experiment designed to investigate the effects of bioethanol-biodiesel blend on fuel spray behaviours, namely spray tip penetration, and spray cone angle. A study of atomisation characteristics—namely droplet size and axial velocity—were also included. This study used biodiesel fuel derived from soybean oil. Bio-ethanol was blended with biodiesel, with the blending ratio set at 10-30% with intervals of 10%. This study revealed that additional bio-ethanol in biodiesel provided little effect on spray tip penetration. However, an increase in spray cone angle was found as the blending ratio of bio-ethanol increases. The experiment also revealed that adding bio-ethanol to biodiesel fuel improved the atomisation performance of the fuel; this is due to the low viscosity of bio-ethanol, which consequently improved fuel evaporation and breakup process.

The previous state-of-art regarding the influence of fuel drop size, ambient condition, viscosity and volatility of the fuel on the engine combustion discussed above indicates their importance. Therefore, in establishing new fuel, assessment of the effect of the fuel properties on spray characteristics is of importance as it affects the atomisation quality and consequently the combustion efficiency. It is noted that most of the studies conducted regarding the effect of fuel properties on fuel spray characteristics are using biodiesel fuel. Considering that the aircraft industry has moved towards using bio-synthetic paraffinic kerosine types of fuel, it is necessary in this work to evaluate the spray characteristics of the selected biofuels – JSPK and CSPK, as the influence of such fuels on the atomisation has not yet been explored.

## 2.3 Requirement of Biofuels Spray Evaluation

In addressing the influence of fuel properties on droplet lifetime and spray penetration, evaluation has been predicted through a spreadsheet analysis prepared by Mazlan (2008), where ethanol is presented as a baseline demonstration fuel. This model focuses on the evaporation of a single droplet formed in a spray from a pressure swirl atomiser. The spreadsheet analysis was built based on the process of heat transfer, which includes droplet motion, energy equation and boiling mass transfer. Equations regarding those processes were taken from the FLUENT 6.3 User Guide.

In such equations, fuel properties—such as density, vapour pressure, and specific heat capacity—are required. With the exception of density, the model developed by Mazlan (2008) did not take into account the variation of vapour pressure, and specific heat capacity with temperature. Therefore, this present study extends and improves the model by including the variation of fuel vapour pressure and heat capacity with temperature to obtain more reliable evaluation.

This study focuses on the bio-SPK type of fuels. However other biofuels, as indicated in Table 2-1, were also chosen for comparison, whereas to investigate the effect of blend fuel on the combustion performance, a blend of 50%, JSPK with 50% kerosine was also performed.

**Table 2-1: Different Types of Biofuels Selected for the Evaluation**

Fuel	Molecular Formula	Fuel composition
Kerosine	$C_{12}H_{23}$	100%
RME	$C_{19}H_{32}O_2$	100%
Ethanol	$C_2H_5OH$	100%
JSPK	* $C_{12}H_{26}$	100%
CSPK	* $C_{12}H_{25.4}$	100%

\*Estimated value – see Appendix C

Equations related to mass, momentum and energy exchange between droplet and air from FLUENT were used and are discussed briefly in this section. Additionally, the findings and derivations of fuel properties over a range of

temperatures to be used in conjunction with the equations above were also included.

### 2.3.1 Physical Modelling of the Liquid Phase

In describing behaviour of a droplet during the evaporation process, equations related to physical modelling of liquid droplet taken from FLUENT is used. In FLUENT the trajectory of droplets is predicted by integrating drag force, gravitational force and additional force which apply on a droplet. This additional force usually includes those forces which necessary in accelerating the fluid surrounding the particle. Accordingly, this study focuses only on the particle's drag. Therefore, forces related to gravity and additional force as in the second and third parts of the right-hand side of the equation (22.2-1) in FLUENT were neglected. By neglecting the gravitational and additional forces, the new equation for predicting the particle motion of the particle is described as follows:

$$\frac{dV_p}{dt} = \frac{18\mu}{\rho_p d_p^2} \frac{C_D \text{Re}_p}{24} (V_\infty - V_p) \quad (1)$$

While the Reynolds number,  $\text{Re}_p$  is defined as

$$\text{Re}_p = \frac{\rho d_p |V_p - V_\infty|}{\mu} \quad (2)$$

The drag coefficient,  $C_d$  in Equation (1) is defined as:

$$C_d = \frac{24}{\text{Re}_p} \left( 1 + \frac{\text{Re}_p^{2/3}}{6} \right) \quad (3)$$

For the condition where the temperature of the fuel's droplet is less than the boiling temperature, a reduction in mass particle over time was calculated according to Equation (4):

$$\frac{dm_p}{dt} = -N_i A_p MW_p \quad (4)$$

The molar flux of the droplet's vapour,  $N_i$  is given as follows:

$$N_i = k_c (C_{i,s} - C_{i,\infty}) \quad (5)$$

While  $C_{i,s}$  was calculated by assuming that the partial pressure of vapour at the interface is equal to the saturated vapour pressure at the particle droplet temperature, as follows:

$$C_{i,s} = \frac{p_{sat}(T_p)}{RT_p} \quad (6)$$

$C_{i,\infty}$  was calculated as in Equation (7) and  $k_c$  was calculated according to Sherwood's number correlation as in Equation (8) below:

$$C_{i,\infty} = X_i \frac{p}{RT} \quad (7)$$

$$Sh_{AB} = \frac{k_c d_p}{D_{i,m}} = 2.0 + 0.6 \left( Re_p \right)^{\frac{1}{2}} Sc^{\frac{1}{3}} \quad (8)$$

Schmidt number,  $Sc$  in equation (8) was calculated as follows:

$$Sc = \frac{\mu}{\rho D_{i,m}} \quad (9)$$

Finally, the changes in droplet temperature were calculated from the heat balance, which is associated with the changes in sensible heat in the droplet and latent heat transfer between the droplet and the continuous phase. By

assuming no radiation heat transfer took place, and rearranging the Equation (22.9-25) from FLUENT, the changes in droplet temperature were calculated using Equation (10) below:

$$\frac{dT_p}{dt} = \frac{hA_p(T - T_p) + \frac{dm_p}{dt} h_{fg}}{m_p C_p} \quad (10)$$

All the above equations were used in conjunction with established fuel properties obtained from literature. In order to assess the evaporation process of droplets, some assumptions were made to simplify the calculation. These are:

1. The droplet is a spherical single droplet which is produced by a pressure swirl atomizer;
2. The initial droplet diameter was assumed to simplify the calculation;
3. No radiation heat transfer was included during the evaporation process;
4. Gas is stagnant and the droplet is evaluated in the stationary condition;
5. The bulk mole fraction of those fuels was assumed as zero, as we are considering that the fuel is evaporating in pure air.

In evaluating the influence of fuel properties on droplet lifetime, the behaviour of the liquid drop during the evaporation process was evaluated.

This numerical calculation was conducted in pure air, at a temperature of 1000K and a pressure of 1 atm. The droplet size produced from the fuel injector was assumed to be 20  $\mu\text{m}$  and the temperature of the fuels was assumed to be 300K. The droplet generated by the fuel injector was assumed to be a sphere owing to its surface tension. The calculation was established in a time step of 10  $\mu\text{s}$ .

The evaporation process of droplet was predicted by setting the initial condition of  $V_p = 100$  m/s,  $d_p = 20\mu\text{m}$ ,  $V_g = 0$  m/s,  $T_g = 1000\text{K}$ ,  $P_g = 101325$  Pa,  $\mu_g = 4.27 \times 10^{-5}$  kg/ms,  $D_0 = 1.00 \times 10^{-3}$ ,  $\theta = 34.89$  and  $\alpha_d = 1.00 \times 10^{-4}$ . In predicting total time taken by a droplet to evaporate completely, steps below are followed.

1. The calculation begins by calculating the Reynolds number using equation (2)
2. From the Reynolds number, drag coefficient,  $C_d$  of the droplet is calculated using equation (3)
3. The changes of velocity of the particle is calculated using equation (1)
4. The change in droplet temperature is calculated using equation (10)
5. Finally, the change of droplet's mass is calculated by using equation (4).

In this calculation, the time step of  $10 \mu\text{s}$  was set until the droplet reaching the boiling temperature where the drop is assumed to vaporise completely. After that, the time step increases to  $1.00 \times 10^{-4}$  sec. The calculation continued until the velocity of the droplet is approaching zero where the change of velocity is almost negligible.

The lifetime of droplet was measured by taking the time when the velocity of droplet is zero. Appendix B shows the calculation of the evaporation and spray penetration of kerosine as an example to show how the calculation was conducted.

## **2.3.2 Finding and Derivation of the Necessary Fuel Properties**

### **2.3.2.1 Kerosine (Jet-A)**

#### ***Density***

The density of kerosine was obtained from graphs in Paleu and Nelias (2007), and its variation towards temperature was calculated using the following equation:

$$\rho = \rho_{20} - 0.718(T - 20) \quad (11)$$

where  $\rho_{20}$  is density of kerosine at  $T = 20^\circ\text{C}$ .  $T$  in the equation (11) refers to temperature in  $^\circ\text{C}$ . The variation of density of kerosine towards temperature is shown in Figure 2-1 below.

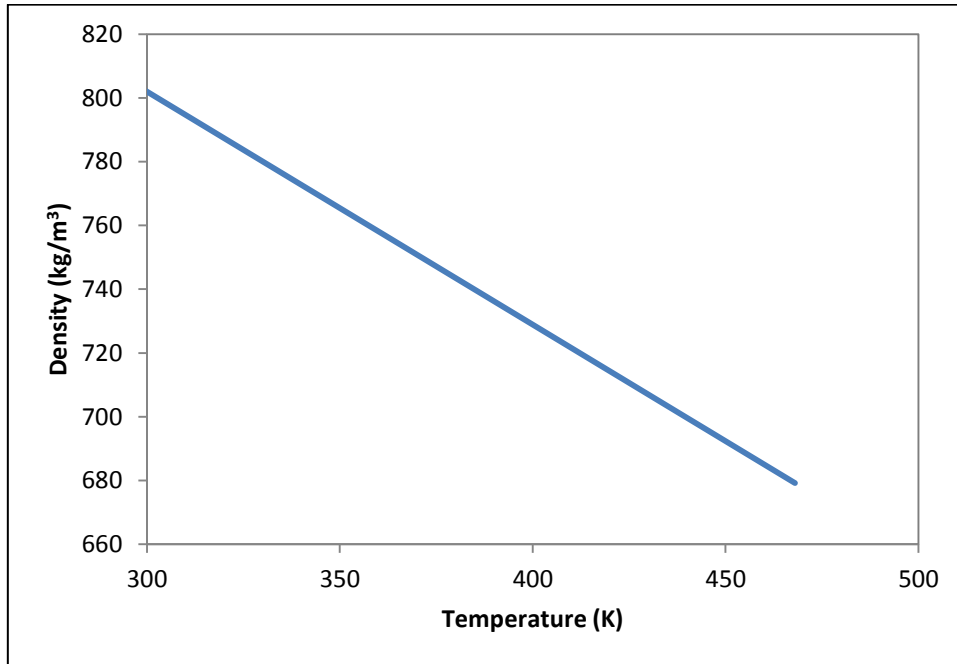


**Figure 2-1: Density of Jet-A as a Function of Temperature**

### ***Vapour Pressure***

Calculation of Jet-A vapour pressure was obtained from the correlation of vapour pressure with temperature (Handbook of Aviation Fuel Properties, 1983) using the following equation:

$$P_v = 188605895 \left( \exp \left( -\frac{4576.45}{T} \right) \right) \quad (12)$$

The graph showing vapour pressure as a function of temperature is shown in Figure 2-2 below. The boiling point of kerosine could be measured from the vapour pressure curve. Moreover, the boiling temperature of kerosine was

measured at  $P=1\text{atm}$ , and the value obtained is  $T_b=461\text{K}$  (which is between  $150^\circ\text{C}$ - $290^\circ\text{C}$  as reported by IARC, 1989).

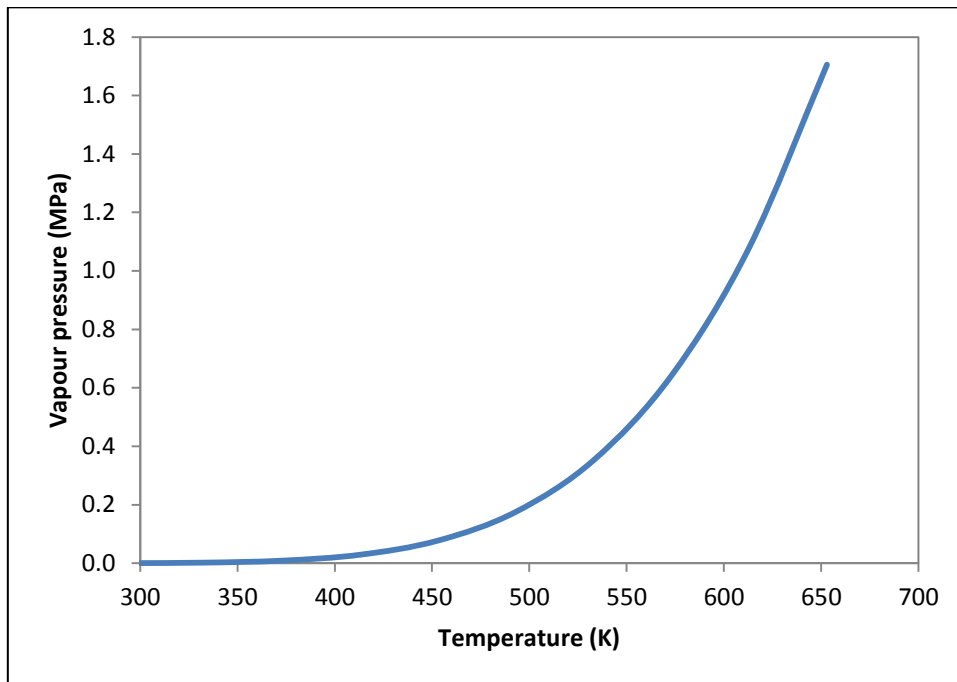


**Figure 2-2: Vapour Pressure of Kerosine as a Function of Temperature**

### **Specific Heat Capacity**

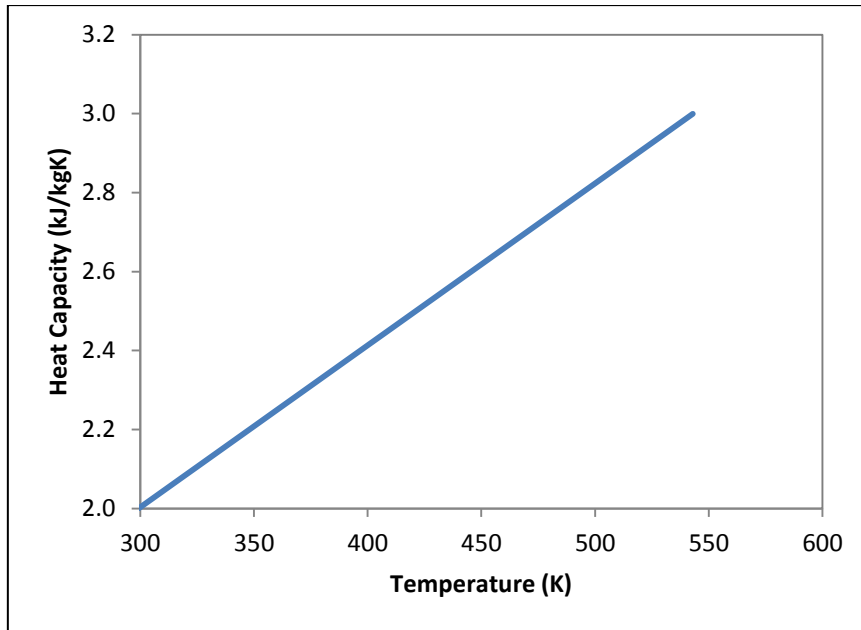


**Figure 2-3: Specific Heat Capacity of Kerosine as a Function of Temperature**

#### **2.3.2.2 Rix Biodiesel (Rapeseed Methyl Ester, RME)**

##### ***Density***

The predicted density of Rix biodiesel as a function of temperature was taken from Halvorsen *et al.* (1993), and is accordingly presented in the graph in Figure 2-4 below.

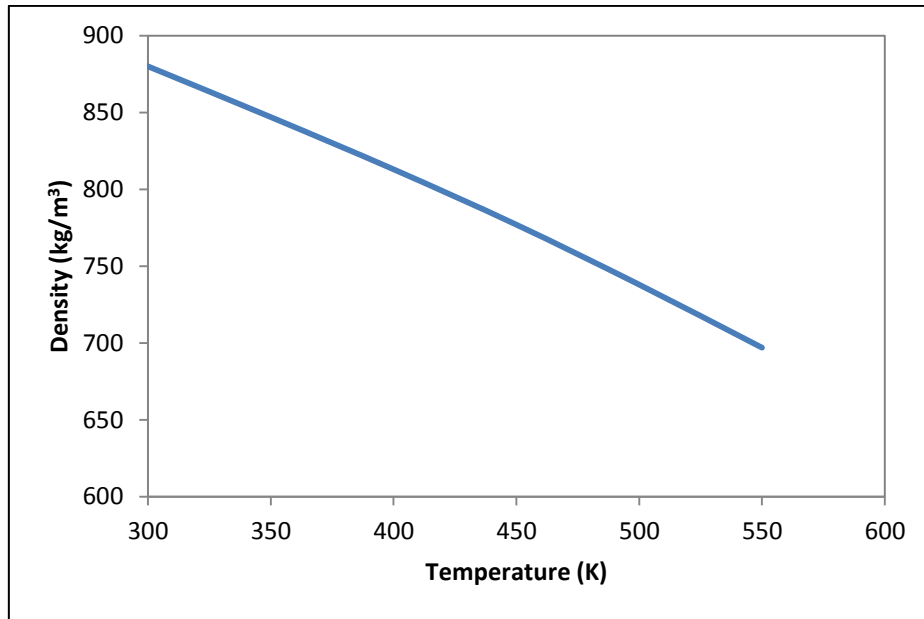


**Figure 2-4: Density of Rix Biodiesel as a Function of Temperature**

### ***Vapour Pressure***

Rix biodiesel comprises several fatty acid methyl esters (FAME). Therefore, its total vapour pressure is based on the mixture of vapour pressure for each fatty acid contained in the biodiesel. It can be calculated using Roul't's law;

$$P_{vmix} = \sum_i P_{vi} x_i \quad (13)$$

where  $P_{vi}$  and  $P_{vmix}$  is the vapour pressure of fatty acid and their mixture respectively, whilst  $x_i$  is the mole fraction of different components of fatty acid.

The mass fraction of Rix biodiesel FAME is given in Table 2-2 below.

**Table 2-2: Rix Biodiesel Fatty Acid Methyl Ester (Rochaya, 2007)**

<b>FAME</b>	<b>FAME Mass fraction</b>
Palmitic 16:0	13.73
Stearic 18:0	5.33
Oleic 18:1	50.96
Linoleic 18:2	19.93
Linolenic 18:3	4.2
Eruric 22:1	5.85

The vapour pressure of each component of FAME present in Rix biodiesel is frequently calculated using the Antoine's equation

$$\log_{10} P = A_{ant} - \frac{B_{ant}}{T + C_{ant}} \quad (14)$$

where A, B and C are the Antoine constant whilst T is the temperature in Kelvin. The Antoine's constant are present in Table 2-3 below.

**Table 2-3: Antoine Constant of FAME (Yuan *et al.*, 2005)**

<b>FAME</b>	<b>A</b>	<b>B</b>	<b>C</b>
C 16:0	9.5714	2229.94	-111.01
C18:0	9.3746	2174.39	-131.23
C18:1	9.9155	2583.52	-96.15
C18:2	8.2175	1450.62	-188.03
C18:3	8.1397	1387.93	-196.16
C 20:0	10.3112	2987.15	-84.56
C20:1	10.3525	3009.62	-81.66
C22:0	10.6867	3380.86	-73.2
C22:1	10.7518	3423.99	-69.43
C24:0	11.0539	3776.89	-62.9

Based on the composition of fatty acid present in the Rix biodiesel and Antoine constant, vapour pressure of Rix biodiesel can be plotted as in Figure 2-5 below:

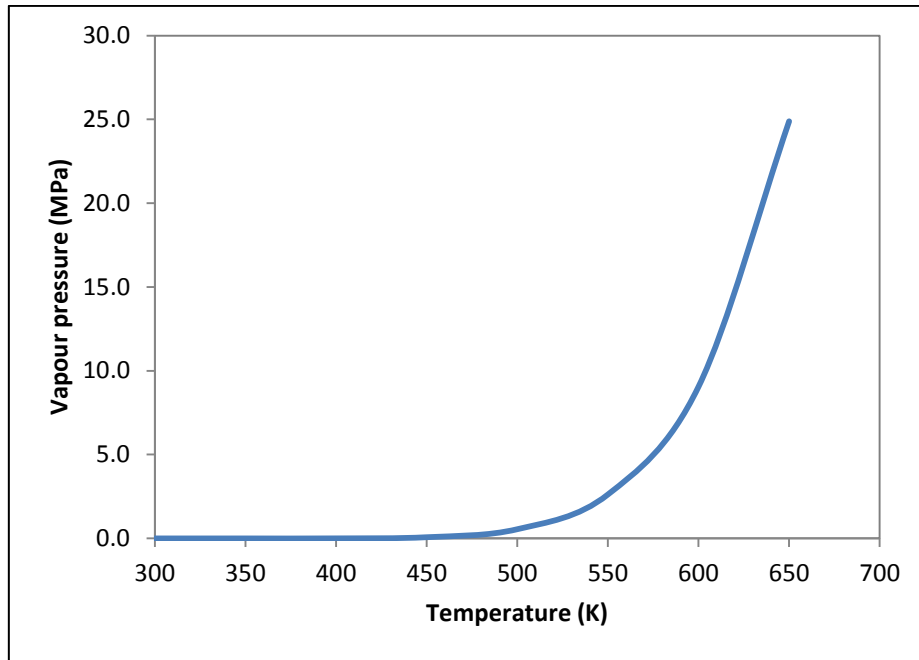


**Figure 2-5: Vapour Pressure of Rix Biodiesel as a Function of Temperature**

From the above vapour pressure curve, the normal boiling point of Rix biodiesel was found to be 623K.

***Specific Heat Capacity***

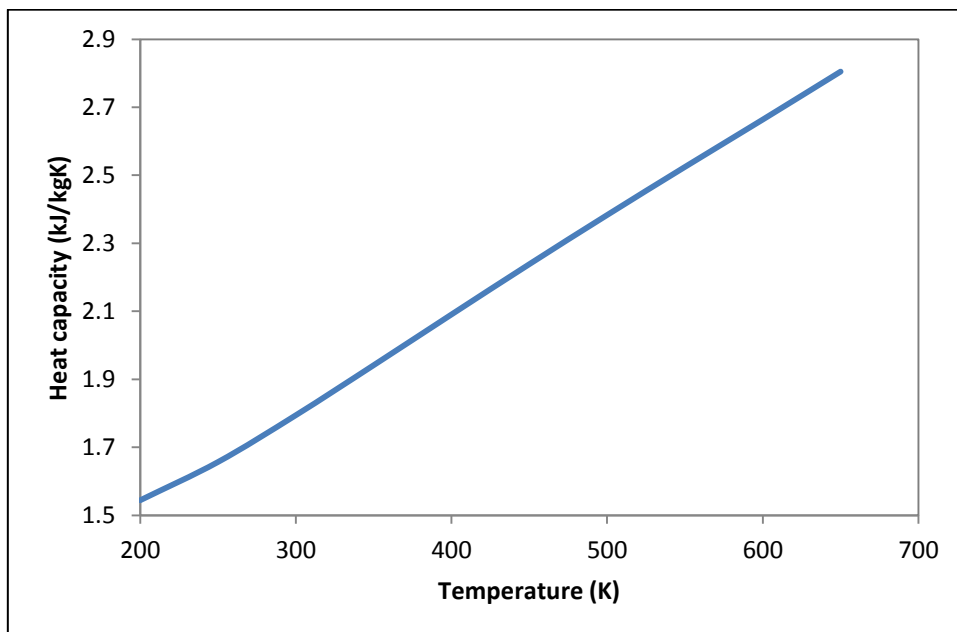


**Figure 2-6: Specific Heat Capacity of RME as a Function of Temperature**

### 2.3.2.3 Ethanol

#### **Density**

The density of ethanol was obtained from Khasanshin and Aleksandrov (1984) and is illustrated in Figure 2-7 below.

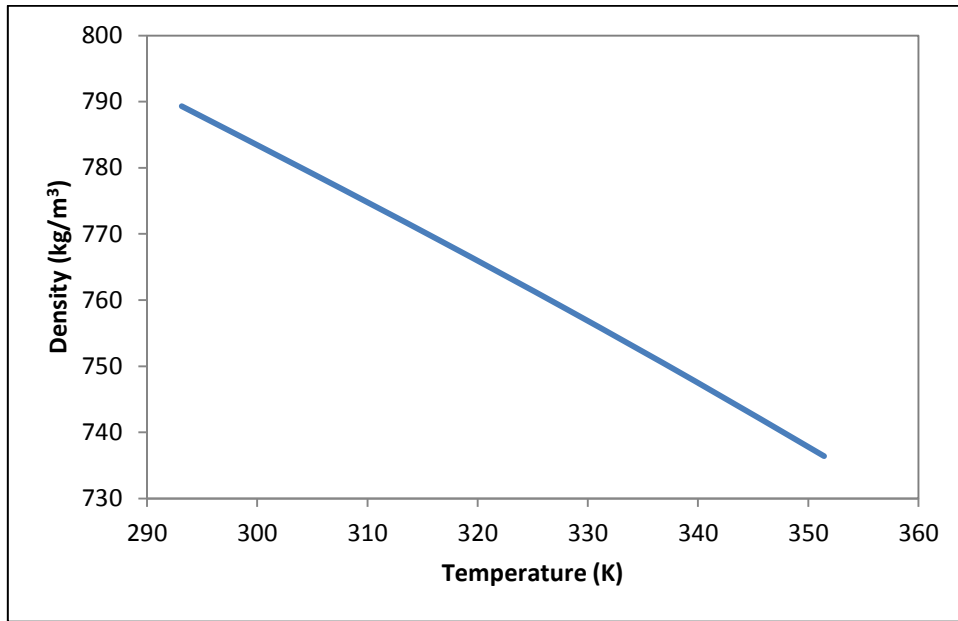


**Figure 2-7: Ethanol's Density Varying with Temperature**

#### **Vapour Pressure**

The temperature dependence of ethanol's vapour pressure was calculated using Equation (15) below (Reid *et al.*, 1987).

$$\ln P = A - \frac{B}{T + C} \quad (15)$$

where A, B and C are constants. T is temperature measured in K whilst P is vapour pressure in kPa.

**Table 2-4: Constants for Ethanol's Vapour Pressure**

Constant	Value
A	16.897
B	3803.980
C	-41.680

Based on Equation (15) above and the vapour pressure constants, the vapour pressure curve of ethanol is presented below.

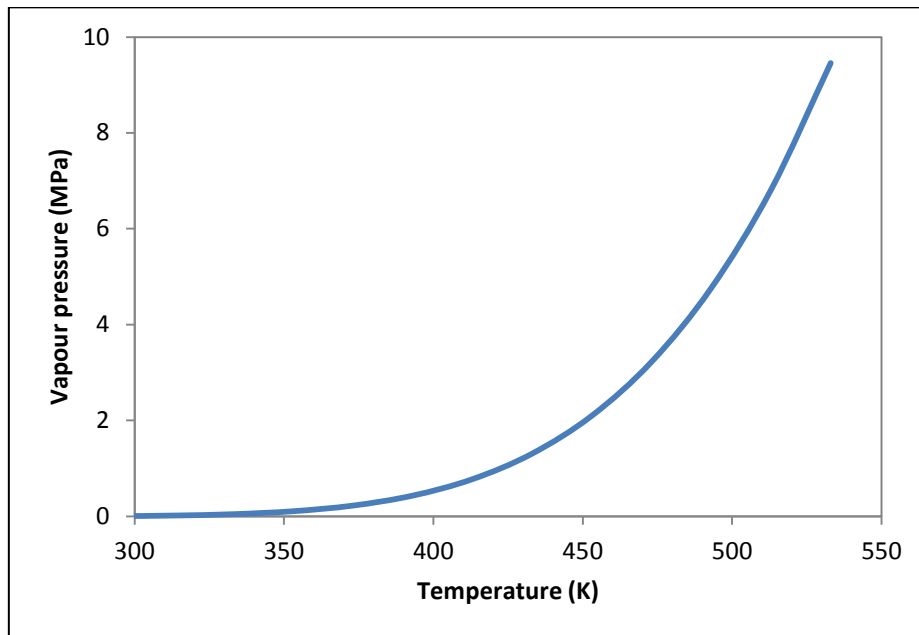


**Figure 2-8: Ethanol's Vapour Pressure as a Function of Temperature**

As shown in the curve, the normal boiling point of ethanol at atmospheric pressure was determined at the point where the curve reaches 1 atm, with the value being found at 352K.

#### **2.3.2.4 Camelina Bio-SPK (CSPK)**

##### ***Density***

The variation of density with temperature for CSPK was obtained as plotted in Kinder (2010) which translated into the following equation:

$$\rho = -0.8(T) + 980.8 \quad (16)$$

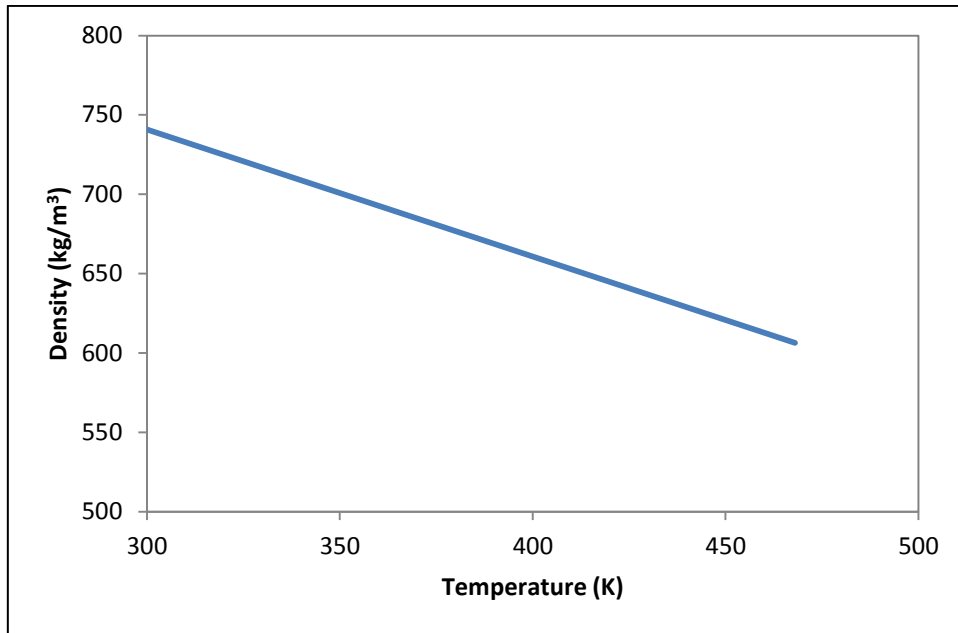


**Figure 2-9: Density of CSPK Reduces as Temperature Increases**

***Vapour Pressure***

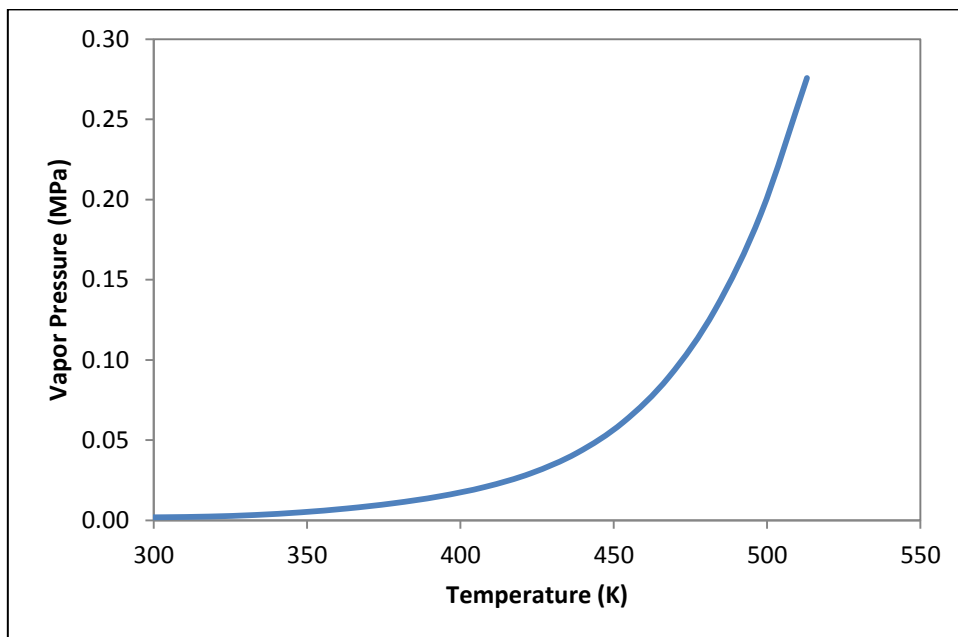


**Figure 2-10: Vapour Pressure of CSPK Varies with Temperature**

## Heat Capacity

In estimating the heat capacity of CSPK, the following equation, as provided in Kinder (2010) is used:

$$C_p = 0.0036(T) + 2.0807 \quad (17)$$

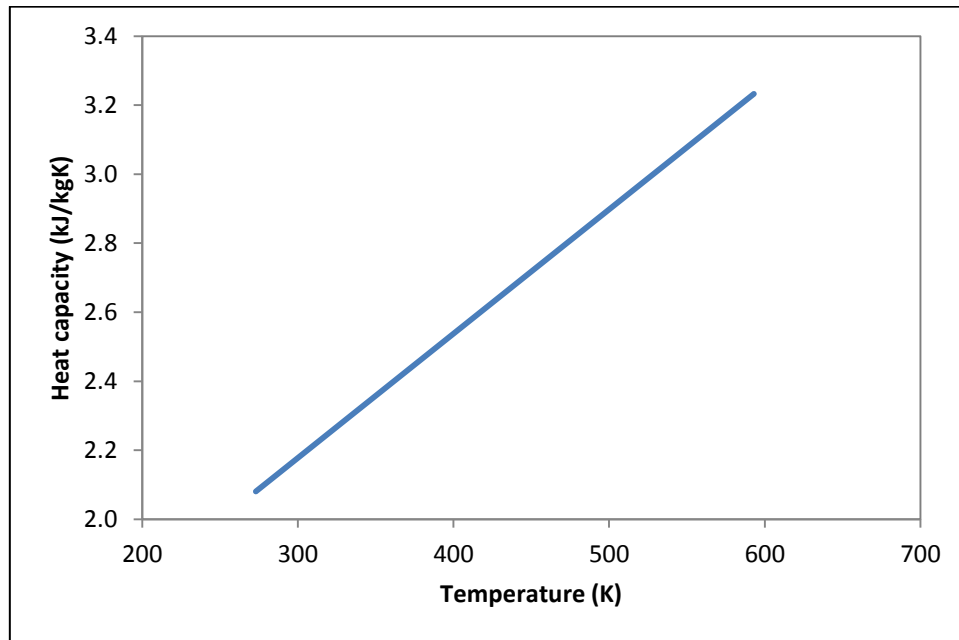


Figure 2-11: Heat Capacity of CSPK Increases Linearly with Temperature

### 2.3.2.5 Jatropha Bio-SPK (JSPK)

#### Density

The variation of density with temperature of JSPK was estimated using an ideal mixture equation in conjunction to the density variation of 50% JSPK with 50% Jet-A with temperature as plotted in (Kinder, 2010). The variation of JSPK density with temperature is presented in Figure 2-12.

$$\rho_{mix} = \sum_i \phi_i \rho_i \quad (18)$$

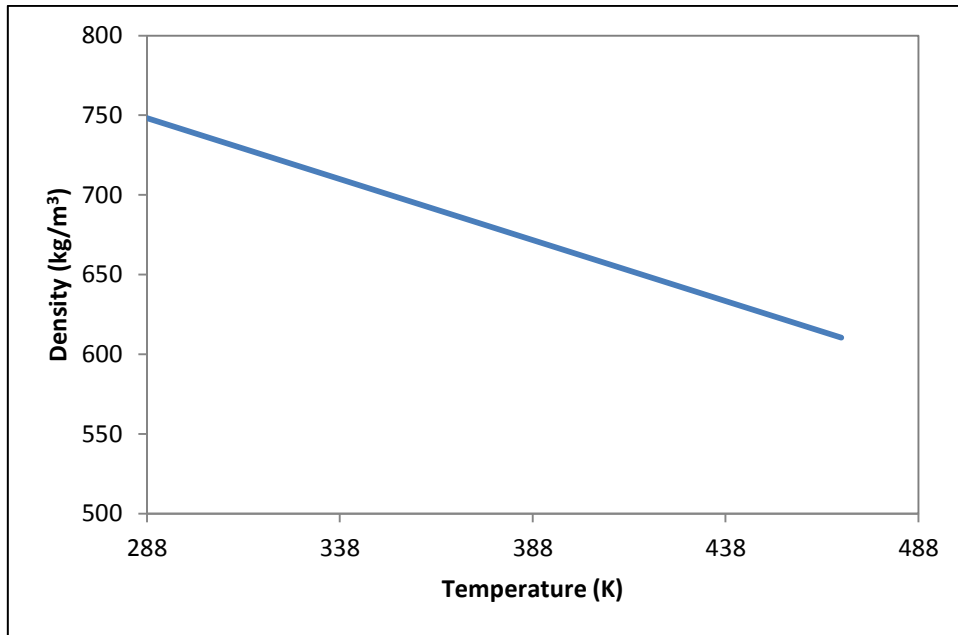


**Figure 2-12: Density of JSPK at Various Temperatures**

### ***Vapour Pressure***

In estimating the vapour pressure of JSPK, the vapour pressure of 50% blend JSPK with 50% Jet-A as in Kinder (2010) was used as a baseline. Therefore the vapour pressure of pure JSPK was estimated by using the equation below:

$$P_{vmix} = \sum_i P_{vi} x_i \quad (19)$$

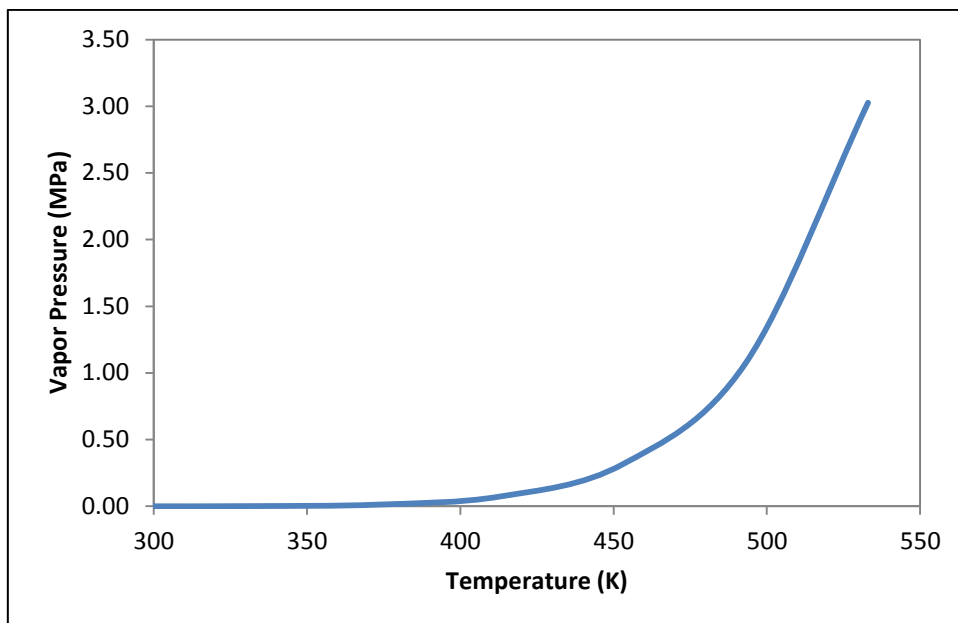


**Figure 2-13: The Variation of Vapour Pressure as a Function of Temperature**

### ***Heat Capacity***

The variation of heat capacity with temperature for JSPK was estimated from the correlation obtained in Kinder (2010).

$$C_p = 0.0035(T) + 2.0796 \quad (20)$$

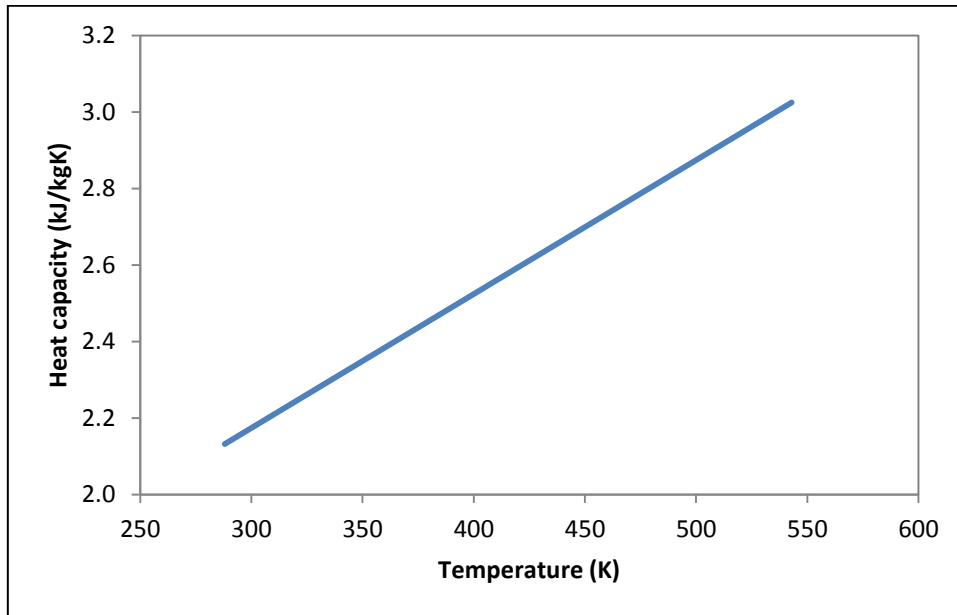


**Figure 2-14: The Variation of Heat Capacity as a Function of Temperature**

## **2.4 Results**

### **2.4.1 The Comparison of Fuel's Properties**

This study focuses on Jatropha Bio-SPK (JSPK) and Camelina Bio-SPK (CSPK) fuel. For comparison, other biofuels, such as ethanol and Rapeseed Methyl Ester (RME) were chosen. The variation of fuel properties with temperature which were used in the evaporation spread sheet analysis—density, heat capacity and vapour pressure—are presented. Those fuel properties are obtained from the literature where accessible. Some properties however are not easily obtained from open literature. In such cases estimation through calculation is necessary. Additionally, the properties of Jet-A also will be provided for purposes of comparison.

### 2.4.1.1 Density

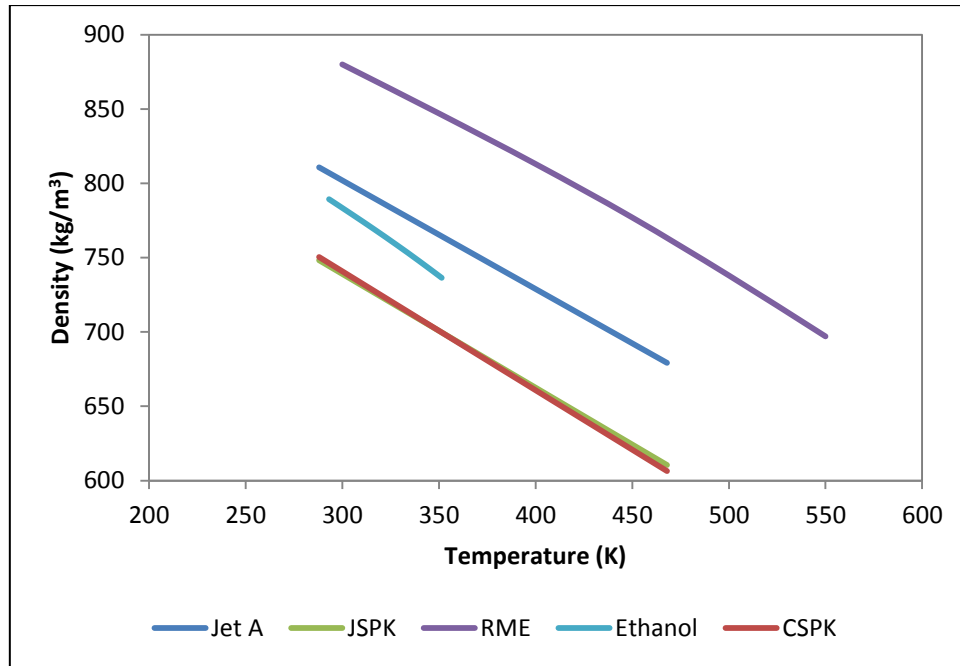


**Figure 2-15: Comparison of Fuels' Density as Function of Temperature**

Figure 2-15 shows the variation of density over temperature for biofuels and Jet-A. Amongst the others it is observed that RME has relatively high density while there is not so much difference between JSPK and CSPK. The high density of RME is probably due to the high molecular weight of the fuel and the component atoms of the fuel molecules. Fuel with high density may provide an advantage regarding the amount of fuel that can be stored in the fuel tank and also the amount of fuel that can be pumped. High density fuel on the other hand is disadvantageous to specific fuel consumption. High density fuel will generate less kinetic energy due to inefficiencies and thermodynamic considerations; hence using this fuel in the engine will increase specific fuel consumption.

Running the engine with fuel with low density may benefit in the specific fuel consumption, but in the case of aircraft, extra storage volume may have to be considered in order to carry the same amount of energy contained in kerosine which consequently increases both the aircraft empty weight and take-off weight. This issue has been discussed in Dagget *et al.* (2006) who explain the

disadvantage of powering the engine with ethanol as it may require an extra of 25% of aircraft weight and 35% of aircraft take-off weight.

As the main purposes of using biofuel in aircraft engine is to reduce the discharged emissions as well as reducing the overdependence of crude oil, however, in order to implement biofuels in the existing aircraft, it is important to make sure that no modification to the aircraft as well as the engine is required. For that reason, the range of density was set up and the density of alternative fuels must lie within that range.

#### 2.4.1.2 Heat Capacity

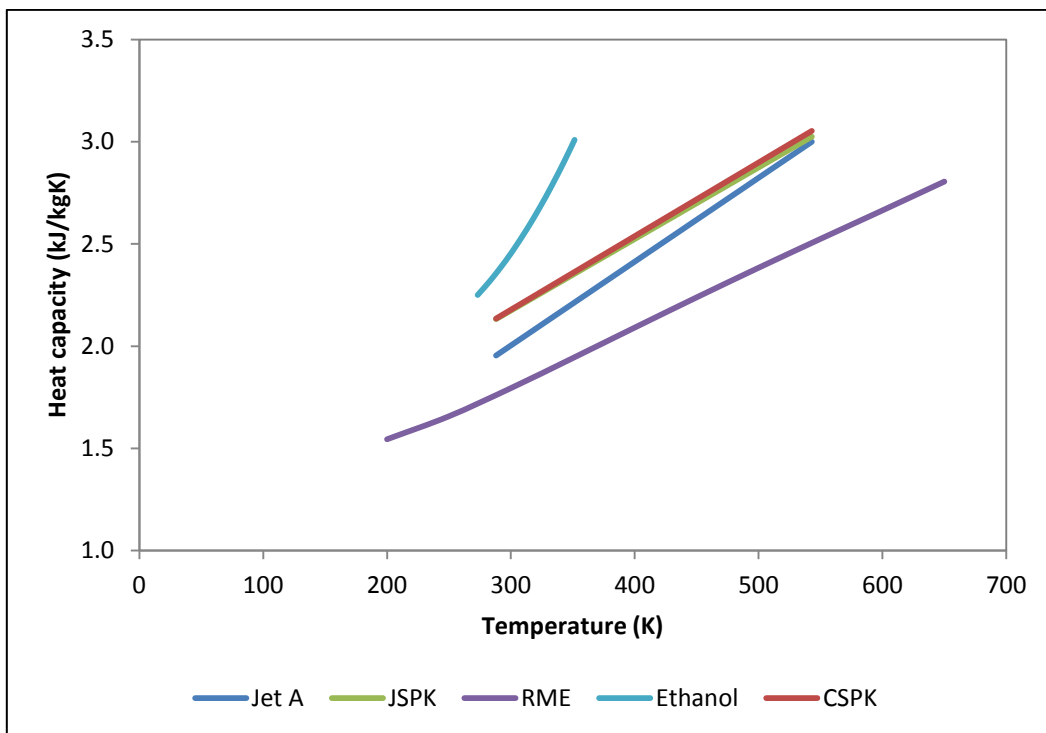


**Figure 2-16: The Comparison of Heat Capacity as a Function of Temperature**

The comparison of specific heat capacity for the biofuels and Jet-A as a function of temperature is presented in Figure 2-16. As observed, all the fuels have almost linear increases of heat capacity with temperature. Notably, ethanol has the highest heat capacity whereas RME is the lowest. Both bio-SPK fuel (JSPK and CSPK) provide high heat capacity in comparison to Jet-A.

### 2.4.1.3 Vapour Pressure

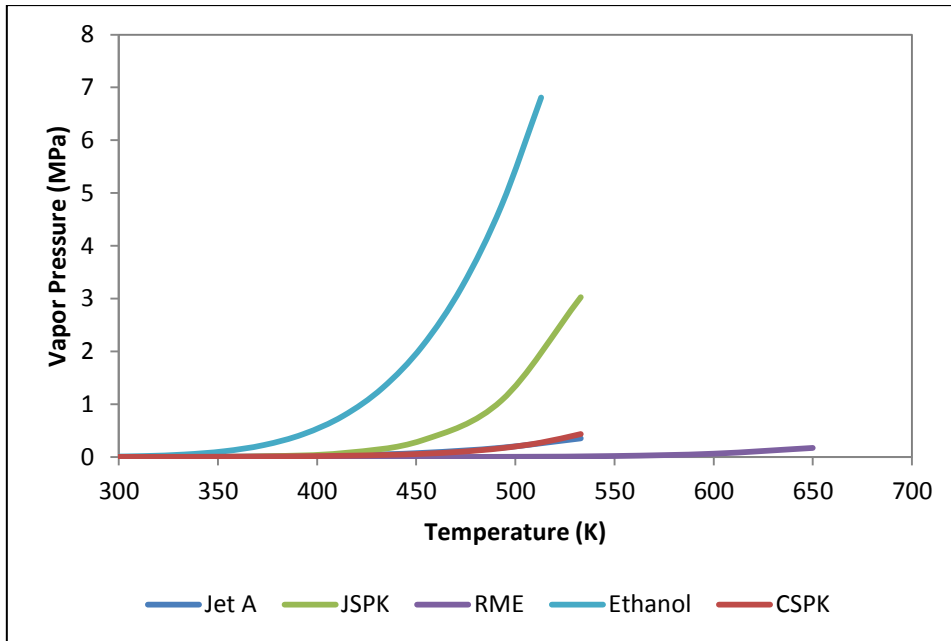


Figure 2-17: The Comparison of Vapour Pressure as a Function of Temperature

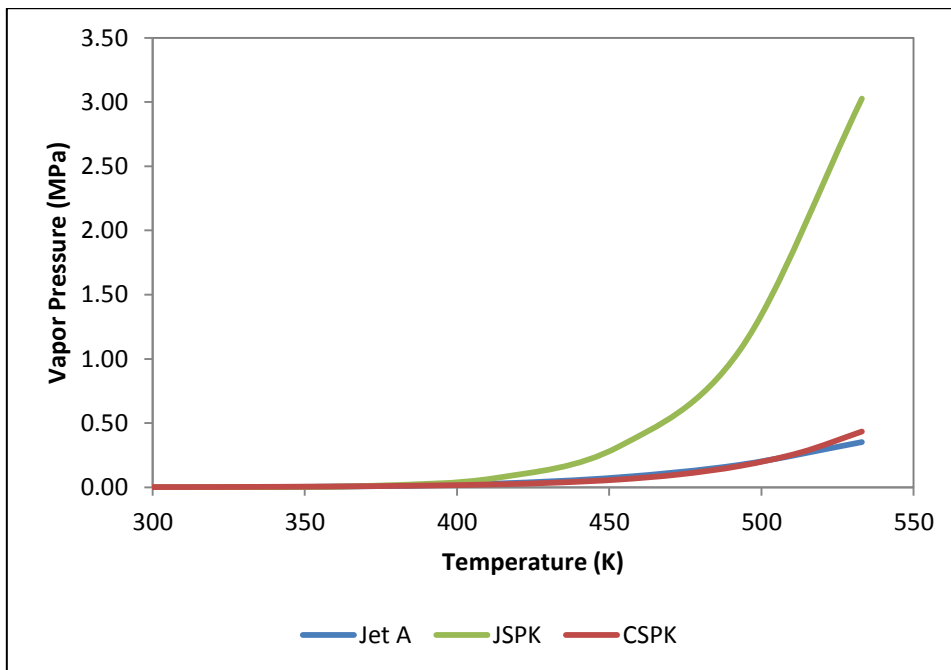


Figure 2-18: The Comparison of Jet-A, JSPK and CSPK as a Function of Temperature

Figure 2-17 presents the comparison of vapour pressure for the biofuels with Jet-A, whereas Figure 2-18 shows the clearer comparison of vapour pressure for JSPK, CSPK and Jet-A. In Figure 2-17, the vapour pressure of ethanol is obviously much higher than that of other fuels whilst RME is the lowest. Of the bio-SPK fuels, JSPK has relatively lower vapour pressure compared to CSPK which has no significant difference with Jet-A. In the process of evaporation, vapour pressure tends to indicate the rate of evaporation which is also important in controlling the level of air pollution. The indication of high and low vapour pressure of the liquid depends on the type of the molecules contained. If the molecules contained in the liquid have relatively strong intermolecular forces, the vapour pressure will be relatively low, whereas low intermolecular forces of molecules will determine the high vapour pressure.

Fuel with high vapour pressure indicates the tendency of the fuel to evaporate easily. It is also known as volatile. However, highly volatile fuel may be hazardous and proper fuel handling may be necessary.

#### 2.4.2 The Evaluation of Droplet Lifetime

Parrilla and Cortes (n.d) define droplet lifetime as the time of a droplet at a given initial size to evaporate and burn completely. According to Lefebvre (1989), the evaluation of droplet lifetime is important as it determines the residence time needed in order to ensure the completion of the combustion process. The droplet lifetimes of the selected fuels were calculated at ambient pressure,  $p_{amb}=1$  bar, initial droplet diameter,  $d_0= 20\mu\text{m}$ , and ambient temperature,  $T_{amb}=1000\text{K}$ .

**Table 2-5: Droplet Lifetime Comparison**

<b>Fuels</b>	<b>Droplet Lifetime (ms)</b>
<b>Jet-A</b>	1.07
<b>RME</b>	1.63
<b>Ethanol</b>	0.04
<b>JSPK</b>	0.97
<b>CSPK</b>	0.90

Table 2-5 shows the comparison of biofuels' droplet lifetime in comparison to Jet-A. It is observed that RME took the longest time to evaporate and consequently may have enough time to burn completely. On the other hand, ethanol took the shortest time which consequently may not have enough time to burn completely. The droplet lifetime of JSPK and CSPK is lower than that of Jet-A, although the difference is not significant.

### 2.4.3 The Comparison of Spray Penetration

Spray penetration determines the propagation distance of a droplet in the combustor during the evaporation process. In order to predict the penetration of the spray, the equation recommended by Sazhin *et al.* (2001) was used,

$$s = \frac{\sqrt{V_{in} D_0 t}}{(1 - \alpha_d)^{1/4} \tilde{\rho}^{1/4} \sqrt{\tan \theta}} \times \left( 1 - \frac{\sqrt{D_0}}{4 \sqrt{V_{in}} (1 - \alpha_d)^{1/4} \tilde{\rho}^{1/4} \sqrt{\tan \theta} \sqrt{t}} \right) \quad (21)$$

where  $s$  is distance measured from nozzle,  $V_{in}$  is the initial velocity,  $D_0$  is nozzle diameter,  $\theta$  is half the angle of the spray cone,  $\alpha_d$  is volume fractions of droplet

in spray,  $t$  is time whilst  $\tilde{\rho} = \frac{\rho_a}{\rho_d}$  is a dimensionless parameter.

Assuming  $D_0 = 1\text{mm}$  and  $\theta = 34.89^\circ$  (Lacava *et al.*, 2004) whilst  $\alpha_d$  was taken as  $1e^{-4}$ , the spray penetration of the biofuels was calculated, and the graph showing their penetration is presented in Figure 2-19 below.

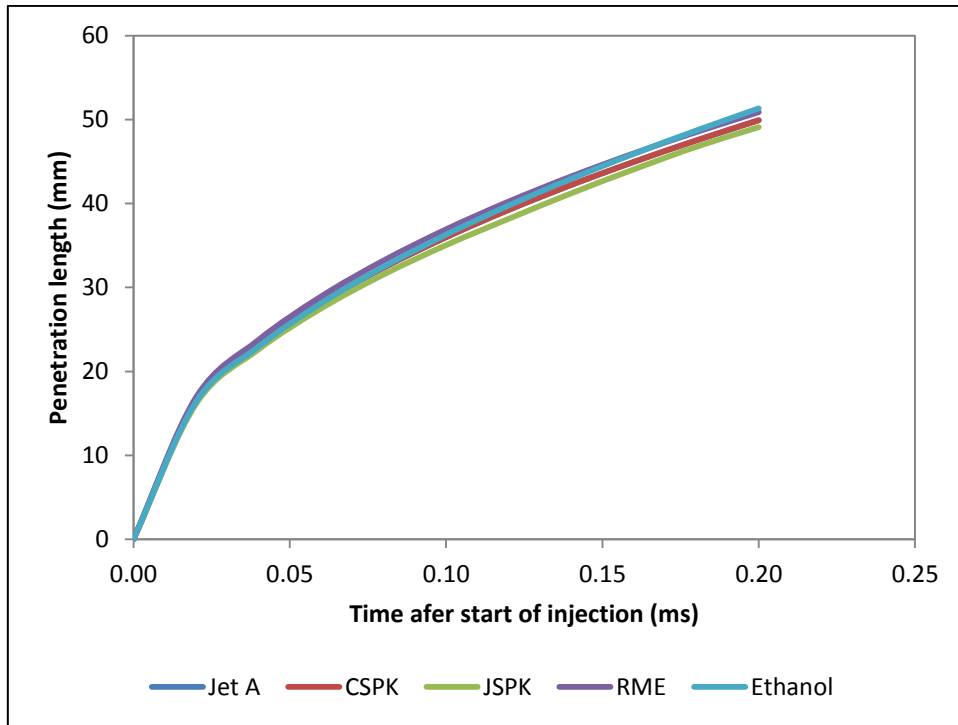


**Figure 2-19: The Comparison of Penetration Length**

Markedly, the spray penetration differences between bio-fuel and kerosine are not clear at the beginning of the injection. However, after 0.04 ms, the differences between kerosine and bio-fuel are observable. To see the picture of the spray behaviour more clearly, the comparison of penetration length measured after 0.08 ms is plotted and presented in Figure 2-20 below.

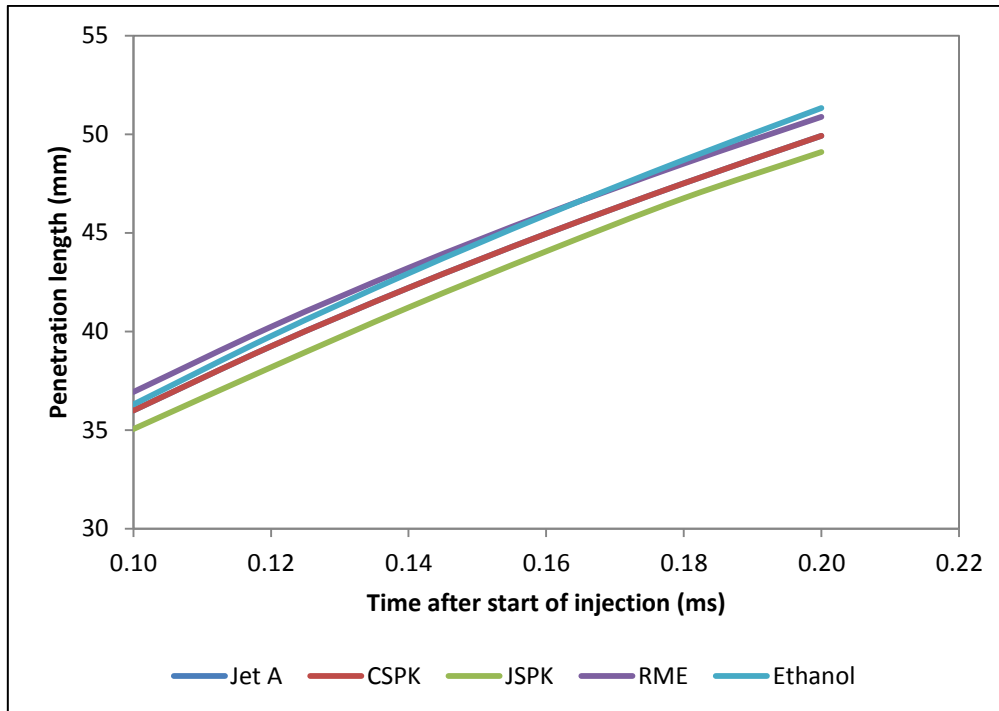


**Figure 2-20: Linear Increases of Spray Penetration Observed After 0.08 ms**

It can be clearly seen that all biofuels penetrate linearly with time. At up to 0.13 ms, the difference between the CSPK and JSPK spray penetration is unobservable. However, at 0.14 ms the difference in spray penetration for CSPK and JSPK is seen with JSPK penetrating longer than CSPK. Among all the biofuels, RME is observed to penetrate the longest (about 43.0 ms) while Jet-A is the shortest.

## 2.5 Discussions

### 2.5.1 The Effect of Boiling Temperature on Droplet Lifetime

According to Prommersberger *et al.* (1998), the droplet lifetimes of different fuels vary due to their different volatility which can be determined by their boiling point. The volatility is found to be proportionately reverse to the normal boiling temperature. High boiling point indicates less volatility, whilst a low boiling point specifies high volatility of the fuel. Essentially, the volatility of the fuel affects the ability of the fuel to vaporise and to form a combustible mixture with air. Greater volatility of the fuel thereby contributes to assisting its evaporation and it burns

more easily. The effect of boiling temperature on droplet lifetime is shown in Table 2-6 where ethanol, recognised as having the lowest boiling temperature, therefore has the shortest droplet lifetime amongst the others, whereas RME which has a high boiling temperature, spent a long time in the system as a liquid before fully evaporating and changing into the gaseous state.

Although it is observed that boiling temperature influenced the lifetime of the droplet, in the case of bio-SPK fuel which has an almost similar boiling temperature to Jet-A, the droplet lifetime of this type of fuel seems to not only depend on the boiling temperature, but also may be influenced by the viscosity of the fuel. The effect of viscosity during the atomisation is noted by Lefebvre and Ballal (2010) who mentioned in their study that more viscous fuel will have poorer fuel atomisation due to its effect on the evaporation rate. This observation concurs with the observations obtained in this work. It is observed that CSPK is less viscous than Jet-A and JSPK, which subsequently has a high rate of evaporation and therefore the lifetime of the droplet is much shorter than that of the others.

**Table 2-6: The Relation between Boiling Temperature and Viscosity with Droplet Lifetime**

<b>Fuels</b>	<b>Approx. Boiling Temperature (K)</b>	<b>Viscosity (mm<sup>2</sup>/sec) measured at -20°C</b>	<b>Droplet Lifetime (ms)</b>
<b>Jet-A</b>	<sup>a</sup> 513.75	<sup>a</sup> 8.00	1.07
<b>RME</b>	<sup>b</sup> 623.00	<sup>b</sup> 4.37 (at 40°C)	1.63
<b>Ethanol</b>	<sup>b</sup> 351.00	<sup>c</sup> 1.82 (at 10°C)	0.04
<b>JSPK</b>	<sup>a</sup> 512.25	<sup>a</sup> 3.663	0.97
<b>CSPK</b>	<sup>a</sup> 515.15	<sup>a</sup> 3.336	0.90

<sup>a</sup>Kinder (2010), <sup>b</sup>Rochaya (2007), <sup>c</sup>Marschall (1990)

### **2.5.2 The Effect of Density on Penetration Length**

In designing a combustor, the penetration of the spray is an important parameter that should be taken into account as it will affect the combustion performance. The penetration of a droplet has to be matched with the combustor size and geometry. If the droplet penetration is too short or

inadequate, the fuel-air mixing is unsatisfactory and the flame will appear in the fuel injector resulting in fuel coke and producing a great deal of soot. If penetration is too long, fuel will impinge on wall surface and combustor which results in the decrease of combustion efficiency and increase of emissions discharge. Thus, it is important to ensure the penetration of a droplet is just enough to avoid soot and at the same time ensuring that all the space in the combustion primary zone is used appropriately.

As mentioned above, the estimation of spray penetration was quantified using the equation recommended by Sazhin *et al* (2001). Most of the variables were kept constant; therefore the penetration length depends only on the fuel density. The influence of fuel density on spray penetration is noticeable, and is presented in Table 2-7 below.

**Table 2-7: The Influence of Density on Spray Penetration**

<b>Fuels</b>	<b>Approximated density (kg/m<sup>3</sup>) measured at 288K</b>	<b>Spray penetration measured at 0.14 ms time after start on injection (mm)</b>
<b>Jet-A</b>	810.7	42.21
<b>RME</b>	880.0	43.22
<b>Ethanol</b>	789.3	42.94
<b>JSPK</b>	749.0	42.21
<b>CSPK</b>	753.0	40.93

At the same time after the start of injection, it is observed that RME penetrates the longest consistent with the high density of the fuel. Although ethanol and JSPK have relatively low density compared to Jet-A, the spray penetration of ethanol is observed to be higher than that of Jet-A, which other factors may affect.

### **2.5.3 The Effect of Fuel's Viscosity on Spray Penetration**

Another factor that might affect the spray penetration is fuel's viscosity, as evident in the findings of this work, especially in comparing the bio-SPK fuels (CSPK and JSPK) with Jet-A. As far as Jet-A and bio-SPK fuels are concerned,

CSPK is known to have the lowest viscosity (3.336 mm<sup>2</sup>/s), followed by JSPK (3.663 mm<sup>2</sup>/sec) and kerosine (8.0 mm<sup>2</sup>/sec) (Kinder 2010), consequently provides the lowest penetration amongst the others. The effect of a fuel's viscosity on spray penetration also is in agreement with Rochaya (2007), who observed an increase in spray penetration as the viscosity of the fuel increased. This observation was obtained due to the high viscous fuel and heavier fuels not being able to be well atomised, hence having an adverse effect on the fineness of atomisation due to there being less air resistance. Therefore, any fuel with low viscosity will have an advantage to the spray atomisation which consequently helps in controlling the pollution discharge.

#### **2.5.4 The Influence of Mixing Biofuel with Kerosine**

As pure biofuel is not suitable for use in aircraft engines due to its low density consequently may require engine modification, mixing biofuel with kerosine is found to be the best solution as far as the emissions are concerned. To quantify the droplet lifetime and spray penetration of the biofuel and kerosine mixture, the evaluation was performed for the blend of 50% JSPK with 50% kerosine (B50).

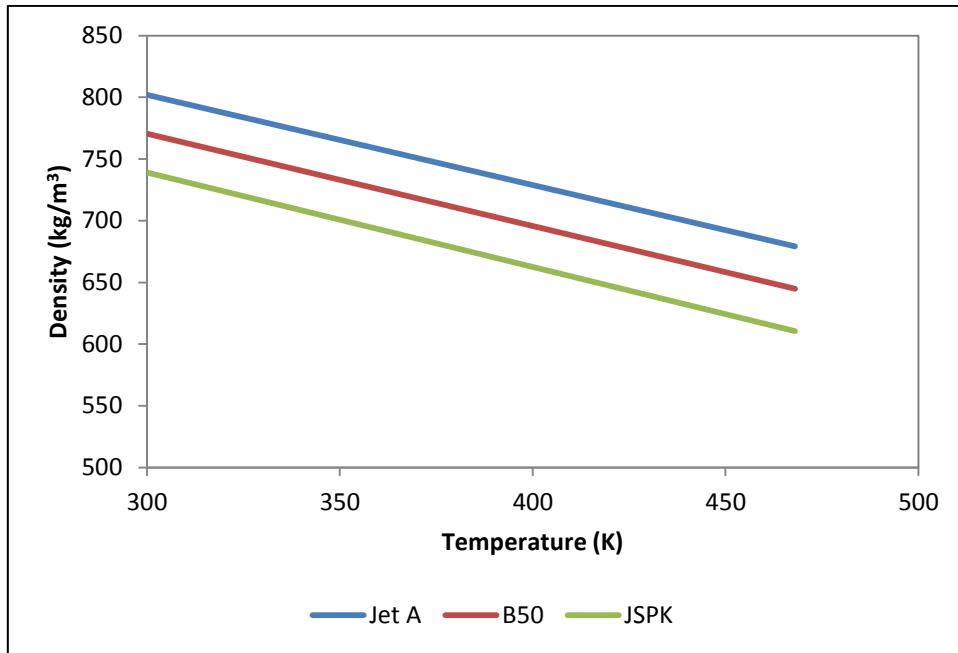


**Figure 2-21: The Comparison of Density between B50, Jet-A and Pure JSPK**

As mentioned earlier, the density of the fuel is related to the amount of fuel that can be stored in the fuel tank and injected into the combustion chamber. Fuel with high density may cause problems for the fuel injector. Therefore, in order to implement highly dense fuel in the combustor chamber, modification to the fuel injector is necessary. In ensuring the gas turbine fuel is able to be operated well without modification to the fuel injector, implementing biofuel in the chamber should accommodate the gas turbine fuel's density range. Blending 50% with 50% Jet-A has increased the fuel's density to be within the gas turbine fuel density range and therefore it can be used in the gas turbine without modification.

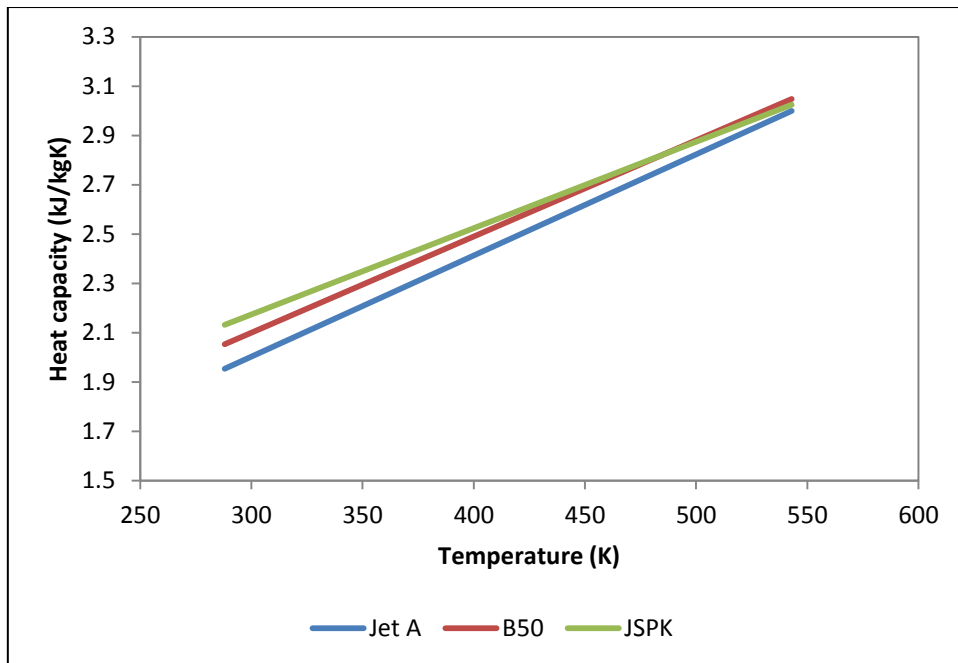


**Figure 2-22: The Comparison of Heat Capacity between B50, Jet-A and Pure JSPK**

By blending JSPK with Jet-A, an improvement in heat capacity is also observed. In comparison to Jet-A, increases in heat capacity of B50 may provide an advantage to the engine thrust.

**Table 2-8: The Comparison of Droplet Lifetime for the Blend Fuel**

Fuels	Fuels composition (%)	Boiling temperature (K)	Droplet Lifetime (ms)
Jet-A	100% Jet-A	513.75	1.07
B50	50% JSPK 50% Jet-A	513.45	1.03
JSPK	100% JSPK	512.25	0.97

As observed, as the percentage of JSPK in the mixture increases, the lifetime of the droplet reduces. This reduction is consistent with the reduction of boiling temperature indicating the increase in the fuel's volatility and increases the tendency of the droplet to evaporate from liquid to the gaseous phases.

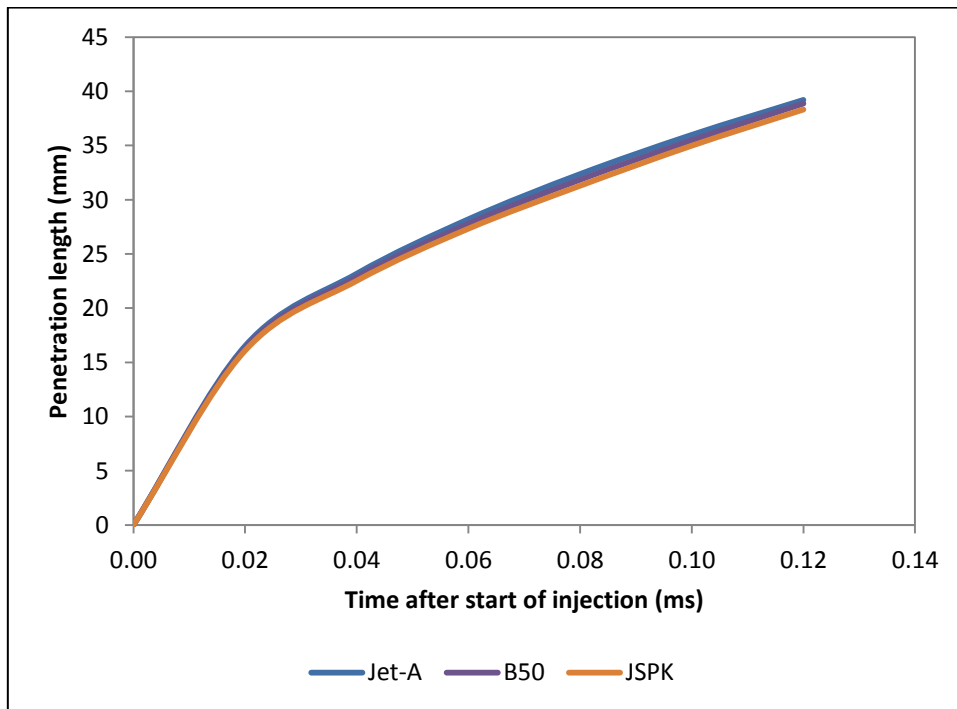


**Figure 2-23: The Comparison of the Penetration Length Predicted between B50, Jet-A, and Pure JSPK**

The comparison of spray penetration for the mixture of JSPK with kerosine is shown in Figure 2-23. Table 2-9 shows the comparison of penetration length measured at 0.12 ms. As expected, blend 50% JSPK with 50% Jet-A reduces the spray penetration due to the reduction of fuel density. The reduction also

corresponds to the reduction of fuel viscosity which also is one of the factors effecting the spray penetration.

**Table 2-9: The Comparison of Penetration Length Measured at 0.12 ms**

<b>Fuels</b>	<b>Fuels composition (%)</b>	<b>Density (15°C) (kg/m<sup>3</sup>)</b>	<b>Viscosity (at - 20°C) (mm<sup>2</sup>/sec)</b>	<b>Penetration length measured at 0.12 ms (mm)</b>
<b>Jet-A</b>	100% Jet-A	810.7	8.000	39.20
<b>B50</b>	50% JSPK 50% Jet-A	779.0	3.606	38.87
<b>JSPK</b>	100% JSPK	749.0	3.663	38.32

## 2.6 Conclusions

The objective of this assessment is to investigate the influence of fuel density, viscosity and volatility on the spray characteristics (i.e. droplet lifetime and spray penetration). This assessment has been established due to the intention of the airline industry of looking towards the utilisation of bio-SPK type of fuel in their aircraft engines. It is known that although factors such as ambient condition have an impact on the spray characteristics, however in case of new fuels which certainly involve difference fuel properties, the influence of such properties becomes essential.

In the present study, two different types of bio-SPK fuels were used, whilst in order to clearly observe the importance of fuel properties on spray characteristics, two other fuels covering a large variation of density, viscosity, and volatility were also used. JSPK and CSPK were used in this study due to the successful test flights conducted using the mixture of these fuels with kerosine in one of the engines. Additionally, RME and ethanol were chosen, representing the high density and volatility of fuel respectively. The influence of fuel properties on spray characteristics was compared with Jet-A as the baseline fuel.

In undertaking the investigation, the properties of the selected fuels were gathered either from the open literature or by estimation through the fuel

composition. The influence of biofuels' properties towards combustor characteristics was tested using the evaporation model taken from FLUENT.

The main properties of the fuel—notably volatility, density and viscosity—mainly affect the combustion performance. Results suggest that high-volatility fuel such as ethanol requires less time compared to low-volatility fuel (RME), which needs additional time to evaporate and change from liquid to the gaseous phase. In addition, the effects of fuel viscosity are found to influence the penetration of the fuel. Notably, fuel which has high viscosity is found to penetrate longer compared with low-viscosity fuel. Besides viscosity, density is also observed to affect the penetration of the spray, although not to a significant extent. In assessing the influence of spray penetration on combustion efficiency, it is an advantage for the fuel that penetrates shorter as too long penetration could induce the impingement of the liquid fuel on the combustor walls which therefore tends to reduce the combustor efficiency and increase the emissions, particularly soot emissions.

In comparison to Jet-A, the low viscosity of JSPK and CSPK provides shorter penetration length which therefore provides an advantage as it reduces the fuel impingement. However, too short penetration will affect the air utilisation and may provide worse combustion due to reduced spray area. Therefore, it is essential to have the spray which penetrates for not too long and not too short in order to ensure an effective combustion rate, and at the same time doesn't encourage any fuel impingement on the combustor walls.

If we consider that pure JSPK, which penetrates shorter than other fuels, will diminish the combustion rate, blending this fuel with Jet-A is ultimately an effective solution as it improves the spray penetration due to the improvement in its viscosity. Additionally, in comparison with pure JSPK, blending JSPK with Jet-A also increases the fuel density, hence being of benefit to the implementation of this fuel in the combustion chamber as no modification is required. JSPK provides shorter droplet lifetime in comparison to Jet-A, which improves the process of evaporation, but implementing JSPK in the chamber is challenging due to the low density of this fuel and therefore might require

modification to the combustor. Therefore, by blending JSPK with Jet-A, the droplet lifetime still can be improved, although the improvement is not significant. Additionally, the density of this fuel is also improved, hence can be used directly in the engine without any engine modification being necessary.

## **3 EVALUATION OF BIOFUELS ENGINE PERFORMANCE**

### **3.1 General Introduction**

Since early 1998, the study of biofuel was performed under experimental conditions, investigating the performance of an engine running with a blend of biofuel and kerosine at a certain percentage. Since then, the interest in biofuel has expanded quickly, from performing the study experimentally in a small scale engine to investigating the performance in a real aircraft engine. For example, Rahmes *et al.*, (2009) investigated the performance of bio-SPK fuel in Boeing aircraft. However, the investigation was performed at off-wing engine ground tests only, which limited the information available relating to other conditions of aircraft in the flight envelope. Therefore, the establishment of this study is essential to increase the amount of information by evaluating the performance of bio-SPK fuel particularly in different flight envelopes.

The establishment of this assessment also was encouraged by the intention in providing different kinds of fuel selection that available in PYTHIA, and to test the ability of PYTHIA in evaluating the biofuel engine performance. For information, PYTHIA is a computer program developed in Cranfield University which is capable to evaluate the performance of all types of engine, whether stationary or aircraft engine. The evaluation can be conducted for both design point and off-design point conditions. Unfortunately, this computer program only evaluates kerosine as the fuel.

### **3.2 Gas Turbines and the Factors that Affect the Performance**

Gas turbine engines have been used for aircraft propulsion, industrial application, and also for marine and land transportation. In general, a gas turbine consists of a compressor, a combustor and a turbine. The function of the compressor is to compress the incoming air to increase its pressure before entering the combustor. In the combustor, fuel is added and will combine with

high-pressure air from the compressor outlet in order for combustion to take place. The power provided through the combustion process is then extracted by the turbine. For aircraft, the useful power extracted by the turbine is accordingly converted into thrust in order to move the aircraft. The schematic diagram of gas turbine engine for aircraft application is shown in Figure 3-1 below.

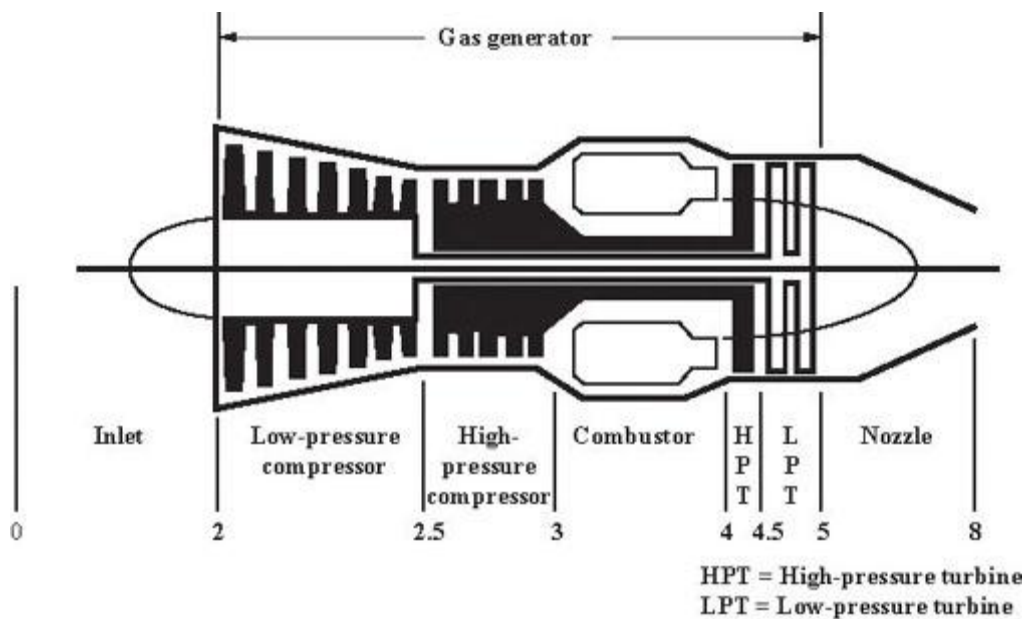


**Figure 3-1: Schematic Diagram of Turbojet Engine (Mattingly, 1996)**

Air temperature, site elevation, humidity and losses are factors which influence the gas turbine engine performance. In addition, fuel type is a further factor potentially affecting the performance (Brooks, 2000). According to Brooks, there are two reasons regarding how fuel type could affect engine performance: heat capacity and low heating value. The influence of heat capacity is due to the work produced from the gas turbine engine being a product of mass flow, heat energy in the combusted gas ( $C_p$ ), and temperature differential across the turbine.

$$W = \dot{m}C_p(T_4 - T_3) \quad (22)$$

Moreover, mass flow  $\dot{m}$  is a sum of compressor airflow and fuel flow, whereas  $C_p$  is a function of fuel elements and the products of combustion.

$$\dot{m} = \dot{m}_a + \dot{m}_f \quad (23)$$

Equation (23) shows a direct proportion of work and  $C_p$ . Brooks (2000) mentioned that work increases as  $C_p$  increases, as indicated by an increase in almost 2% more work output of natural gas (methane) than distillate oil, owing to higher specific heat of natural gas. A high specific heat of natural gas is due to the higher content of water vapour produced by higher hydrogen to carbon ratio.

The influence of the low heating value of fuel on turbine output is shown in Figure 3-2. It can be seen that in the case of fuel comprising only hydrocarbon ( $C_xH_y$ ) with no inert gas and oxygen atoms, the turbine output is proportional with LHV. In the case of fuel containing a large amount of inert gas, turbine output will be inversely proportional to LHV. However, this becomes a problem, and therefore needs to be considered when burning lower heating values fuel.

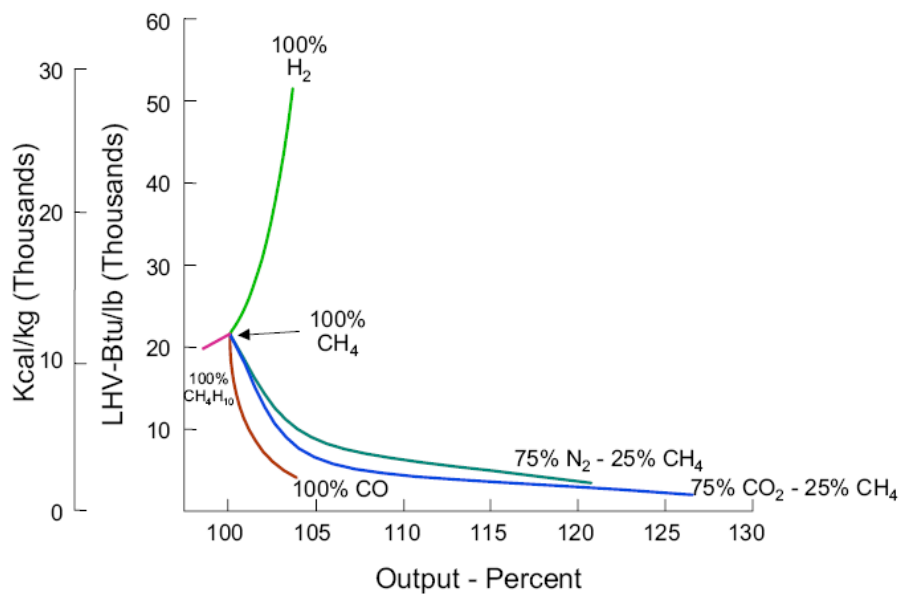


**Figure 3-2: Effect of Fuel Heating Value on Turbine Output (Brooks, 2000)**

Another factor corresponding to fuel type that might affect gas turbine performance is the fuel-air-ratio (Palmer, 1945), as shown in Figure 3-3.

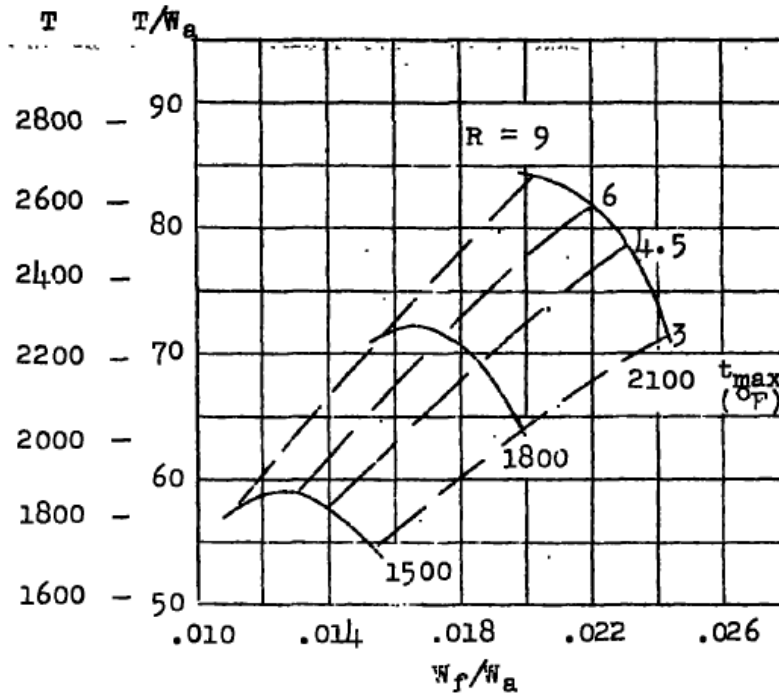


**Figure 3-3: Effect of FAR, Pressure Ratio and Maximum Temperature on Thrust at Sea Level (Palmer, 1945)**

In his study, Palmer concluded that although the maximum thrust has a close relationship with pressure ratio, fuel-air ratio and combustion chamber temperature, it is nevertheless recognised that at any particular temperature, the influence of fuel-air ratio towards thrust is more pronounced than changes in pressure ratio.

### 3.3 Requirement for the Engine Performance Evaluation

Two bio-fuels are considered in this work—Camelina Bio-synthetic Paraffinic kerosine (CSPK) and Jatropa Bio-synthetic Paraffinic kerosine (JSPK)—both of which have recently been used in flight tests. The evaluation of engine performance in this study focuses on the blend of CSPK, and JSPK at 20%, 40%, 60% and 80% with kerosine respectively in order to provide information for optimisation work later.

Cranfield University owns an engine performance software with the capability of simulating the performance of any type of gas turbine engine whether it is stationary gas turbine or aircraft gas turbine engine—both in design point and off-design point condition. A previous version of PYTHIA which has been used to simulate engine performance (PYTHIA version 2.8) only provides the capability of simulating kerosine (Jet-A), Diesel, UK Natural gas (UKna), and Africa Natural gas (AFna). In order to simulate CSPK and JSPK in PYTHIA, the gas properties of the fuels have to be introduced into the software. In order to achieve this, the gas properties data for CSPK and JSPK have to be generated before they can be used in PYTHIA.

The evaluation of CSPK and JSPK in aircraft engines has been carried out in two different conditions: design point and constant mass flow condition. The results obtained from these two conditions are assessed by comparing them with Jet-A as a baseline fuel.

### **3.3.1 Computer Tools Used**

Two computer tools were used for this assessment – NASA's chemical equilibrium (CEA) and PYTHIA.

NASA CEA was used to generate tabulated data consisting of the JSPK and CSPK fuel properties over wide range of temperature, pressure, fuel-air ratio and water-air ratio. The properties that were generated include density, heat capacity, enthalpy, entropy, gamma, and viscosity.

PYTHIA is a 0D engine performance computer tool available in Cranfield University using gas-path analysis technique. This well-established engine performance tool has been developed in Cranfield with it's well-known capability of evaluating any type of gas turbine engine either in design point or off-design point condition.

### 3.3.2 Fuels' Caloric Properties Data Generation

The performance of aircraft engines running with bio-fuel has been evaluated using PYTHIA. PYTHIA is a 0D computer program able to evaluate engine performance including engine deterioration and engine diagnostics with the use of a gas-path analysis technique. The capability of PYTHIA in terms of evaluating gas turbine engines—both at design point and off-design point—has already been established. For instance, (Naeem *et al.*, 1998) used PYTHIA to assess the implications of engine deterioration for fuel usage in F-18 aircraft.

The capability of PYTHIA regarding evaluating engines running with bio-fuels has not yet been evaluated; therefore, this study took the opportunity to introduce, apply and evaluate bio-fuels in PYTHIA. In this case, the caloric properties of bio-fuels which are required in PYTHIA—heat capacity, enthalpy, viscosity, gamma, entropy and gas constant—have to be introduced into the software.

Tabulated data containing fuel calorific properties over a wide range of temperatures, pressures, fuel-air ratio and water-air ratio for the bio-fuels' properties has been developed based on work conducted by Kamunge (2011), who developed a FORTRAN code in conjunction with NASA's chemical equilibrium program (CEA) (McBride, J. B. and Gordon, S., 1996) to generate the caloric properties for dry air, moist air, UK Natural gas and Hydrogen. Kamunge also introduced the interpolation routine in the code allowing more accurate data reading. The use of NASA CEA in generating fuel caloric properties has also been implemented in the study conducted by Sethi (2008).

Since the bio-fuels considered in this study are not included in NASA CEA thermodynamics' library, alternatively, other information—such as molecular formula and the heat of formation of the fuels—are required; however, this cannot be easily obtained in open literature, hence the molecular formula of the fuels is estimated from the composition of carbon and hydrogen in the fuel, whilst the heat of formation is estimated by calculating backwards from the heat of the combustion of fuels. The calculation of the molecular formula and heat of

formation for the selected bio-SPK fuels – JSPK and CSPK can be found in Appendix C.

**Table 3-1: Estimation of Molecular Formula and Enthalpy of Formation for JSPK and CSPK**

Fuel	JSPK	CSPK
% of Carbon (*)	85.4	85.4
% of Hydrogen (*)	15.5	15.1
Heat of Combustion (MJ/kg) (*)	44.3	44.0
Chemical formula	C <sub>12</sub> H <sub>26</sub>	C <sub>12</sub> H <sub>25.4</sub>
Heat of Formation (kJ/mol)	-330.50	-335.45

\* (Kinder and Rahmes, 2009)

### 3.3.3 Validation of Data Generation

In validating the fuel's caloric properties data generated, the percentage difference of the fuel's data is compared with data available in Powell *et al*, (1955). Due to the inconsistency of the predicted fuel's molecular formula with the molecular formula considered in Powell *et al* (1955) (C<sub>n</sub>H<sub>2n</sub>), some errors are expected. Therefore importantly, it should be highlighted that the purpose of comparison of data generated in this work to data obtained by (Powell *et al.*, 1955) is not to verify the accuracy but rather to evaluate whether the tabulated data generated of the chosen bio-fuels are reasonable and dependable for use.

In evaluating the percentage difference of data generated to data available in literature, Equation (24) below is used.

$$\frac{GP_{ref} - GP_{table}}{GP_{ref}} \times 100 \quad (24)$$

where:

GP<sub>ref</sub> is reference to the caloric property obtained from literature

GP<sub>table</sub> is the caloric property obtained in this work.

Comparisons of caloric property for dry air and moist air have been evaluated in (Kamunge, 2011); therefore, this is not going to be repeated in this work.

Comparisons for JSPK and CSPK relative to data from literature were performed at an equivalence ratio of 0.25 and at a pressure of 10 atm. The comparison was carried out at a low temperature ranging from 300K–1000K, and at high temperature ranging between 1200K and 3000K.

### 3.3.4 Evaluation of Bio-fuel in Two-Spool High Bypass Turbofan Aircraft Engine

To demonstrate the performance of bio-fuels in aircraft engines, the evaluation of bio-fuels was carried out in a two-spool high bypass turbofan engine (Figure 3-4). Simulation was achieved through PYTHIA, an engine performance computer tool owned by Cranfield University which already integrated with the generated caloric properties data, and also was modified to be able to assess biofuels. The two-spool high bypass turbofan engine (Figure 3-4) was translated into PYTHIA, as shown in Figure 3-5.

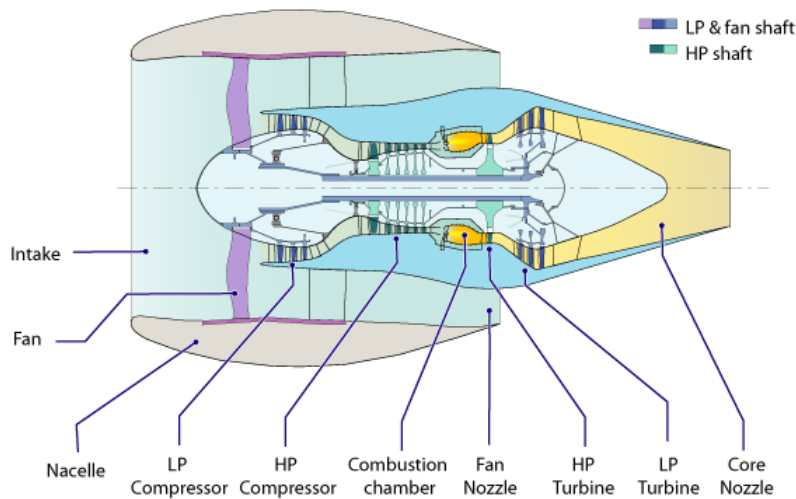


**Figure 3-4: Components in Two Spool High Bypass Turbofan Engine**

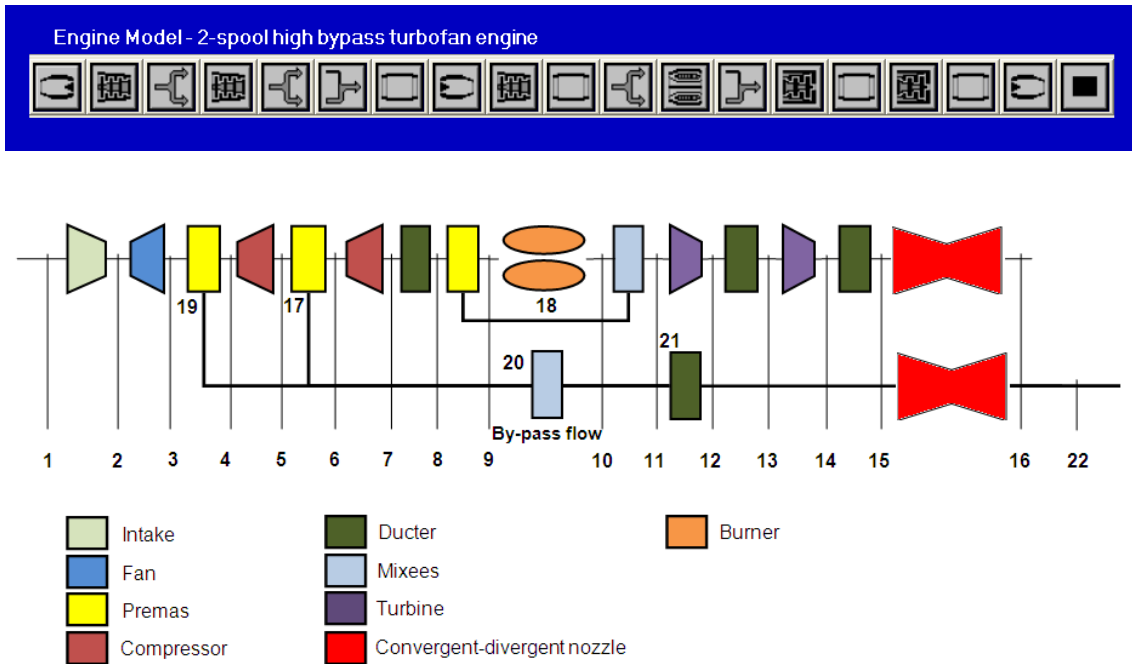


**Figure 3-5: Schematic Diagram of Two Spools High Bypass Turbofan Engine used in this Work**

The evaluation of bio-fuels in a two-spool high bypass turbofan engine was achieved through two case studies, as follows:

### 1. Design Point

In this case, the engine was simulated using engine parameters of a two-spool high bypass turbofan engine, available in the public domain. The cruise condition was considered to be evaluated as design point, as most of the civil aircraft are operated primarily at this condition. The engine characteristics regarding a two-spool high bypass turbofan engine flying at cruise were obtained from public domain (<http://www.jet-engine.net/civtfspec.html>). This includes altitude, Mach number and thrust generated. Based on this information, other engine parameters such as component efficiencies, pressure ratios for each engine component, air bleeds, air flow rate and TET were estimated to achieve as close as possible to the thrust generated in that

condition. The engine characteristics' parameters at the cruise condition used in this work are presented in Table 3-2.

**Table 3-2: Parameters for the Chosen Engine**

<b>Parameter</b>	<b>Unit</b>	<b>Value</b>
Altitude	m	10668
W	kg/sec	130
M		0.8
TET	K	1660.0
BPR		5.46
FPR		1.8
IPCPR		1.811
HPCPR		10.0
OPR		32.6
Power off take from HPT	kW	200

## 2. Constant Mass Flow Condition

The other case that was considered in this work was a constant mass flow condition. In this alternative off-design condition, the same engine characteristic parameters as in design point were applied. Only TET was disabled. At constant mass flow condition, the amount of air and fuel flow was kept constant for all the blends during the simulation. Considering that the LBO margin between Jet-A and the chosen Bio-SPKs fuel can be viewed as equivalent (Rahmes *et al.*, 2009), this case was selected in an attempt to provide the constant LBO condition between the fuels. In order to do that, the amount of fuel fed into the combustor was fixed at an amount that allows the engine to burn lean (equivalence ratio < 1). Considering that LBO for Jet-A is equivalent to the chosen Bio-SPK fuel, therefore the same amount of fuel was considered to be fed into the combustor as Jet-A (baseline fuel).

For both conditions, the evaluation was performed for pure bio-fuels (100% bio-fuels), and as 20%, 40%, 60%, and 80% of biofuel which blends with 80%, 60%, 40% and 20% of Jet-A respectively.

## 3.4 Results

### 3.4.1 Data Validation

The validation of gas properties data generated from NASA CEA for JSPK and CSPK was achieved by comparing the values with those obtained from (Powell *et al.*, 1955). As mentioned above, (Powell *et al.*, 1955) generated data for chemicals with a molecular formula of  $C_nH_{2n}$ . Comparing data regarding JSPK ( $C_{12}H_{26}$ ) and CSPK ( $C_{12}H_{24.5}$ ) obtained from this work alongside with data gathered by (Powell *et al.*, 1955), some error is observed, though not considered to be significant. The average of error produced is shown in Table 3-3 below.

**Table 3-3: Average Error of Data Generated Relative to Data from Literature**

	Low temperature		High temperature	
	JSPK (%)	CSPK (%)	JSPK (%)	CSPK (%)
<b>Density</b>	0.14	0.10	0.15	0.11
<b>Heat capacity, <math>C_p</math></b>	0.11	0.07	0.30	0.25
<b>Enthalpy differentiation, <math>\Delta H</math></b>	0.25	0.25	0.30	0.30
<b>Entropy differentiation, <math>\Delta S</math></b>	0.30	0.30	1.00	1.00

At both low and high temperature, the average error of JSPK and CSPK in relation to the molecular formula of  $C_nH_{2n}$  is similar for both  $\Delta H$  and  $\Delta S$ . However, for density and heat capacity, the average error of CSPK is less than JSPK owing to the lesser difference between the molecular formula of CSPK with the molecular formula used in the literature.

The comparison between data generated for JSPK and CSPK with data available from the literature do not show any significant differences. The highest difference is reported at a high temperature of 1%. Apparently, the differences are not significant and therefore the data generated is acceptable and able to be used for further engine performance evaluation.

### 3.4.2 Engine Performance Validation

The predicted engine performance calculated in this work was compared with the engine performance predicted in the experimental work from Rahmes *et al.*, (2009) who conducted an off-wing engine ground test for 50% Jatropha-Algae/50% Jet-A. It appears that, the fuel blend used in this off-wing engine ground test was not similar to that evaluated in this work, although they are of the same family. The fuel used in the off-wing ground test is a mixture of two bio-SPK fuels with Jet-A, while fuel used in this research is a mixture of one bio-SPK fuel with Jet-A. However, the total composition of bio-SPK fuel in the mixture was taken as the same. Although the fuel mixture in the literature is different to the one used in this work, it is not expected to have significant difference in the trends.

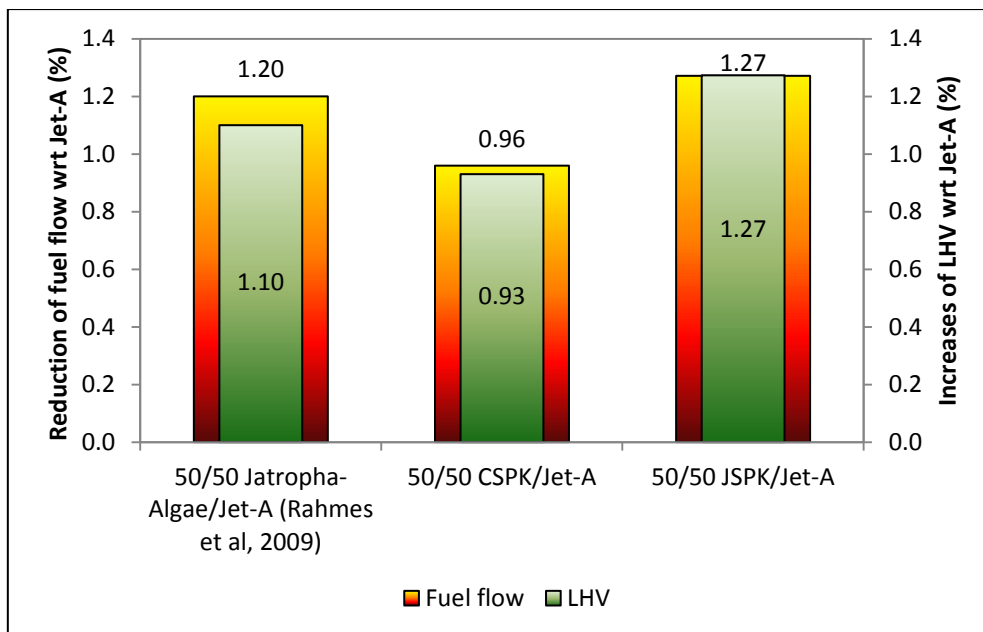


**Figure 3-6: The comparison of Fuel flow and Heating Value with Literature**

Figure 3-6 shows the percentage difference of fuel flow reduction and percentage difference of increased LHV wrt Jet-A over the fuels used in this work and in the literature. It is observed that the reduction of fuel flow expected from this research work is consistent with the reduction of fuel flow predicted in the literature. As expected, the relationship between the fuel flow reductions

predicted in this research work is consistent with the increases of LHV as predicted in the literature.

This comparison assessment summarises that the calculated molecular formula and enthalpy of formation used in generating the caloric properties data as the input for PYTHIA can be relied upon and the capability of PYTHIA of conducting the engine performance evaluation is dependable.

### **3.4.3 The Influence of Biofuel Mixture during Cruise Condition**

The performance of the two-spool high bypass turbofan engine running with the selected fuel composition was simulated at a design point condition (cruise) by implementing the engine configuration as in Table 3-2. First, the simulation was conducted with Jet-A as the baseline fuel. Then, the simulation was carried out for the other fuel compositions by changing the percentage of biofuel and the heating value of the fuel. None of the other engine parameters were changed. Finally the comparison of thrust, fuel flow and specific consumption for the difference of fuel composition were compared with Jet-A.

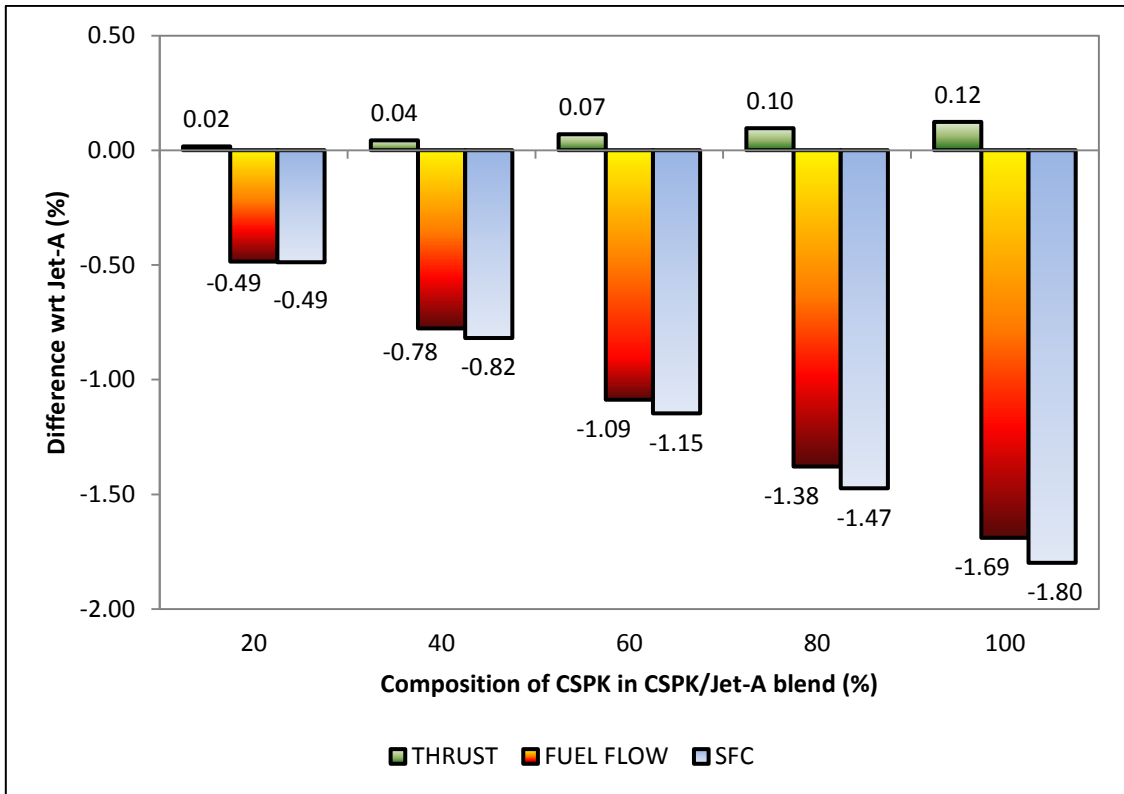


**Figure 3-7: Comparison of Thrust, Fuel Flow, and SFC of Pure CSPK and CSPK/Jet-A blend with Jet-A**

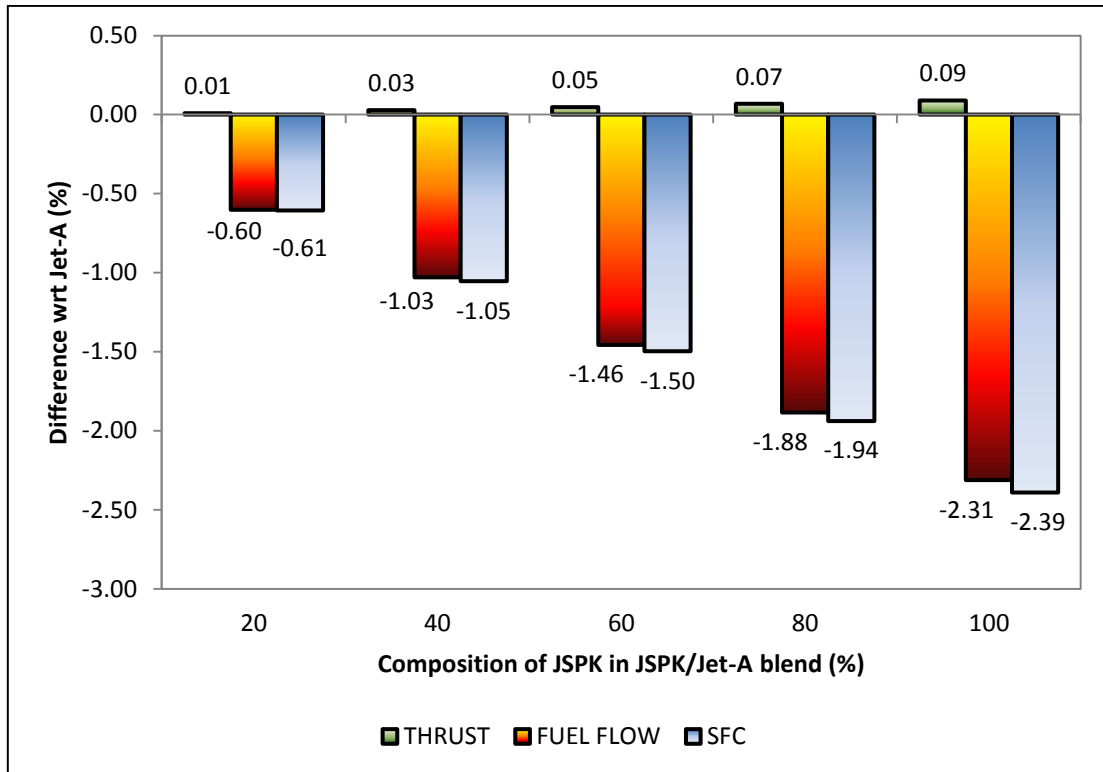


**Figure 3-8: Comparison of Thrust, Fuel Flow, and SFC of JSPK/Jet-A blend with Jet-A**

Figure 3-7 and Figure 3-8 show the percentage difference of engine thrust, fuel consumption and SFC predicted from the implementation of CSPK and JSPK either as a pure or by blend with Jet-A in two-spool high bypass turbofan engines. Both fuels show the same trend in terms of predicted thrust, fuel flow and SFC. Both fuels show increases in thrust, reduction in fuel flow and improvement in SFC, although the improvement is considered small and not significant. The same trend is also observed as the composition of bio-SPK fuel in the blend increases.

The highest increases in thrust, reduction of fuel flow and improvement in SFC are observed when 100% of bio-SPK fuel was used. Between both fuels, CSPK provides higher improvement in thrust (0.12%) compared to JSPK (0.09%). However, the fuel flow and SFC of the two-spool high bypass engine simulated at design point condition were reduced (improved) by 2.31% and 2.39%, respectively as JSPK was used as opposed to CSPK.

### 3.4.4 The Influence of Biofuel Mixture at Constant Mass Flow Condition

This alternative off-design condition was simulated to evaluate the performance of pure bio-fuels and the blends for thrust and SFC when the same amount of fuel is supplied to the combustor. The similar engine characteristics as at design point condition were applied, while TET was disabling. In this condition, the amount of fuel supplied is assumed as 0.52 kg/s, leading to FAR = 0.02 (Equivalence ratio ~ 0.4). The percentage difference of thrust, TET and SFC of JSPK and CSPK and the blend with Jet-A were presented.

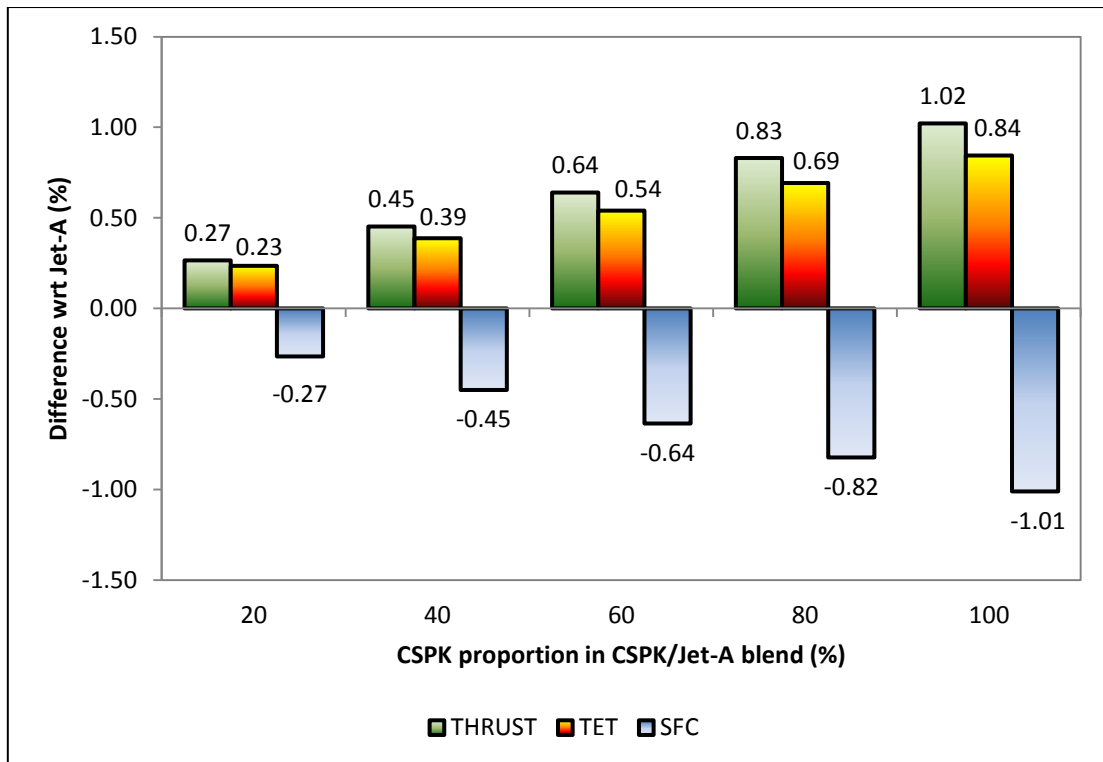
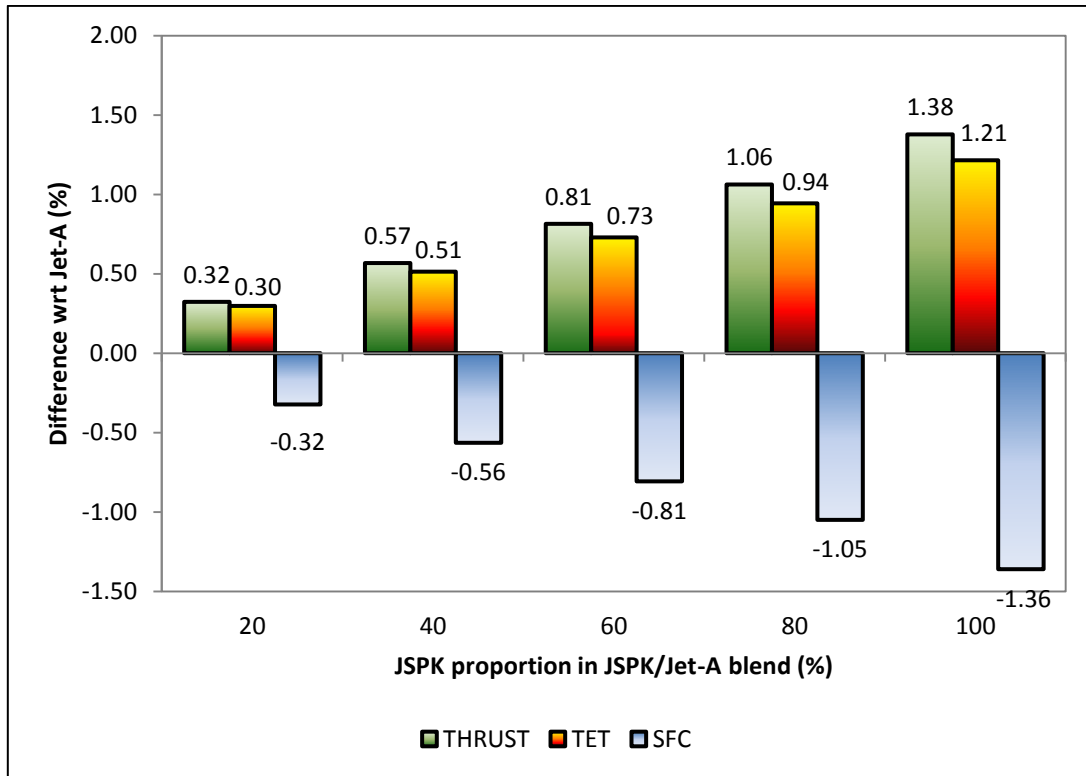


Figure 3-9: Comparison of Thrust, TET, and SFC of CSPK/Jet-A blend Compared to Jet-A



**Figure 3-10: Difference of Thrust, TET, and SFC of JSPK/Jet-A blend Compared to Jet-A**

Both fuels show the same trend in terms of the increases in thrust, TET and improvement (reduction) in SFC. The same trend is also observed as the percentage of biofuel in the mixture increases. The production of thrust, increases of TET and improvement in SFC are observed to be changed linearly with the percentage of biofuel in the mixture. Implementing 100% of CSPK and 100% JSPK in the aircraft engine provides the highest thrust and better improvement in SFC compared to blending it with Jet-A. However, in comparison to CSPK, JSPK produced more thrust and improved SFC by 1.38% and 1.36% respectively. The increases of thrust produced by JSPK and CSPK are consistent with the increases in TET which are known to be proportionate to the thrust generation.

## **3.5 Discussion**

### **3.5.1 The Influence of LHV on the Engine Thrust**

Both assessments (at cruise and constant mass flow condition) show an improvement in thrust owing to high value of LHV of the selected fuels (JSPK = 44.3 MJ/kg; CSPK = 44.0 MJ/kg) in comparison to Jet-A (43.2 MJ/kg). The improvement in thrust is also observed as the percentage of biofuel in the mixture increases.

The effect of LHV on engine performance, particularly thrust, has been widely known, and so will not be discussed in detail in this work. However, it is worth mentioning here that these results are consistent with Brooks (2000), who correlates the work with LHV in a gas turbine engine. In the case of fuel that comprises only a hydrocarbon ( $C_xH_y$ ) component, work from a gas turbine engine is found to be directly proportional to LHV. But for fuel with inert gas content, the correlation is found to be inversed proportionally. Considering that fuels chosen in this study are in  $C_xH_y$  format, the effect of LHV on thrust is pronounced.

### **3.5.2 The Effect of Heat Capacity on Engine Thrust**

Another factor that might influence the increases in thrust generated by an aircraft engine is fuel's heat capacity, as observed in Figure 3-11. The thrust generated by 100% CSPK is much higher than 100% JSPK. This difference is observed to not be significantly affected by high LHV but rather due to high heat capacity of CSPK in comparison to JSPK. It is observed that due to high heat capacity, CSPK produced the most thrust amongst the others.

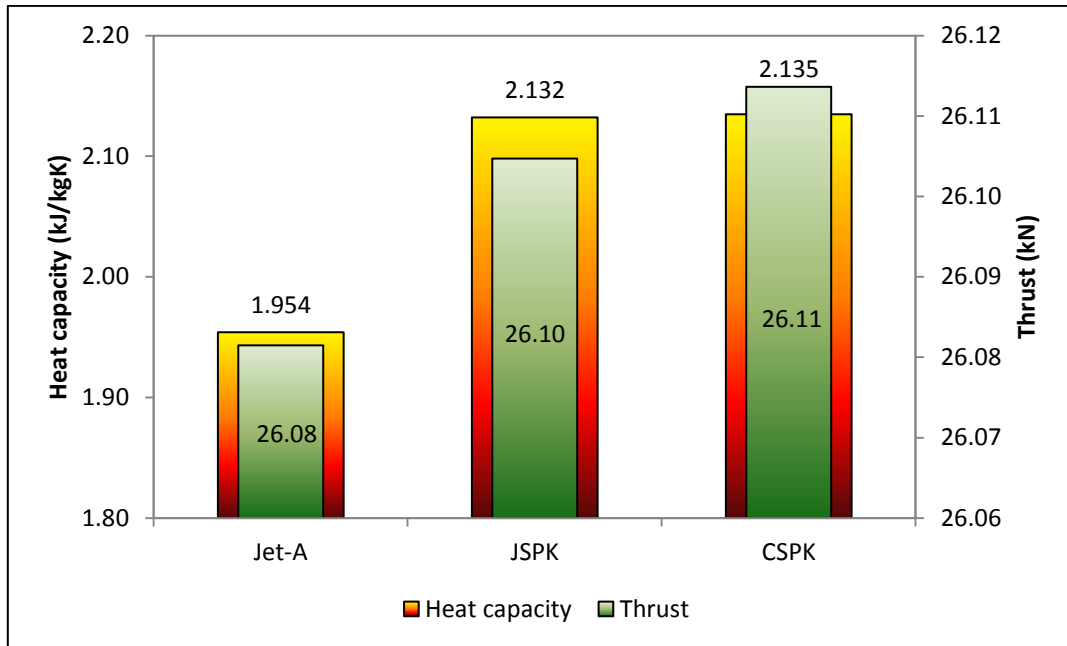


**Figure 3-11: The Effect of Heat Capacity on Engine Thrust**

The increases of engine thrust are observed to be correlated with the increases of velocity at the nozzle core exit. Thrust of a turbofan can be calculated by totalling the amount of thrust generated from the core stream and thrust from the fan stream. Accordingly equation (25) as described in Mattingly (1996) can be used.

$$F = \frac{\dot{m}_C}{g_c} (V_9 - V_0) + \frac{\dot{m}_F}{g_c} (V_{19} - V_0) \quad (25)$$

Rearrange equation (25) and replacing the initial velocity,  $V_0$  with  $a_0$  and  $M_0$ , and the ratio of fan flow to the core flow with  $\alpha$  (bypass ratio), the generation of engine thrust can be expanded as equation below

$$\frac{F}{\dot{m}_0} = \frac{a_0}{g_c} \frac{1}{1 + \alpha} \left[ \frac{V_9}{a_0} - M_0 + \alpha \left( \frac{V_{19}}{a_0} - M_0 \right) \right] \quad (26)$$

$\frac{V_9}{a_0}$  in equation (26) can be replaced into equation (27) in which the relation between the velocity and the temperature ratio of the turbine  $\tau_t$  can be observed. In this equation, the turbine temperature ratio is calculated from the

total power required for the turbine to drive the compressor and the fan (equation 28).

$$\frac{V_9}{a_0} = \sqrt{\frac{2}{\gamma - 1} \frac{\tau_\lambda}{\tau_r \tau_c} (\tau_r \tau_c \tau_t - 1)} \quad (27)$$

$$\dot{W}_t = (\dot{m}_c + \dot{m}_f) c_p (T_{t4} - T_{t5}) \cong \dot{m}_0 c_p T_{t4} (1 - \tau_t) \quad (28)$$

Equation (28) shows the correlation of engine thrust,  $\tau_t$  with the turbine power out,  $\dot{W}_t$  which also is proportional to the heat capacity of the fuel. Following to that relation, it is noted that as the heat capacity of the fuel is increased, the power out of the turbine also increases and therefore increases the engine thrust. Although the increases are not significant, in order to compare fuels, the contribution of heat capacity has to be taken into account.

### 3.5.3 The Effect of Fuel Density on Fuel Consumption

The effect of fuel's density on the fuel consumption was investigated.

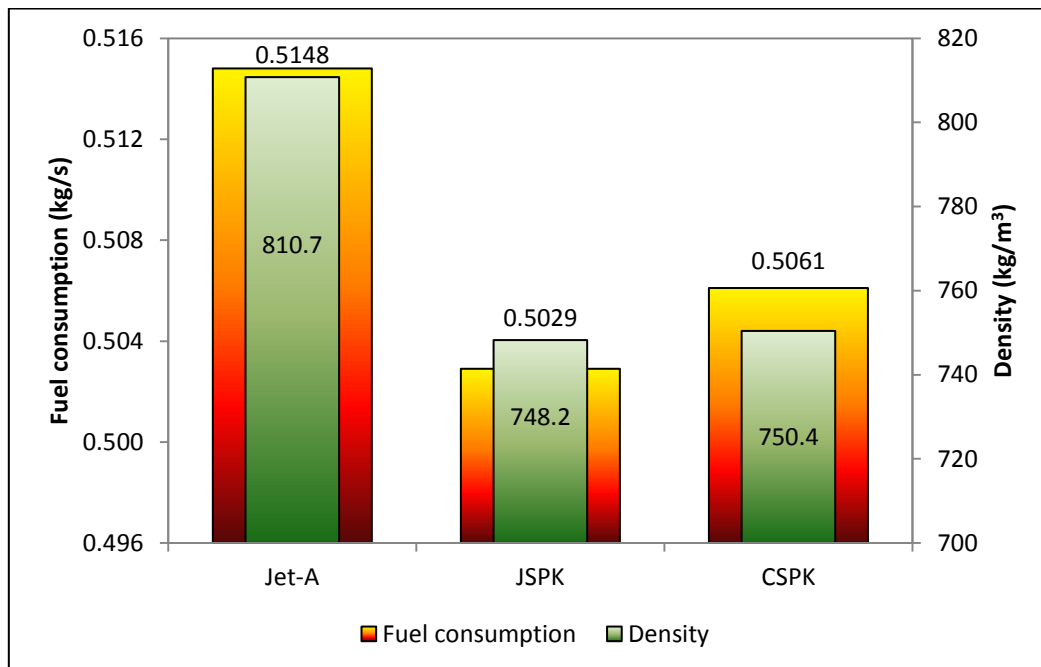


Figure 3-12: The Effect of Fuel Density on Fuel Consumption

The evaluation of the effect of density on the fuel consumption showed that the fuel consumed by the engine increases with increases in fuel density. Density of the fuel depends on the composition of the fuel. According to Aviation Fuels Technical Review, fuel with less density has high energy content per unit weight while the high density fuel has low energy content per unit volume. In order to accommodate the TET value set in the cruise simulation, the fuel injector has to inject a larger mass of dense fuel due to its low energy content, on the other hand, only small quantity of mass has to be injected for the less dense fuel. This is advantageous towards the reduction of fuel consumption, but in the case of an aircraft which will usually take off with the fuel's tank full, a more dense fuel with high energy per unit volume is much preferred.

### **3.6 Conclusions**

This chapter provides an assessment of the engine performance of two-spool high bypass turbofan engines running with bio-SPK fuel, namely JSPK and CSPK. The assessment was conducted as 100% of bio-SPK fuel and as blend at 20%, 40%, 60%, and 80% of the fuel with 80%, 60%, 40% and 20% of Jet-A respectively. For validation purposes, the blend of 50% bio-SPK fuel with 50% Jet-A was also evaluated, as only this mixture is available in the literature. Two types of engine condition were considered – design point condition (cruise) and constant mass flow condition. For both conditions, the characteristics of the engine were kept constant but only TET was disabled during the constant mass flow evaluation.

The in-house engine performance computer tool PYTHIA, which was integrated with the set of fuel caloric properties data generated from NASA CEA, was used for the evaluation. The generation of fuel caloric properties data was validated by comparing the data with the data of the chemical with the molecular formula as close as possible to the estimated molecular formula of the selected biofuels. The difference of the generated data is very small and dependable to be used.

The comparison of fuel flow and LHV of 50% bio-SPK with 50% Jet-A evaluated in this research work is consistent with that predicted in the literature. It is

therefore summarised that the predicted molecular formula and enthalpy of formation of the selected biofuels in this work used in generating caloric properties data as the input in PYTHIA is dependable. This also indicates that the capability of PYTHIA in evaluating biofuels is valid.

The evaluation and comparison of thrust, fuel flow, TET and SFC of pure bio-SPK fuels and their blend with Jet-A were presented. At design point condition where the engine was considered to be operated at cruise, both bio-SPK fuels were observed to produce more thrust than Jet-A. The improvement of engine performance wrt Jet-A increases as the percentage of biofuel in the mixture increases. For each bio-SPK fuel, the highest thrust is produced by implementing 100% of the fuel in the engine. However, between JSPK and CSPK, CSPK is found to generate higher thrust than JSPK. The same trend is also observed for fixed fuel conditions where both fuels improved the thrust correspondingly.

Implementing bio-SPK fuels in the aircraft engine either with 100% or by blending it with Jet-A, is observed to reduce the consumption of fuel and improve the SFC which consequently improved (increased) the efficiency. Similarly with thrust, the highest reduction of fuel flow is found when the engine was running with 100% bio-SPK fuel. However, the highest reduction of fuel flow is observed when 100% of JSPK was used.

The comparison of TET measured during the constant mass flow condition evaluation shows consistent increases as percentage of bio-SPK fuel in the mixture increases, which corresponded to the increases of thrust. Although TET increases, the increases are small and do not exceed the maximum temperature allowed for the turbine. Therefore the increases can be considered acceptable.

Factors were identified which influence the improvement in the engine performance focused on in this research. Considering that both evaluations were conducted using the same engine characteristics and engine condition,

therefore the observation of  $s$  that may influence those improvements correspond to the properties of the bio-SPK fuel itself.

The first and foremost factor influencing those improvements is high low heating value (LHV) of the bio-SPK fuels in comparison to Jet-A. This heating value increases as the percentage of bio-SPK fuel in the blend increases and therefore indicates the increase of thrust. Besides LHV, heat capacity was also identified as influencing the generation of thrust. Heat capacity of the selected bio-SPK fuels is relatively higher than Jet-A and consequently increases the thrust by providing high velocity at the nozzle exit. In addition, the effect of density is also observed to influence the reduction of fuel flow during the design point condition. This is due to the fuel injector that has to inject more dense fuel in comparison to less dense. Through this assessment, the capability of bio-SPK fuel in providing an improvement in engine performance was noted.

## **4 EVALUATION OF BIOFUELS ENGINE EMISSIONS**

### **4.1 General Introduction**

World-wide demand for air transport has steadily risen, leading to increased concern regarding the environmental impact. It has indeed become a great challenge to meet the demand whilst considering the effect of pollution emitted from the aircraft combustor which negatively affects human health and environment. The formation rate of pollution emissions may correspond to various factors such as the aircraft flight operation and fuel properties.

As aforementioned, the concern about using biofuels in aircraft engines becomes an interested topic, as it is observed to be able to alleviate problems regarding formation of pollution, especially  $\text{NO}_x$ , and to reduce the dependency of aviation industries on crude oil. As a result of this anxiety, studies of the influence of biofuels on engine emissions have been developed extensively in order to provide further information regarding developing future greener aircraft.

In moving towards that intention, this research is initiated in order to extend the biofuel information regarding engine emissions. Considering that Cranfield University has developed an engine emissions tool, this research work is also developed to take the opportunity of expanding the fuel selection in HEPHAESTUS (in-house engine emissions tool) and to test the ability of HEPHAESTUS in predicting the biofuels emissions.

### **4.2 Formation of Pollutant Emissions and Its Impact on the Environment and Human Health**

The process of combustion consists of mixing air and fuel, igniting and burning which consequently produces heat and emissions as products. For an aero-engine, the process of emissions formation produced from the combustion process is shown below.

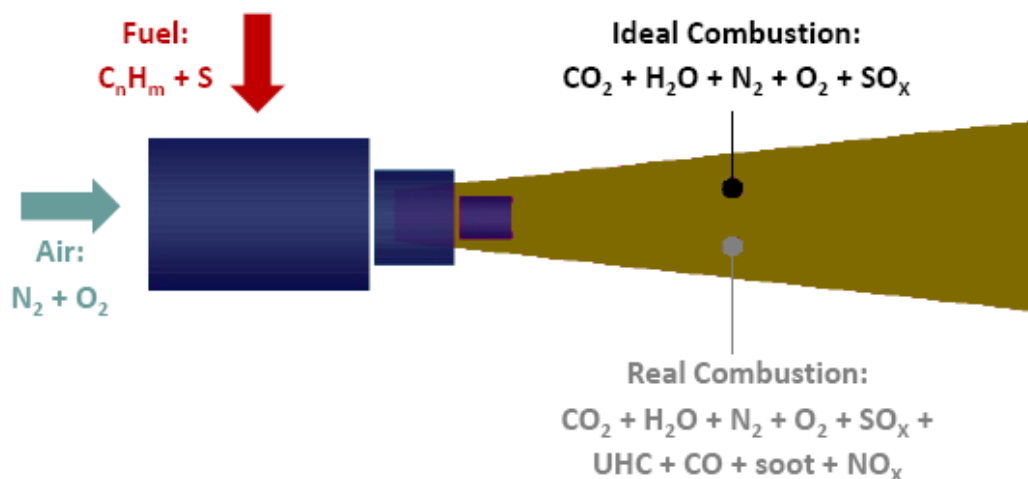


**Figure 4-1: The Formation of Emissions from the Aero-engine (Norman et al., 2003)**

The pollution dispersed from gas turbine engine is generated through an ideal and actual combustion processes. In the ideal combustion process, the production of emissions such as carbon dioxide (CO<sub>2</sub>), water (H<sub>2</sub>O) and sulphur dioxide (SO<sub>2</sub>) are related directly to the composition of the fuel and the amount of fuel burnt during the combustion.

However, in the real process of combustion, hundreds of reactions are involved, which produce additional emissions to the ideal combustion emissions. This actual process of combustion produces pollution such as carbon monoxide (CO), unburnt hydrocarbon (UHC), nitrogen oxide (NO<sub>x</sub>), soot, sulphur trioxide (SO<sub>3</sub>), sulphuric acid (H<sub>2</sub>SO<sub>4</sub>) and sulphur dioxide (SO<sub>2</sub>) also called SO<sub>x</sub>. The rate of these additional emissions depends on the amount of fuel burnt and the condition of the combustor during the operation condition such as temperature and pressure and air-fuel ratio. The quantities of pollution emissions vary with the operating condition, especially for CO, UHC and NO<sub>x</sub> (Table 4-1). With the extensive growth of the aviation industry, developing a combustor with low emissions becomes a top priority. Considering that the range of emissions are formed in different operating conditions and processes, therefore designing a combustion chamber that produces low emissions in all operating conditions becomes a great challenge.

**Table 4-1: Difference in Emission Level during Different Operating Condition (Penner *et al.*, 2013)**

<b>Emission</b>	<b>Idle</b>	<b>Take off</b>	<b>Cruise</b>
CO <sub>2</sub>	3160	3160	3160
H <sub>2</sub> O	1230	1230	1230
SO <sub>x</sub>	0.8 – 1.2	0.8 – 1.2	0.8 – 1.2
CO	10 - 60	< 1	1 – 3.5
UHC	0 - 12	< 0.5	0.2 – 1.3
NO <sub>x</sub>			
Short haul	3 - 6	10 - 53	8 - 12
Long haul	3 - 6	20 - 65	11 - 16

Emissions generated by aero-engines will impact on both the environment and human health. The contribution of aircraft emissions to global warming and climate change are notified. Instead of CO<sub>2</sub> as the most notable impact on climate change, other impacts associated with aviation are NO<sub>x</sub> and contrails.

The level of these emissions depends on the duration of flight. In the Sustainable Aviation report dated November 2008, the substantial proportion of these emissions is occurred at cruise altitudes. Typically, subsonic aircraft flies within the range of altitude of 30000 – 40000 ft and spends the longest time at cruise. During cruise, the amount of fuel burned increases. The generation of NO<sub>x</sub> also increases as the amount of fuel burned increases. It is reported that through the complex set of reactions involving the sunlight, high amount of NO<sub>x</sub> released during cruise will increase the ozone concentrations and consequently causing the global warming. The increase of atmospheric ozone concentrations let in the sunlight direct to the Earth but kept heat from escaping. This is called greenhouse effect. Generally when the sun shines the Earth, the sunlight will be absorbed and radiated back into the atmosphere as the heat. Unfortunately the greenhouse will trap this heat and rising the Earth temperature which causing the climate change and affecting the environment.

These impacts were summarised and reported by the United States Environmental Agency (1999), as follows:

**Table 4-2: The Impact of Aircraft Pollution onto Human Health and Environment**

<b>Pollution</b>	<b>Health Impact</b>	<b>Environment Impact</b>
Ozone	Lung function impairment, effects on exercise performance, increased airway responsiveness, increased susceptibility to respiratory infection, pulmonary inflammation and lung structure damage	Crop damage, damage to trees and decreased resistance to disease for both crops and other plants
Carbon Monoxide	Cardiovascular effects	Similar health effects on animals as on humans
Nitrogen Oxide	Lung irritation and lower resistance to respiratory infection	Acid rain, visibility degradation, particle formation, contribution towards ozone formation
Particulate Matter	Premature mortality, aggravation of respiratory and cardiovascular disease, changes in lung function and increased respiratory symptoms, changes to lung tissues and structure, and altered respiratory defence mechanisms.	Visibility degradation and monument and building soiling, safety effects for aircraft from reduced visibility
Volatile Organic Compounds	Eye and respiratory tract irritation, headaches, dizziness, visual disorders, and memory impairment.	Contribution towards ozone formation, odours and some direct effect on buildings and plants.

### **4.3 Effect of Fuel Properties on Emissions**

The effect of fuel properties on emissions—notably NO<sub>x</sub>, CO, UHC and smoke/soot—gathered from previous studies are presented in this section. Not much information relating to the effect of fuel properties on pollutants has been found for aircraft gas turbine engines. Most of the previous studies on this topic were concerned with the pollutants from the diesel engine, which run with a bio-diesel-type fuel. Although it is not quite relevant to this work, which focuses on aircraft engines, it is nevertheless considered worth observing whether there is any relationship between those discussed in the literature and those that obtained from this work.

## Nitrogen Oxide (NO<sub>x</sub>)

The overall formation of NO<sub>x</sub> is contributed from three pathways, i.e. thermal-NO<sub>x</sub>, fuel-NO<sub>x</sub>, and prompt-NO<sub>x</sub>. Among these three, thermal-NO<sub>x</sub> is the main contributor to the formation of NO<sub>x</sub> generated from a gas turbine. Thermal-NO<sub>x</sub> is produced by the oxidation of atmospheric (molecular) nitrogen in high temperature regions of the flame and in the post-flame gases. Thermal-NO<sub>x</sub> is usually predicted using the Zeldovich mechanism. As mentioned in Gupta (2004), the flame temperature depends on the fuel properties, preheat temperature, and oxygen concentration.

A study conducted by (McCormick *et al.*, 2001) investigated the effects of bio-diesel properties on NO<sub>x</sub> and particulate matter (PM) in a heavy truck engine, and accordingly found a correlation between density with NO<sub>x</sub> and PM emissions. The observations show that the formation of NO<sub>x</sub> increases as the density of the fuel increases; an observation consistent with that obtained by (Signer *et al.*, 1996), cited by (McCormick *et al.*, 2001), who reported approximately 3–4% increases of NO<sub>x</sub> for 3.5% increases in density. The increases are owing to the fuel injector, which has to inject a larger mass of dense fuel at a given speed and load, thus resulting in the burner burning more fuel, and producing more NO<sub>x</sub> (McCormick *et al.*, 1997).

As opposed to fuel density, the fuel's boiling temperature is another property potentially affecting NO<sub>x</sub> emissions (McCormick *et al.*, 1997). Notably, fuel with a high boiling temperature may require a longer time to be heated to boil and vaporise, which consequently reduces the rate of droplet evaporation and thus leads to the consumption of a smaller fraction of the fuel in premixed relative to diffusion burn combustion. However, the effect of boiling temperature in NO<sub>x</sub> formation still needs to be clarified.

In the case of the aircraft engine, the difference between the ratio of hydrogen and carbon (H/C) content in the biofuel in comparison to H/C ratio of kerosine is one of the factors influencing the tendency to NO<sub>x</sub> formation. A study conducted

by (Rahmes *et al.*, 2009) shows that the differences in H/C ratio lower the flame temperature and accordingly reduce NO<sub>x</sub>.

### Smoke/soot

As is well-known, the production of soot in a gas turbine engine is mainly due to the incomplete combustion of hydrocarbon fuels, which usually occurs in the hottest part of the primary zone. Moreover, it can also occur anywhere in the combustion zone where mixing between fuel and air is inadequate (Acosta and Beckel, 1989), and in the region where the fuel-air ratio is higher than 1.5 (fuel-rich region). Since it is important for aircraft to operate at relatively low or possibly without any visible smoke emissions, it is therefore necessary to monitor the amount of soot—not only to fulfil this requirement but also as indicator of the satisfactory operation of the combustor.

The formation of a local fuel-rich region in the combustor chamber is controlled by the fuel volatility and fuel viscosity, as these properties will affect the mean drop size, penetration and evaporation of fuel spray, whilst the molecular structure of the fuel will control the resistance of carbon or soot production. Studies conducted by Butze and Ehlers (1975) and Blazowski and Jackson (1978), cited by Acosta and Beckel, (1989), show that the tendency for soot increases with the reduction of hydrogen content, whilst other studies state that more soot will be produced by fuel containing a high concentration of polycyclic aromatics than fuel with a low concentration (Naegli *et al.*, 1983), (Naegli and Moses, 1980), cited by Acosta and Beckel (1989).

The effect of fuel properties on the formation of soot was also investigated by (McCormick *et al.*, 2001), who found that the tendency of soot to occur is unchanged, although density is increased. Unfortunately, however, there is a critical density where soot is found to increase dramatically.

The investigation into the effect of flame temperature and fuel composition on soot formation was conducted by Naegeli *et al.*, (1983), who found that, although the tendency of soot to form is higher if the flame temperature

increases, increase in soot is nevertheless much greater when the H/C of the fuel is lower.

### CO and UHC

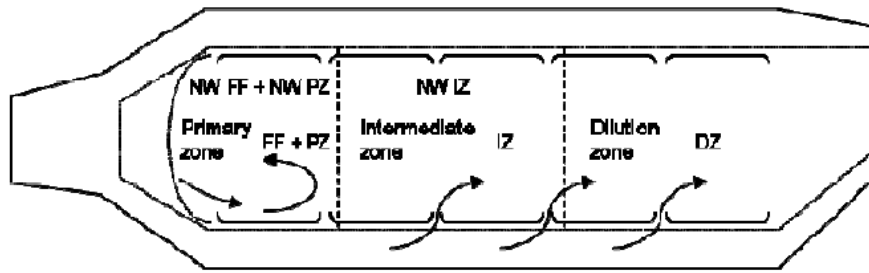
The formation of CO and UHC is usually associated with poor atomisation, which depends on the properties of fuels, such as surface tension, viscosity and specific gravity. Another factor potentially affecting the formation of CO and UHC is a lower flame temperature, which will lead to more incomplete carbon oxidation (Rahmes *et al.*, 2009).

## **4.4 Engine Emissions Evaluation Requirements**

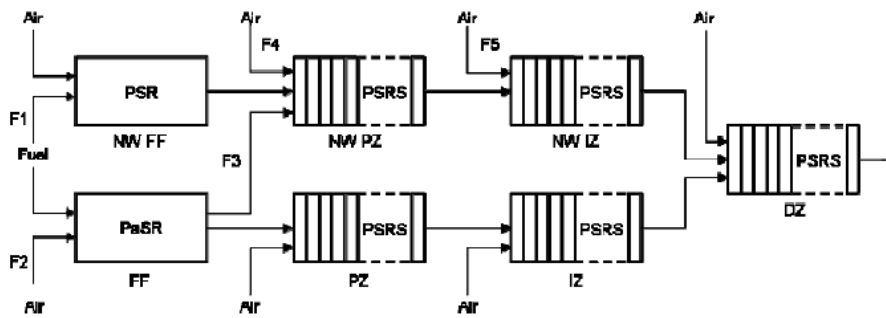
### **4.4.1 Introduction to the HEPHAESTUS**

The amount of emissions generated by an engine running with biofuels is predicted with the use of an emissions software, known as HEPHAESTUS, which was developed by a previous PhD student at Cranfield University (Celis, 2010). This software consists of models representing the conventional combustor, which includes a partially-stirred reactor (PSR) and a series of perfectly-stirred reactors. The arrangement of these reactors is shown in Figure 4-2.

- A partially-stirred reactor (PSR) that represents flame front (FF) (first part of combustor primary zone)
- A series of perfectly-stirred reactors (PSRS) which represents combustor primary zone (PZ), intermediate/secondary zone (IZ), and combustor dilution zone (DZ).



(a)



(b)

**Figure 4-2: The Arrangement of PSR and PaSR in Representing the Combustor (Celis, 2010)**

Emissions that can be predicted using this software include  $\text{NO}_x$ , CO, UHC and soot/smoke. The capability of this software of predicting the emissions from kerosine has been verified. In general, the levels of such pollutants were observed to follow the trends provided by the ICAO databank. However, only the prediction of  $\text{NO}_x$  and CO is considered reliable currently and can be used for further evaluation. Due to difficulties in modelling the kinetics of UHC and soot, for the time being the author of HEPHAESTUS has advised us not to evaluate UHC and soot as the prediction is not accurate.

In order to use the software, input data, such as engine parameters and the geometry of the combustion chamber, are needed. The engine parameters required consist of fuel total temperature, ambient flight altitude, ambient temperature, ambient relative humidity, air total temperature and air total pressure at the combustor inlet, total air mass flow rate and fuel mass flow rate.

The engine parameters can be obtained from engine performance software (PYTHIA version 4.0). As there is no information available for the fuel total temperature and combustion chamber geometry, those values are kept constant, as per the value used in Celis (2010).

To predict the biofuel emissions, some modifications in the HEPHAESTUS source code have been introduced. The modifications are carried out on a 'chemistry' module which uses NASA CEA to compute chemical equilibrium conditions, such as equilibrium temperature, equilibrium density, combustion products mass fraction and the concentration at the exit of a given chemical reactor. As biofuels selected in this work are not included in the NASA CEA library, therefore, the information, such as molecular formula and the heat of formation of the bio-fuels, is required in order to feed the programme and predict the chemical equilibrium conditions. The molecular formula and heat of the formation of bio-fuels chosen in this work however are not easy to find in open literature. Therefore, those values are predicted based on the information available. For instance, the molecular formula of the selected bio-fuels are predicted based on the composition of carbon and hydrogen in the molecule, whilst the enthalpy of formation was predicted by calculating backwards using the value of the heat of combustion.

Another modification to the source code was also conducted in the 'fuel' module. The modification includes an additional case so as to simulate biofuels. In this module, a sub-routine was introduced in order to calculate the blend fuel properties.

Modification has also been introduced in the 'global' module, where a greater number of elements are implemented in order to allow the user to insert the amount of carbon, hydrogen, nitrogen, sulphur, oxygen and argon contained in the fuel, as well as the weight of the fuel, the name of the fuel, and also the coefficients needed in order to calculate the heat capacity.

The HEPHAESTUS input file also was modified to enable the user to insert the composition of biofuel in the mixture.

#### **4.4.2 Engine emissions evaluation**

The evaluation of engine emissions was performed for both bio-SPK fuels – JSPK and CSPK as a pure and also by blending it at 20%, 40%, 60%, and 80% with 80%, 60%, 40%, and 20% of Jet-A respectively in order to see how the difference of NO<sub>x</sub> and CO are changing with the fuel's composition. The evaluation was performed at cruise and constant mass flow conditions. The input files for those blends and conditions are presented in Appendix E.

### **4.5 Results**

#### **4.5.1 The Comparison of NO<sub>x</sub> and CO with the Literature**

To validate the formation of NO<sub>x</sub> and CO predicted in this work with the literature, the evaluation of engine emissions was performed for the blend of 50% bio-SPK fuel with 50% of Jet-A based on the emissions data available in the literature that used fuel from the same family. In the literature, the prediction of NO<sub>x</sub> and CO was performed experimentally for the blend of 50% Jatropha-Algae bio-SPK with 50% of Jet-A. Although biofuel used in this experiment is different from fuel used in this research, and considering that this is only the information available, the difference in the results is not expected to be extensive taking into account the compositions consistency in reported results.

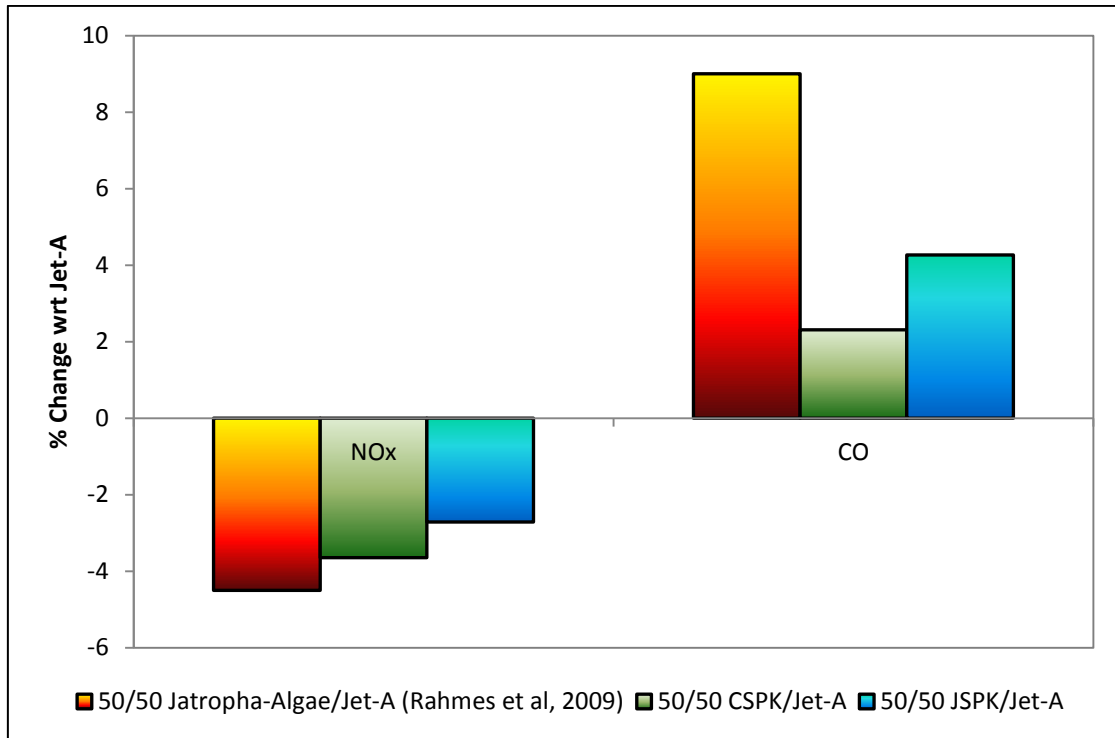


**Figure 4-3: The Comparison of Engine Emissions Predicted in this Work with Literature**

Data used for the validation is obtained from Rahmes *et al.*, (2009) who conducted off-wing engine ground tests for 50% Jatropha-Algae/50% Jet-A. In their tests, they observed a slight reduction of NO<sub>x</sub> (~5%) and increase of CO (~9%), NO<sub>x</sub> and CO, which are at least partly consistent with that predicted in this work although quantitatively different. The reduction of NO<sub>x</sub> obtained in this work is about 3% - 4% while CO is observed increases about 2% - 4%. It is clear that the precise emissions may vary among various Bio-SPKs. However, considering that little information is available on this topic, results from Rahmes *et al.*, (2009) was referenced as a benchmark as the variation in emissions among various Bio-SPKs is not expected to be extensive based on the consistency of the composition of reported results. This validation assessment summarised that the ability of the modified HEPHAESTUS in evaluating biofuel emissions is considered acceptable.

#### 4.5.2 Formation of NO<sub>x</sub> during Cruise Condition

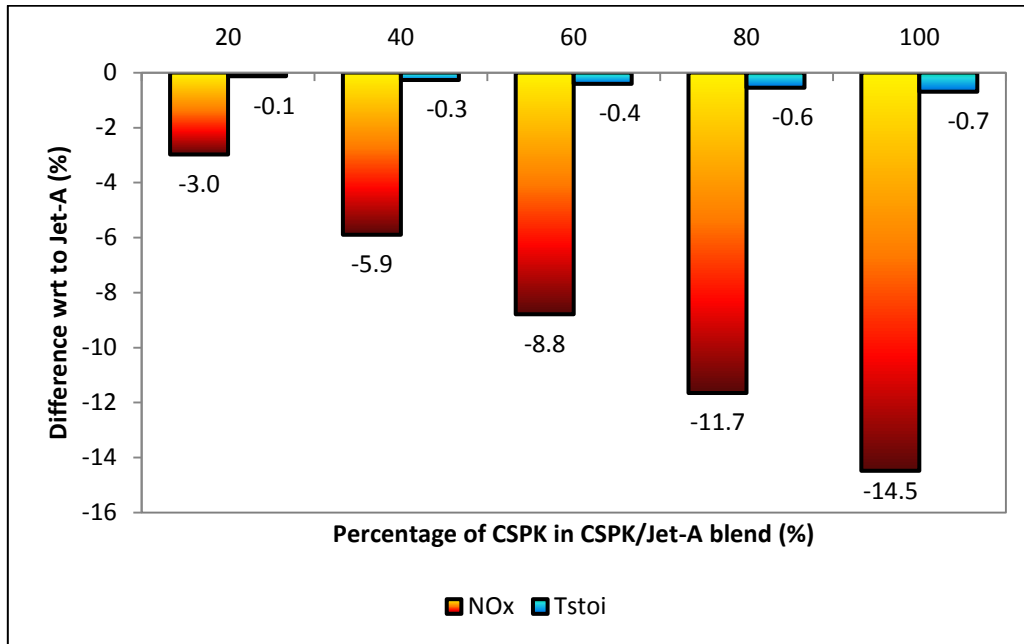


**Figure 4-4: Percentage Difference of NO<sub>x</sub> and Adiabatic Flame Temperature as a Function of CSPK Level**

The percentage difference of NO<sub>x</sub> formation and adiabatic flame temperature of CSPK and the blends relative to Jet-A are shown in Figure 4-4. As Jet-A is mixed with CSPK, the reduction in NO<sub>x</sub> and adiabatic flame temperature of CSPK and the blends relative to Jet-A is observed. The formation of NO<sub>x</sub> and flame temperature is found to be reduced linearly with the percentage of CSPK in CSPK/Jet-A mixture. The reduction in NO<sub>x</sub> is consistent with reduction in flame temperature as thermal-NO<sub>x</sub> was considered. Injecting 100% of CSPK in the combustor produced the highest reduction in adiabatic flame temperature and consequently in NO<sub>x</sub>.

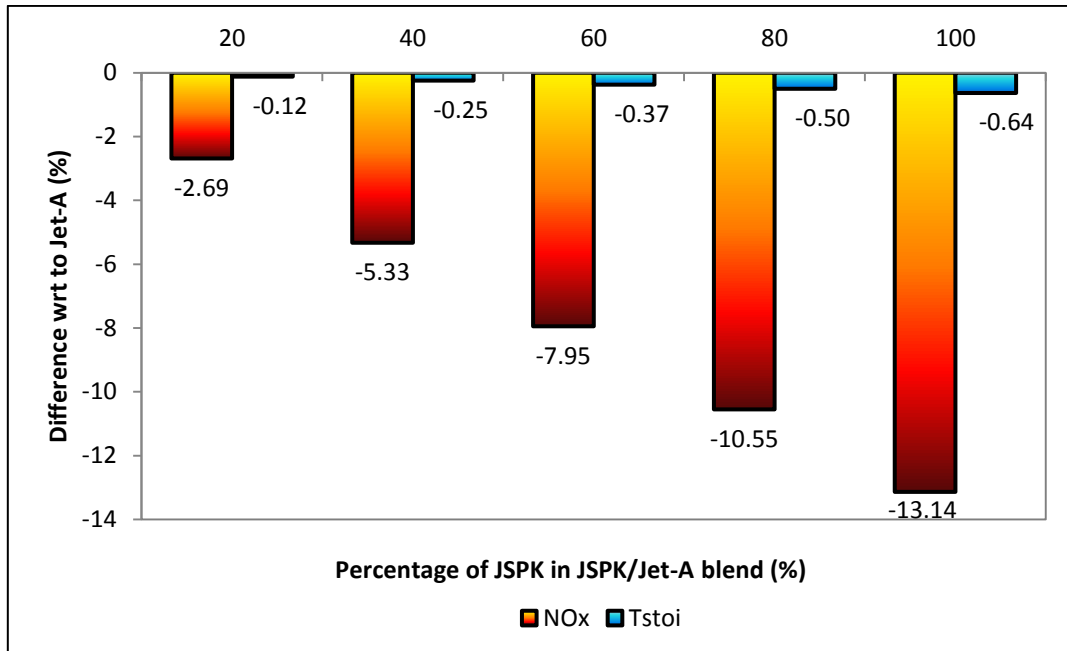


**Figure 4-5: Percentage Difference of NO<sub>x</sub> Pollution and Adiabatic Flame Temperature as a Function of JSPK level**

Similar trends are also observed for JSPK. Blending JSPK with Jet-A at any percentage is found to reduce NO<sub>x</sub> formation. The reduction is also consistent with the reduction of adiabatic flame temperature of the mixture. Both NO<sub>x</sub> and adiabatic flame temperature are found to reduce linearly with increases of JSPK percentage in the mixture. The higher the percentage of JSPK in the mixture, the higher the percentage of NO<sub>x</sub> that becomes available to pollute the atmosphere. Implementing 100% of JSPK in the combustor chamber reduces NO<sub>x</sub> by about 13.1% which is also the highest amongst the other percentages of JSPK.

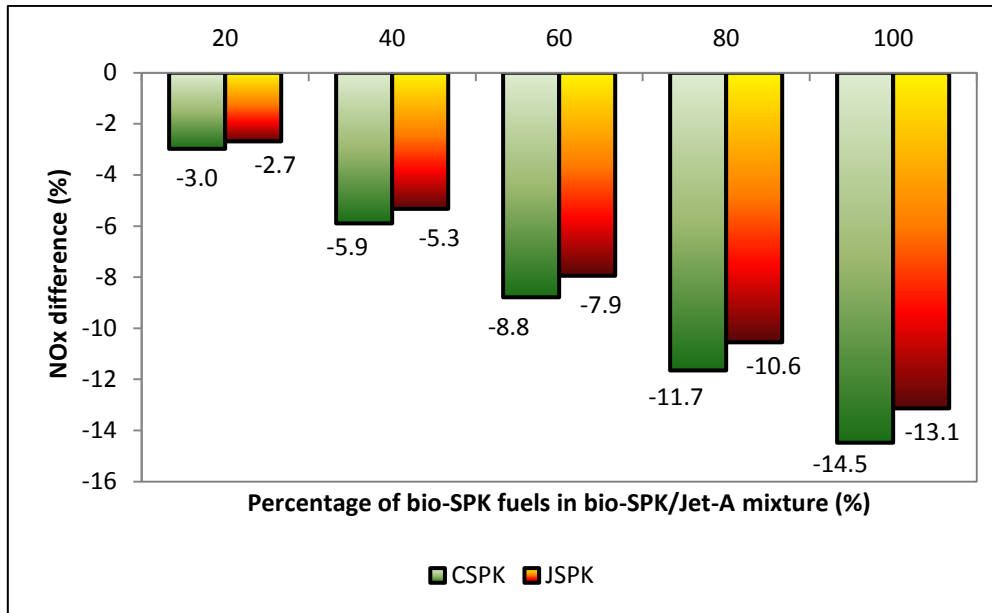


**Figure 4-6: Percentage Difference of NO<sub>x</sub> as a Function of Biofuel Percentage**

As mentioned above, at cruise condition the production of NO<sub>x</sub> for both selected bio-SPK fuels (JSPK and CSPK) is reduced constantly with the percentage of bio-SPK fuel in the bio-SPK/Jet-A mixture. Comparing between the selected bio-SPKs, the production of NO<sub>x</sub> is much improved by implementing any percentage of CSPK rather than JSPK. However the difference between them is not significant.

### 4.5.3 Formation of CO during Cruise Condition

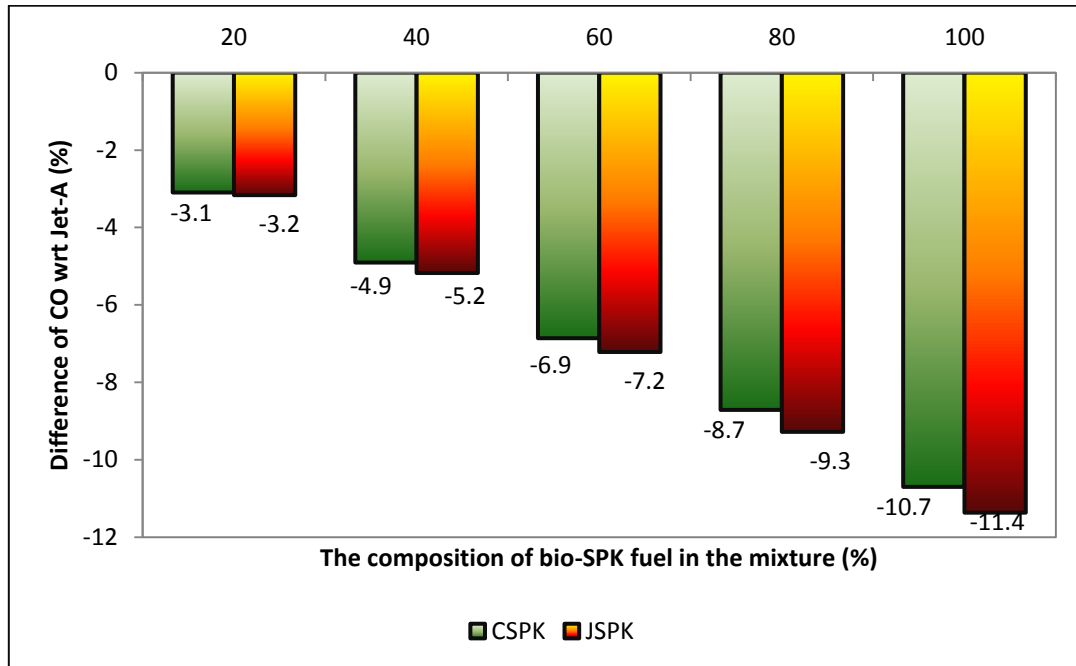


**Figure 4-7: The Reduction of CO during Cruise Condition as a Function of Biofuel Composition**

Figure 4-7 shows the percentage difference of CO formation between Jet-A and the blended fuel during cruise. It appears that the formation of CO is reduced significantly. The reduction of CO is found to be linear with the percentage of biofuel in the mixture. Comparing each biofuel, the highest reduction of CO is observed to be contributed by implementing 100% of JSPK in the engine (reduction about 11.4%). At any percentage of biofuel, implementing JSPK in the mixture however reduces CO more than when blending CSPK in Jet-A, although the difference between JSPK/Jet-A mixture and CSPK/Jet-A mixture is small.

#### 4.5.4 Formation of NO<sub>x</sub> during Constant Mass Flow Condition

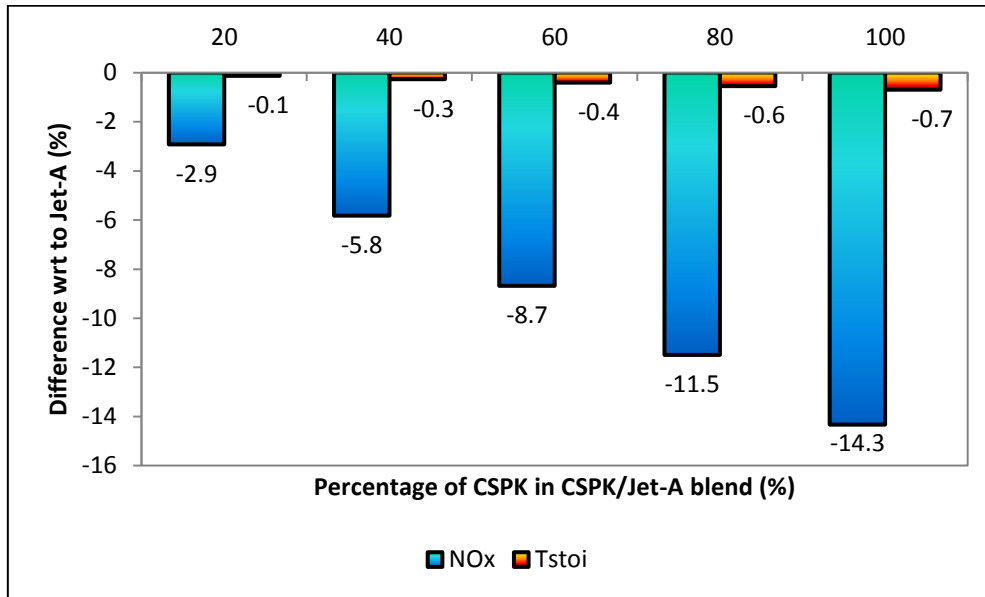


**Figure 4-8: Percentage Difference of NO<sub>x</sub> and Adiabatic Flame Temperature as a Function of CSPK Percentage Quantified at Constant Mass Flow Condition**

The percentage difference of NO<sub>x</sub> generated for different percentages of CSPK during constant mass flow condition relative to Jet-A is plotted in Figure 4-8. Quantitatively, it is observed that as the percentage of CSPK in the CSPK/Jet-A mixture increases, the reduction of NO<sub>x</sub> generated increases too. The highest reduction of NO<sub>x</sub> is observed when 100% of CSPK was utilised. The reduction of NO<sub>x</sub> observed in this assessment is also consistent with the reduction in flame temperature, as again, the formation of NO<sub>x</sub> considered in this work is relative to the flame temperature.

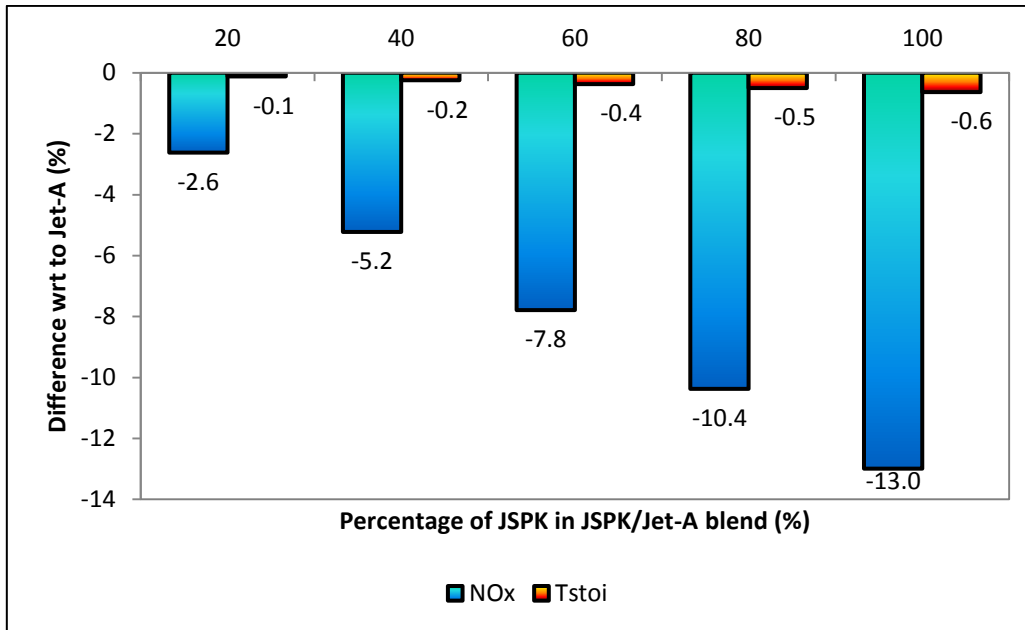


**Figure 4-9: Percentage Difference of NO<sub>x</sub> and Adiabatic Flame Temperature as a Function of JSPK Level at Constant Mass Flow Condition**

The similar trend in NO<sub>x</sub> reduction is also experienced if JSPK is implemented. Linear reduction of NO<sub>x</sub> with a percentage of JSPK in the mixture is quantified. As observed, implementing pure or 100% JSPK in the combustion chamber reduced NO<sub>x</sub> significantly. The reduction of NO<sub>x</sub> is also consistent with the reduction of flame temperature.

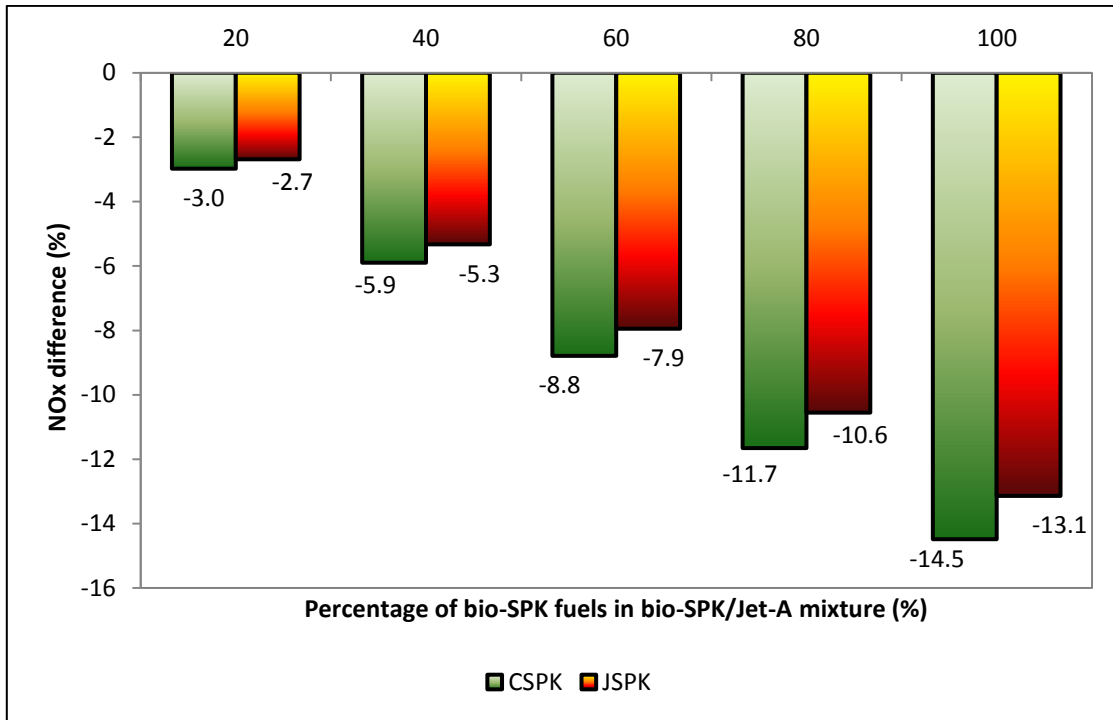


**Figure 4-10: Percentage Difference of NO<sub>x</sub> Generated as a Function of Biofuel Mixture during Constant Mass Flow Condition**

Figure 4-10 shows the comparison of percentage reduction of NO<sub>x</sub> between CSPK and JSPK relative to Jet-A during the constant mass flow condition. Both fuels show reduction in NO<sub>x</sub> as the percentage of biofuel in the mixture increases. CSPK is observed to produce more NO<sub>x</sub> compared to JSPK although the difference is not significant.

#### 4.5.5 Formation of CO during Constant Mass Flow Condition

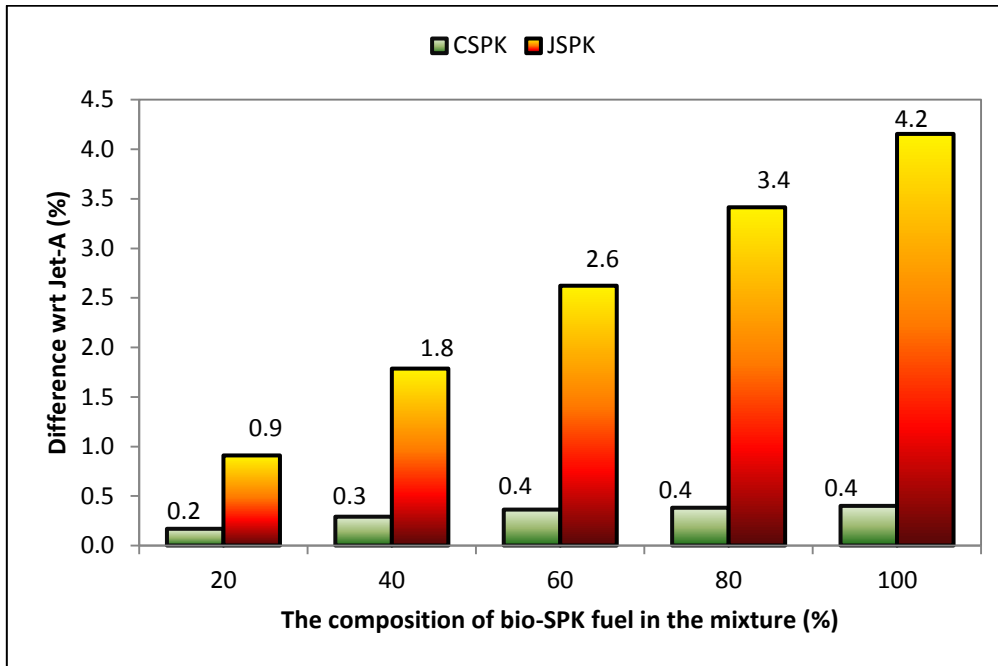


**Figure 4-11: Percentage difference of CO between JSPK and CSPK relative to Jet-A during the constant mass flow condition**

At constant mass flow condition, the CO formation of JSPK, CSPK and the blend relative to Jet-A is observed to increase linearly with the increases in the blend percentage. For each type of biofuel, the highest CO is observed to be generated when JSPK and CSPK is utilised purely. However, the highest CO is generated when 100% of JSPK is used. Based on the comparison above, significant difference of CO is obtained when Jet-A is blended with JSPK rather than blend Jet-A with CSPK.

#### 4.6 Discussion

As is well-known, besides ambient conditions, flight profile and engine parameters, the fuel properties also are one of the factors that influence the  $\text{NO}_x$  and CO formation. As in this evaluation the flight altitude and ambient conditions were not changed, therefore, the formation of  $\text{NO}_x$  and CO measured in this assessment was primarily influenced by the properties of the evaluated fuels.

#### **4.6.1 The Effect of LHV, Heat Capacity and FAR on Combustor Outlet Temperature and NO<sub>x</sub> Formation**

The reduction of NO<sub>x</sub> formation during cruise and constant mass flow conditions is observed to be consistent with the reduction of the flame temperature. This is due to the assumption that NO<sub>x</sub> formation assumed in this work is predominantly by thermal-NO<sub>x</sub> over prompt-NO<sub>x</sub>, while the fuel bound-NO<sub>x</sub> is neglected due to the very small percentage of nitrogen in the fuel (< 0.1 for CSPK and JSPK) (Kinder and Rahmes, 2009).

As quoted in Baukal (2001), adiabatic flame temperature is the temperature at which the enthalpy of the products of combustion equals the sum of enthalpy of the reactants plus the heat released by the combustion process. The correlation between adiabatic flame temperature with LHV, FAR and heat capacity is given by Borman and Ragland (1998) as Equation (29) below. In comparing one fuel with another, these three criteria – LHV, FAR and heat capacity have to be considered and are worthy of investigation, as the influence of these criteria might be significant.

$$T_f = T_0 + \frac{FAR}{1 + FAR} \frac{LHV}{C_p} \quad (29)$$

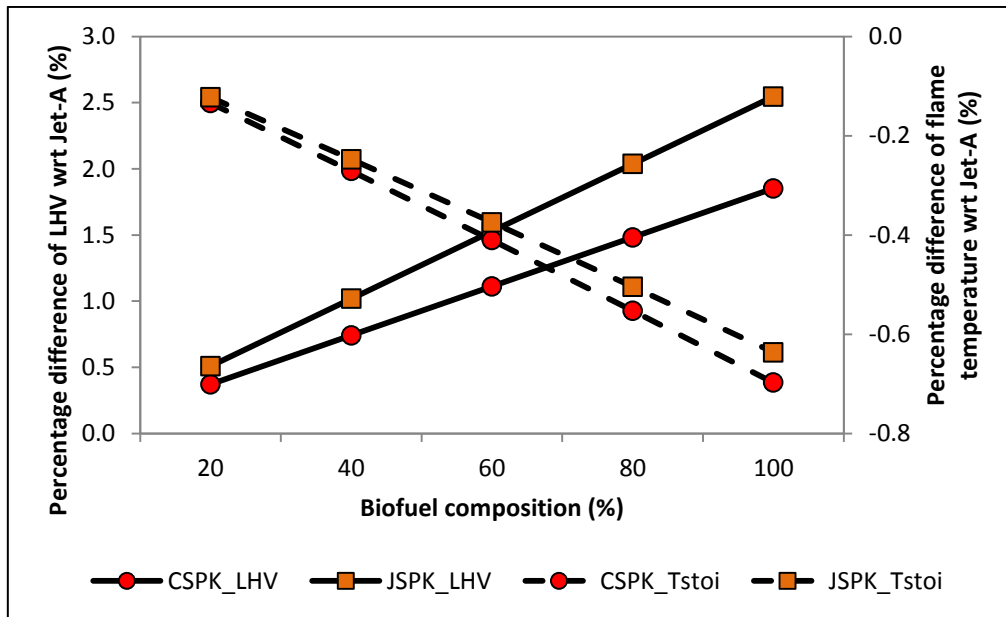


**Figure 4-12: The Effect of LHV on Flame Temperature as a Function of Biofuel Composition**

Figure 4-12 shows the effect of LHV as one of the factors that influence the flame temperature. It shows that the percentage difference of LHV wrt Jet-A increases as the composition of biofuel in the mixture increases. Increases of biofuel composition however, experience reduction in flame temperature. Apparently the effect of LHV on flame temperature is not observed.

As quoted in Borman and Ragland (1998), a larger heating does not necessarily imply a higher stoichiometric flame temperature because the stoichiometric fuel-air ratio must be considered. Therefore the investigation on the effect of fuel-air ratio on flame temperature is conducted. As predicted, the consistency between the reductions of FAR with flame temperature is shown in Figure 4-13. This observation is also consistent with the observation in Lefebvre (1999) who discovered the effect of FAR on flame temperature. In his observation, at constant pressure and temperature, reduced FAR will reduce the flame temperature due to the increases in specific heat of the combustion.

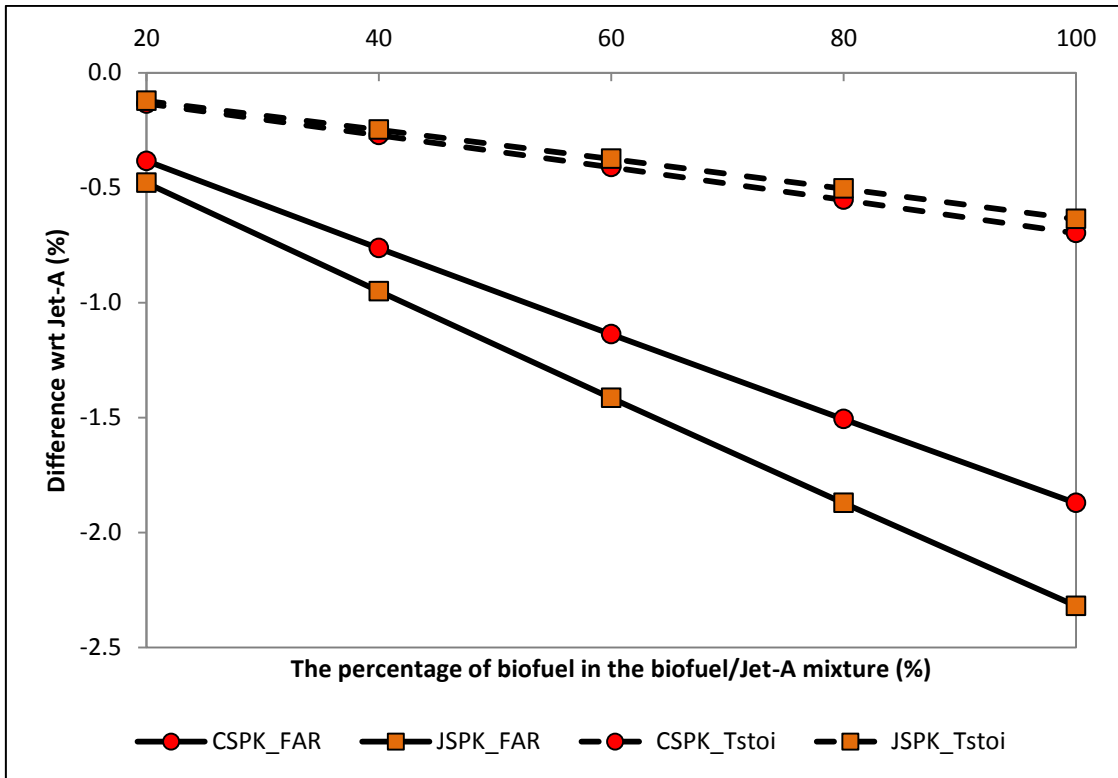


**Figure 4-13: The Effect of FAR on Flame Temperature as a Function of Biofuel Composition**

Besides LHV and AFR, the influence of heat capacity on flame temperature is also observed. Notably, heat capacity increases as the composition of biofuel in the mixture increases, and consequently reduces the flame temperature.

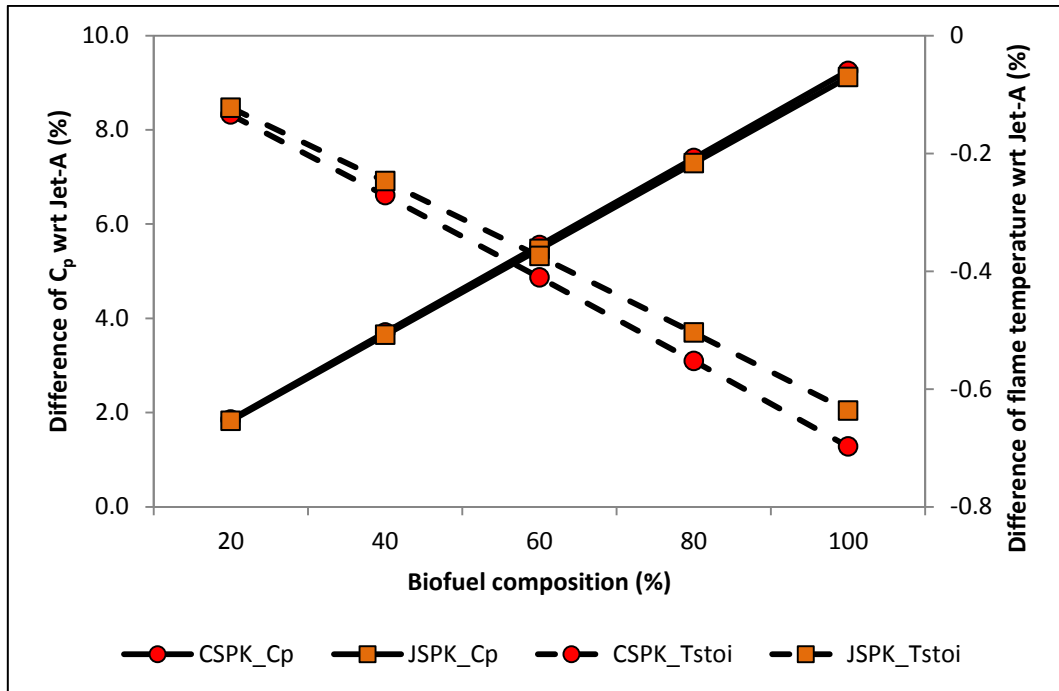


**Figure 4-14: The Effect of  $C_p$  on Flame Temperature as a Function of Biofuel Composition**

#### 4.6.2 The Effect of Boiling Temperature on $NO_x$ Formation

The formation of  $NO_x$  may also potentially be affected by high boiling temperature of the fuel (McCormick *et al.*, 1997). Notably, fuel with a high temperature may require a longer time to boil and vaporise, which consequently reduces the rate of droplet evaporation and leads to the consumption of a smaller fraction of the fuel in the premixed state, relative to diffusion burn combustion. However, the effect of boiling temperature on  $NO_x$  formation still needs to be clarified.

With this in mind, the influence of the boiling temperature on  $NO_x$  was also investigated.

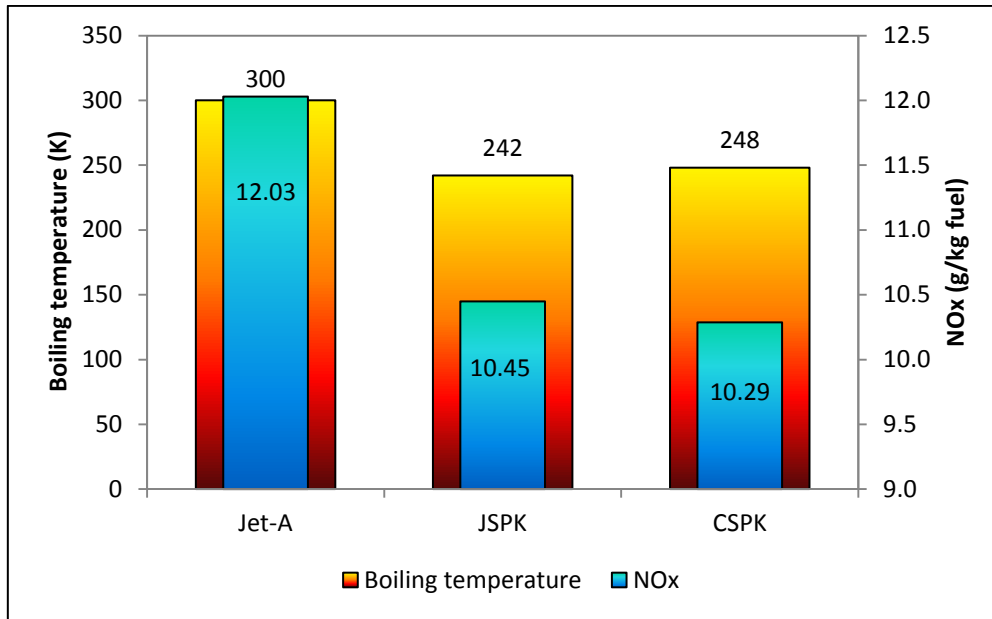


**Figure 4-15: The Effect of Boiling Temperature on NO<sub>x</sub>**

As reported in Rahmes *et al.*, (2009), the maximum boiling temperature of pure CSPK and pure JSPK is approximately 248K and 242K, respectively, whilst the maximum boiling temperature of Jet-A is 300K. The low boiling temperature of CSPK and JSPK in comparison to Jet-A is beneficial to the reduction of NO<sub>x</sub> with respect to Jet-A. In this observation, the effect of boiling temperature on NO<sub>x</sub> formation is in agreement with the findings of McCormick *et al.*, (1997).

#### 4.6.3 The effect of fuel density on NO<sub>x</sub> formation

Reduction in NO<sub>x</sub> is also found to have a close relationship with fuel density, consistence with the observations made by (McCormick *et al.*, 2001 and McCormick *et al.*, 1997). This is due to the amount of fuel injected into the combustor chamber in order to accommodate a certain engine speed, which is lower for the case of less dense fuel. As a result, less fuel is burnt and less NO<sub>x</sub> generated. The influence of density in NO<sub>x</sub> formation is observed in this assessment, especially in the case of cruise condition, where the evaluation was performed based on the amount of fuel consumed by the engine to accommodate the constant TET.

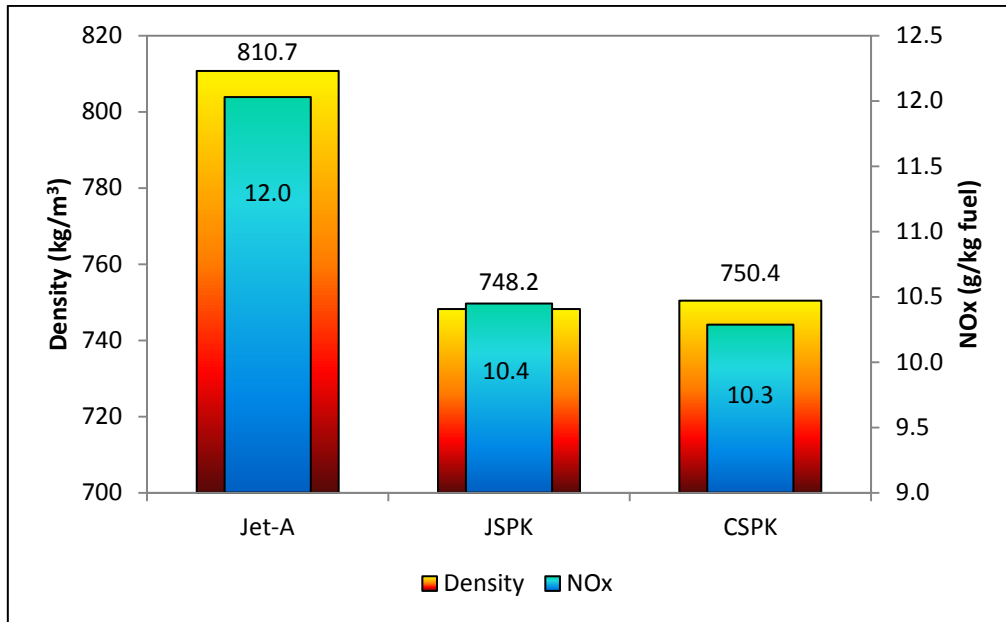


**Figure 4-16: The Influence of Density on NO<sub>x</sub> Formation**

The influence of density on NO<sub>x</sub> is shown in Figure 4-16, which is plotted as a function of Jet-A, 100% JSPK, and 100% CSPK. It is observed that the formation of NO<sub>x</sub> for 100% JSPK and 100% CSPK is reduced compared to Jet-A. The reduction is consistent with the low density of these fuels, which apparently corresponds to the low amount of fuel the engine has consumed.

#### **4.6.4 The Effect of Flame Temperature on CO Formation at constant mass flow condition**

As is known, the formation of CO is due to incomplete combustion of the fuel. The production of CO due to the incompleteness of combustion may be affected by low flame temperature due to the fact that colder temperatures will lead to more incomplete oxidation of carbon atoms (Rahmes *et al.*, 2009). The effect of low flame temperature on CO formation is observable in this work (Figure 4-17). Both CO and flame temperature are observed to decrease linearly with the composition of biofuel in the mixture. As expected, the reduction in flame temperature nonetheless is observed to correspond to the increases in AFR.

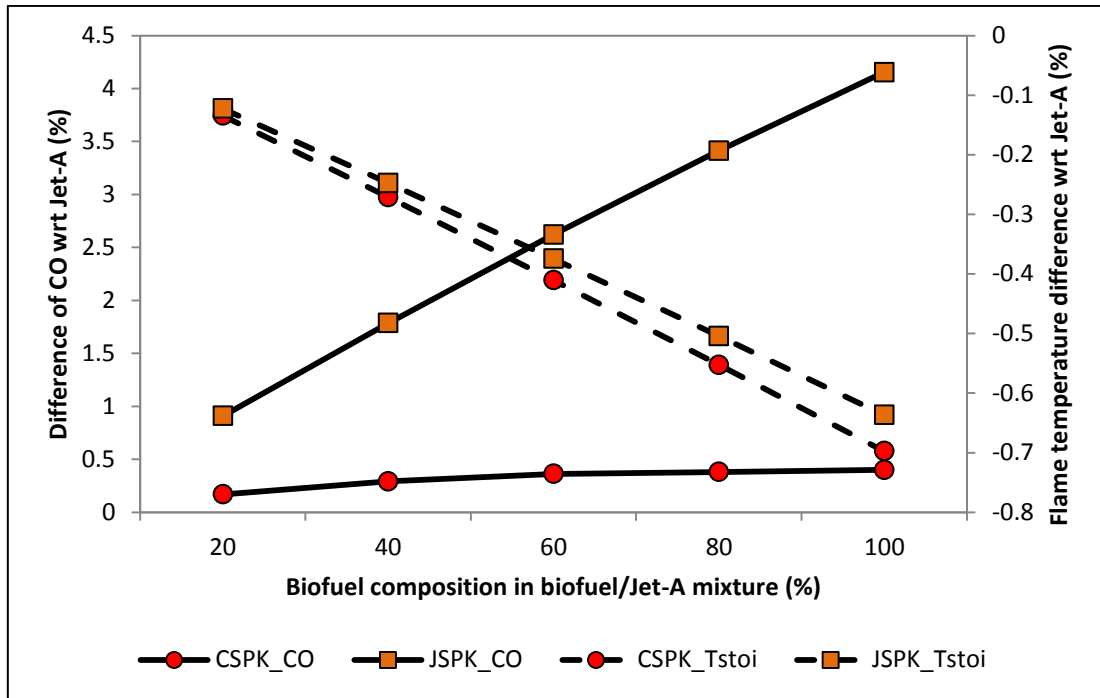


Figure 4-17: The Effect of Flame Temperature on CO Formation

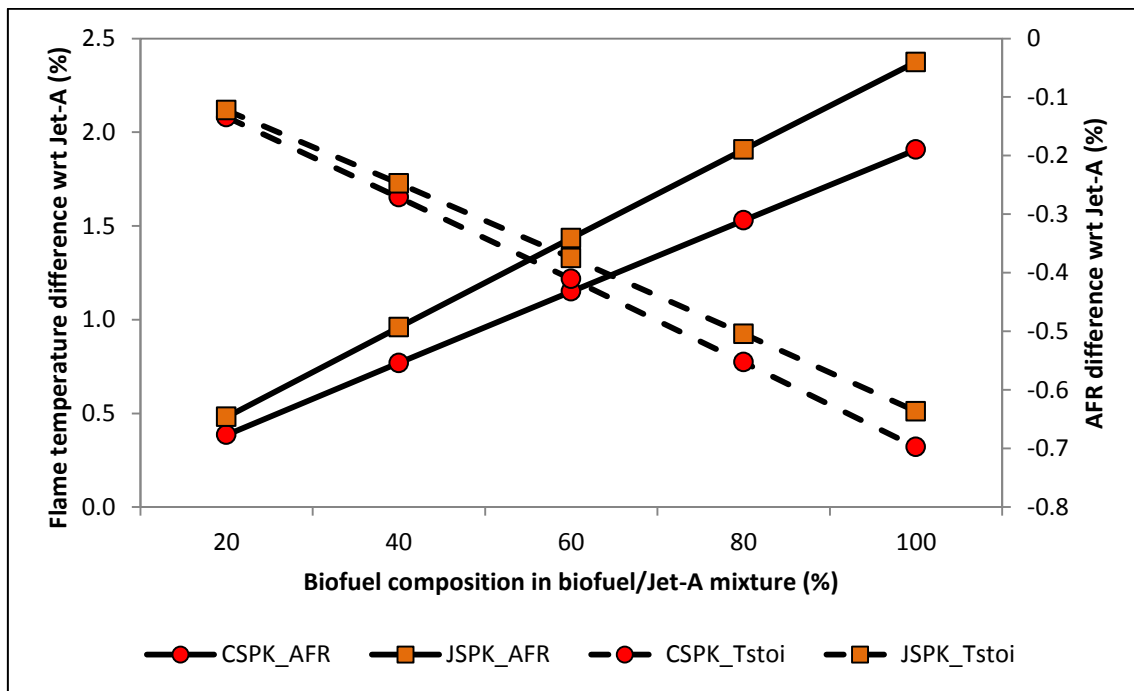


Figure 4-18: The Effect of AFR on Flame Temperature

#### **4.6.5 The Effect of Fuel Volatility on Evaporation Rate and CO Formation at Cruise Condition**

Although flame temperature may influence the CO formation due to incomplete combustion, flame temperature itself is not the only factor that affects the CO formation, especially during the cruise condition. It was mentioned in Lefebvre (1985) that the formation of CO is much higher at the low pressure conditions where the evaporation rates are relatively slow. Therefore, any factors that influence the evaporation rate cannot be ignored as they will have direct impact on the volume available for chemical reaction and therefore the emission of CO. The evaporation rate may be affected by the fuel volatility. Volatility is inversely proportional with boiling temperature. Literally, fuel with low boiling temperature is more volatile and will evaporate much faster than fuel with high boiling temperature. For instance, the boiling temperature of pure CSPK and pure JSPK is approximately 248K and 242K, respectively, whilst the maximum boiling temperature of Jet-A is 300K. Between these three fuels, the boiling temperature of JSPK is much lower and it is consequently more volatile than other fuels. This results in increases in the evaporation rate due to the propensity of the liquid fuel to evaporate into the gaseous state and helps the completion of combustion, which therefore suggests the reduction of CO.

#### **4.7 Conclusions**

This exercise evaluates engine emissions of a two-spool high bypass turbofan engine which operated at a cruise condition and at constant mass flow condition. The evaluation of engine emissions was completed using an in-house engine computer tool (HEPHAESTUS). Two types of bio-SPK fuel were chosen for the assessment: JSPK and CSPK – both of these fuels have been used in some of test flights as a mixture with Jet-A. To achieve the successful of this assessment, the modification was performed in HEPHAESTUS source code to allow the emission calculation for biofuel and the mixture of the biofuel with Jet-A. To enable HEPHAESTUS to predict the combustion properties of the

selected fuel, molecular formulae and enthalpy of formation of the fuel were introduced into the source code.

The evaluation of biofuel emission was conducted as a pure and as a blend of 20%, 40%, 60%, 80% with 80%, 60%, 40%, and 20% of Jet-A respectively. Additionally, the mixture of 50% of biofuel with 50% Jet-A also was performed in order to compare the result given by HEPHAESTUS with result from the literature. The evaluation of biofuel emission was focused on  $\text{NO}_x$  and CO formations as only these pollutants are observed to follow the trend provided by ICAO and considered reliable at the moment. The comparison of  $\text{NO}_x$  and CO predicted from HEPHAESTUS is observed to follow the trend given in the literature, although quantitatively different.

The effect of blending biofuel with Jet-A was evaluated at cruise and at constant mass flow condition. At both conditions, increasing the percentage of biofuel in the mixture reduced  $\text{NO}_x$ . Whilst at cruise, reduction in CO was observed, but increases of CO at constant mass flow condition were noted. Reduction of  $\text{NO}_x$  in both conditions is consistent with reduction of flame temperature as the generation of  $\text{NO}_x$  considered in HEPHAESTUS is based on thermal- $\text{NO}_x$ . From the literature, the flame temperature corresponds to LHV, heat capacity and AFR. However, in this assessment, only heat capacity and AFR are observed to have impact on the reduction of flame temperature. Besides flame temperature, the other factors observed to affect the reduction in  $\text{NO}_x$  formation are the low boiling temperature and low density of the biofuel.

The reduction of flame temperature on the other hand is observed to increase the generation of CO at constant mass flow condition owing to the incompleteness of carbon oxidation. However, low flame temperature was found to be not the only factor that affects the CO formation, especially during cruise condition. The reduction of CO during cruise is found to be related to the improved atomisation process which is related to the fuel volatility.

## 5 OPTIMISATION ASSESSMENT

### 5.1 Introduction

The concern about overdependence on crude oil and increases of pollution into the atmosphere has eventually encouraged researchers to conduct studies to find solution to these problems. A wide range of studies has been established which also comprises the area of optimisation in order to explore the feasibility of reaching the optimal solution, especially in the areas of aircraft design, aircraft trajectories, and aircraft operations for minimising operating cost, fuel consumption and ensuring minimal environmental impact.

Antoine and Kroo (2004), for example have established a multi-objective optimisation work to determine the optimal aircraft configuration between the conflicting objectives of low noise, emissions and operating costs. This study has successfully been achieved through the use of a multi-objective genetic algorithm that was integrated with the noise and engine models. In other research, Bower and Kroo (2008) conducted multi-objective optimisation work in the area of aircraft design focusing on minimising of direct operating costs, CO<sub>2</sub> emissions and NO<sub>x</sub> emissions. Furthermore, Celis (2010) has established a multi-objective optimisation work in the field of aircraft trajectories and engine cycles for low emissions and fuel consumption. As far as the fuel consumption is concerned, Singh *et al* (2012) has reviewed the area that might prove important and worth being explored particularly in the area of fuel consumption optimisation. This includes the areas of technology and product design, operation and performance, infrastructure and also the area of alternative fuels and fuels properties. Currently, none of the studies have focused on the area of alternate fuels which would take into account the combination of fuel consumption, engine performance, and engine emissions. Therefore this concern was selected to be evaluated in this work as it seems a demand that requires attention.

As discussed in the previous chapter, the interest towards biofuels has grown in which many experimental studies and flight tests have been conducted to evaluate the performance of biofuels. Details about the flight tests can be found in Chapter 1 (Table 1-1). However, these studies only focused on a certain percentage of blends. Usually, the evaluation was performed for the mixing of at least up to 50% of alternative fuel with kerosene due to density limitation highlighted for gas turbine fuel. None of these studies however were focused on the optimal percentage of biofuel that can be blended with Jet-A. Therefore it is crucial in this work to identify this issue, and for that reason, the establishment of an optimisation work was proposed at this stage. The main objective of this assessment is to obtain the trade-off that exists between engine performance and emissions impact for the selected test case and to find the optimal solution for the design problem focused in this work. At this stage, the feasibility of integrating the engine performance and emissions requirement in the optimisation tool is explored and the quantitative analysis of the trade-off between the engine performance and emissions is performed.

## **5.2 Optimisation in general**

In general, optimisation is about obtaining an optimal design in achieving the requirement of the design objectives within the specific settings of design constraints. There are two types of optimisation that are usually considered during the decision making, which usually depend on the objectives of the problem. The objectives that have to be achieved may include minimising the risks, maximising reliability, minimising cost, maximising efficiency, etc.

The two types of optimisation are single objective optimisation and multi-objective optimisation. In single objective optimisation, the optimiser has to find the best solution of either minimum or maximum value of single objective function. On the other hand, for multi-objective optimisation, it always deals with conflicting objectives and as a consequence, there will be no single optimal solution. These conflicting objectives lead to the set of compromised solutions,

which are also known as the trade-off, non-dominated, non-inferior or Pareto-optimal solutions.

There are numerous types of optimisation algorithms that can be implemented during the design process, such as Genetic Algorithm, Tabu Search, Simulated Annealing (SA), and Evaluation Strategies (ES) (Jaeggi *et al*, 2008). Although different types of algorithm may be used during the optimisation process, parameters associated with the problem such as design variables, design objectives and design constraints are important and have to be properly defined.

### **5.3 Requirement for the Optimisation Assessment**

#### **5.3.1 About GATAC – The Optimisation Framework**

This optimisation was performed using a framework called GATAC, by utilising the information and computer tools used for the performance and emission evaluation. GATAC is an optimisation tool that has been developed for the CLEAN SKY project (Sammut *et al*, 2012). GATAC comprises two components – GATAC core and Model Suite. GATAC core is the component where the optimisation takes place whilst Model Suite is the component where all the execution models are stored. Both these components will communicate with each other in transferring data. To operate GATAC, a set of dictionaries are required to be prepared. They are Model dictionary, Optimiser dictionary, Daemon dictionary, Setup dictionary, Setup Model dictionary, and Connectors dictionary, which are written in XML format. Further explanation of the components in GATAC including the function and requirement of each dictionary required are presented in GATAC User's Manual (Sammut *et al*, 2012). Interestingly, GATAC can be accessed through Graphical User Interface (GUI) which enables the user to more easily build a test case without writing the XML dictionaries. Within GUI, the Setup Dictionary, Case Handler and Hosts Environment dictionary will be automatically created, easy to edit and manageable. In performing the optimisation, GATAC implemented the so-called non-dominated searching genetic algorithm multi-objective (NSGAMO). The

capability of GATAC in evaluating the optimisation has been tested through a series of test cases either with or without constraints. The Pareto front generated for both test cases showed a good agreement with the theoretical Pareto front used as reference. The close matches between these two Pareto fronts confirms that either with or without constraints, the optimisation evaluation is satisfactorily handled by GATAC. Further explanation about the evaluation can be found in Sammut *et al* (2012).

### **5.3.2 Non-dominated Searching Genetic Algorithm (NSGA) - based Optimiser**

GATAC implements a genetic algorithm based optimiser, particularly non-dominated searching genetic algorithm (NSGA) in performing the optimisation. NSGA has been broadly utilised in solving optimisation problems. NSGA has not only been used in solving the problems related to aeronautical applications (Kroo, 2004) but also in the area of chemical reaction engineering (Nandasana *et al*, 2003), electrical (MahdaviNejad, 2011) and in the area of product design (Nanda, n.d). The application of NSGA in solving the problem is known to benefit from fast selection and easy converging (Popov, 2005). NSGA also has remarkable potential and offers a tremendous approach to solving multi-objective optimisation problems (Srinivas and Deb, 1995). The advantage of NSGA in performing the multi-objective optimisation problems has also been discovered through the comparative study conducted by Ciriuc and Leon (2010). In their study, the comparison between NSGA with weighted genetic algorithm and vector evaluated genetic algorithm (VEGA) particularly in examining their capability in handling test cases which generate the convex Pareto-optimal front, concave Pareto-optimal front and discontinuous Pareto-optimal front was observed. According to Ciriuc and Leon (2010), in comparison to weighted genetic algorithm and VEGA, NSGA is the most efficient algorithm particularly in generating good approximation for every shape of Pareto-optimal front which is crucial, especially in obtaining the trade-off to solve the real-world engineering problems.

The process of NSGA is well-explained elsewhere in the literature and can be summarised as follows. NSGA is initiated by generating a set of random solutions called population. Each solution in this set will progress after every iteration/generation. This is called chromosome. If optimal solution is unlikely to be met at the first iteration, the process will be repeated. The creation of the next generation starts from the new chromosomes called offspring. This offspring is formed by either merging two chromosomes from the latest chromosome using a crossover operator, or by modifying a chromosome using a mutation operator. Methods such as random selection or stochastic universal sampling are used in generating new chromosomes. The process is repeated until the algorithm converges and the optimal solution is provided. The optimal solution is different between single and multi-objective optimisation. For single objective optimisation, the optimal solution represents the best solution provided from the final population, while for multi-objective optimisation the optimal solution is presented through the form of Pareto front.

### **5.3.3 Test cases Implementation**

Two test cases were carried out throughout this optimisation assessment. Both test cases aim to reveal a trade-off that exist between the engine thrust and emissions discharged, particularly NO<sub>x</sub> and CO for the specified mission profile. In this assessment, the mission is to explore the prospective percentage of biofuel in the biofuel/Jet-A mixture in providing lower emissions and high engine thrust. It is noted that due to the aim of reducing the dependency of Jet-A in the aircraft engine, the maximum percentage of biofuel in the mixture is a priority. However, several issues were identified in which the evaluation has to take into account the limitation of fuel's density and the TET which will affect the combustor operation.

The first test case is optimising the percentage of CSPK while the second test case is optimising the percentage of JSPK. Both test cases use the same set-up configuration as in Figure 5-1. The difference is only at the properties of the input handler where the Genes/Variables (I01, I02, I03) are stored. For the first

test case, the minimum and maximum value of I02 (which refers to the percentage of JSPK) is set to be 0, while for the second test case, the minimum and maximum value of I01 (which refers to the percentage of CSPK) is set to be 0. Design parameters, design objectives and design constraints chosen for such test cases are listed below. For test case 1, the design parameters setting is follow as in Table 5-1 while Table 5-2 represents the design parameters for test case 2. However, both these test cases have the same design objectives and design constraints as presented in Table 5-3.

**Table 5-1: List of Design Parameters (Test case 1)**

Gene/Variable	Description	Minimum	Maximum
I01	Percentage of CSPK	0	100
I02	Percentage of JSPK	0	0
I03	Fuel flow rate	0.51	0.7

**Table 5-2: List of Design Parameters (Test case 2)**

Gene/Variable	Description	Minimum	Maximum
I01	Percentage of CSPK	0	0
I02	Percentage of JSPK	0	100
I03	Fuel flow rate	0.51	0.7

**Table 5-3: List of Design Objectives and Design Constraints**

Objective/ Constraint name	Description	Minimum	Maximum	Objective/ Constraint Type	Normalisation Factor
F1	Objective 1 (NO <sub>x</sub> – g/kg fuel)	0.0	20.0	Minimisation	ObjectiveMin
F2	Objective 2 (CO – g/kg fuel)	0.0	10.0	Minimisation	ObjectiveMin
F3	Objective 3 (Thrust - N)	26000.0	100000.0	Maximisation	ObjectiveMax
F4	Constraint 1 (TET - K)	0.0	1800.0	Greater than minimum	GreaterThan
F5	Constraint 2 (Fuel's density – kg/m <sup>3</sup> )	775.0	840.0	Less than maximum	LessThan

In the table, the minimum and maximum value represents the lower limit and upper limit for each objectives and constraints. For this assessment, the main optimiser settings selected are as follows:

**Table 5-4: The Optimiser Set up**

Population size	200.0
Initialisation factor	10.0
Creation scheme	mo2. creators. DoubleTriLinearCrossover mo2. creators. DoubleBoundedSBX mo2. creators. DoubleDynamicVectorMutate
Creation selectors	mo2. selectors. StochasticUniversalSampling mo2. selectors. StochasticUniversalSampling mo2. selectors. RandomSelection
Creation rates	0.45, 0.45, 0.1
Stopping criteria (maximum generation)	200.0
Selection pressure	2.0

Within this set up, total evaluations performed by NSGAMO in generating the Pareto front are 41601.

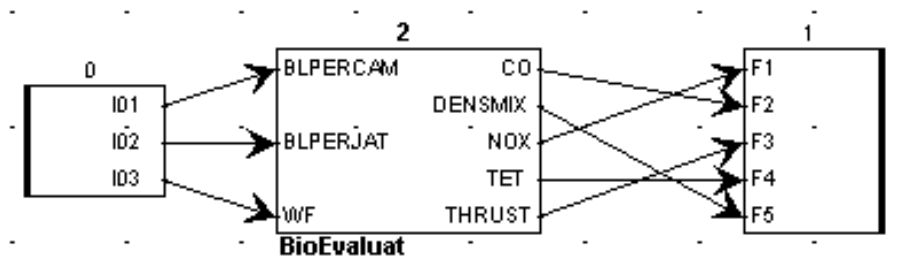


**Figure 5-1: The Test Case Configuration Set up in GATAC Framework**

As shown in Figure 5-1, Block 0 represents the Input Handler component, Block 1 represents the Output Handler component while Block 2 represents the Evaluation Model component. Input Handler component is the component that interfaces the optimiser to the model set up, while Output Handler component interfaces the model set up with the optimiser. The Evaluation Model is the component that responsible to read the input from Input Handler, performing the

engine performance and engine emissions evaluation, and provides the output to the Output Handler.

#### **5.3.4 Comparative Study with MOTS2**

In addition to NSGAMO, MOTS also has usually been implemented in solving problems related to design process. The process of MOTS and the implementation of MOTS in solving the design process problem are discussed broadly in literature, such as in (Jaeggi *et al*, 2008), Armento and Arroyo (2004), and Connor and Tilley (1998).

In order to explore whether there will be an agreement between the solution given by NSGAMO with MOTS2, the optimisation assessment also was conducted using MOTS2 (Jaeggi *et al*, 2008). The assessment was conducted for both test cases providing the same design variables, design objectives, and design constraints. Within this assessment, the comparison in Pareto front generated from both algorithms is performed in order to investigate the design space covered in generating the solutions, and the number of evaluations required for each algorithm in generating Pareto front. Furthermore, the trend for the trade-off, extreme designs, and compromise designs obtained from both optimisers were explored.

In MOTS2 the total number of evaluations was set for 2000 evaluations. The Pareto front generated and the extreme and optimal designs obtained were compared with results obtained from NSGAMO.

In the previous section, total number of evaluations required for NSGAMO to generate Pareto front is 41601, with the evaluations taking approximately four days to complete on a single high performance processor. In order to investigate the total number of evaluations and time consumed for MOTS2 to complete the same solutions, MOTS2 was set firstly to perform a smaller number of iterations. The design space covered was assessed by comparing the generated Pareto front with the NSGAMO Pareto front. The extreme designs were also extracted within the MOTS2 Pareto front and were compared

with the extreme designs obtained from NSGAMO. Through this assessment, the comparison in NSGAMO and MOTS performance was explored. It was found that MOTS2 produced very similar results and an equally filled out Pareto front within only 2000 iterations; requiring only 8 hours cpu time on the same computer.

## **5.4 Results and Discussions**

### **5.4.1 Trade studies – Test case 1**

In this test case, the trade-off investigation for the test case 1 design problem is presented. In this test case, design variables used are the percentage of CSPK and fuel flow. While parameters used as the objective functions are  $\text{NO}_x$ , CO, and thrust and while the constraints selected are TET, and density. Both of the constraints selected are hard constraints in which each of them has to be satisfied.

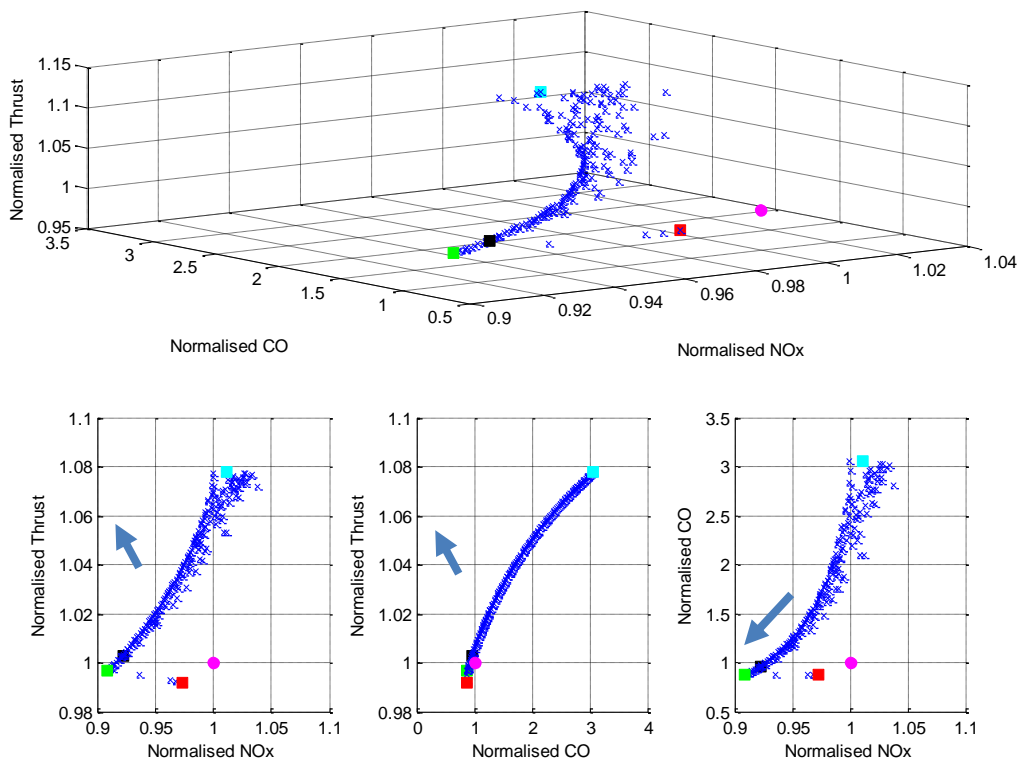


**Figure 5-2: 3D and 2D Plots of NSGAMO Optimisation Result (Blue (x) – Pareto front, Magenta (circle) – datum point, Green (square) – Min NO<sub>x</sub> design (Design A), Red (square) – Min CO design (Design B), Cyan (square) – Max Thrust design (Design C)) for test case 1**

Figure 5-2 presents the 3D Pareto surface and the corresponding 2D projections which represent the trade-off between NO<sub>x</sub> and thrust, CO and thrust, and NO<sub>x</sub> and CO. Arrow shows the target directions. In each trade-off, three extreme designs represent the minimum NO<sub>x</sub>, minimum CO, and maximum thrust in comparison to the baseline point (Jet-A) is included. The trade-off between the formation of NO<sub>x</sub> and thrust generation, and between the CO and engine thrust is clearly shown. However, very little trade-off between NO<sub>x</sub> and CO is evident.

### 5.4.2 Extreme Designs – Test case 1

Table 5-5 and Table 5-6 show details of the extreme designs and the improvement of the designs in comparison to datum. These extreme designs summarise the percentage of CSPK in CSPK/Jet-A mixture and the amount of fuel injected for the extreme optimised designs having minimum NO<sub>x</sub> (Design A), minimum CO (Design B), maximum thrust (Design C) in comparison to datum point (Jet-A).

**Table 5-5: Comparison between the Optimiser Solutions with Baseline Point**

Objective function	Datum/ baseline point	Design A (Min NO <sub>x</sub> )	Design B (Min CO)	Design C (Max Thrust)
Percentage of CSPK (%)	0	57.9	5.9	50.4
Percentage of Jet-A (%)	100	42.1	94.1	49.6
Fuel flow rate (kg/s)	0.52	0.51	0.51	0.60
NO <sub>x</sub> emission (g/kg fuel)	9.6	8.8	9.4	9.7
CO emission (g/kg fuel)	0.1150	0.1009	0.1007	0.3510
Thrust (N)	26154.20	26072.62	25938.66	28182.92

**Table 5-6: Improvement of Objective Functions for Each Solution Relative to Baseline Point**

Objective Functions	Improvement Relative to Baseline Point (%)		
	Design A	Design B	Design C
NO <sub>x</sub> (g/kg fuel)	9.1	2.7	-1.1
CO (g/kg fuel)	12.2	12.4	-205.0
Thrust (N)	-0.3	-0.8	7.8
Fuel Flow (kg/s)	1.9	1.9	-15.0

In Design A, the resulting optimised design shows the highest reduction of 9.09% in NO<sub>x</sub>, with the penalty of 0.3% reduction in thrust. The reduction in CO is observed for this design. However the reduction is not much compared to Design B. For this design, the blend of 57.898% of CSPK with 42.102% Jet-A is obtained. This design also illustrates the reduction in fuel flow by 1.9%.

Design B yields the highest reduction in CO formation relative to Design A and Design C, although the reduction in NO<sub>x</sub> is observed. With this design, CO is reduced by about 12.4% with a penalty of 0.8% due to reduction in engine thrust. This design however, shows the little use of CSPK in the mixture, with the reduction of 1.9% of fuel flow being observed.

Accordingly, to achieve the maximum thrust design (Design C), the blend of 50.4% CSPK with 49.6% Jet-A is required. With this design, the relatively higher increase of thrust is reported. This is consistent with the amount of fuel consumed as the thrust is proportionate with the fuel consumed. However, due to the high amount of fuel consumed, this design has to suffer the largest penalty of CO.

#### **5.4.3 Compromise Design – Test case 1**

Prior to choosing the compromise design, the design problem defined earlier has to be considered. As the intention of this assessment is to reduce the dependency on conventional fuel and minimise emissions generated while improving or the aircraft performance (engine thrust), therefore, it is important in this evaluation to consider the optimal percentage of biofuel that satisfies the objective functions selected. Although Design C is observed to improve the engine thrust, it also generates high NO<sub>x</sub> and CO due to the increases in fuel consumed. Design B is noted to offer a reduction in both NO<sub>x</sub> and CO, although the reduction in engine thrust is noted and considered acceptable. But this is only achievable by mixing a very small percentage of biofuel which therefore is still unable to fulfil the defined requirement. Design A on the other hand, reduces NO<sub>x</sub> and CO although the reduction of CO is small compared to Design B. Within this design however, a small reduction in engine thrust is noted.

The trade-off study has shown the correlation of the emissions generation and the production of engine thrust with the percentage mixture of biofuel/Jet-A, and the fuel flow. It was observed that in order to have the highest engine thrust the blend of biofuel with Jet-A is essential as it increases LHV and heat capacity of the fuel, hence increasing the thrust. Additionally, it is also necessary to inject more fuel. Blending biofuel with Jet-A also is necessary in order to have low NO<sub>x</sub> emissions due to a reduction in flame temperature as the percentage of biofuel in the mixture increases. In contrast, to have low emissions, blending biofuel with Jet-A is not mandatory as the amount of fuel injected becomes more important. This is due to the reduction in flame temperature as the percentage of biofuel in the mixture increases, which leads to incomplete combustion. Furthermore, it is also observed that in obtaining low emissions, the amount of fuel injected has to be reduced. Based on this investigation, a compromise design was selected within the Pareto-optimal front that more or less satisfies the objective function. The comparison of optimal design selected and the improvement relative to datum point is presented in Table 5-7.

**Table 5-7: The Comparison of Optimal Design and the Improvement Relative to Datum Point**

<b>Objective function</b>	<b>Datum/ baseline point</b>	<b>Optimal design</b>	<b>Improvement relative to baseline (%) (0.51 – 0.7)</b>
Percentage of CSPK (%)	0	57.24	-
Percentage of Jet-A (%)	100	42.76	-
Fuel flow rate (kg/s)	0.52	0.517	0.57
NO <sub>x</sub> emission (g/kg fuel)	9.6	8.9	7.80
CO emission (g/kg fuel)	0.12	0.11	4.34
Thrust (N)	26154.20	26228.89	0.3

#### **5.4.4 Trade Studies – Test case 2**

Similar to test case 1, this test case was set up to obtain the trade-off existing between the selected objective functions: NO<sub>x</sub>, CO and thrust. However, regarding test case 1, this test case was established to optimise the percentage

of JSPK in the JSPK/Jet-A mixture within the certain range of fuel flow. As for test case 1, this test case also implemented the same design constraints. The evaluation was performed using a similar optimiser method at similar population size, which accordingly generated the same total number of evaluations. The Pareto-optimal front obtained is presented in Figure 5-3 with projections of the 3D Pareto set between  $\text{NO}_x$  and thrust, CO and thrust, and  $\text{NO}_x$  and CO included. Figure 5-3 shows definite trade-off between the objectives functions selected. However, very small trade-off is observed for the case of  $\text{NO}_x$  and CO.

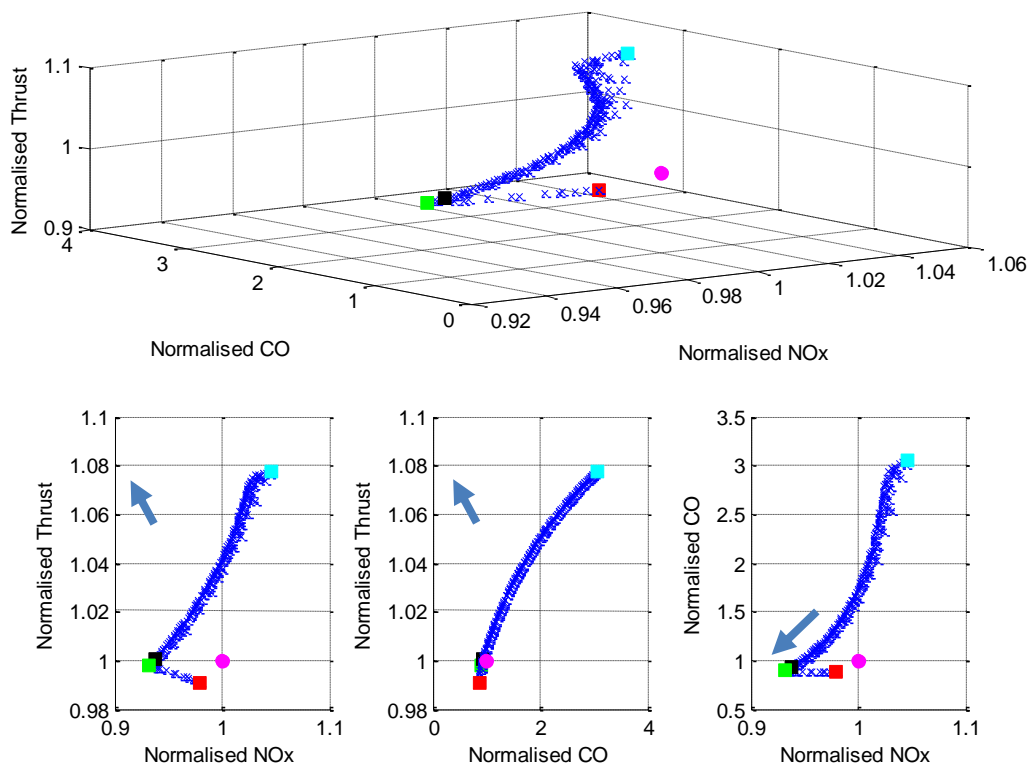


**Figure 5-3: 3D and 2D Plots of NSGAMO Optimisation Result (Blue (x) – Pareto front, Magenta (circle) – datum point, Green (square) – Min  $\text{NO}_x$  design, Cyan (square) – Max Thrust design, Red (square) – Min CO design) for test case 2 – Arrow Shows the Target Direction**

#### 5.4.5 Extreme Designs - Test case 2

An analysis of the trade-off presented above has led to three extreme design points which have the minimum  $\text{NO}_x$  (Design A), minimum CO (design B) and

maximum thrust (Design C) which corresponds to the percentage of JSPK in the mixture with the amount of fuel consumed. Table 5-8 shows details of those three extreme design points while the improvement of those points relative to datum point (Jet-A) is given in Table 5-9.

Design A illustrates the need for mixing 46.72% of JSPK with 53.28% of Jet-A in obtaining the minimum NO<sub>x</sub>. This design also yields a reduction of 10.7% of CO and 0.2% reduction in thrust. Design B on the other hand illustrates the possibility of having the minimum CO by using almost 100% Jet-A, but it has to be injected as a small amount of fuel which therefore reduces the thrust generated by 0.9%. Design B also yields a reduction in NO<sub>x</sub> but this reduction is not significant in comparison to Design A. Design C which corresponds to high thrust design illustrates the mixture of 30.99% of JSPK with 69.01% of Jet-A which has to be injected at relatively high amount of fuel. However, as the penalty, this design has to suffer high increases of NO<sub>x</sub> and CO.

**Table 5-8: Comparison between the Optimiser Solutions with Baseline Point**

<b>Objective function</b>	<b>Datum/ baseline point</b>	<b>Design A Min NO<sub>x</sub></b>	<b>Design B Min CO</b>	<b>Design C Max thrust</b>
Percentage of JSPK (%)	0	46.72	0.36	30.99
Percentage of Jet-A (%)	100	53.28	99.64	69.01
Fuel flow rate (kg/s)	0.52	0.51	0.51	0.60
NO <sub>x</sub> emission (g/kg fuel)	9.6	9.0	9.4	10.1
CO emission (g/kg fuel)	0.115	0.103	0.101	0.351
Thrust (N)	26154.20	26100.24	25913.87	28177.27

**Table 5-9: Improvement of Objective Functions for Each Solution Relative to Baseline Point**

Objective Functions	Improvement relative to datum point (%)		
	Design A Min NO <sub>x</sub>	Design B Min CO	Design C Max thrust
NO <sub>x</sub> (g/kg fuel)	6.85	2.05	-4.59
CO (g/kg fuel)	10.7	12.4	-205.3
Thrust (N)	-0.2	-0.9	7.7
Fuel Flow (kg/s)	1.9	1.9	-15.0

#### 5.4.6 Compromise Design – Test case 2

The compromise design for this test case was selected based on the criteria defined earlier. Considering the three extreme designs discussed above, none of these designs fulfil the objectives of the design problem. Both Design A and Design B show the possibility of reduction in NO<sub>x</sub> and CO; however the increase in thrust is unsatisfactory. Design C on the other hand satisfies the thrust objective function but not for CO and NO<sub>x</sub>. For that reason, the optimal design has been chosen in order to ensure that the objective functions are satisfied. The optimal solution selected shows improvements in all specified objective functions although the improvements are not significant.

**Table 5-10: The Optimal Solution and the Improvement Relation to Datum Point**

Objective function	Datum/ baseline point	Optimal solution	Improvement relative to baseline (%) (0.51 – 0.7)
Percentage of JSPK (%)	0	46.51	-
Percentage of Jet-A (%)	100	53.49	-
Fuel flow rate (kg/s)	0.52	0.513	1.35
NO <sub>x</sub> emission (g/kg fuel)	9.6	9.0	6.28
CO emission (g/kg fuel)	0.115	0.107	6.96
Thrust (N)	26154.20	26169.59	0.06

### 5.4.7 Comparison between NSGAMO with MOTS2

As aforementioned, the design space was covered by MOTS2 using only 2000 evaluations and a cpu time of just 32191 seconds; about 8 hours to completion. The Pareto front generated compare well with the Pareto front generated by NSGAMO but this routine took far larger evaluations and time.

#### 5.4.7.1 The Pareto front Comparison

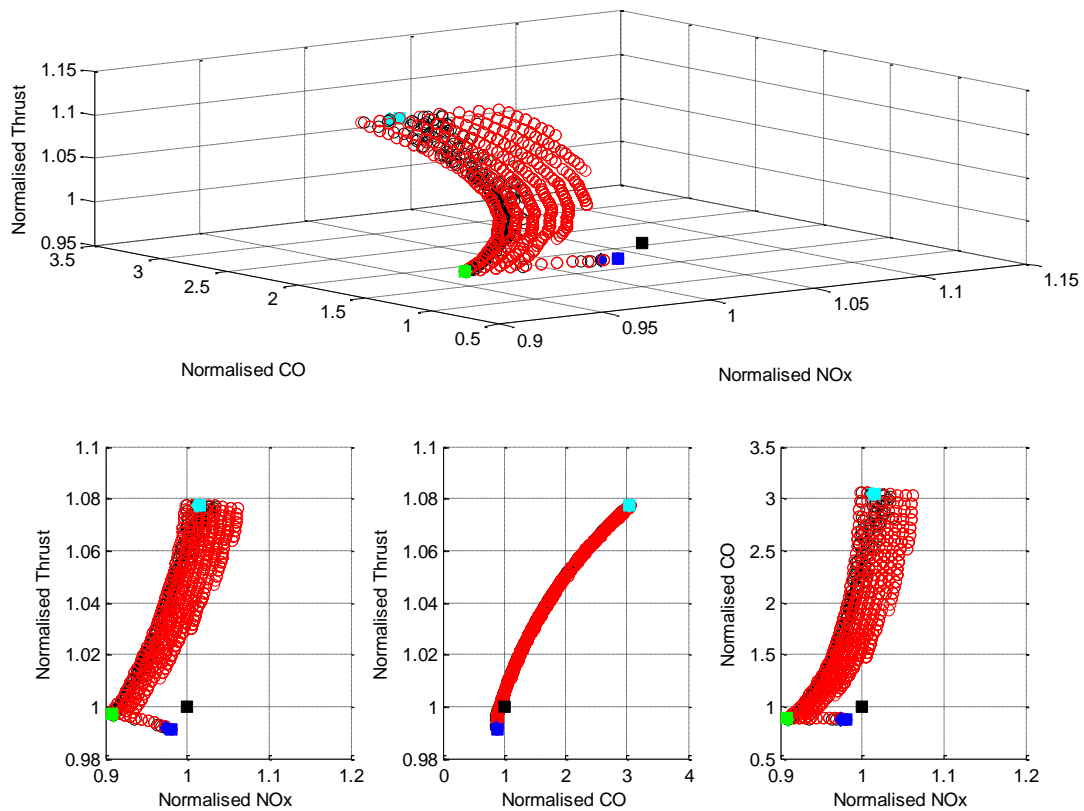


**Figure 5-4: The Comparison of Pareto Front for Test Case 1 - (Red circle - MOTS2 Pareto Front, Black circle – NSGAMO Pareto Front, Black square – Datum point, Cyan square – Max thrust design (MOTS2), Cyan diamond – Max thrust design (NSGAMO), Green square – Min NOx design (MOTS2), Green diamond – Min NOx design (NSGAMO), Blue square – Min CO design (MOTS2), Blue square – Min CO design (NSGAMO))**

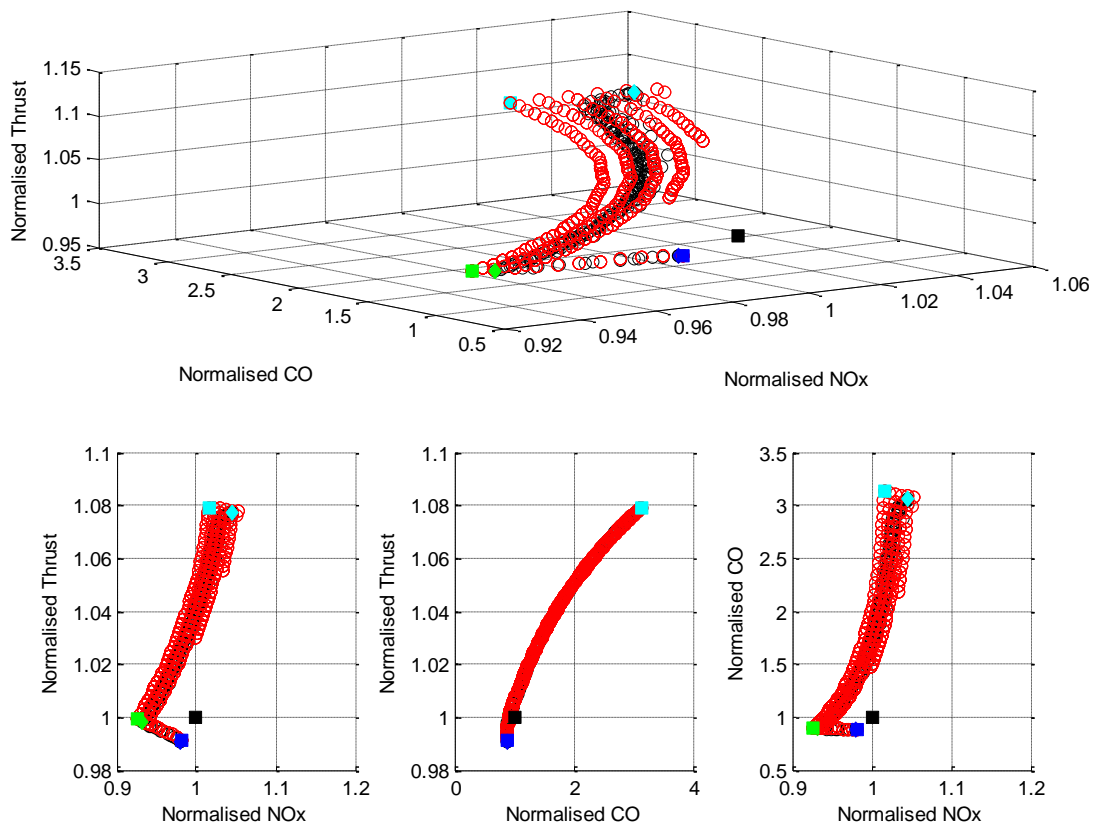


**Figure 5-5: The Comparison of Pareto Front for Test Case 2 (Red circle - MOTS2 Pareto Front, Black circle – NSGAMO Pareto Front, Black square – Datum point, Cyan square – Max thrust design (MOTS2), Cyan diamond – Max thrust design (NSGAMO), Green square – Min NOx design (MOTS2), Green diamond – Min NOx design (NSGAMO), Blue square – Min CO design (MOTS2), Blue square – Min CO design (NSGAMO))**

For both optimisations, the set up for the evaluated test cases is the same as indicated in Table 5-1, Table 5-2, and Table 5-3. The difference only relies on the number of evaluation. As aforementioned, the design space was covered by MOTS2 using only 2000 evaluations, and a cpu time of just 32191 seconds; about 8 hours to completion. The Pareto front generated compare well with the Pareto front generated by NSGAMO but this routine took far larger evaluations and time. The comparison of 3D Pareto surface and the 2D projections obtained between MOTS and NSGAMO however shows similar shape and trade-off

which suggests the successful of those optimisers in handling the selected design problem.

#### 5.4.7.2 Extreme Designs Comparison

##### Test case 1

**Table 5-11: The Comparison of Extreme Designs Solution given between NSGAMO and MOTS2 – Test case 1**

Objective function	Datum/ baseline point	NSGAMO			MOTS2		
		Design A Min NO <sub>x</sub>	Design B Min CO	Design C Max thrust	Design A Min NO <sub>x</sub>	Design B Min CO	Design C Max thrust
Percentage of CSPK (%)	0	46.72	0.36	30.99	59.0	0	47.2
Percentage of Jet-A (%)	100	53.28	99.64	69.01	41.0	100	52.8
Fuel flow rate (kg/s)	0.52	0.51	0.51	0.60	0.51	0.51	0.6
NO <sub>x</sub> emission (g/kg fuel)	9.6	9.0	9.4	10.1	8.8	9.4	9.8
CO emission (g/kg fuel)	0.115	0.103	0.101	0.351	0.102	0.101	0.350
Thrust (N)	26154.20	26100.24	25913.87	28177.27	26086.70	25923.70	28182.10

Test case 2

**Table 5-12: The Comparison of Extreme Designs Solution given between NSGAMO and MOTS2 – Test case 2**

Objective function	Datum/ baseline point	NSGAMO			MOTS2		
		Design A Min NO <sub>x</sub>	Design B Min CO	Design C Max thrust	Design A Min NO <sub>x</sub>	Design B Min CO	Design C Max thrust
Percentage of JSPK (%)	0	46.72	0.36	30.99	53.0	0	53.0
Percentage of Jet-A (%)	100	53.28	99.64	69.01	47.0	100.0	47.0
Fuel flow rate (kg/s)	0.52	0.51	0.51	0.60	0.51	0.51	0.60
NO <sub>x</sub> emission (g/kg fuel)	9.6	9.0	9.4	10.1	9.0	9.4	9.8
CO emission (g/kg fuel)	0.115	0.103	0.101	0.351	0.104	0.101	0.359
Thrust (N)	26154.20	26100.24	25913.87	28177.27	26137.70	25923.70	28225.40

In order to explore the objective designs evaluated in NSGAMO and MOTS2, the extreme conditions obtained from each of the Pareto fronts was compared. Table 5-11 and Table 5-12 show the extreme design conditions between MOTS2 and NSGAMO. As shown, both optimisers predict the same fuel flow that has to be injected in satisfying the design objectives. However, differences have been noted in the fuel percentage. In comparison to NSGAMO, MOTS2 predicts larger percentage of JSPK and CSPK that can be used in the engine in order to satisfy the design objectives.

### 5.4.7.3 Compromise Design Comparison

The comparison of the compromise designs obtained from NSGAMO and MOTS2 for Test Case 1 and Test Case 2 are presented.

**Table 5-13: The Comparison of Optimal Design between NSGAMO and MOTS2 - Test Case 1**

<b>Objective function</b>	<b>Datum/ baseline point</b>	<b>Optimal design (NSGAMO)</b>	<b>Improvement relative to baseline (%)</b>	<b>Optimal design (MOTS)</b>	<b>Improvement relative to baseline (%)</b>
Percentage of CSPK (%)	0	57.24	-	59.0	-
Percentage of Jet-A (%)	100	42.76	-	41.0	-
Fuel flow rate (kg/s)	0.52	0.517	0.57	0.518	0.38
NO <sub>x</sub> emission (g/kg fuel)	9.6	8.9	7.8	8.9	7.7
CO emission (g/kg fuel)	0.115	0.110	4.34	0.113	2.72
Thrust (N)	26154.20	26228.89	0.3	26264.70	0.42

**Table 5-14: The Comparison of Optimal Design between NSGAMO and MOTS2 - Test case 2**

<b>Objective function</b>	<b>Datum/ baseline point</b>	<b>Optimal solution (NSGAMO)</b>	<b>Improvement relative to baseline (%)</b>	<b>Optimal solution (MOTS2)</b>	<b>Improvement relative to baseline (%)</b>
Percentage of JSPK (%)	0	46.51	-	47.7	-
Percentage of Jet-A (%)	100	53.49	-	52.3	-
Fuel flow rate (kg/s)	0.52	0.513	1.35	0.514	1.15
NO <sub>x</sub> emission (g/kg fuel)	9.6	9.0	6.3	9.0	6.2
CO emission (g/kg fuel)	0.115	0.107	6.96	0.109	5.2
Thrust (N)	26154.20	26169.59	0.06	26205.60	0.20

Table 5-13 and Table 5-14 present the comparison in optimal design solution selected for MOTS2 and NSGAMO, with the improvement relative to datum point is included. The optimal solution selected for MOTS shows close value with optimal solution selected for NSGAMO. The optimal solution for test case 1 (CSPK/Jet-A mixture) suggests the mixture of 59% CSPK with 41.0% Jet-A which yield to the improvement of 7.7% in NO<sub>x</sub>, 2.7% for CO, and 0.4% for engine thrust. While for test case 2 (JSPK/Jet-A mixture), the mixture of 47.7% JSPK with 53.3% of Jet-A is selected as it improves NO<sub>x</sub> by 6.2%, CO by 5.2%, and engine thrust by 0.2%.

## **5.5 Conclusions**

This chapter provides an optimisation assessment in finding the optimal fuel mixture in order to encounter overdependence on the conventional/crude oil and the formation of pollution emissions. As far as the aviation industry is concerned, it is also necessary for the airline company to reduce or at least maintain the operating cost via the reduction of fuel consumed without upsetting

the aircraft performance. Therefore, in addition to the requirement of reducing the emissions generated, the possibility of the fuel mixture improving or at least maintaining the engine thrust has also been evaluated.

In accomplishing this design problem, design variables, design objectives and design constraints are properly defined. Two test cases have been conducted. For test case 1, design variables selected are CSPK percentage and fuel flow, while for test case 2, JSPK percentage and fuel flow are selected. In both test cases, the objective functions of minimising  $\text{NO}_x$ , minimising CO, and maximising thrust are chosen, while the constraints of maximum TET and range of fuel density are defined. The optimisation assessment has been conducted in GATAC (optimisation framework) which implements the Non-dominated Sorted Genetic Multi-objective (NSGAMO) algorithm. In accomplishing the optimisation exercise, GATAC was linked with the BioEvaluate.exe which integrated with the computer tools used for the engine performance and emissions evaluation. The optimisation was allowed to run for a maximum of 200 population generations with 41601 numbers of evaluations being performed.

Within this set up, the trade-offs between the  $\text{NO}_x$  and thrust, CO and thrust, and  $\text{NO}_x$  and CO are obtained and analysed. The trade-offs highlighted the feasibility of integrating tools used in the engine performance and emissions evaluation within GATAC environment particularly for the selected design problem. It also showed that the genetic algorithm optimisation method implemented in GATAC is able to handle this particular designed problem.

The optimisation assessment also was conducted using MOTSS2 to explore the difference in the solutions given between both optimisers. In this exercise, the similar problem designs were set and the evaluations were performed for 2000 evaluations. To explore the difference, the trend of the Pareto front, the extreme designs and the optimal solution given by MOTSS2 are compared with the solution given by NSGAMO. It is noted that for both test cases implemented, MOTSS2 and NSGAMO provided the same trend in Pareto surfaces and revealed correspondingly similar trade-off that exists between the engine thrusts

and emissions discharged. This observation suggests the successful of both optimisers - MOTS2 and NSGAMO in handling the specified design problems.

Three extreme designs representing minimum  $\text{NO}_x$ , minimum CO, and maximum thrust obtained from the trade-offs analysis are compared and discussed. The compromise designs for both optimisers are selected and observed to be reasonably closed.

In case of NSGAMO, for test case 1 (optimising CSPK/Jet-A mixture) the compromise design suggests the mixture of 57.24% of CSPK with 42.76% Jet-A is essential, to yield an improvement (reduction) of  $\text{NO}_x$  by 7.8%, reduction of CO by 4.34%, and improvement (increase) in engine thrust by 0.3%. For test case 2 (optimising JSPK/Jet-A mixture), the compromise design selected suggests the use of 46.51% JSPK/53.49% Jet-A to be implemented in the aircraft engine. This design yields the reduction of  $\text{NO}_x$  by 6.3% and CO by 6.96%. An improvement of 0.06% in engine thrust is noted with this compromise design.

Meanwhile, in case of MOTS2, the compromise design selected for test case 1 suggests the mixture of 59% CSPK with 41.0% Jet-A which improves  $\text{NO}_x$  by 7.7%, 2.7% for CO, and 0.4% for engine thrust. While for test case 2 (JSPK/Jet-A mixture), the mixture of 47.7% JSPK with 53.3% of Jet-A is selected. Within this design, the improvement of  $\text{NO}_x$  by 6.2%, CO by 5.2%, and engine thrust by 0.2% are obtained.

## **6 CFD MODELLING APPROACH**

### **6.1 General Introduction**

As mentioned in Celis (2010), HEPHAESTUS was developed mainly as the sensitivity analysis tool in which the trends of the predicted emissions are more important than the absolute level. It is clearly mentioned in Celis (2010) that in modelling HEPHAESTUS, combustion phenomena such as evaporation process, flow recirculation and turbulence are neglected to provide simplification. Combustion modelled in HEPHAESTUS is also assumed to have well-mixed criteria by introducing the perfectly stirred reactor model which assumes the perfect mixing, hence representing the turbulence process. Within these assumptions, the trend of predicted emissions generated is appropriate to follow the trend provided by ICAO data although under-estimated absolute values are pronounced.

Corresponding to this issue, an assessment was performed in which the practical issues related to the HEPHAESTUS combustion modelling are explored. The assessment was conducted by simulating the combustion in the CFD tool, which is known to be able to test new ideas and solve the fluid problem successfully without the need of high cost experimental studies (Parson *et al*, 2008). Within this assessment, the influence of those assumptions towards the temperature profile and the generation of NO<sub>x</sub> are observed. This assessment was performed only for Jet-A due to little information being available in open literature about the biofuels reaction rate. In solving the turbulence problem, the RANS based turbulence model is used. The assessment was performed with two other colleagues – Gilberto Materano and Janthanee Dumrongsak.

### **6.2 The Comparison of RANS model with DNS and LES models**

In the combustor, the process of turbulence is important as it provides the mixing between the reactant and the oxidiser. There are several models available in CFD usually used in modelling turbulence which are RANS

(Reynolds-Averaged Navier-Stokes), DNS (Direct Numerical Simulation) and LES (Large Eddy Simulation). The comparison of RANS, DNS, and LES has been discussed widely.

DNS is a turbulence model that solves governing equations of flow fields, chemical species concentrations and temperature by setting the numerical grid space below the minimum eddies in these fields. In comparison to RANS and LES, DNS provides the highest numerical accuracy and because of that it is effectively applicable to the basic research. Unfortunately, practical application of this method in the combustion field is very difficult as it requires a huge number of grid points and gives high loads to the computer. Conversely, RANS has been used frequently in practical applications. Using this method, the governing equations are solved by averaging them over time and replacing the resulted Reynolds stresses and turbulent scalars fluxes terms with turbulence model. The advantage of this method is it reduces the number of grid points and computer loads, hence is widely adopted for practical engineering applications. However, for the case of combustion, the accuracy given by RANS is not as accurate as that given by LES, due to its weakness in predicting the unsteady turbulent motions. In the combustor, rapid mixing and short combustion times are deemed essential to having the proper flame stabilisation, which is consequently characterised by very complicated flow patterns such as swirling flows, breakdowns of large-scale vertical structures, and recirculation regions. The limitation of RANS also corresponds to the disability of the code to capture counter-gradient diffusion and other unsteady phenomena in gas turbine combustors (Cannon *et al*, 2003). As the result, the accuracy of the pollution predictions is not fully achieved using RANS simulation. Alternatively, LES method can be used. LES solves the governing equations for relatively large eddies and calculates the remaining small eddies using the models. Advantageously with this method the unsteady turbulent motions are able to be solved. Solving LES gives high loads to computer but high accuracy in the solution is obtained. Although the accuracy of RANS is uncertain especially in solving the combustion problem, a RANS solution is essential in initializing the LES combustor simulation.

Although the RANS solution is known as inaccurate due to its inability in tackling the issue of unsteady turbulent motions associated with the combustion phenomena, the choice of using RANS in solving the turbulence model is appropriate to provide initial study of the difference in temperature profile and NO<sub>x</sub> generation predicted in HEPHAESTUS.

### 6.3 Problem description

It is important to mention here that in order to assess the HEPHAESTUS combustion model in CFD, the 3D model was established based on the 1D model considered in HEPHAESTUS. In HEPHAESTUS, the combustor is represented in four sections; flame front (FF), primary zone (PZ), intermediate zone (IZ) and dilution zone (DZ) (Figure 6-1) with the length and area of each section shown in Table 6-1. Additionally, HEPHAESTUS considers certain fraction of air for the core and for the wall cooling (Table 6-2).

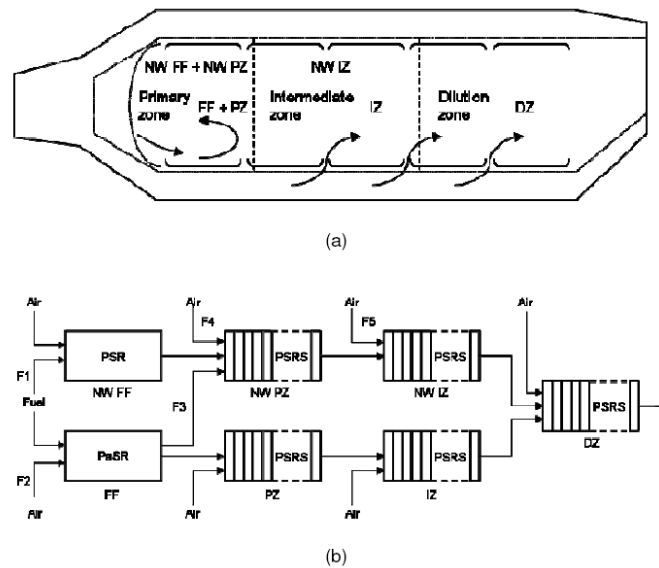


**Figure 6-1: Configuration of Combustor Considered in HEPHAESTUS**

**Table 6-1: Combustor Geometry**

	FF	PZ	IZ	DZ
Inlet area (m <sup>2</sup> )	0.20617	0.20617	0.20617	0.20617
Outlet area (m <sup>2</sup> )	0.20617	0.20617	0.20617	0.20617
Length (m)	0.03125	0.03125	0.09375	0.09437

**Table 6-2: Fraction of Air at the Core and Wall of the Combustor Section**

F1	F2	F3	F4	F5
0.15	0.60	0.15	0.20	0.20

Based on the air fraction and total air mass flow given, the amount of air injected into the core and the wall for each section in the chamber was calculated and is shown in Table 6-3.

**Table 6-3: Amount of Air Entering Each Section of the Combustor**

Combustor section	Air (kg/s)
FF core	0.23442
PZ core	0.31256
IZ core	0.31256
FF wall	0.078
PZ wall	0.078
IZ wall	0.078
DZ wall	0.7814
<b>Total</b>	<b>1.95322</b>

Additionally, with the known value of the fuel flow rate, the chamber pressure, air temperature and the fuel temperature, the area for the core and wall cooling and area of the fuel injector were calculated by assuming the fuel's velocity as 40 m/s, while the air velocity of 10 m/s and 6 m/s were assumed for core and wall respectively using the equations below.

From the equation of state, density of the fuel and density of air were calculated as follows:

$$\rho = \frac{P}{RT} \quad (30)$$

From the known total mass flow of air and fuel, the volumetric flow rate of air and fuel was calculated using the following equation:

$$\dot{V} = \frac{\dot{m}}{\rho} \quad (31)$$

Using the velocity as assumed above, the area of the fuel injector and the area for the core and wall cooling were calculated as follows:

$$A = \frac{\dot{V}}{V} \quad (32)$$

These areas are important in calculating the diameter of the fuel injector and the diameter of the holes that represent the core cooling. Additionally, the number of holes which are homogenously arranged through the combustor zone can also be obtained. However, in the case of the wall cooling, the annular ring was used considering the limitation in the combustor size.

The chamber was meshed using non-structural mesh with the total cells of 154 235.

### Combustor configuration

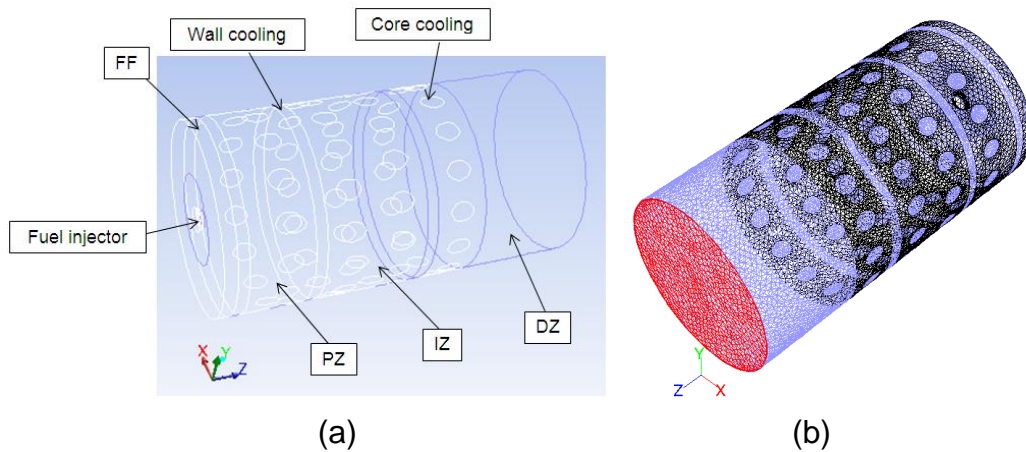


**Figure 6-2: (a) The combustor configuration showing the location of the fuel injector, holes for the core cooling and annular ring for the wall cooling along the chamber (b) The combustor with the total cells of 154 235 non-structural mesh**

## CFD simulation methodology

The simulation was performed using RANS with the boundary condition used is presented in Table 6-4. The simulation was conducted using only 1/10 section of the whole combustor.

**Table 6-4: Combustion Chamber Boundary Condition**

Operating pressure (Pa)	1160903
Total mass flow air (kg/s)	1.95322
Total mass flow fuel (kg/s)	0.04168
Temperature of air (K)	736.51
Temperature of air (K)	288.15

## **6.4 Results and Discussion**

### **6.4.1 Comparison of Combustor Temperature Profile**

It is worth mentioning here that in order to investigate the fluid behaviour considered in HEPHAESTUS and also to justify the practical issues related to the developed model, the CFD 3D model was established based on the 1D model (HEPHAESTUS). Figure 6-3 shows the plot of the temperature predicted by HEPHAESTUS for the wall and for the core of the combustor in comparison to CFD. In HEPHAESTUS, temperature calculated for each section is a mean temperature. Therefore, in order to obtain the mean temperature in CFD, the adaptation from the volume integral for each section is applied.

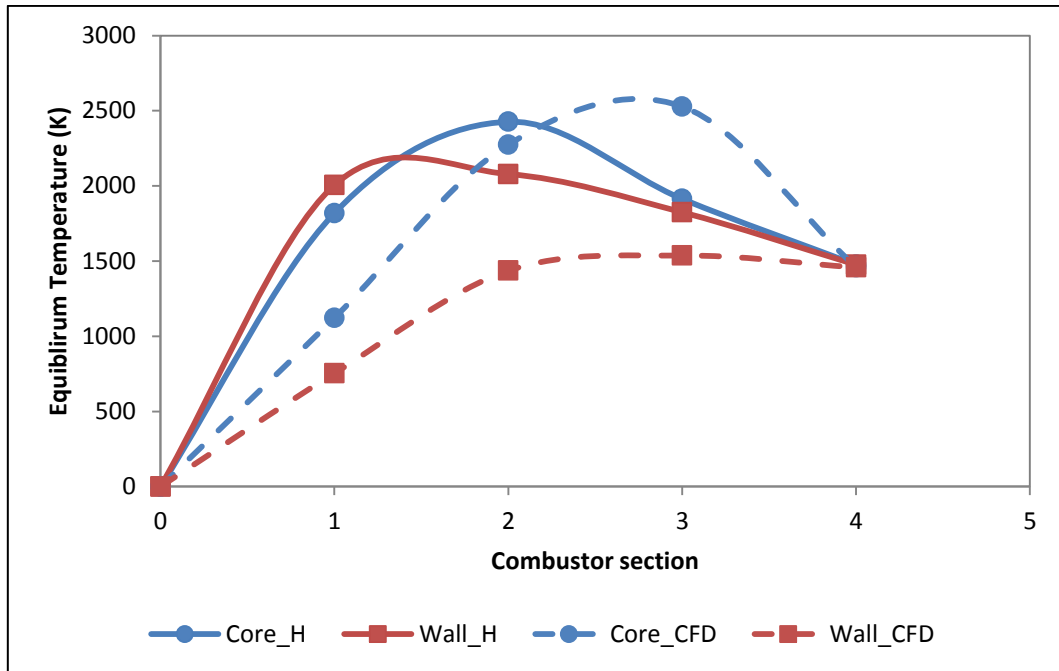


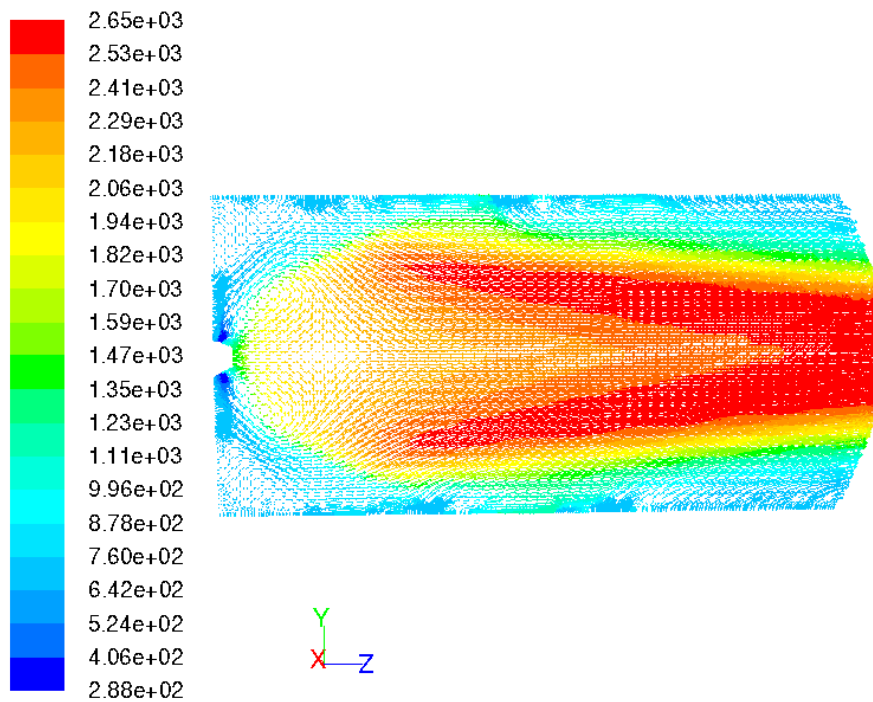
**Figure 6-3: The Temperature Profile of HEPHAESTUS (H) in Comparison to CFD (1 = FF, 2 = PZ, 3 = IZ, 4 = DZ)**

Generally the temperature profile predicted by HEPHAESTUS is in agreement with CFD. Both tools predicted an increase in temperature due to the combustible process, followed by the reduction in temperature particularly at the dilution zone. Although HEPHAESTUS provides an agreement in temperature profile with CFD, as far as the absolute temperature is concerned, significant difference is observed particularly at the combustor upstream although almost consistent temperature is recorded downstream.

Furthermore, it is observed that the flame temperature recorded in HEPHAESTUS appears at the primary zone, while the flame temperature recorded in CFD appears at the intermediate zone. The difference in the flame location and high temperature reported in HEPHAESTUS is due to the assumption that the combustor is well-mixed, and the turbulence is assumed to be well-enough for the combustion to take place as soon as the fuel is injected into the chamber. Additionally, other phenomenon regarding the real combustor process such as droplet evaporation and recirculation are also neglected.

As mentioned above, HEPHAESTUS was developed by representing the FF as the partial stirred reactor (PaSR) while the sequence of perfectly stirred reactor (PSRS) was established in modelling the PZ, IZ and DZ. The reason for establishing PaSR in the FF is to simulate the initial mixing and reaction of the fuel with the swirled air which takes into account the inhomogeneities in this region, while the establishment of the PSRS in the PZ, IZ and DZ was to provide the perfect mixing of the fuel and oxidiser; as such the inclusion of flow recirculation is negligible. As a consequence of the perfect mixing assumed (through the establishment of PSRS) in the PZ, the perfect mixing between the reactant and the oxidiser is achieved, therefore providing the combustible mixture which suggests the reason of the maximum flame temperature is recorded in this region.

However in CFD, the mixing of fuel and oxidiser is established through the turbulence generated from the recirculation process through the difference in velocity of the air and fuel. In order to generate recirculation, hence mixing the fuel and oxidiser, the velocity of the fuel and the velocity of the air were assumed in the beginning of the simulation. Figure 6-4 depicts the temperature velocity vector across the combustor which shows that the assumption made for the fuel flow and airflow velocity is good enough in providing the turbulence/recirculation within the FF region hence initially mixing the fuel and oxidiser. The velocity assumed for the fuel flow and airflow also has been observed in maintaining the flame to be located in the centre of the combustor. Further downstream the FF region, the turbulence is progressing towards the PZ region. The additional air supplied into the combustor in the PZ zone provides higher recirculation region and substantially initiates the flame development in which the temperature starts increasing. However, it is observed that the well-mixing of the fuel and oxidiser occurred at the IZ where the maximum temperature is recorded, which accordingly represents the reason of the difference in maximum temperature location between CFD and HEPHAESTUS.



Velocity Vectors Colored By Static Temperature (k)

Sep 13, 2012  
ANSYS FLUENT 12.1 (3d, dp, pbns, spe, rke)

**Figure 6-4: Velocity Vector of the Static Temperature**

### 6.4.2 The Comparison of NO<sub>x</sub> Generation

The generation of NO<sub>x</sub> was predicted via the post-processing where a converged combustion flow field solution is first obtained before the NO<sub>x</sub> prediction can be performed. In this assessment, only thermal-NO<sub>x</sub> is considered where the Zeldovich mechanisms are employed. As far as NO<sub>x</sub> generation is concerned, the comparison of NO<sub>x</sub> predicted in HEPHAESTUS is compared with NO<sub>x</sub> predicted in CFD (Table 6-5). The comparison shows significant difference of NO<sub>x</sub> predicted. In order to explain this difference, some concerns are highlighted.

**Table 6-5: The Comparison of Temperature and NO<sub>x</sub> between HEPHAESTUS and CFD**

	<b>CFD</b>	<b>HEPHAESTUS</b>	<b>Difference (%)</b>
Temperature (K)	2650	2426.23	-8.4
EINO <sub>x</sub> (g/kg fuel)	50.4	9.4	-81.3

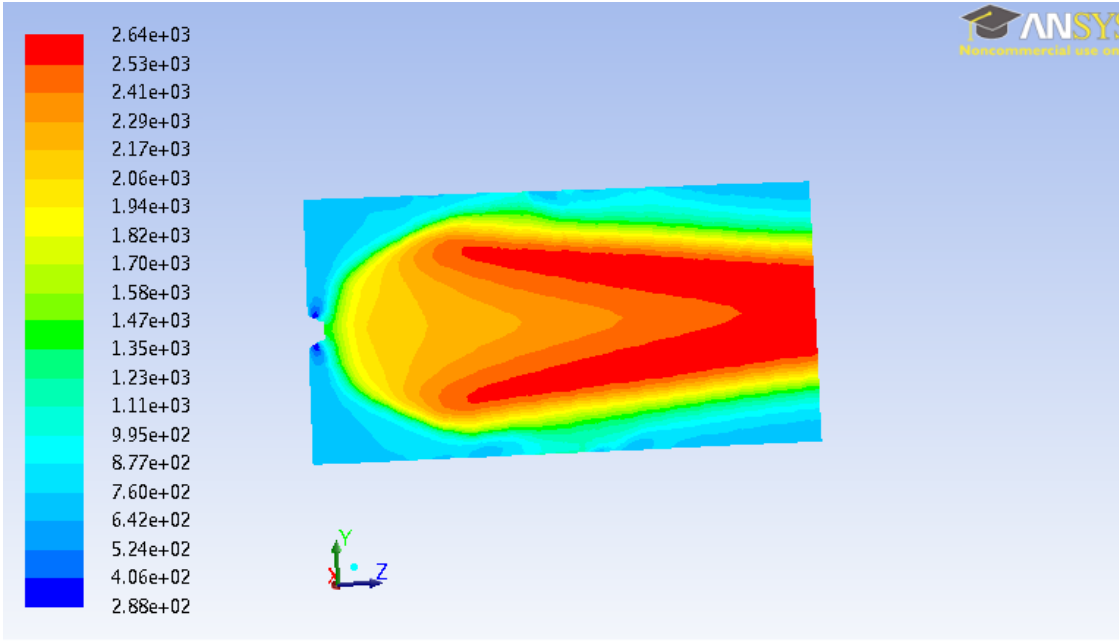
As mentioned above NO<sub>x</sub> considered in both tools is thermal-NO<sub>x</sub> which was calculated based on Zeldovich mechanisms. As known, the extended Zeldovich mechanism is very sensitive to temperature; therefore any difference in temperature will have impact on the NO<sub>x</sub> formation. As depicted in the table, the temperature predicted in HEPHAESTUS is lower than the predicted temperature given in CFD. This reduction consequently reduced NO<sub>x</sub> generation. The sensitivity of temperature with NO<sub>x</sub> is as yet unknown. CFD however predicts an increase of twice NO<sub>x</sub> for every 90K difference in temperature (FLUENT, 2001). From the table it is observed that every 1% reduction in temperature effects a 10% reduction in NO<sub>x</sub>.

Additionally, the difference in NO<sub>x</sub> between HEPHAESTUS and CFD is observed due to the inconsistency in the temperature profile which shows the dissimilarity in the location of maximum flame temperature previously discussed, due to the assumption of fast and well-mixed reaction between reactant and air considered in HEPHAESTUS. In addition, this inconsistency may be affected by neglecting the real combustion phenomena such as fuel droplet evaporation, combustion instability and flow recirculation within the chamber.

The effect of recirculation zone on NO<sub>x</sub> formation is noted in Schefer and Sawyer (1977) who observed that maximum NO<sub>x</sub> is generated within the recirculation zone due to relatively high temperatures and long residence time characteristics of this region. Therefore, by neglecting this phenomenon, the prediction of NO<sub>x</sub> may not be dependable. This is also strongly supported by Celis (2010). For the test case he considered, the under-predicted formation of NO<sub>x</sub> in comparison to the ICAO data is obtained, which was believed to be due

the approach of how the residence time was calculated. In HEPHAESTUS the residence time was calculated through the proportionality of residence time on density and reactor volume, and inversely proportional to the mass flow rate. Through this calculation, the estimation of residence time is relatively short and provides under-estimation of  $\text{NO}_x$ . Celis (2010) also discovered that if he doubled the residence time in the PZ and IZ of the combustor section to represent the flow recirculation, the increases in  $\text{NO}_x$  would be approximately doubled too, which is much closer to the  $\text{NO}_x$  provided in the ICAO data.

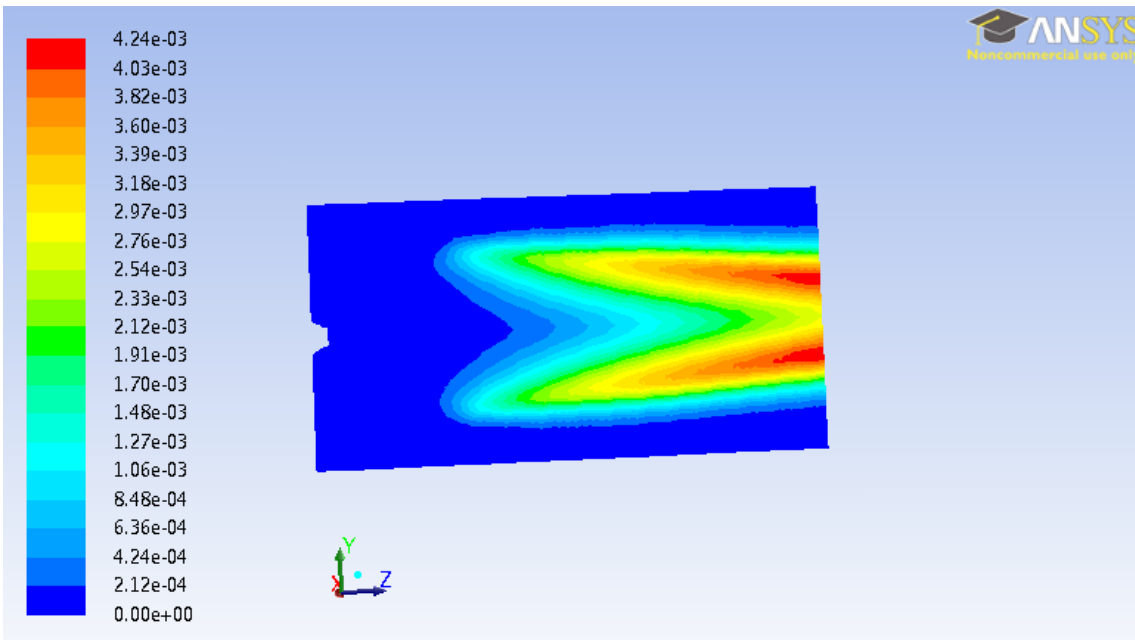
It is observed in Figure 6-5 that although the flame is well-located at the centre of the chamber, due to the length considered in HEPHAESTUS, the flame is found to be positioned downstream close to the exit, which suggests the so-called blow-out condition. The temperature contours also clearly show the growth of the flame temperature which is starting to develop at the PZ, achieves the maximum at the IZ and continuously propagates towards the combustor exit which therefore suggests the high mass fraction of  $\text{NO}_x$  downstream in the chamber (Figure 6-6). This also represents one of the reasons owing to the significant discrepancy in  $\text{NO}_x$  formation between CFD and HEPHAESTUS.



Contours of Static Temperature (k)

Nov 15, 2012  
ANSYS FLUENT 14.0 (3d, pbns, spe, rke)

**Figure 6-5: The Temperature Contour Shows the Maximum Temperature which Recorded at the IZ**



Contours of Mass fraction of Pollutant no

Nov 15, 2012  
ANSYS FLUENT 14.0 (3d, pbns, spe, rke)

**Figure 6-6: The Contour of NO<sub>x</sub> Mass Fraction Shows the Highest NO<sub>x</sub> Mass Fraction Downstream of the Chamber**

It is important to mention that although the Zeldovich mechanism is applied in both tools, the difference in the kinetic rate constants which correspond to the reaction rate parameter: Pre-exponential factor in the Arrhenius Equation (A), Activation energy in the Arrhenius equation ( $E_a$ ), and temperature exponent in the Arrhenius equation ( $\beta$ ), also become one of the factors that provides the significant difference in the prediction of  $\text{NO}_x$  formation. The influence of different kinetic rate parameters towards the prediction of  $\text{NO}_x$  formation has been observed in Hernandez *et al.* (1998) who modelled and compared  $\text{NO}_x$  emission results by changing the A,  $\beta$ , and  $E_a$  in the reactions below, as used by different authors.



From the results, the influence of reaction parameters was observable especially in (R1) and (R4) which correspondingly dispersed  $\text{NO}_x$  for up to 68% and 20% respectively. This observation suggested that a different approach in modelling  $\text{NO}_x$  may provide different  $\text{NO}_x$  prediction, thus more reliable experimental data especially for the main reaction that affects the  $\text{NO}_x$  formation is essential.

In order to check the effect of the reaction parameters considered in this work, the reaction parameters used in HEPHAESTUS are compared with the reaction rate used in CFD. The reaction parameters considered in both tools are presented in Table 6-6 below.

**Table 6-6: The Comparison of Reaction Parameters Considered in HEPHAESTUS and CFD for Each Elementary Reaction**

	Elementary Reaction	CFD (Hanson and Salimian, 1984)			HEPHAESTUS (Celis, 2010)		
		A	$\beta$	$E_a/R$	A	$\beta$	$E_a/R$
1.	$O + N_2 \rightarrow NO + N$	$1.8 \times 10^8$	0	38370	-	-	-
2.	$NO + N \rightarrow O + N_2$	$3.8 \times 10^7$	0	- 425	$1.204 \times 10^{10}$	0	0
3.	$N + O_2 \rightarrow NO + O$	$1.8 \times 10^4$	0	- 4680	$1.204 \times 10^{10}$	0	- 3550
4.	$NO + O \rightarrow N + O_2$	$3.81 \times 10^3$	0	- 20820	-	-	-
5.	$N + OH \rightarrow H + NO$	$7.1 \times 10^7$	0	- 450	$4.214 \times 10^{10}$	0	0
6.	$NO + H \rightarrow N + OH$	$1.7 \times 10^8$	0	- 24560	-	-	-
7.	$H + N_2O \rightarrow N_2 + OH$	-	-	-	$3.01 \times 10^{10}$	0	- 5400
8.	$O + N_2O \rightarrow N_2 + O_2$	-	-	-	$3.612 \times 10^{10}$	0	- 1200
9.	$O + N_2O \rightarrow NO + NO$	-	-	-	$4.816 \times 10^{10}$	0	- 1200

As shown in Table 6-6, the first six reactions represent the forward and backward extended Zeldovich mechanism. As observed, CFD considered all the reaction elements of extended Zeldovich mechanism, but not all of the reactions elements are considered in HEPHAESTUS. For each Zeldovich reaction considered in HEPHAESTUS, the difference in the reaction parameters also is noted. In addition to the Zeldovich mechanism, HEPHAESTUS also considered additional reactions which represent the contribution of  $N_2O$  to  $NO_x$  formation. This comparison clarifies the influence of reaction constants and the difference in number of reactions considered towards the generation of  $NO_x$ . The effect of the reaction constants toward  $NO_x$  generation is further explored by changing the reaction constants considered in Celis (2010) with the reaction constants suggested in Miller and Bowman (1989). The reaction elements however are kept as the same.

**Table 6-7: The Reaction Considered in Modified HEPHAESTUS**

	Elementary Reaction	HEPHAESTUS (Celis, 2010)			Modified HEPHAESTUS (Miller and Bowman, 1989)		
		A	$\beta$	$E_a/R$	A	$\beta$	$E_a/R$
1.	$NO + N \rightarrow O + N_2$	$1.204 \times 10^{10}$	0	0	$3.27 \times 10^9$	3	0
2.	$N + O_2 \rightarrow NO + O$	$1.204 \times 10^{10}$	0	- 3550	$6.4 \times 10^6$	0	- 3160.5
3.	$N + OH \rightarrow H + NO$	$4.214 \times 10^{10}$	0	0	$3.8 \times 10^{10}$	0	0
4.	$H + N_2O \rightarrow N_2 + OH$	$3.01 \times 10^{10}$	0	- 5400	$7.6 \times 10^{10}$	0	- 7650
4.	$O + N_2O \rightarrow N_2 + O_2$	$3.612 \times 10^{10}$	0	- 1200	$1.1 \times 10^{11}$	0	- 14195.25
6.	$O + N_2O \rightarrow NO + NO$	$4.816 \times 10^{10}$	0	- 1200	$1.1 \times 10^{11}$	0	- 14195.25

**Table 6-8: The Comparison of NO<sub>x</sub> between the Initial HEPHAESTUS,  
Modified HEPHAESTUS and CFD**

	CFD	HEPHAESTUS (Celis, 2010)	Difference wrt CFD (%)	Modified HEPHAESTUS (Miller and Bowman, 1978)	Difference wrt CFD (%)
Temperature (K)	2640	2426	8.1	2426	8.1
EINO <sub>x</sub> (g/kg fuel)	50.372	9.406	81.3	34.071	32.4

It is observed that modified HEPHAESTUS, using reaction constants given by Miller and Bowman (1984) has increased the NO<sub>x</sub> generation by 3.6 times larger than the original HEPHAESTUS, which uses the reaction constants considered in Celis (2010), and the prediction for the NO<sub>x</sub> is also observed to be much closer to the NO<sub>x</sub> predicted in CFD (32.4% reduction in comparison to the 81.3% reduction predicted in HEPHAESTUS). This suggests that proper experimental data is crucial in order to have accuracy in the result.

#### **6.4.3 The Comparison Result between HEPHAESTUS with URANS and LES for the case of Generic Combustor**

The practical issues related to the simplifications and assumptions considered in HEPHAESTUS also were explored for the case of generic combustor. In this investigation, a 3D generic combustor was modelled in FLUENT by establishing the boundary condition considered in HEPHAESTUS. The simulation was performed by Dumrongsak (2012), who implemented URANS and LES model to model the turbulence inside the chamber. Detail about the simulation can be obtained in Dumrongsak (2012).

In order to explore the influence of assumptions considered in HEPHAESTUS, the boundary condition and the combustor geometry of the generic combustor were provided into the HEPHAESTUS input file, and the comparison of temperature at the combustor outlet, flame temperature, and the generation of NO<sub>x</sub> were performed.

**Table 6-9: The Boundary Condition for the Generic Combustor**

Total mass flow air (kg/s)	19.535
Total mass flow fuel (kg/s)	0.417
Temperature of air (K)	737
Temperature of air (K)	288

**Table 6-10: Average Control Volume of the Generic Combustor**

	FF	PZ	IZ	DZ
Inlet area (m <sup>2</sup> )	0.018	0.020	0.021	0.020
Outlet area (m <sup>2</sup> )	0.018	0.020	0.021	0.020
Length (m)	0.070	0.070	0.073	0.350

**Table 6-11: The Temperature Predicted by HEPHAESTUS for Each Zone of the Generic Combustor**

Combustor Section	Temperature (K)
Flame Front (FF)	1818.22
Primary Zone (PZ)	2426.53
Intermediate Zone (IZ)	1913.46
Dilution Zone (DZ)	1475.75

**Table 6-12: The Comparison of Outlet Temperature, Flame Temperature and NO<sub>x</sub> Generation between HEPHAESTUS and CFD Simulation**

	Outlet Temperature (K)	Flame Temperature (K)	EINO <sub>x</sub> (g/kg fuel)
CFD – URANS (Dumrongsak, 2012)	1452.00	2766.57	81.0
CFD – LES (Dumrongsak, 2012)	1512.00	2490.00	10.0
HEPHAESTUS (Celis, 2010)	1475.75	2426.23	0.797
HEPHAESTUS (Miller and Bowman, 1978)	1475.75	2426.23	3.650

Table 6-12 shows the comparison in temperature outlet, flame temperature and NO<sub>x</sub> generation for both version of HEPHAESTUS and the turbulence models used in the CFD simulation. In regard to the outlet and flame temperature, it is noted that HEPHAESTUS predicted the value to be reasonably close with the CFD simulation (URANS and LES). However, significant difference is observed for the formation of NO<sub>x</sub>. As far as thermal-NO<sub>x</sub> is concerned, the difference in

NO<sub>x</sub> formation is found to be proportionate with the flame temperature however due to simplification and assumptions considered in the initial HEPHAESTUS, the under-predicted value is observed. Little improvement is obtained as the reaction rate considered in Miller and Bowmann (1978) was used.

Additionally, in case of HEPHAESTUS, the flame is found to be located at the PZ due to the highest temperature recorded in this region (Table 6-11). While in case of CFD, the highest temperature is recorded at the PZ (Dumrongsak, 2012). The difference in the flame location is nonetheless due to the assumption considered in HEPHAESTUS in which the turbulence phenomenon was neglected.

## **6.5 Conclusions**

This assessment was proposed in order to explore the behaviour of the flow inside the combustor considered in HEPHAESTUS by transforming the combustor geometry, the air fraction, fuel flow, temperature and pressure of the combustor into the 3D model suitable for CFD. The comparison in temperature profile across the combustor and the generation of NO<sub>x</sub> is presented. In terms of trends, the temperature profile predicted in HEPHAESTUS is in agreement with the temperature profile predicted in CFD, although differences in the absolute value and the location of the maximum flame temperature are observed. Such differences nonetheless are due to the assumption considered and are negligible of other combustor phenomenon. Additionally, this assessment clarified the effect of different reaction equations and reaction constants towards NO<sub>x</sub> generation which therefore requires proper experimental data to achieve consistency in the accuracy. In order to obtain close agreement with CFD, HEPHAESTUS has to consider using different reaction constants, for example the one suggested in Miller and Bowman (1978) for predicting NO<sub>x</sub>.

## **7 GENERAL RESULTS AND DISCUSSIONS**

This research work was proposed generally to evaluate and optimise the biofuel combustion technologies designed to reduce the pollution discharged from civil aircraft engines. To be more specific, the research was established in order to investigate the influence of biofuels regarding spray characteristics, which are known as one of the factors controlling pollution formation. The capability of biofuels is further explored through the examination of their effects on engine performance and emissions. The following optimisation work explores the trade-off between engine performance and emissions in order to identify the optimal fuel design based on the engine performance and emission requirements. Several tasks have been identified in the course of this research. The results obtained from the tasks are summarised here.

### **7.1 Biofuel's Spray Behaviour Evaluation**

As part of the combustion efficiency evaluation, this research work was developed to expand the work of Mazlan (2008) who conducted a numerical study focusing on predicting the droplet lifetime and spray penetration as one of the factors influencing fuel spray characteristics and the formation of pollution of a gas turbine engine. The work conducted by Mazlan (2008) used ethanol as a baseline fuel. The prediction of droplet lifetime and spray penetration was quantified by implementing the ethanol's properties into the equations related to motion, energy and boiling mass transfer taken from FLUENT. In expanding this research work, the droplet lifetime and spray penetration was evaluated for other biofuels (JSPK, CSPK and RME) and the comparison with kerosine was conducted.

From the investigation, ethanol recorded the shortest droplet lifetime while the longest was recorded by RME. Droplet lifetime indicates the time taken by the liquid fuel droplet to evaporate into a gaseous state, before it can be mixed properly with air in order to start the combustion. Droplet lifetime is noted as proportionate to the volatility of the fuel, whilst the volatility of the fuel can be

estimated in inverse proportion to the fuel boiling temperature. Fuel with high boiling temperature is less volatile than fuel with low boiling temperature. As observed, ethanol has low boiling temperature, hence is more volatile than other fuels which simultaneously require less time to evaporate from liquid to gaseous state, while the reverse is the case for RME. Furthermore, boiling point itself is not the only factor which influences the lifetime of the droplet, as the effect of viscosity is also noted. With regard to spray penetration, the prediction was carried out using the equation recommended in Sazhin (2001). As far as this equation is concerned, the prediction of penetration length depends on the density of the fuel. Although the influence of fuel density on penetration length is observed, this however is only valid in the case of RME, whilst other factors such as viscosity are found to influence the penetration length. More viscous fuel is noted to penetrate longer than less viscous fuel. This observation was obtained due to high viscous fuel being unable to be well-atomised. Nonetheless, this will have an adverse effect on the fineness of atomisation due to there being less air resistance. This suggests that any fuel with low viscosity will have an advantage regarding spray atomisation which consequently helps in controlling the pollution discharge. The influence of viscosity on spray penetration was observed in this work and also coincided with the findings of studies conducted in Rahmes *et al* (2009).

Furthermore, the effect of blending bio-SPK fuel with kerosine is investigated. In this assessment, the effect of mixing 50% JSPK with 50% Jet-A (B50) on droplet lifetime and spray penetration was observed. Additionally, the comparison of fuel properties is presented. The consideration of blending pure JSPK with Jet-A is due to the low density of JSPK, which unfortunately cannot be feasibly implemented in existing aircraft due to the modifications needing to be made. It is noted that in comparison to pure JSPK, mixing 50% JSPK with 50% Jet-A has increased the fuel's density to lie within the density range consequently feasible for use in existing aircraft engines. Advantageously, the boiling temperature and viscosity of this mixture is still lower than that of Jet-A, providing shorter droplet lifetime and spray penetration. Therefore, it is important to ensure that in selecting the biofuel to reduce emissions and

dependency on crude oil, properties such as density, viscosity and boiling temperature (as the indication to the fuel's volatility) are taken into account.

## **7.2 Biofuel's Engine Performance Evaluation**

The effect of biofuels on combustion was also evaluated with regard to the performance of the engine focusing on engine thrust, fuel consumption and specific fuel consumption. The evaluation was carried out using an in-house engine performance computer tool called PYTHIA, which was integrated with the fuel's caloric properties data generated using NASA CEA software. The quantification of engine performance was conducted for a civil aircraft flying at cruise and at a constant mass flow condition. However, for this evaluation, only JSPK and CSPK were considered, and simulated both as pure and as a blend with Jet-A.

In generating the caloric properties data, the molecular formula and enthalpy of formation were employed. The tabulated caloric properties data is generated for wide range of temperature, pressure, FAR and WAR. A set of data containing the fuel's density, heat capacity, enthalpy and entropy is generated for pure JSPK and CSPK. The data is validated by comparing the percentage difference with data from the component which has closer molecular formula to JSPK and CSPK. The validation shows a small difference, therefore it is concluded that the data set is dependable to be used for the engine performance evaluation.

The performance of CSPK and JSPK on engine performance was evaluated for two different conditions – design point condition which focused on cruise; and alternative off-design condition which focused on the constant mass flow condition. In both conditions, engine characteristics such as flight altitude, ambient temperature, ambient pressure, air mass flow, engine component efficiencies and pressure ratio are kept constant. The only difference is in the TET setting. At design point condition, the value for TET was fixed, therefore the prediction of engine thrust, fuel flow and SFC is dependent on the fixed value set for TET. Whereas at constant mass flow condition, the TET was

disabled whilst the fuel flow rate was fixed in order to provide the so-called constant LBO condition.

At both conditions, increases in engine thrust were noted as the percentage of biofuels increased. Noticeably at cruise condition, the reduction in fuel flow was noted and subsequently improves the SFC. Meanwhile, at the constant mass flow condition where the fuel flow is fixed, the increases in engine thrust are consistent with the increases in TET. The improvement (increases) in engine thrust are observed corresponding to high LHV of the biofuels in comparison to Jet-A. High heat capacity of biofuels is also observed to affect the increases in engine thrust by increasing the temperature of the engine downstream, consequently increasing the nozzle exit velocity which is important in calculating the engine thrust. At cruise condition, the reduction in fuel flow is observed as consistent with the increases in the biofuel's percentage in the biofuel/Jet-A mixture. The reduction of fuel flow is observed to correspond to the density of the fuel. It is noted that fuel with less density has high energy content per unit weight and therefore in order to accommodate the constant TET set during the cruise, only a small amount of fuel is required. The effect of fuel density is also observed at constant mass flow condition which is observable from the increases of TET.

### **7.3 Biofuel's Engine Emissions Evaluation**

Additionally, the evaluation of the influence of JSPK and CSPK was carried out with regard to their effect on engine emissions with the attention focused on NO<sub>x</sub> and CO formation. The formation of such pollutions was conducted using HEPHAESTUS, an in-house engine emissions computer tool, where the parameters of the engine are mandatory.

In this assessment, both biofuels – CSPK and JSPK were also evaluated as pure and also as a blend with Jet-A. The emissions evaluation was conducted at the same condition considered in engine performance evaluation. The formations of pollutions considered in this assessment are NO<sub>x</sub> and CO. In comparison to Jet-A, both conditions show significant decreases of NO<sub>x</sub> as the

percentage of the biofuel in the mixture increases. At cruise condition, the formation of CO is reduced, but increases in CO are observed at constant mass flow condition. The reduction in NO<sub>x</sub> pollution is consistent with the reduction of flame temperature as thermal-NO<sub>x</sub> was considered. The reduction of flame temperature is observed to correspond with the reduction of FAR which depends on the composition of the fuel. Additionally, the reduction in NO<sub>x</sub> is also observed to correspond with the low density of the biofuel, resulting in a low amount of fuel injected into the chamber. Besides low flame temperature and low density, low boiling temperature of biofuels is also found to affect the NO<sub>x</sub> formation. Fuel with high boiling temperature requires a longer time to boil and vaporise, which consequently reduces the rate of droplet evaporation and leads to the consumption of a smaller fraction of the fuel in the premixed state relative to diffusion burn combustion. Although implementing biofuel in the engine lowers the flame temperature, substantially helping in reducing NO<sub>x</sub>, this on the other hand increases the CO formation particularly during the constant mass flow condition. Whereas during cruise, the reduction of CO is observed notably due to the small amount of fuel injected stemming from low density of biofuels.

In validating the biofuel emission results, the formation of NO<sub>x</sub> and CO predicted in this work was compared with data obtained from Rahmes *et al* (2009) who conducted off-engine ground tests for the mixture of 50% Jatropha-Algae with 50% Jet-A. It is worth mentioning that since the fuels used in the experiment differ from those used in this research; clearly the precise emissions may vary. However, as this is the only information available the data was referenced as a benchmark with certain limitations, as follows: Firstly, although the fuels utilised in both studies are different, those fuels were produced through the same chemical processes (deoxygenation and isomerization) in order to provide the so-called fit-for-purpose fuel. Therefore, the use of emissions data from this fuel is considered acceptable as those fuels utilised in the experiment and the present research work can be categorised as the fuel from the same family. Secondly, using this data is considered acceptable due to the consistency of the biofuel's composition in the mixture used in the experiment and in this research

work. The comparison results show the consistency in the trend, but the prediction of CO in this research work is slightly lower than that measured from the experimental work.

## **7.4 Optimisation Assessment**

As density of JSPK and CSPK is lower than that of kerosine, the implementation of this fuel may require modification to the existing gas turbine engine. However, JSPK and CSPK can still be implemented in gas turbine engines by blending with kerosine at a certain percentage in order to maintain the density within the range of density allowed. For that reason, the optimisation of the biofuel percentage was included in this research by taking into account the problem related to the fuel consumption, engine thrust and engine emissions. Additionally, the establishment of this exercise nonetheless to test the integration of the optimiser with the performance and emissions model for the selected problem. This exercise was performed using GATAC optimisation tool which implemented the non-sorted multi-objective genetic algorithm (NSGAMO).

Two cases were evaluated. The first case was established to optimise the percentage of CSPK in the biofuel/kerosine mixture, while the second case was developed to optimise the percentage of JSPK in the biofuel/kerosine mixture. For both cases, the percentage of biofuel ranging from 0% to 100% and the fuel flow ranging from 0.51 kg/s to 0.7 kg/s were selected as the design variables. As for the objectives function, minimum NO<sub>x</sub>, minimum CO and maximum engine thrust were chosen. Considering the condition such as maximum temperature that the turbine can withstand, and also due to the density range of the gas turbine fuel, the maximum temperature of 1800K and density ranging from 775 kg/m<sup>3</sup> to 840 kg/m<sup>3</sup> were set as the design constraints. In this evaluation, the baseline point corresponded to the formation of NO<sub>x</sub>, CO and thrust generated by the engine running which was operated at 0.52 kg/s of Jet-A.

In each case, three extreme points indicating the minimum design of  $\text{NO}_x$ , minimum design of CO and maximum design of engine thrust were obtained from the Pareto front generated by the optimiser. For the first case which was established to optimise the maximum percentage of CSPK in the mixture, it is noted that to achieve the minimum design of  $\text{NO}_x$ , CSPK has to be mixed with Jet-A at the percentage of 58 and 42 respectively and has to be injected at 0.51 kg/s. In comparison to the baseline point (Jet-A), this design yields a 9.09% decrease in  $\text{NO}_x$ , 12.16% decrease in CO, with the penalty being a 0.31% decrease in engine thrust. In achieving the minimum design of CO, the mixture of 6% of CSPK with 94% of Jet-A which injected at the fuel flow rate of 0.51 kg/s is essential. Relative to Jet-A, this design produces 2.71% reduction in  $\text{NO}_x$ , and 12.36% reduction in CO. However, the penalty of 0.82% in engine thrust is noted. Meanwhile, the maximum engine thrust design is achievable by injecting 0.6 kg/s of the mixture of 50.4% CSPK with 49.6% Jet-A which increases the engine thrust of 7.75%, relative to the baseline point. Although considerably low penalty in  $\text{NO}_x$  is obtained, unfortunately, this design suffers relatively large increases of CO which therefore is particularly ineffective. Based on these extreme points, the compromise design of 57.24% CSPK mix with 42.76% of Jet-A was selected.

Meanwhile, for the second test case, in order to obtain the minimum  $\text{NO}_x$  design, the mixture of 47% of JSPK with 53% of Jet-A is essential. This mixture having to be injected at the rate of 0.51 kg/s. In comparison to the baseline point, this design provides a reduction of 6.85 % of  $\text{NO}_x$ , 10.69% of CO and a penalty of 0.21% in engine thrust. In contrast, the minimum CO design is achieved by implementing almost 100% of Jet-A at the fuel rate of 0.51 kg/s yielding to the reduction of 2.05% of  $\text{NO}_x$  and 12.39% of CO. Unfortunately, a penalty of 0.91% of engine thrust is observed. In achieving the maximum design of engine thrust, the mixture of about 31% JSPK with 69% Jet-A should be injected at the fuel rate of 0.60 kg/s. This design yields a 7.74% increase in engine thrust but suffers a large increase in CO and  $\text{NO}_x$ . For this test case, the mixture of 46.51% of JSPK with 53.49% of Jet-A is chosen as the compromise design. The compromise designs for both cases specify the maximum

percentage of biofuel that is feasible to blend with Jet-A in order to alleviate the problem regarding the overdependence on crude oil. Additionally, both compromise designs indicate the improvement (reduction) in fuel flow which also becomes the advantage.

In order to compare the solution given by NSGAMO, the optimisation assessment was conducted using MOTS2. Similar trend in Pareto surfaces are obtained and the same trend of trade-off exists between the engine emissions and engine thrust are revealed. This comparable solution suggests the capability of both optimisers – MOTS2 and NSGAMO in handling the specified design problems.

To further explore the solution given between both optimisers, the extreme conditions and the compromise designs selected from both optimisers were compared. In case of NSGAMO, for test case 1 (optimising CSPK/Jet-A mixture) the compromise design suggests the mixture of 57.24% of CSPK with 42.76% Jet-A is essential, yielding an improvement (reduction) of  $\text{NO}_x$  by 7.80%, reduction of CO by 4.34%, and improvement (increase) in engine thrust by 0.3%. For test case 2 (optimising JSPK/Jet-A mixture), the compromise design selected suggests the use of 46.51% JSPK/53.49% Jet-A to be implemented in the aircraft engine. This design yields the reduction of  $\text{NO}_x$  and CO by 6.28% and 6.96% respectively. An improvement of 0.06% in engine thrust is noted with this compromise design. Meanwhile, in case of MOTS2, the compromise design selected for test case 1 suggests the mixture of 59% CSPK with 41.0% Jet-A which improves  $\text{NO}_x$  by 7.73%, CO by 2.72%, and 0.42% for engine thrust. While for test case 2 (JSPK/Jet-A mixture), the mixture of 47.7% JSPK with 53.3% of Jet-A is selected. Within this design, the improvement of  $\text{NO}_x$  by 6.15%, CO by 5.22%, and engine thrust by 0.20% are obtained.

## 7.5 CFD Modelling Approach

In exploring the practical issues related to HEPHAESTUS combustion modelling, the simulation through CFD package was performed considering the ability of CFD in visualising and solving most of the fluid problem. This exercise was established in order to visualize the behaviour of the fluid inside the chamber and to evaluate the influence of assumptions considered in HEPHAESTUS. In conducting the exercise, the CFD 3D model was established based on the 1D model provided by HEPHAESTUS. In this assessment, the comparison of average temperature distributed within the combustor chamber and the formation of  $\text{NO}_x$  were made. The evaluation however was conducted only for Jet-A as not enough information was obtained for biofuel.

In terms of trends, the distribution of temperature at the core and at the wall predicted in HEPHAESTUS is in agreement with the average temperature predicted in CFD although inconsistency in absolute temperature is observed.

In regard to the location of maximum temperature, HEPHAESTUS predicted the highest temperature at the PZ of the combustor while in case of CFD, the highest temperature is recorded at the IZ, with 8.1% higher than temperature predicted by HEPHAESTUS. This maximum temperature is important as it represents the combustion flame and therefore reflects the thermal- $\text{NO}_x$  formation.

The inconsistency in the maximum flame location recorded between HEPHAESTUS and CFD is due to the assumption considered in HEPHAESTUS which is impractical in reality. In general, HEPHAESTUS considers the homogeneous well-mixed between the fuel and oxidiser. Therefore as soon as the fuel is injected into the chamber, the combustion process will take place. This assumption leads the flame to be located within the PZ and therefore the maximum flame temperature is recorded in this zone. Instead of well-mixed, HEPHAESTUS also neglects other phenomena occurring in the combustion chamber such as fuel evaporation, combustion unsteadiness and flow recirculation. In contrast, the 3D model developed in CFD is non-mixed

where the mixture of the fuel and oxidizer is controlled by the turbulence. Additionally, as far as the liquid fuel is concerned, the evaporation process that changes the liquid into the gaseous phase will be taking place before mixing with the air and starting the combustion. This phenomenon explains the difference in the flame that happens to be located at the downstream of the combustor instead of PZ as predicted in HEPHAESTUS.

The comparison in  $\text{NO}_x$  formation shows the significant difference as HEPHAESTUS under-predicts  $\text{NO}_x$  with 81% difference. Instead of the difference in flame location, and the neglecting of some combustion phenomena, the significant difference in  $\text{NO}_x$  is associated with the reaction constants used implied by Celis (2010) in HEPHAESTUS. In order to improve the result, reaction constants suggested by Miller and Bowman (1978) were employed. With these constants,  $\text{NO}_x$  prediction is much closer to CFD result (with the difference of 32.36% being obtained). It is worth mentioning here that  $\text{NO}_x$  generated in both tools is the thermal- $\text{NO}_x$  where the temperature becomes important. Considering the temperature recorded in HEPHAESTUS is lower than the temperature predicted in CFD, therefore the formation of  $\text{NO}_x$  predicted in HEPHAESTUS is smaller than that predicted in CFD.

## **8 CONCLUSIONS AND FUTURE WORKS**

### **8.1 Conclusions**

This research work was developed to provide a methodology to assess and optimise biofuel combustion, addressing issues related to overdependence on crude oil and increases of pollution generated. More specifically, the research was mainly intended to quantitatively evaluate and optimise biofuel combustion technologies taking into account both engine performance and emissions of a civil aircraft engine. This research was also intended to expand the work of Mazlan (2009), on evaporation analysis by providing the work with different types of biofuel and improving the analysis with more reliable data. In addition, this research intended to use computer tools available in Cranfield University, and when necessary to modify the existing computer tools and to introduce the related information in the tools to perform the proposed tasks in this work.

Generally, the main contribution of this work to the existing knowledge comprises the following:

1. The development of a so-called greener-based methodology for assessing the potential of biofuels in reducing the dependency on conventional fuel and the amount of pollution emission generated,
2. The prediction of fuel spray characteristics as one of the major controlling factors regarding emissions,
3. The evaluation of engine performance and emission through the adaptation of a fuel's properties into the in-house computer tools,
4. The development of optimisation work to obtain a trade-off between engine performance and emissions, and
5. The development of CFD work to explore the practical issues related to the HEPHAESTUS engine emission combustion modelling.

Based on these objectives and contributions it is concluded that this research work was successfully completed and the expected outcomes were achieved.

In accomplishing this research several specific works were identified and divided into several parts. These specific works include those related to the initial literature review, which justified the need and motivation for the research; the processes involving collection of fuel properties, integration of fuel properties into the in-house computer tools developed at Cranfield University, evaluation exercises via those improved tools, optimisation assessment by integrating those tools into the optimiser, and last but not least a CFD exercise to explore and provide an insight into the practical issues related to the effect of assumptions considered in the HEPHAESTUS combustion emission modelling.

To be more specific, the first part of this research indicated the previous state-of-the-art of problems that have been faced by the airline industries regarding crude oil and the impact of tremendous environmental challenges. Additionally, this part indicated different approaches recommended in encountering those problems. Literally, in order to counter overdependence on crude oil and to reduce the environmental impact of aircraft, the changing in aircraft engine operation, changing in aircraft configuration, changing in aircraft operations and traffic management, and replacing the conventional fuel with alternative fuels are proposed. However, the last alternative was found to be the most feasible alternative, especially within the short term. Therefore, this part provided the initial literature review on biofuels, comprising the types of biofuel and the challenges faced regarding the implication of the fuels as the replacement in the aircraft engine. Considering the interest from airline industries towards biofuels, this part also provided several successful flight tests and the outcomes either from experimental or numerical studies in regard to their performance and emissions.

To further continue this research, the second part dealt with the analysis of spray characteristics generally, or droplet lifetime and spray penetration specifically as one of the emissions controlling factors. The analysis was conducted by comparing different types of alternative fuels in conjunction with the variation of fuel properties with temperature to provide more versatile and more dependable results. This analysis was established as the continuity of the

work conducted in Mazlan (2008) who used ethanol as the baseline fuel. Other fuels used for this assessment are Rapeseed Methyl Ester (RME), Jatropha Bio-synthetic Paraffinic Kerosine (JSPK) and Camelina Bio-synthetic Paraffinic Kerosine (CSPK). The outcomes obtained from this assessment concluded that the fuel properties of volatility, viscosity and density are the main factors that affect the droplet lifetime and the penetration of the spray and which consequently influence the combustion performance. Less volatile fuel will easily evaporate and therefore has shorter droplet lifetime compared to highly volatile fuel. Fuel with high density and high viscosity will have longer spray penetration in comparison to less dense and less viscous fuel. It is however, mandatory to ensure that the properties of the prospective alternative fuel satisfy the gas turbine engine requirement in order to ensure that no modification to the engine should be necessary. One of the important properties is density of the fuel. In order to ensure that no modification to the engine is necessary the density of the alternative fuel should be within the range of 775 – 840 kg/m<sup>3</sup>. Most of the alternative fuels however, do not comply with that requirement, unless by blending it with the conventional fuel. For that reason, the investigation onto the effect of blends 50% JSPK with 50% Jet-A on droplet lifetime and spray penetration was performed. The results obtained concluded that those properties were improved and therefore provided improvement in the spray characteristic and combustion performance accordingly.

The influence of biofuels on engine performance was tested in the third part of this research work. Considering the potential of bio-synthetic paraffinic kerosine types of fuel, only CSPK and JSPK were used for this evaluation. The assessment was conducted through an engine performance computer tool available in Cranfield University. The properties required for the evaluation were generated and integrated into the software before conducting the assessment. The generated fuel properties were validated and were proven dependable. The effect of biofuels on engine performance was tested in a two-spool high bypass turbofan engine, simulated to be operated at cruise condition and at constant mass fuel flow condition. The assessment indicated improvement in engine thrust due to high low heating value of biofuels in comparison to that of

conventional fuel. The amount of fuel flow consumed by the engine operated with biofuel was improved (reduced) due to the high heat capacity of biofuel.

Furthermore, this research work also focused on comparison of the pollution emission formation generated by biofuels with the pollution generated from Jet-A. This assessment was conducted using the in-house engine emission computer tool (HEPHAESTUS) with the improvement in the code introduced to enable the tool to evaluate biofuel. The emissions comparative study between biofuels and Jet-A was performed by comparing  $\text{NO}_x$  and CO generated from JSPK and CSPK evaluated as pure and as blends with Jet-A. The evaluation was conducted at cruise and at constant mass flow condition. The emissions comparative results have shown a reduction in  $\text{NO}_x$  at both conditions. The reduction of CO was observed during cruise whilst the increases of CO were observed at the constant mass flow condition. The reduction of  $\text{NO}_x$  is due to the reduction of flame temperature due to thermal- $\text{NO}_x$  as considered. It is also concluded that the  $\text{NO}_x$  reduction also corresponds to the high boiling temperature of biofuel which provides rapid evaporation process and produces a smaller fraction of the fuel in the premixed state, relative to diffusion burn combustion. At constant mass flow condition, the effect of low flame temperature is observed to correspond to the increases of CO whilst at cruise, the reduction in CO is observed to correspond to the volatility of the fuel which improves the evaporation rate of the fuel, hence helping the completion of the combustion.

Due to poor fuel properties, the utilisation of biofuel in aircraft engine is not easy and as a result, the modification to the engine and the aircraft itself is necessary. The only option is to blend the biofuel with Jet-A. Therefore, an optimisation work was established with the mission aiming to find the maximum percentage of biofuel that minimises  $\text{NO}_x$  and CO, whilst maximising the engine thrust, within the specific range TET and fuel density appropriate to the circumstances associated with the limitations of the aircraft engine. This assessment also provided an exploration to the feasibility of integrating the information and computer tools used in the previous assessment in the multi-

objective genetic algorithm optimiser tool at the conceptual design stage, thereby allowing a quantitative analysis of the trade-off between the engine performance and environmental impact. The optimisation assessment was developed in order to produce the optimal designs based on the specific mission's profile and constraints mentioned above. The mixture of CSPK with Jet-A, and the mixture of JSPK with Jet-A were considered. This approach was successful in highlighting the trade-off that exists between the engine performance and emissions. For each case, three extreme designs were analysed and the compromise design was selected. The comparison of solution given by NSGAMO was compared by evaluating the specified test cases using MOTS2, in which both test cases evaluated in NSGAMO also were evaluated in MOTS2. Through the comparison, the similar trend of Pareto surfaces and trade-off that exists between the design objectives is observed. The reasonable close comparison for each extreme designs and compromise designs between NSGAMO and MOTS for both test cases also are observed.

In order to explore the practical issues related to the assumptions considered in the engine emissions combustion modelling, the CFD work was conducted by adopting and establishing the setting in the emission software into the CFD simulation. The CFD simulation was performed only for Jet-A. The comparison of  $\text{NO}_x$  formation and temperature profile across the chamber predicted in HEPHAESTUS was compared with the  $\text{NO}_x$  and the average temperature measured in CFD. The profile of temperature predicted in HEPHAESTUS shows an agreement with the profile of average temperature measured in CFD. However, due to the well-mixed assumption considered in HEPHAESTUS, the maximum flame temperature is recorded at PZ instead of IZ as recorded by CFD. This difference also was affected due to neglecting the combustion phenomena such as evaporation process, combustion unsteadiness and flow recirculation.

The effect of such assumptions also influence the generation of  $\text{NO}_x$ . As far as the  $\text{NO}_x$  is concerned, HEPHAESTUS under-predicted  $\text{NO}_x$  with 81% difference noted. In addition to the assumptions considered above, the discrepancy was

observed due to the reaction constants considered. In tackling this problem, different reaction constants were implemented in HEPHAESTUS and are found to improve  $\text{NO}_x$  difference by 31%. This assessment nonetheless clarified the effect of different reaction equations and reaction constants towards  $\text{NO}_x$  generation which therefore requires proper experimental data to achieve consistency in the accuracy.

## **8.2 Future Works**

This biofuel research work has covered the area of fuel spray characteristics as one of the major factors controlling the formation of pollution from the combustor. In order to deliver further continuation of the research in regard to biofuel, performance and emission generated from biofuel were evaluated. Moreover, this research work also focused on the optimisation assessment in establishing the optimal percentage of biofuel in the biofuel/Jet-A mixture. Last but not least, this research also covered the exploration into the influence of assumptions considered in emission computer tool by comparing the results with CFD simulation. As biofuel is the focus of attention nowadays, further works on biofuel are necessary in terms of development, with either a direct or indirect relation to this research work. Nevertheless, all research areas covered in this work deserve special attention.

### **1. Evaluation using Algae type of fuel**

Despite JSPK and CSPK, other fuel that currently becomes attention is algae type of fuel. This fuel was recognised as being more promising, as it will not compete with other food crops, etc, thus reserves to be evaluated. In order to conduct assessment for this type of fuel, the detailed properties of algae is required. Once the properties are gathered, they can be used directly in the evaporation spreadsheet analysis to evaluate its spray characteristics. In evaluating the engine performance of algae type of fuel, set of caloric properties data over range of temperature, pressure, FAR and WAR is necessary and has first to be introduced in PYTHIA. This data can be generated by NASA CEA with the information regarding to molecular formula and enthalpy of formation are required. It is also important to introduce algae in HEPHAESTUS for emissions evaluation.

### **2. Evaluate biofuel engine performance and emissions at full aircraft trajectories**

The evaluation of engine performance and emissions performed in this work has focused only on the cruise condition, which was recognised as being a

condition where the aircraft spends the longest time during its flight operation. Since full aircraft flight trajectory comprises take-off, climb, cruise, and descent, the evaluation of biofuels during this trajectory therefore deserves to be conducted. In order to perform this evaluation, the profile of this trajectory has to be determined.

### **3. Evaluate the biofuel engine emissions using the improved version of HEPHAESTUS**

Study conducted by Pervier (2011) has improved HEPHAESTUS by modifying the initial HEPHAESTUS established in Celis (2010). The modification has been made involved the eliminating of wall section, and also by modifying the fuel distribution. Within this modification, the prediction of emissions specifically  $\text{NO}_x$  is not only follow the trend provided from ICAO, but qualitatively, the prediction is much closer to the ICAO data, hence the prediction of  $\text{NO}_x$  is much reliable compare to the one that used in this work. Further explanation about the modification can be found in Pervier (2010). Therefore, it is important in the future to establish a research work that focuses on the integration of biofuel in this improved version of HEPHAESTUS.

is also noted that due to the assumptions considered in initial HEPHAESTUS, the prediction of  $\text{NO}_x$  in comparison to CFD is significant. Therefore, it becomes important in the future to improve HEPHAESTUS by including the evaporation process, flow recirculation, turbulent phenomena, and the used of appropriate reaction rates and constants in order to provide reliable results. Other research areas that deserve to be considered include the performance of the CFD simulation through the use biofuel as the reactant. In this research work, the CFD simulation was conducted using only Jet-A. Additionally, the simulation of CFD utilising biofuel may not be achievable in this work due to the difficulties associated with getting the reaction step and reaction rate of this fuel. Based on this consideration, it is worth noting that, if, in the future, further work is developed in getting all the

information pertinent to biofuels, this may perhaps be achieved through the conduction of an experiment in order to perform biofuel simulation in CFD.

**4. Perform an optimisation study using the improved version of HEPHAESTUS and to conduct a parallel coordinate study**

In area of optimisation study, it is worth in the future to conduct the fuel design optimisation using the improved version of HEPHAESTUS. It is also recommended to conduct a parallel coordinate study in order to help and further analyse a set of data given from the optimiser. A parallel coordinate study is informative such as to give better understanding which variables in a dataset that highly important in defining the objective functions.

**5. Conduct biofuel optimisation study for different flight trajectory**

From the information obtained in the research area mentioned above, there may be the capacity to initiate an optimisation work later on. The optimisation of flight trajectory was performed in the research work of Celis; however, focus was directed towards only Jet-A. Therefore, the flight trajectory optimisation, with the use of biofuel, is worth performing.

**6. Conduct CFD study on biofuels**

Other research areas that deserve to be considered include the performance of the CFD simulation through the use biofuel as the reactant. In this research work, the CFD simulation was conducted using only Jet-A as consideration was given only to validating the HEPHAESTUS result before its utilisation in the optimisation work. Additionally, the simulation of CFD utilising biofuel may not be achievable in this work due to the difficulties associated with getting the reaction step and reaction rate of this fuel. Based on this consideration, it is worth noting that, if, in the future, further work is developed in getting all the information pertinent to biofuels, this may perhaps be achieved through the conduction of an experiment in order to perform biofuel simulation in CFD.

## 9 REFERENCES

1. Acosta, W. A. and Beckel, S. A. (1989), Fuel Properties Effect on the Performance of a Small High Temperature Rise Combustor, 25th Joint Propulsion Conference co-sponsored by the AIAA, ASME, SAE, and ASEE, July 10-12, 1989, Monterey, California, pp. 1.
2. Anderson, R. W., Patil, P. B., Chin, J., Nicholls, J. A., Mirsky, W., Lyons, V., (1976), The Effect of Drop Size on Emissions from the Primary Zone of a Gas Turbine Type Combustor, 16<sup>th</sup> Symposium (International) on Combustion, The Combustion Institute
3. Antoine N. E., and Kroo, I. M., (2004), Multiobjective Aircraft Design Optimization for Low Noise and Emissions, 24<sup>th</sup> International Congress of the Aeronautical Sciences (ICASS 2004).
4. Antoine, N. E. and Kroo, I. M. (2005), Framework for Aircraft Conceptual Design and Environmental Performance Studies, AIAA JOURNAL, vol. 43, no. 10, pp. 2100-2109.
5. Armento, V. A., and Arroyo, J. C., (2004), An Application of a Multi-Objective Tabu Search Algorithm to a Bicriteria Flowshop Problem, Journal of Heuristics, No. 10, pp. 463 – 481
6. Baukal, C. E. Jr., (2001), The John Zink Combustion Handbook, John Zink Company LLC, CFRC Press LLC
7. Baylor Institute for Air Science, (1998), Renewable Aviation Fuels Development Center, Development of Bio-based Fuels for Aircraft Turbine Engines-final report
8. Blazowski, W. S. and Jackson, T. A. (1978), Evaluation of Future Jet Fuel Combustion Characteristics, AFAPL-TR-77-93.
9. Borman, G. L., and Rangeland, K. W., (1998), Combustion Engineering, McGraw-Hill
10. Bower, G. C., and Kroo, M. I., (2008), Multi-objective Aircraft Optimization for Minimum Cost and Emissions Over Specific Route Networks, 26<sup>th</sup> International Congress of the Aeronautical Sciences (ICAS 2008).

11. Brooks, F. J., (2000), GE Gas Turbine Performance Characteristics, GER-3567H, GE Power Systems Schenectady, NY. ([http://site.ge-energy.com/prod\\_serv/products/tech\\_docs/en/gas\\_turbines.htm](http://site.ge-energy.com/prod_serv/products/tech_docs/en/gas_turbines.htm))
12. Butze, H. F. and Ehlers, R. C. (1975), Effect of Fuel Properties on Performance of a Single Aircraft Turbojet Combustor, NASA TM X-71789.
13. Cannon, S. M., Smith, C. E., and Anand, M. S., (2003), LES Predictions of Combustor Emissions in an Aero Gas Turbine Engine, 39<sup>th</sup> AIAA/ASME/SAE/ASEE Joint Propulsion Conference and Exhibit, 20 – 23 July 2003, Huntsville, Alabama
14. Celis, C. (2010), Evaluation and Optimisation of Environmentally Friendly Aircraft Propulsion Systems (PhD thesis), Cranfield University, UK
15. CFD Inc. (2001), Chapter 17. Modelling Pollutant Formation
16. Circiu, M. S., and Leon, F., (2010), Comparative Study of Multiobjective Genetic Algorithms, Buletinul, Institutului Politehnic Din Iasi, Publicat de, Universitatea Tehnica Gheorghe Asachi din Iasi.
17. Conference on Aviation and Alternative Fuels, (2009), International Civil Aviation Organization, Working Paper, CAAF/09-WP/09, Rio de Janeiro, Brazil, 16 to 18 November 2009
18. Connor, A. M., and Tilley, D. G., (1998), A Tabu Search Method for the Optimization of Fluid Power Circuits, Proceedings of the Institution of Mechanical Engineers, Part 1: Journal of Systems and Control Engineering.
19. Dagget, D. L., Hendricks, R. C., Walther, R. and Corporan, E. (2007), Alternate Fuels for use in Commercial Aircraft, , The Boeing Company.
20. Dagget, D., Hadaller, O., Hendricks, R., Walther, R., (2006), Alternative Fuels and Their Potential Impact on Aviation, The 25<sup>th</sup> Congress of the International Council of the Aeronautical Sciences (ICAS) hosted by the German Society for Aeronautics and Astronautics, Vol. NASA/TM—2006-214365, September 3–8, 2006, Hamburg, Germany, pp. 1 - 8.

21. Datta, A., and Som, S. K., (1999), Effects of Spray Characteristics on Combustion Performance of a Liquid Fuel Spray in a Gas Turbine Combustor, *International Journal of Energy Research*, 23: 217-228
22. Demirbas, A. (2007), Progress and Recent Trends in Biofuels, *Progress Energy Combust Sci*, vol. 33, pp. 1-18.
23. Dimech, E., Chircop, K., Xuereb, M., Muscat, R., Camilleri, W., Karumbaiah, D. N., Pervier, H., (2011), GATAC User Manual V2.
24. Dumrongsak, J., (2012), Numerical Study of Helicopter Combustor and Exhaust Emissions Using Large Eddy Simulation, 21<sup>st</sup> Review Report, Cranfield University, UK
25. Ellis, W., Lear, W., Singh, B., Srivivisan, A., Crittenden, J. and Sherif, S. (2008), "Flameless Combustion of Biofuels in Semi-closed Cycle Gas Turbine", 46th AIAA Aerospace Sciences Meeting and Exhibition.
26. FLUENT 6.3 User Guide
27. Fuller, E. N., Schettler, P. D. and Giddings, J. C. (1966), A New Method for Prediction of Binary Gas-Phase Diffusivity Coefficients, *Industrial and Engineering Chemistry*, vol. 58, no. 5, pp. 18-27.
28. GAO Report (2009), Aviation and Climate Change, Aircraft Emissions Expected to Grow, but Technological and Operational Improvements and Government Policies Can Help Control Emissions, GAO-09-554, United States Government Accountability Office, Report to Congressional Committees.
29. Giannelos, P. N., Zannikos, F., Tournas, S. L. E. and and Anastopoulos, G. (2002), Tobacco Seed Oil as and Alternative Diesel Fuel: Physical and Chemical Properties, *Industrial Crops and Products*, vol. 16, pp. 1-9.
30. Greene, D. L. (1992), Energy-efficiency Improvement Potential of Commercial Aircraft, *Ann Rev Energy Environ*, vol. 17, pp. 537-573.
31. Gupta, A. K., (2004), Thermal Characteristics of Gaseous Fuel Flames using High Temperature Air, *Journal of Engineering Gas Turbine Power*, 126 (1), pp. 9 -19

32. Habib, Z., Parthasarathy, R. and Gollahalli, S. (2009), Performance and Emission Characteristics of Biofuel in a Small-scale Gas Turbine Engine, *Applied Energy*, vol. 87, no. 5, pp. 1701-1709.
33. Halvorsen, J. D., Mammel, W. C. and Celements, L. D. (1993), Density Estimation for Fatty Acids and Vegetable Oils Based on Their Fatty Acid Composition, *Journal of the American Oil Chemists' Society*, vol. 70, no. 875, pp. 880.
34. Handbook of Aviation Fuel Properties, (1983), Coordinating Research Council, Report No. 530
35. Hanson, R. K., and Salimian, S., (1984), Survey of Rate Constants in H/N/O Systems, *Combustion Chemistry*, pp. 361
36. Hernandez, J. J., Collado, J. P., and Sanz-Argent, J., (1998), Role of the Chemical Kinetics on Modelling NO<sub>x</sub> Emissions in Diesel Engines, *Official J. Eur. Communities*, L350, 1- 56
37. <http://www.grc.nasa.gov/WWW/k-12/airplane/winglets.html>
38. <http://www.jet-engine.net/civtfspec.html>
39. International Agency for Research on Cancer (IARC). (1989). Volume 45, Occupational Exposures in Petroleum Refining; Crude oil and Major Petroleum Fuels, Summary of Data Reported and Evaluation, p203
40. International Civil Aviation Organization (2002), Annual Civil Aviation Report, *ICAO J*, 57 (6), 12:20
41. Jaeggi, D. M., Parks, G. T., Kipouros, T., Clarkson, P. J., (2008), the Development of Multi-Objective Tabu Search Algorithm for Continuous Optimisation Problems, *European Journal of Operational Research*, Vol. 185, pp. 1192 – 1212
42. Jha, S. K., Fernando, S., and To, S. D. F., (2007), Flame Temperature Analysis of Biodiesel Blends and Components, An ASABE Meeting Presentation, Paper Number: 076234, American Society of Agricultural and Biological Engineers.

43. Kamunge, D. (2011), A Non-Linear Weighted Least Squares Gas Turbine Diagnostic Approach and Multi-Fuel Performance Simulation, PhD Thesis, Cranfield University, UK
44. Khasanshin, T. S. and Aleksandrova, A. A., (1984), Thermodynamic Properties of Ethanol and Atmospheric Pressure, Journal of Engineering Physics and Thermophysics., Vol. 47., no. 3., pp. 1046 - 1052
45. Kinder, J. D. and Rahmes, T. (2009), Evaluation of Bio-derived Synthetic Paraffinic Kerosene (Bio-SPK), The Boeing Company.
46. Kinder, J. D., (2010)., Research Report: Evaluation of Bio-Derived Synthetic Paraffinic Kerosenes (Bio-SPKs), The Boeing Company UOP United States Air Force Research Laboratory
47. Klopper, H. (2010), First Biofuel-Powered Military Helicopter Takes Flight, available at:  
[http://www.boeing.com/Features/2010/09/bds\\_feat\\_rnlaf\\_09\\_07\\_10.html](http://www.boeing.com/Features/2010/09/bds_feat_rnlaf_09_07_10.html) (accessed August 10).
48. Krishna, C. R., (2007), Performance of the Capstone C30 Microturbine on Biodiesel Blends, Bookhaven National Laboratory
49. Kroo, I., (2004), Aeronautical Applications of Evolutionary Design, VKI Lecture Series on Optimization Methods and Tools for Multicriteria/Multidisciplinary design, November 15 – 19, 2004
50. Kuhn, M., ( 2009), Azul Looks to Sugar Cane to Power Embraer E-Jet .
51. Lacava, P. T., Bastos-Netto, D., and Pimenta, A. P. (2004) Design Procedure and Experimental Evaluation of Pressure Swirl Atomizer. 24th International Congress of the Aeronautical Sciences
52. Le Clercq, P., Aigner, M., (2009), Impact of Alternative Fuels Physical Properties on Combustor Performance, 11th Triennial International Annual Conference on Liquid Atomization and Spray Systems, (ICLASS), Vail, Colorado, USA

53. Lee, J. J., (2010), Can We Accelerate the Improvement of Energy Efficiency in Aircraft Systems?, *Energy Conversion and Management*, 189-196
54. Lee, J. J., Lukacho, S. P., Waitz, I. A. and Schafer, A. (2001), Historical and Future Trends in Aircraft Performance, Cost and Emissions, *Ann Rev Energy Environ*, vol. 26, pp. 167-200.
55. Lefebvre, A. H. (1989), *Atomization and Sprays*, Hemisphere Publishing Corporation.
56. Lefebvre, A. H., and Ballal, D. P., (2010), *Gas Turbine Combustion: Alternative Fuels and Emissions*, CRC Press
57. Lefebvre, A. H., (1985), Fuel Effects on Gas Turbine Combustion - Ignition, Stability, and Combustion Efficiency, *Transactions of ASME, Journal of Engineering for Gas Turbine and Power*
58. Lefebvre, A. H., (1999), *Gas Turbine Combustion, Second Edition*, Taylor and Francis Group
59. MahdaviNejad, R. A., (2011), Modeling and Optimization of Electrical Discharge Machining of SiC Parameters, Using Neutral Network and Non-dominated Sorting Genetic Algorithm (NSGA II), *materials Sciences and Applications*, vol. 2, pp. 669 – 675
60. Marschall, E., (1990), Viscosity of Selected Binary, ternary, and Quaternary Liquid Mixtures, *J. Chem. Eng. Data*, 35, 375 - 381
61. Mattingly, J. D. (1996), *Elements of Gas Turbine Propulsion*, McGraw-Hill Inc.
62. Mazlan, N. M. (2008), *Combustion Performance of Liquid Fuels Derived from Biomass*, MSc thesis, Cranfield University, UK.
63. McBride, J. B. and Gordon, S., (1996), *Computer Program for Calculation of Complex Chemical Equilibrium Compositions and Applications, User's Manual and Program Description*.
64. McCormick, R. L., Graboski, M. S., Alleman, T. L., Herring, A. M. and Tyson, K. S. (2001), "Impact of Biodiesel Source Material and Chemical Structure on Emissions of Criteria Pollutants from a Heavy-Duty Engine", *Environ. Sci. Technol.*, vol. 35, pp. 1742-1747.

65. McCormick, R. L., Ross, D. J. and Graboski, M. S. (1997), "Effect of Several Oxygenates on Regulated Emissions from Heavy-Duty Diesel Engines", *Environ. Sci. Technol.*, vol. 31, pp. 1144-1150.
66. Melanie, T., (2006), Baere Aerospace, West Lafayette, IN
67. Miller, J. A., and Bowman, C. T., (1989), Mechanism and Modelling of Nitrogen Chemistry in Combustion, *Progress in Energy and Combustion Science*, Vol. 15, pp. 287 – 338
68. Morsi, S. A., and A. J. Alexander.,(1972), An Investigation of Particle Trajectories in Two-Phase Flow Systems, *J. Fluid Mech.*, 55 (2): 193 - 208
69. Myhre, G. and Stordal, F. (2001), On the Trade-off of the Solar and Thermal Infrared Radiative Impact of Contrails, *Geophys Res Lett*, vol. 28, no. 3119, pp. 3122.
70. Naeem, M., Singh, R. and and Probert, D. (1998), Implications of engine deterioration for fuel usage", *Applied Energy*, vol. 2-3, no. 59, pp. 125-146.
71. Naegeli, D. W., Dodge, L. G. and Moses, C. A. (1983), Effect of Flame Temperature and Fuel Composition on Soot Formation in Gas Turbine Combustors, *Combustion Science and Technology*, vol. 35, no. 1-4, pp. 117-131.
72. Naegli, D. W. and Moses, C. A. (1980), Effect of Fuel Molecular Structure on Soot Formation in Gas Turbine Engines, ASME.
73. Naegli, D. W., Dodge, L. G. and Moses, C. A. (1983), The Sooting Tendency of Fuels Containing Polycyclic Aromatics in a Research Combustor, *Journal of Energy*, vol. 7, no. 2, pp. 168.
74. Nanda, J., (n. d), Multiobjective Genetic Algorithm for Product Design, Industrial and Manufacturing, Engineering Department, Penn State University, University Park, PA 16802
75. Nandasana, A. D., Ray, A. K., and Gupta, S. K., (2003), Applications of the Non-Dominated Sorting Genetic Algorithm (NSGA) in Chemical Reaction Engineering, *International Journal of Chemical Reactor Engineering*, Vol. 1

76. Norman, P. D., Lister, D. H., Lecht, M., Madden, P., Park, K., Penanhoat, O., Plaisance, C., Renger, K., (2003), Development of the Technical Basis for a New Emissions Parameter Covering the Whole Aircraft Operation: NEPAIR, final technical report, Technical Report Contract Number G4RD-CT-2000-00182, European Community
77. O'Keeffe, N., (2010), Planting Hope.
78. Pachidis V. A., (2006), Gas Turbine Performance Simulation (unpublished Thermal Power MSc course notes), School of Engineering, Department of Power Propulsion and Aerospace Engineering.
79. Paleu, V. and Nelias, D. (2007), On Kerosine Lubrication of Hybrid Ball Bearings, International Conference on Diagnosis and Prediction in Mechanical Engineering Systems (DIPRE'07), 26 - 27 October 2007, Galati, Romania, pp. 50.
80. Palmer, C. B. (1945), Performance of Compressor-Turbine Jet Propulsion Systems, L5E17, Langley Memorial Aeronautical Laboratory Langley Field, VA.
81. Palmer, F. H., (1986), Vehicle Performance of Gasoline Containing Oxygenates., International Conference on Petroleum Based and Automotive Applications, Institution of Mechanical Engineers Conference Publications, MEP, London, UK, pp. 33 – 46
82. Park, S. H., Suh, H. K., Lee, C. S., (2009), Effect of Bioethanol-Biodiesel Ratio on Fuel Spray Behavior and Atomization Characteristics, Energy and Fuels, 23: 4092-4098
83. Parrilla, J and Cortes, C., Modelling of Droplet Burning for Rapeseed oil as Liquid Fuel, Department of Mechanical Engineering, Centro Politecnico Superior, University of Zaragoza, Spain.
84. Parsons, D., Nanduri, J., Celik, I., Strakey, P., (2008), Assessment of Emissions Prediction Capability of RANS based PDF Models for Lean Premixed Combustion of Methane, Proceedings of the 2008 Technical Meeting of the Central States Section of The Combustion Institute

85. Penner, J. E., Lister, D. H., Griggs, D. J., Dokken. D. J., McFarland, M., (2013), Aviation and the Global Atmosphere, IPCC Special Reports on Climate Change – online versions.
86. Pervier, H., (2011), Emissions Modelling for Engine Cycle and Aircraft Trajectory Optimisation, Second Year Review Report, Cranfield University, UK
87. Pierce, J. B., Rochaya, D., Jasuja, A. K. and Moss, J. B. (2007), AFTUR Final Report: Modelling of Droplet Evaporation and Spray Formation for Alternative Fuels, WP 3, Sub-task 3.1.2, Cranfield University, UK
88. Pikunas, A., Pukalskas, S., Grabys, J., (2003), Influence of Composition of Gasoline – Ethanol Blends on Parameters of Internal Combustion Engines, Journal of KONES Internal Combustion Engines, vol. 10.
89. Popov, A., (2005), Genetic Algorithms for Optimization, Programs for Matlab Version 1.0 User Manual
90. Powell, H. N., Suci, S. N., Brinkley Jr, S. R., Edwards, H. E. and Fremont, H. A. (1955), Properties of Combustion Volume 1: Thermodynamic Properties, 1st ed, McGraw Hill Book Company Inc, General Electric Company, Cincinnati, Ohio.
91. Prommersberger, K., Maier, G. and Wittig, S. (1998), Validation and Application of a Droplet Evaporation Model for Real Aviation Fuel, Symposium on Gas Turbine Engine Combustion, Emissions and Alternative Fuels, 12-16 October 1998, Lisbon, Portugal.
92. Prommersberger, K., Maier, G., and Wittig, S., (1998), Validation and Application of a Droplet Evaporation Model for Real Aviation Fuel, Symposium on Gas Turbine Engine Combustion, Emissions and Alternative Fuels, Lisbon, Portugal, 12-16 October 1998.
93. Rahmes, T. F., Kinder, J. D., Henry, T., M., Crenfeldt, G., LeDuc, G. F., Zombanakis, G. P., Abe, Y., Lambert, D. M., Lewis, C., Juenger, J. A., Andac, M. G., Reilly, K. R., Holmgren, J. R., McCall, M. J. and Bozzano, A. G. (2009), Sustainable Bio-Derived Synthetic Paraffinic

- Kerosine (Bio-SPK) Jet Fuel Flights and Engine Tests Program Results, 9th AIAA Aviation Technology, Integration, and Operations Conference, 21-23 September 2009, Hilton Head South Carolina
94. Reid, R. C., Prausnitz, J. M. and Poling, B. E. (1987), The Properties of Gases and Liquids, 4th ed, , New York, USA.
  95. Reid, R. C., Prausnitz, J. M. and Sherwood, T. L. (1977), The Properties of Gases and Liquids, 3rd ed, USA: McGraw Hill Book Company.
  96. Rink K. K., and Lefebvre A. H., (1989), The Influences of Fuel Composition and Spray Characteristics on Nitric Oxide Formation, Combustion Science and Technology, Vol. 68, Issue 1 - 3
  97. Rochaya, D. (2007), Numerical Simulation of Spray Combustion using Bio-mass Derived Liquid Fuels (PhD thesis), Cranfield University, UK
  98. Sahoo, P. K., Das, L. M., Babu., M. K. G., Arora, P., Singh, V. P., Kumar., N. R., Varyani., T. S., (2009), Comparative Evaluation of Performance and Emission Characteristics of Jatropha, Karanja, Polanga Based Biodiesel as Fuel in Tractor Engine, Fuel, vol. 88, pp. 1698 – 1707
  99. Sammut, M., Muscat, R., Xuereb, M., Chircop, K., Camilleri, W., Dimech, E, Karumbiah, D., N., and Pervier, H., (2012), GATAC V2.1.1 User Manual
  100. Sausen, R., Gierens, K., Ponater, M. and Schumann, U. (1998), "A Diagnostic Study of the Global Distribution of Contrails Part 1: Present Day Climate", Theoretical and Applied Climatology, vol. 61, no. 3-4, pp. 127-141.
  101. Sazhin, S. S., Feng., G. and Heikal, M. R. (2001), A Model for Fuel Spray Penetration, Fuel, vol. 80, pp. 2171-2180.
  102. Schefer, R. W., and Sawyer, R. F., (1977), Lean Premixed Recirculating Flow Combustion for Control of Oxides of Nitrogen, Symposium (International) on Combustion, vol. 16, Issue. 1, pp. 119 - 134

103. Sethi, V. (2008), Advanced Performance Simulation of Gas Turbine Components and Fluid Thermodynamic Properties (PhD thesis), Cranfield University, Cranfield University
104. Sharma, N. Y., Datta, A., Som, S. K., (2001), Influences of Spray and Operating Parameters on Penetration of Vaporizing Fuel Droplets in a Gas Turbine Combustor, Applied Thermal Engineering, 21: 1755-1768
105. Sharma, N. Y., Som, S. K., (2002), Influence of Fuel Volatility on Combustion and Emission Characteristics in a Gas Turbine Combustor at a Different Inlet Pressures and Swirl Conditions, Proc Instn Mech Engrs Vol 216 Part A: J Power and Energy
106. Sharp, J. G. (1951), Fuels for Gas-Turbine Aero-Engines, Aircraft Engineering
107. Signer, M., H., P., Mercogliano, R. and Stein, H. (1996), European Programme on Emissions, Fuels and Engine Technologies (EPEFE)-Heavy Duty Diesel Study, 961074, SAE Technical Paper.
108. Sims, R., Taylor, M., Saddler, J. and Mabee, W. (2008), From 1st to 2nd Generation Biofuel Technologies: An Overview of Current Industry and RD&D Activities, International Energy Agency
109. Singh, V., Sharma, S. K., and Vaibhav, S., (2012), Identification of Dimensions of the Optimization of Fuel Consumption in Air Transport Industry: A Literature Review, Journal of Energy Technologies and Policy, ISSN 2224 – 3232 (paper) ISSN 2225 – 0573 (online), Vol. 2, No. 7
110. Sobie, B., (2010), Salicornia Shortage Scuppers First Mexican Biofuels Flight, Flight International, 26 January – 1 February 2010, p 11
111. Srinivas, S., and Deb, K., (1995), Multiobjective Optimization Using Nondominated Sorting in Genetic Algorithms, Evolutionary Computation 2 (3), pp. 221 – 248
112. Tuttle, J. H, Shisler, R. A., Bilger, R. W., Mellor, A. M., (1975), Emissions from Aircraft Fuel Nozzle Flames, Purdue University Combustion Laboratory, Report PURDU-CL-75-04

113. Useful Information about Conventional and Alternate Fuels and Their Feedstocks, National Renewable Energy Lab, National Bioengineering Center, June 2004
114. Warwick, G., (2009), Green Day.
115. Yuan, W., Hansen, A. C. and Zhang, Q. (2005), Vapor Pressure and Normal Boiling Point Predictions for Pure Methyl Esters and Biodiesel Fuels, Fuel, vol. 84, pp. 943-950.

## 10 APPENDICES

### 10.1 Appendix A - List of Publications

Conference and Proceedings:

- Mazlan, N. M., Savill, M., Kipouros, T., Li, Y. G., 2012, "A Numerical Study into the Effects of Bio-synthetic Paraffinic Kerosine Blends with Jet-A for Civil Aircraft Engine" GT2012-68754, Proceedings of ASME Turbo Expo 2012, Copenhagen, Denmark
- Mazlan, N. M., Savill, M., Kipouros, T., 2011, "Computational Evaluation of Combustion Performance for Liquid Jet Fuels Derived from Biomass", 3<sup>rd</sup> CEAS Air and Space Conference, 21<sup>st</sup> AIDAA Congress, Venice, Italy



# Appendix B - Continues

5.10E-04	1.0E-05	1.9841E-05	9.84E-01	461	0.69	101325	689.277	0.353	1.261E-04	0	3.813E-02	6.41E-02	-5.860E+03	-5.860E-02	2.819E-12	2000	0.068	3.704	6911	1.237E-09	1000	251000	9.72E+04	2.54E-02	0	1.15E-06	1.093E+02	1.489E-01	3.776E-03	-1.835E-08	-1.835E-13	-3.705E-09	-3.705E-04	0.000E+00	0.000E+00	5.114E-04	8.080E-02
5.20E-04	1.0E-05	1.9838E-05	9.84E-01	461	0.63	101325	689.277	0.353	1.261E-04	0	3.488E-02	7.00E-02	-5.357E+02	-5.357E-02	2.818E-12	2000	0.068	3.704	6908	1.236E-09	1000	251000	9.72E+04	2.54E-02	0	1.15E-06	1.093E+02	1.475E-01	3.741E-03	-1.834E-08	-1.834E-13	-3.704E-09	-3.704E-04	0.000E+00	0.000E+00	5.114E-04	8.159E-02
5.30E-04	1.0E-05	1.9834E-05	9.83E-01	461	0.58	101325	689.277	0.353	1.261E-04	0	3.190E-02	7.65E-02	-4.897E+03	-4.897E-02	2.816E-12	2000	0.068	3.704	6906	1.236E-09	1000	251000	9.72E+04	2.54E-02	0	1.15E-06	1.093E+02	1.462E-01	3.707E-03	-1.833E-08	-1.833E-13	-3.703E-09	-3.703E-04	0.000E+00	0.000E+00	5.114E-04	8.237E-02
5.40E-04	1.0E-05	1.9830E-05	9.83E-01	461	0.53	101325	689.277	0.353	1.261E-04	0	2.918E-02	8.35E-02	-4.478E+03	-4.478E-02	2.815E-12	2000	0.068	3.704	6904	1.236E-09	1000	251000	9.72E+04	2.54E-02	0	1.15E-06	1.093E+02	1.449E-01	3.675E-03	-1.831E-08	-1.831E-13	-3.702E-09	-3.702E-04	0.000E+00	0.000E+00	5.114E-04	8.315E-02
5.50E-04	1.0E-05	1.9827E-05	9.83E-01	461	0.48	101325	689.277	0.353	1.261E-04	0	2.669E-02	9.12E-02	-4.095E+03	-4.095E-02	2.813E-12	2000	0.068	3.704	6902	1.235E-09	1000	251000	9.72E+04	2.54E-02	0	1.15E-06	1.093E+02	1.437E-01	3.644E-03	-1.830E-08	-1.830E-13	-3.701E-09	-3.701E-04	0.000E+00	0.000E+00	5.114E-04	8.391E-02
5.60E-04	1.0E-05	1.9823E-05	9.82E-01	461	0.44	101325	689.277	0.353	1.261E-04	0	2.442E-02	9.97E-02	-3.745E+03	-3.745E-02	2.812E-12	2000	0.068	3.704	6900	1.235E-09	1000	251000	9.72E+04	2.54E-02	0	1.15E-06	1.093E+02	1.425E-01	3.615E-03	-1.829E-08	-1.829E-13	-3.700E-09	-3.700E-04	0.000E+00	0.000E+00	5.114E-04	8.467E-02
5.70E-04	1.0E-05	1.9819E-05	9.82E-01	461	0.40	101325	689.277	0.353	1.261E-04	0	2.234E-02	1.09E+03	-3.425E+03	-3.425E-02	2.810E-12	2000	0.068	3.704	6899	1.234E-09	1000	251000	9.72E+04	2.54E-02	0	1.15E-06	1.093E+02	1.414E-01	3.587E-03	-1.828E-08	-1.828E-13	-3.700E-09	-3.700E-04	0.000E+00	0.000E+00	5.114E-04	8.543E-02
5.80E-04	1.0E-05	1.9815E-05	9.82E-01	461	0.37	101325	689.277	0.353	1.261E-04	0	2.044E-02	1.19E+03	-3.133E+03	-3.133E-02	2.808E-12	2000	0.068	3.704	6898	1.234E-09	1000	251000	9.72E+04	2.54E-02	0	1.15E-06	1.093E+02	1.403E-01	3.560E-03	-1.827E-08	-1.827E-13	-3.699E-09	-3.699E-04	0.000E+00	0.000E+00	5.114E-04	8.617E-02
5.90E-04	1.0E-05	1.9812E-05	9.81E-01	461	0.34	101325	689.277	0.353	1.261E-04	0	1.870E-02	1.30E+03	-2.866E+03	-2.866E-02	2.807E-12	2000	0.068	3.704	6897	1.233E-09	1000	251000	9.72E+04	2.54E-02	0	1.15E-06	1.093E+02	1.393E-01	3.534E-03	-1.826E-08	-1.826E-13	-3.698E-09	-3.698E-04	0.000E+00	0.000E+00	5.114E-04	8.691E-02
6.00E-04	1.0E-05	1.9808E-05	9.81E-01	461	0.31	101325	689.277	0.353	1.261E-04	0	1.711E-02	1.42E+03	-2.622E+03	-2.622E-02	2.805E-12	2000	0.068	3.704	6896	1.233E-09	1000	251000	9.72E+04	2.54E-02	0	1.15E-06	1.093E+02	1.384E-01	3.510E-03	-1.825E-08	-1.825E-13	-3.698E-09	-3.698E-04	0.000E+00	0.000E+00	5.114E-04	8.764E-02
6.10E-04	1.0E-05	1.9804E-05	9.81E-01	461	0.28	101325	689.277	0.353	1.261E-04	0	1.565E-02	1.55E+03	-2.399E+03	-2.399E-02	2.804E-12	2000	0.068	3.704	6896	1.232E-09	1000	251000	9.72E+04	2.54E-02	0	1.15E-06	1.093E+02	1.374E-01	3.486E-03	-1.824E-08	-1.824E-13	-3.697E-09	-3.697E-04	0.000E+00	0.000E+00	5.114E-04	8.837E-02
6.20E-04	1.0E-05	1.9801E-05	9.80E-01	461	0.26	101325	689.277	0.353	1.261E-04	0	1.432E-02	1.69E+03	-2.195E+03	-2.195E-02	2.802E-12	2000	0.068	3.704	6895	1.232E-09	1000	251000	9.72E+04	2.54E-02	0	1.15E-06	1.093E+02	1.366E-01	3.464E-03	-1.824E-08	-1.824E-13	-3.697E-09	-3.697E-04	0.000E+00	0.000E+00	5.114E-04	8.909E-02
6.30E-04	1.0E-05	1.9797E-05	9.80E-01	461	0.24	101325	689.277	0.353	1.261E-04	0	1.311E-02	1.85E+03	-2.008E+03	-2.008E-02	2.801E-12	2000	0.068	3.704	6895	1.231E-09	1000	251000	9.72E+04	2.54E-02	0	1.15E-06	1.093E+02	1.357E-01	3.442E-03	-1.823E-08	-1.823E-13	-3.696E-09	-3.696E-04	0.000E+00	0.000E+00	5.114E-04	8.981E-02
6.40E-04	1.0E-05	1.9793E-05	9.79E-01	461	0.22	101325	689.277	0.353	1.261E-04	0	1.199E-02	2.02E+03	-1.838E+03	-1.838E-02	2.799E-12	2000	0.068	3.704	6895	1.231E-09	1000	251000	9.72E+04	2.54E-02	0	1.15E-06	1.093E+02	1.349E-01	3.422E-03	-1.822E-08	-1.822E-13	-3.696E-09	-3.696E-04	0.000E+00	0.000E+00	5.114E-04	9.052E-02
6.50E-04	1.0E-05	1.9790E-05	9.79E-01	461	0.20	101325	689.277	0.353	1.261E-04	0	1.097E-02	2.21E+03	-1.682E+03	-1.682E-02	2.797E-12	2000	0.068	3.704	6895	1.230E-09	1000	251000	9.72E+04	2.54E-02	0	1.15E-06	1.093E+02	1.341E-01	3.402E-03	-1.821E-08	-1.821E-13	-3.695E-09	-3.695E-04	0.000E+00	0.000E+00	5.114E-04	9.122E-02
6.60E-04	1.0E-05	1.9786E-05	9.79E-01	461	0.18	101325	689.277	0.353	1.261E-04	0	1.004E-02	2.41E+03	-1.539E+03	-1.539E-02	2.796E-12	2000	0.068	3.704	6895	1.230E-09	1000	251000	9.72E+04	2.54E-02	0	1.15E-06	1.093E+02	1.334E-01	3.384E-03	-1.821E-08	-1.821E-13	-3.695E-09	-3.695E-04	0.000E+00	0.000E+00	5.114E-04	9.192E-02
6.70E-04	1.0E-05	1.9783E-05	9.78E-01	461	0.17	101325	689.277	0.353	1.261E-04	0	9.189E-03	2.63E+03	-1.408E+03	-1.408E-02	2.794E-12	2000	0.068	3.704	6895	1.230E-09	1000	251000	9.72E+04	2.54E-02	0	1.15E-06	1.093E+02	1.327E-01	3.366E-03	-1.820E-08	-1.820E-13	-3.694E-09	-3.694E-04	0.000E+00	0.000E+00	5.114E-04	9.261E-02
6.80E-04	1.0E-05	1.9778E-05	9.78E-01	461	0.15	101325	689.277	0.353	1.261E-04	0	8.408E-03	2.87E+03	-1.289E+03	-1.289E-02	2.793E-12	2000	0.068	3.704	6895	1.229E-09	1000	251000	9.72E+04	2.54E-02	0	1.15E-06	1.093E+02	1.320E-01	3.349E-03	-1.819E-08	-1.819E-13	-3.694E-09	-3.694E-04	0.000E+00	0.000E+00	5.114E-04	9.330E-02
6.90E-04	1.0E-05	1.9775E-05	9.78E-01	461	0.14	101325	689.277	0.353	1.261E-04	0	7.694E-03	3.14E+03	-1.180E+03	-1.180E-02	2.791E-12	2000	0.068	3.704	6896	1.229E-09	1000	251000	9.72E+04	2.54E-02	0	1.15E-06	1.093E+02	1.314E-01	3.333E-03	-1.819E-08	-1.819E-13	-3.694E-09	-3.694E-04	0.000E+00	0.000E+00	5.114E-04	9.399E-02
7.00E-04	1.0E-05	1.9771E-05	9.77E-01	461	0.13	101325	689.277	0.353	1.261E-04	0	7.041E-03	3.42E+03	-1.080E+03	-1.080E-02	2.790E-12	2000	0.068	3.704	6896	1.228E-09	1000	251000	9.72E+04	2.54E-02	0	1.15E-06	1.093E+02	1.308E-01	3.317E-03	-1.818E-08	-1.818E-13	-3.693E-09	-3.693E-04	0.000E+00	0.000E+00	5.114E-04	9.467E-02
7.10E-04	1.0E-05	1.9767E-05	9.77E-01	461	0.12	101325	689.277	0.353	1.261E-04	0	6.443E-03	3.75E+03	-9.982E+02	-9.982E-02	2.788E-12	2000	0.068	3.704	6897	1.228E-09	1000	251000	9.72E+04	2.54E-02	0	1.15E-06	1.093E+02	1.302E-01	3.302E-03	-1.818E-08	-1.818E-13	-3.693E-09	-3.693E-04	0.000E+00	0.000E+00	5.114E-04	9.534E-02
7.20E-04	1.0E-05	1.9764E-05	9.77E-01	461	0.11	101325	689.277	0.353	1.261E-04	0	5.895E-03	4.09E+03	-9.045E+02	-9.045E-02	2.786E-12	2000	0.068	3.704	6897	1.227E-09	1000	251000	9.72E+04	2.54E-02	0	1.15E-06	1.093E+02	1.296E-01	3.288E-03	-1.817E-08	-1.817E-13	-3.693E-09	-3.693E-04	0.000E+00	0.000E+00	5.114E-04	9.601E-02
7.30E-04	1.0E-05	1.9760E-05	9.76E-01	461	0.10	101325	689.277	0.353	1.261E-04	0	5.395E-03	4.47E+03	-8.279E+02	-8.279E-02	2.785E-12	2000	0.068	3.704	6895	1.227E-09	1000	251000	9.72E+04	2.54E-02	0	1.15E-06	1.093E+02	1.291E-01	3.274E-03	-1.817E-08	-1.817E-13	-3.692E-09	-3.692E-04	0.000E+00	0.000E+00	5.114E-04	9.676E-02
7.40E-04	1.0E-05	1.9756E-05	9.76E-01	461	0.09	101325	689.277	0.353	1.261E-04	0	4.936E-03	4.89E+03	-7.578E+02	-7.578E-02	2.783E-12	2000	0.068	3.704	6899	1.226E-09	1000	251000	9.72E+04	2.54E-02	0	1.15E-06	1.093E+02	1.286E-01	3.261E-03	-1.816E-08	-1.816E-13	-3.692E-09	-3.692E-04	0.000E+00	0.000E+00	5.114E-04	9.733E-02
7.50E-04	1.0E-05	1.9753E-05	9.75E-01	461	0.08	101325	689.277	0.353	1.261E-04	0	4.517E-03	5.34E+03	-6.936E+02	-6.936E-02	2.782E-12	2000	0.068	3.704	6899	1.226E-09	1000	251000	9.72E+04	2.54E-02	0	1.15E-06	1.093E+02	1.281E-01	3.249E-03	-1.816E-08	-1.816E-13	-3.692E-09	-3.692E-04	0.000E+00	0.000E+00	5.114E-04	9.799E-02
7.60E-04	1.0E-05	1.9749E-05	9.75E-01	461	0.07	101325	689.277	0.353	1.261E-04	0	4.138E-03	5.83E+03	-6.349E+02	-6.349E-02	2.780E-12	2000	0.068	3.704	6900	1.225E-09	1000	251000	9.72E+04	2.54E-02	0	1.15E-06	1.093E+02	1.276E-01	3.237E-03	-1.815E-08	-1.815E-13	-3.691E-09	-3.691E-04	0.000E+00	0.000E+00	5.114E-04	9.864E-02
7.70E-04	1.0E-05	1.9745E-05	9.75E-01	461	0.07	101325	689.277	0.353																													

## 10.3 Appendix C - Calculation of Molecular Formula and Enthalpy of Formation

### 1. Calculating molecular formula

From D5291 test, percentages of carbon and hydrogen atoms in JSPK and CSPK are as follows (ref):

<b>Fuel</b>	<b>CSPK</b>	<b>JSPK</b>
% C	85.4	85.4
% H	15.1	15.5
% N	< 0.10	< 0.10
C/H	5.7	5.5

The estimation of the molecular formula for the fuels was done by estimating their empirical formula from the percentage of carbon and hydrogen in the fuels (by assuming that the fuel contained carbon and hydrogen essentially only, and the nitrogen composition in the fuel is negligibly small). Empirical formula can be then calculated as follows:

- i. Assume 100% of compound is equal to 100g to change the percentage to grams
- ii. Convert the grams to mole by dividing the element with its molecular weight
- iii. Divide each number of the moles by the least number
- iv. Multiply the results to remove the fractions

Fuel composition	JSPK		CSPK	
	C	H	C	H
% of composition	85.4	15.5	85.4	15.1
Molar mass of the composition (g/mol)	12	1	12	1
Number of mole	85.4/12 = 7.12	15.5/1 = 15.5	85.4/12 = 7.12	15.1/1 = 15.1
Divide by the least number	7.12/7.12 = 1	15.5/7.12 = 2.18	7.12/7.12 = 1	15.1/7.12 = 2.12
<b>Empirical formula</b>	<b>C<sub>1</sub>H<sub>2.18</sub></b>		<b>C<sub>1</sub>H<sub>2.12</sub></b>	

Assuming the average carbon content in bio-SPK is similar to that in kerosine (C=12), multiplying the empirical formula of JSPK and CSPK by 12 leads to molecular formula for JSPK and CSPK of C<sub>12</sub>H<sub>26</sub> and C<sub>12</sub>H<sub>25.4</sub> respectively.

## 2. Calculating enthalpy of formation

D5291 test also provides the heat of combustion for JSPK and CSPK which are:

Fuel	JSPK	CSPK
Net heat of combustion (MJ/kg)	44.3	44.0

### Example: Enthalpy of formation of JSPK

Balancing the chemical stoichiometric equation of JSPK:



From the general equation of heat of combustion:

Heat of combustion = {The sum of all heats of formation of the products} – {The sum of all heats of combustion of the reactants}

Heat of combustion = {Heat of combustion of CO<sub>2</sub> (g) + Heat of formation of H<sub>2</sub>O (g)} – {Heat of formation of C<sub>12</sub>H<sub>26</sub> (g) + Heat of formation of O<sub>2</sub> (g)}

Convert 44.3 MJ/kg to kJ/mole = 7534.9 kJ/mole

Rearrange the equation:

$$7534.9 \text{ kJ/mole} = \{12(-393.5) + 13(-241.8)\} - \{\text{Heat of formation of } \text{C}_{12}\text{H}_{26} + (37/2)(0)\}$$

Heat of formation of  $\text{C}_{12}\text{H}_{26} = -330.50 \text{ kJ/mole}$

**The same calculation also was done for CSPK**

## 10.4 Appendix D - Equations of Mixing Properties of Two Fuels

### 1. Enthalpy, $H_{mix}$

$$H_{mix} = \frac{\sum x_i \rho_i H_i}{\sum x_i \rho_i} = \frac{x_1 \rho_1 H_1 + x_2 \rho_2 H_2}{x_1 \rho_1 + x_2 \rho_2}$$

### 2. Entropy, $S_{mix}$

$$S_{mix} = \frac{\sum x_i \rho_i S_i}{\sum x_i \rho_i} = \frac{x_1 \rho_1 S_1 + x_2 \rho_2 S_2}{x_1 \rho_1 + x_2 \rho_2}$$

### 3. Gas constant, $R_{mix}$

$$R_{mix} = \frac{\sum x_i \rho_i R_i}{\sum x_i \rho_i} = \frac{x_1 \rho_1 R_1 + x_2 \rho_2 R_2}{x_1 \rho_1 + x_2 \rho_2}$$

### 4. Heat capacity, $C_{p,mix}$

$$C_{p,mix} = \sum x_i C_p = x_1 C_{p1} + x_2 C_{p2}$$

## 10.5 Appendix E - Hephaestus Input File

Design point

Jet-A

Table 10-1: HEPHAESTUS Input File for Jet-A at Cruise Condition

Engine Parameters	Design point condition
	Jet-A
Ambient flight altitude (m)	0
Ambient temperature (K)	288.15
Ambient relative humidity	0
Air total temperature at the combustor inlet (K)	720.52
Air total pressure at the combustor inlet (atm)	19.39423
Total air mass flow rate (kg/s)	119.510
Fuel mass flow rate (kg/s)	2.6570
Fuel total temperature (K)	400



**Table 10-2: Engine Parameters of CSPK and the Blend as an Input file for HEPHAESTUS**

<b>Engine Parameters</b>	<b>20BC/80KE</b>	<b>40BC/60KE</b>	<b>60BC/40KE</b>	<b>80BC/20KE</b>	<b>100BC</b>
Ambient flight altitude (m)	0	0	0	0	0
Ambient temperature (K)	288.15	288.15	288.15	288.15	288.15
Ambient relative humidity	0	0	0	0	0
Air total temperature at the combustor inlet (K)	720.52	503.46	510.08	513.45	515.49
Air total pressure at the combustor inlet (atm)	19.39425	19.39424	19.39422	19.39422	19.39423
Total air mass flow rate (kg/s)	119.510	119.510	119.510	119.510	119.510
Fuel mass flow rate (kg/s)	2.6443	3.3023	3.2720	3.2516	3.2354
Fuel total temperature (K)	400	400	400	400	400

**Table 10-3: Engine Parameters of JSPK and the Blends as an Input File for HEPHAESTUS**

<b>Engine Parameters</b>	<b>20BJ/80KE</b>	<b>40BJ/60KE</b>	<b>60BJ/40KE</b>	<b>80BJ/20KE</b>	<b>100BC</b>
Ambient flight altitude (m)	0	0	0	0	0
Ambient temperature (K)	288.15	288.15	288.15	288.15	288.15
Ambient relative humidity	0	0	0	0	0
Air total temperature at the combustor inlet (K)	720.52	503.46	510.08	513.45	515.49
Air total pressure at the combustor inlet (atm)	19.39424	19.39422	19.39420	19.39420	19.39420
Total air mass flow rate (kg/s)	119.510	119.510	119.510	119.510	119.510
Fuel mass flow rate (kg/s)	2.6409	3.2939	3.2595	3.2352	3.2150
Fuel total temperature (K)	400	400	400	400	400

**Table 10-4: Hephaestus Input File for Constant Mass Flow Evaluation**

<b>Engine Parameters</b>	<b>Design point condition</b>
	<b>Jet-A</b>
Ambient flight altitude (m)	0
Ambient temperature (K)	288.15
Ambient relative humidity	0
Air total temperature at the combustor inlet (K)	720.52
Air total pressure at the combustor inlet (atm)	19.39423
Total air mass flow rate (kg/s)	119.510
Fuel mass flow rate (kg/s)	2.6570
Fuel total temperature (K)	400